NASA TECHNICAL TRANSLATION

NASA TT F-590

NASA TT F-590

TRANSFER OF MICROWAVE RADIATION IN THE ATMOSPHERE

Transactions of the Main Geophysical Observatory
Im. A. I. Voyeykov, No. 222

K. S. Shifrin, Editor

Hydrometeorological Press, Leningrad, 1968

NATIONAL AERONAUTICS AND SPACE ADMINISTRATION • WASHINGTON, D. C. • JULY 1969

TRANSFER OF MICROWAVE RADIATION IN THE ATMOSPHERE

Transactions of the Main Geophysical Observatory
Im. A. I. Voyeykov, No. 222

K. S. Shifrin, Editor

Translation of "Perenos Mikrovolnovogo Izlucheniya v Atmosfere"
Trudy Glavnaya Geofizicheskaya Observatoriya
Im. A. I. Voyeykova, Vypusk 222. Hydrometeorological Press, Leningrad, 1968

NATIONAL AERONAUTICS AND SPACE ADMINISTRATION

For sale by the Clearinghouse for Federal Scientific and Technical Information
Springfield, Virginia 22151 – CFSTI price $3.00

This collection contains the results of both theoretical and experimental investigations of thermal emission from the atmosphere and the underlying surface in the centimeter and millimeter regions of the spectrum. The problem of microwave radiation in a cloud-free atmosphere, in clouds and in precipitation are studied; the reflection and radiation of the rough surface of the sea and the ice cover are investigated and the contrasts in radiobrightness temperature of the ice fields, the zone of cloud cover, precipitation and the regions of increased humidity are evaluated. The possibility of using radio emission is evaluated from the viewpoint of solving inverse problems, i.e., sounding of the atmosphere and the underlying surface from aircraft.

This collection is intended for scientific researchers, engineers, candidates and students concerned with problems of the physics of the atmosphere, radiophysics and radio engineering.

TABLE OF CONTENTS

FROM THE EDITOR

This collection is called to the attention of the readers and contains work from colleagues of the Main Geophysical Observatory im. A.I. Voyeykov, Main Administration of the Hydrometeorological Service, The Institute of Radio Engineering and Electronics, Academy of Sciences, USSR and the Leningrad Military Academy of Engineering im. A.F. Mozhayskiy, and concerns natural thermal emission from the atmosphere and the Earth's surface in the centimeter and millimeter regions of the spectrum. Although the energy of this radiation is very small, for example, for λ = 1 cm, it is approximately 10^8 times smaller than for λ = 1 μm; contemporary microwave radiometers have such a high sensitivity that it can be easily measured.

The research published in this collection has been developed during the period 1964 - 1967 and shows that the natural radio emission contains important information concerning the temperature of the Earth's surface, the ice fields on the sea, the humidity of the atmosphere and the zones of cloud cover and precipitation. A closer analysis of this radiation permits determining the vertical profiles of the temperature, the pressure and humidity and studying the characteristics of roughness, thickness of the ice cover, etc.

The use of a huge radio window in the Earth's atmosphere for gathering meteorological information is quite promising. In the near future a microwave radiometer, installed on an artificial Earth satellite will operationally supply a forecast of the most important data and, we must hope, will permit the forecasts to be substantially improved qualitatively. This is the ultimate purpose of this work, reports of which the reader will find in the pages of this collection.

NATIONAL AERONAUTICS AND SPACE ADMINISTRATION

TECHNICAL TRANSLATION EVALUATION

Budget Bureau No. 104-R037
Approval Expires: Sept. 30, 1969

TO: THE USERS OF THIS TRANSLATION →

NASA TTF NO. 590

MAINTAINING THE QUALITY OF NASA TRANSLATIONS REQUIRES A CONTINUOUS EVALUATION PROGRAM. PLEASE COMPLETE AND MAIL THIS FORM TO AID IN THE EVALUATION OF THE USEFULNESS AND QUALITY OF THE TRANSLATING SERVICE.

THIS PUBLICATION *(Check one or more)*

- ☐ FURNISHED VALUABLE NEW DATA OR A NEW APPROACH TO RESEARCH.
- ☐ VERIFIED INFORMATION AVAILABLE FROM OTHER SOURCES.
- ☐ FURNISHED INTERESTING BACKGROUND INFORMATION.
- ☐ OTHER *(Explain)*: _____

FOLD LINE FOLD LINE

TRANSLATION TEXT *(Check one)*

- ☐ IS TECHNICALLY ACCURATE.
- ☐ IS SUFFICIENTLY ACCURATE FOR OUR PURPOSE.
- ☐ IS SATISFACTORY, BUT CONTAINS MINOR ERRORS.
- ☐ IS UNSATISFACTORY BECAUSE OF *(Check one or more)*:
  - ☐ POOR TERMINOLOGY.
  - ☐ NUMERICAL INACCURACIES.
  - ☐ INCOMPLETE TRANSLATION.
  - ☐ ILLEGIBLE SYMBOLS, TABULATIONS, OR CURVES.
  - ☐ OTHER *(Explain)*:

FOLD LINE FOLD LINE

REMARKS

FROM

DATE

NOTE: REMOVE THIS SHEET FROM THE PUBLICATION, FOLD AS INDICATED, STAPLE OR TAPE, AND MAIL. NO POSTAGE NECESSARY.

NASA Form 1332 AUG 66

GPO 915-777

CUT ALONG THIS LINE

CUT ALONG THIS LINE

INVESTIGATION OF THE FIELD OF MICROWAVE RADIATION IN THE ATMOSPHERE

K.S. Shifrin, Yu. I. Rabinovich, G.G. Shchukin

ABSTRACT: The possibility of using microwave technology in satellite meteorology is examined. In this respect the advantages are discussed of radiometric systems in comparison with the infrared technology used for solving a number of meterological problems. The possibility is investigated of determining the temperature and type of underlying surface and of determining the overall water content of the atmosphere. The possibilities are examined of using microwave technology in meteorology. Of greatest interest is the use of this range for solving the so-called inverse problems, i.e., determination of the basic meteorological elements in the atmosphere from measurements obtained at the upper boundary of the atmosphere from artificial Earth satellites.

Introduction.

The use of artificial Earth satellites (AES) for meteorological investigations has changed the content and significantly increased the amount of information concerning the condition of the atmosphere and the Earth's surface which is available to investigators. High altitudes are necessary for a satellite to remain aloft for a prolonged period of time; and it is here that the physical properties of the surrounding atmosphere are insignificant from the viewpoint of the annual processes. Therefore, meteorological measurements in the ordinary sense of the word have no meaning for the meteorological AES. It is the characteristics of the electromagnetic field, i.e., its angular and spectral structure, that are measured on such a satellite as well as the polarization properties. The problem involves investigating what information concerning the lower layers of the atmosphere and the Earth's surface are included in these characteristics and finding methods for obtaining it. /5*

From this viewpoint, the visible and infrared parts of the spectrum have been studied that are "traditional" for atmospheric physics. However, great possibilities are found in the longer wave lengths, i.e., the millimeter and centimeter ones.

* Numbers in the margin indicate pagination in the foreign text.

Generally speaking, the Earth's atmosphere has three "windows" of transparency for electromagnetic radiation:

(1) The visible and near IR-window (Optical) ($0.3\ \mu m \leq \lambda \leq 1\ \mu m$);

(2) The IR-window ($8\ \mu m \leq \lambda \leq 12\ \mu m$);

(3) The radio window ($2.5\ mm \leq \lambda \leq 20\ m$).

Figure 1 shows a schematic representation of these "windows" in the spectrum.

The short-wave boundary of the radio window is determined by the absorption in H_2O and O_2 (rotational-vibrational bands), and the long-wave boundary is determined by the penetration of the ionosphere. The radio window possesses a notable characteristic, i.e., the radiation from $\lambda \geq 3$ cm passes almost freely through the cloud cover of the Earth. Since the clouds cover, on the average, 55% of the Earth's surface, this window gives us the unique possibility of seeing beneath the cloud and finding the processes which occur between the cloud and the Earth. In particular we find here the possibility of differentiating between rain clouds and rain-free clouds and even of measuring the intensity of precipitation from the clouds. Microwave radiation is also feasible to use for investigating certain other problems.

In principle, the use of microwave radiation for problems of /6
probing may be done in two ways: (a) the use of an active locator on board the AES; (b) the use of natural heat radiation from the atmosphere. The first means has been discussed in detail in the meteorological literature for some time now. Thus, in 1960, Kiegler and Krawitz [1] described a specially constructed radar designed for operation on board AES. The weight of the radar (without antenna) was 20 kg, the average power requirement was 36 W. Detailed data on the possibility of an active radar on board AES (methods of radar scanning, required resolving power, etc) are given in monograph [2] (Chapter 7). The basic difficulty with active location is the guarantee of a suitable supply source and its stabilization.

Now let us look at the second method, i.e., the use of thermal radio emission.

In the present article we look at the possibility of the microwave range for solving problems of probing the atmosphere. Let us evaluate its advantages and disadvantages in comparison with the visible and the IR-radiations and describe the method and preliminary results of aircraft measurements.

Measurement of thermal radiation from celestial bodies in the radio range is the basic purpose of radioastronomy. From this viewpoint the problem under discussion can be reduced to developing a method of radioastronomical investigations of the planet Earth from AES. Let us add that in observations from the Earth

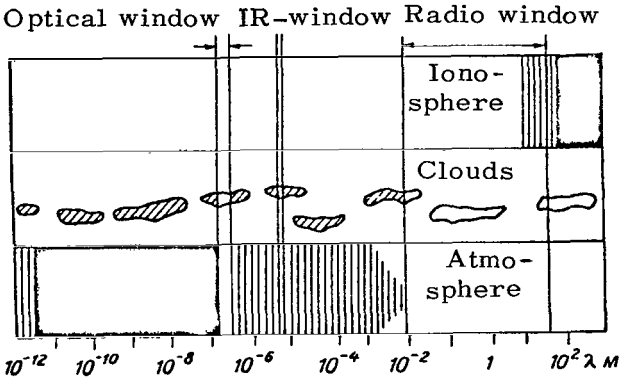

Fig. 1

the natural microwave radiation from the Earth's atmosphere, hydrometeors found in it, and the elements of the Earth's surface has for some time now been the subject of investigation for radioastronomers. This radiation seems to radioastronomers to be a noise that must be known in order to be able to properly exclude it from a signal being observed. For meterologists, however, it is this "noise" itself that is the subject of investigation.

1. Methodological Problems.

Energy Resolving Power and Time Constant.

At first glance the possibility of measuring thermal radiation from the atmosphere and the Earth in the microwave region may seem to be remarkable. In fact, in this range the spectral brightness of an absolute black body B is described by the Rayleigh-Jeans formula (long-wave approximate formulas of Planck) /7

$$B = \frac{2\nu^2}{c^2} kT = \frac{2kT}{\lambda 2} = 2.76 \cdot 10^{-23} \frac{T}{\lambda 2} \text{ W/ster}\cdot\text{cm}^2\cdot\text{Hz}.$$

Since the radiation from a black body is of Lambert type, the total energy of radiation (luminous emittance) F per 1 cm^2 will be

$$F = \pi B = 8.67 \cdot 10^{-23} \frac{T}{\lambda 2} \text{ W/cm}^2\cdot\text{Hz}.$$

From the formula it is clear that we are concerned here with very weak radiations. With transition, for example, from λ = 10 μm to λ = 10 cm, the values of B and F are decreased by 10^8 times.

There is one significant fact however that saves the situation. This involves the microwave radiometers possessing a significantly greater sensitivity than the black radiation receivers. For a radio receiver the minimally detectable power is determined by the Nyquist formula $P_r = kT\,\Delta f \approx 4\cdot 10^{-21}$ W (when T = 300° K, Δf = 1 Hz)[1], whereas for a black IR-receiver we have $P_{IR} = 4T^{5/2}$

[1] It is curious that this threshold is similar to the threshold of the human eye (10^{-21} W) and is better than the radiation receivers which we have available at the present time.

$(2\sigma kA\Delta f)^{1/2} \approx 5.5 \cdot 10^{-12}$ W (when T = 300° K, Δf = 1 Hz, the area of the IR-receiver A = 1 mm^2). Consequently,

$$\frac{P_r}{P_{IR}} \approx 10^{-9}.$$

Thus, the large difference in sensitivity of the microwave radiometer and the IR-receiver overlaps the decrease in energy of radiation such that measurements are found to be completely feasible.

Physically the large difference in sensitivity is due to the fact that in an ideal radio receiver the effective pass band width is equal to its band, whereas in a black receiver it overlaps the entire band of radiation from the black body. Thus the noise level of an IR-receiver is found to be considerably higher than in a microwave radiometer.

If a selective IR-receiver is used, the effective width of its band will be lowered and, respectively, so will the threshold. Thus, for example, for contemporary photoelectric receivers of radiation we may have a threshold on the order of 10^{-15} W or even 10^{-17} W for λ = 1 μm. As a result the signal-to-noise ratio in IR-receivers is found to be higher than in radiometers. To increase it in these latter we have recourse to the effect of signal pileup. With a high noise level we must make our observation for a prolonged period of time so that as a result of noise interference, the relative noise of the useful signal will increase. Thus, the inertia in radiometers (time constant) is found to be considerably greater than the inertia in IR-detectors.

The question as to the time constant for our problem is very important. In fact, each second is 8 km in the AES trajectory, and if, for example, as we find in highly sensitive astronomical radiometers, the time constant is on the order of 100 seconds, then the signal that is registered will be a result of integration of the field on the 800 km trajectory. It is only slightly probable that in this instance we could, for example, determine the shower source in an extent of 6 - 10 km. Fortunately, the actual situation is not so bad. The time constants of the radiometers, installed on aircraft, may be set up from several seconds to hundreds of seconds, it would seem because of a slight loss in the energy sensitivity. This sensitivity (measured in degrees) is found to be in this case on the order of 0.5 - 5° K as a function of wave length. /8

Angular Resolving Power and Scattering of Antennas.

The angular resolving power β of any optical system is determined by the Rayleigh criterion $\beta \approx 1.22 \frac{\lambda}{D}$. It is associated

with the diffraction pattern of the incipient image and corresponds to the angular distance of the first dark ring in the formula for a corona[2]. Transition from the infrared to the centimeter range means an increase in λ by 10^3 - 10^4 times and with a constant diameter of the objective (antenna) a corresponding increase in β.

Considerable difficulties arise here. For example, if we wish to have a radiotelescope for λ = 1 cm with the same resolving power as in an optical telescope with a diameter of 20 cm for λ = 0.5 μm, then the diameter of the radio telescope must be made equal to 5 km! In radioastronomy, decreases in β are achieved both due to an increase in the diameters of the antennas and by the use of special radio interferometric methods whose effect is similar to the effect of diffraction grids in optics. In fact with antennas having a diameter of 0.5 m, we may have $\beta \approx 2 - 6°$ for aircraft and satellite radiometers. For AES from an altitude of 500 km this gives a spot with a diameter of 20 - 60 km.

It seems to us that it is important to increase the angular resolving power for a number of meteorological applications of radiometry. Here we have the following possibilities: the use of inflated or hinged antennas and also the use of interferometry connected with the movement of the carrier.

One other troublesome fact is associated with the low resolving power of antennas in the microwave range. The side lobes of the antenna radiation pattern are found to be significantly unfolded from the axis of the major lobe, such that a significant flow of radiation arrives at the antenna outside the major lobe. In order to characterize this property of the antenna, we introduce the so-called scattering coefficient. If we place the antenna in an isotropic field of radiation, the scattering coefficient will be equal to the amount of power entering the system through the side lobes. For example, if we take no special measures to suppress the side lobes, the scattering coefficient of a single-mirror parabolic antenna will then be about 0.3 - 0.4. This means that 30 - 40% of the power of the isotropic field will enter the antenna from the lateral directions, and if "hot" bodies are located in the lateral directions, their parasitic effect may prevent measurements from being made generally.

In practice at the present time we can manufacture aircraft and satellite antennas with a scattering coefficient of 0.15 - 0.20. This all results in the necessity of taking "scattering" into account during absolute measurements of microwave radiation.

---

[2] For example, in [4] (p. 149) we have for the first dark ring $\rho\beta = 3.832$, $\beta = \frac{3.832}{\pi} \frac{\lambda}{D} = 1.22 \frac{\lambda}{D}$.

2. Characteristics of Propagation in the Atmosphere and Reflection from the Earth's Surface.

Propagation in Gases.

In the radio range, because of the comparatively long waves, /9
substantial significance is given to absorption associated with dipole transitions, electrical and magnetic. Of the atmospheric gases only in molecules of O_2 and H_2O are there pronounced dipole moments, magnetic in O_2 and electric in H_2O. All other molecules (N_2, CO_2, H_2, A_2, He, Ne) have neither electric nor magnetic moments, therefore in the range of centimeter and millimeter waves the absorption coefficient for them will be practically zero. We can neglect in this case the transitions that are associated with higher multipole orders such as, for example, electrical quadrupole orders, etc.

It is easy to see this if we look at the ratio of the intensity of quadrupole I_{qu} and dipole I_d transitions

$$\frac{I_{qu}}{I_d} \sim \left(\frac{a}{\lambda}\right)^2 \sim \frac{10^{-16}}{\lambda^2},$$

where a is the radius of the atom (approximately 10^{-8} cm) and λ is the wave length in centimeters.

In the radio range this value is completely insignificant. Moreover the higher multipole transitions are not substantial. In optics it seems this is not so. An oxygen molecule in fundamental state possesses a magnetic moment that is associated with the presence of spin in the molecule equal to $\hbar$.

The structure of the levels is found to be quite complex, and in particular, leads to a complete system of lines near $\lambda = 0.5$ cm. The distance between centers of the lines is on the order of 0.01 - 0.02 cm and at normal atmospheric pressure we usually observe a solid band that is slightly distorted by small maxima and minima.

Figure 2 shows a theoretical profile of the band for two values of the half-width of the lines, 0.02 cm^{-1} (broken curve) and 0.05 cm^{-1} (solid curve). The points indicate experimental data. On the ordinate axis, the absorption is given in db/km.[3]

---

[3] In radiophysics, for the attenuation factor α, two units are used: cm^{-1} or neper/cm and db/km. With transition from α in cm^{-1} to α in db/km we must multiply α by $10^6 \log e = 0.4343.10^6$. The reverse conversion from db/km to cm^{-1} is accomplished by multipli-

At the band maximum (when λ = 0.5 cm), $\alpha \approx$ 15 db/km = $3.5 \cdot 10^{-5}$ cm^{-1} and the intensity is decreased by 10 times even on a path of 667 m. For λ = 1 cm, $\alpha \approx 0.014$ db/km and the same attenuation in intensity will occur even on a path of 700 km.

Besides the band λ = 0.5 cm, in O_2 a still stronger single line λ = 0.25 cm is observed as well as two windows of transparency λ = 0.315 cm and λ = 0.93 cm.

Along with resonance absorption, in O_2 molecules we can observe still another very weak, non-resonance absorption corresponding to Debye absorption for dipole molecules. In the range $\lambda \approx$ 2 - 25 cm this absorption will be altogether about 0.006 db/km, or 10^{-8} cm^{-1}, and further on it will be decreased sharply. /10

A molecule of water possesses in fundamental state a significant electric moment. On the strength of specific selection rules for molecules of asymmetric gyroscopic type, such as the H_2O molecule is, the non-resonance absorption will be absent in it. As far as the resonance transitions are concerned, they basically fall into the IR-region. Only the transition, which corresponds to a wave length of λ = 1.348 cm, enters the centimeter range; further on there follow the lines λ = 0.164 cm and λ = 0.09 cm in the millimeter range, etc.

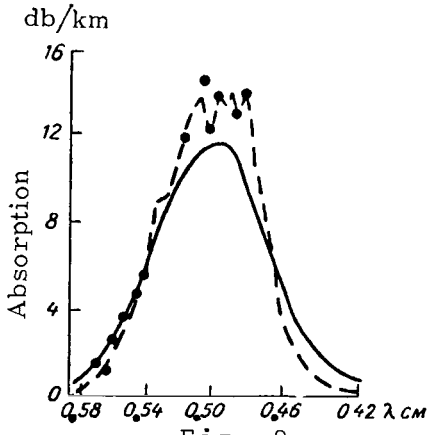

Fig. 2

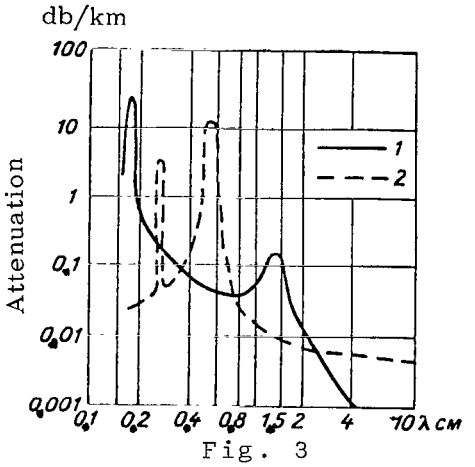

Fig. 3

footnote #3 cont.

cation by $\frac{10^{-6}}{0.4343} = 0.2303 \cdot 10^{-5}$. Let us add that the change in intensity of radiation on the trajectory x may be written in two identical expressions.

$$I = I_0 e^{-\alpha(cm^{-1}) \times (cm)}$$

$$I = I_0 \cdot 10^{-0.1\alpha(db/km) \times (km)}.$$

From Figure 3 we have compiled the absolute values of α for H_2O (1), corresponding to a vapor content of 7.5 g/m^3, and for O_2 (2) at normal pressure.

Hydrometeors.

The attenuation of radio emission in hydrometeors is determined by the value of the parameter $\rho = \frac{2\pi a}{\lambda}$. For aerosols and clouds $\rho << 1$, and for the scattering coefficient k_r and the attenuation factor k, per particle, we have (see [4], p. 86):

$$k_r = 24\pi^3 \frac{v^2}{\lambda^4} \left| \frac{m^2 - 1}{m^2 + 2} \right|^2,$$

$$k = \frac{36\pi nx}{|m^2 + 2|^2} \frac{v}{\lambda}.$$

Since $k_r << k$, the scattering here can then be virtually ignored in comparison with the absorption. For water in the centimeter region (from λ = 0.5 cm to λ = 10 cm) the value is

$$\frac{nx}{|m^2 + 2|^2} \approx \frac{1}{\lambda}.$$

/11

Thus we find that

$$k \approx \frac{v}{\lambda 2}.$$

By substituting all numerical constants the attenuation factor will be

$$\alpha = \frac{0.1R}{\lambda 2} \text{ km}^{-1}.$$

Here R is given in g/m^3, and λ in centimeters. For λ = 1 cm and R = 3 g/m^3, we find consequently that α = 0.3 km^{-1}.

Thus, clouds absorb centimeter radiation rather weakly.

For the precipitations, the parameter $\rho \approx 1$. In Table 1 we give values of k_r, k and $\bar{\lambda}$, the probabilities of survival of photons for the smallest and largest particles of the precipitation.

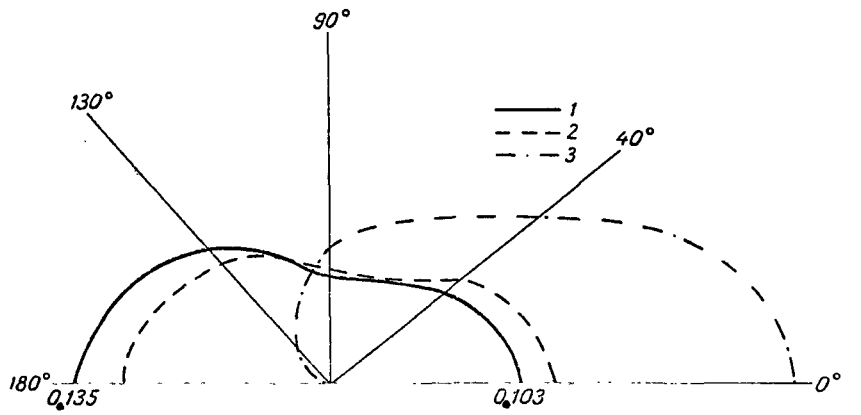

Fig. 4.

D см	$\lambda = 3{,}2$ см			$\lambda = 10$ см		
	k_{γ}, см^2	k см^2	$\bar{\lambda}$	k_{γ} см^2	k см^2	$\bar{\lambda}$
0,05	$4 \cdot 10^{-8}$	$9 \cdot 10^{-6}$	$4 \cdot 10^{-3}$	$3 \cdot 10^{-10}$	$7 \cdot 10^{-7}$	$4 \cdot 10^{-4}$
0,5	0,06	0,2	0,3	$3 \cdot 10^{-4}$	$2 \cdot 10^{-3}$	0,15

Table 1.

For particles with D = 0.5 cm the probability of survival of photons during a single act of scattering is significant. This means that a significant scattering will occur and with a large optical thickness of the layer, the frequency of the scattering process must be taken into account. To compute the brightness of the layer in taking scattering into account, data must be available on the characteristic curve of the scattering. These computations have been made in [5]. Unlike the spherically symmetrical radiation from the individual drop, the characteristic curve of the scattering of the drops is nonsymmetrical. For small particles it is significantly extended backwards; with an increase in ρ, the Mie effect comes into play and it begins to be extended forward. Figure 4 shows, an illustration of this effect, the characteristic curves for ρ, equal to 0.5 (1), 1.0 (2), 1.7 (3) and λ = 1.35 cm.

Reflection from the Earth's Surface.

There does exist a small amount of data on the values of reflection in the centimeter region, but there is very little on the angular structure of the beam reflected from real, rough surfaces. For the characteristics of the degree of roughness of a body we use the Rayleigh criteria /12

$$h \cos \varphi \ll \frac{\lambda}{16}.$$

Here h is the height of the roughness and θ is the zenith angle of incidence of the rays. The "smoothness" of a body depends on wave length. A body that is smooth for certain wave lengths will be rough for shorter waves.

Measurements give approximately the following values of the emission coefficients in the normal direction for λ = 3.2 cm (Table 2).

Table 2.

Underlying Surface	Emission Coefficient
Sea Water	40
Forest	98-99
Swamp	85
Field with thawed patches of Earth	75
Sea Foam, Breakers	99-100
Earth	50

Most significant here is this large deviation of the degree of blackness of the water from unity. In the centimeter range, water must be assumed as a surface that is almost a mirror, unlike in the IR-range, where it is similar to a black body. This means that the properties of water, in particular change in its salinity, exert influence on the emission coefficient.

3. Determination of Temperature and Type of Underlying Surface.

The significant variations in the degree of blackness with change in the character of the underlying surface represent a substantial feature of the microwave range. Whereas for the majority of underlying surfaces in the IR-range the coefficient of blackness in the normal direction is near to unity and varies comparatively little, in the microwave range it varies significantly as a function of the type of underlying surface. This fact, which makes determination of the temperature more difficult from the radiation makes the problem of determining the boundary between surface of different types easier. For a known type of surface the radiation is uniquely determined by its temperature.

Let us look at the possibilities of determining the temperature of the surface.

Precision of Converting Radiation into Temperature.

For a nonblack body the relationship between radiation B and temperature T can be described by the formula

$$B = \varepsilon(\lambda) E(\lambda, T),$$

where E is the Planck function, $\varepsilon(\lambda)$ is the degree of blackness of the body.

With a given error in determining the radiation B, the error in T will vary for different segments of the Planck curve. From the relationship /13

$$E(\lambda, T) = \frac{B}{\varepsilon(\lambda)} = \tau$$

we find

$$T = \Phi(\tau),$$

where Φ (T) is a function that is inverse to E(T).

Let $\Delta_1 = \left|\frac{dB}{B}\right|$ and $\Delta_2 = \left|\frac{d\varepsilon}{\varepsilon}\right|$ be the absolute values of the relative errors in the quantities B and ε. Obviously

$$dT = \frac{d\Phi}{d\tau}\frac{B}{\varepsilon}\left(\frac{dB}{B} - \frac{d\varepsilon}{\varepsilon}\right),$$

$$\left|\frac{dT}{T}\right| = \left|\frac{\tau d\Phi}{\Phi d\tau}\right|(\Delta_1 + \Delta_2),$$

$$\left|\frac{dT}{T}\right| = |q|(\Delta_1 + \Delta_2).$$

Let us denote

$$q(x) = \frac{\tau d\Phi}{\Phi d\tau} = \frac{\tau dT}{T d\tau} = \frac{E}{T}\frac{dT}{dE} = \frac{1}{\frac{T}{E}\frac{dE}{dT}} = \frac{1}{M(x)}.$$

The quantity M(x) was tabulated in [6] as a function of $x = \frac{\lambda}{\lambda_m}$. The values q(x) are given on Table 3.

Table 3.

x	0	0,1	0,2	0,5	1,0	2	3	∞
$q(x)$	0	0,0201	0,0403	0,101	0,201	0,370	0,488	1,00

In our case λ_m = 10 μm. Consequently, with measurements in the IR-range (λ = 10μm, x = 1) the error in determining the temperature will be 5 times less than with measurements having the same accuracy in the centimeter range (x = ∞), i.e., with transition to the microwave radiation we have a slight loss here.

Influence of the Atmosphere.

The influence of the atmosphere, however, indicates otherwise. If we ignore the effect of reflection of brightness of the sky from the Earth, the measured biightness is determined by the formula

$$T=(1-R^2)T_0e^{-\int_0^\infty \tau\sec\theta} + \int_0^\infty T(z')\alpha(z')\sec\theta dz' e^{-\int_{z'}^\infty \tau\sec\theta}.$$

The First term describes the radiation from the Earth, attenuated by the atmosphere and arrived at the observer; the second term describes the radiation from the atmosphere, incident on the radiometer; the quantity R^2 is the energy coefficient of reflection, the quantities represent the optical thickness of the entire atmosphere and the layer from the level z'.

To evaluate the influence of the atmosphere on the microwave radiation let us look at data from calculations of the radiation at the upper boundary of the atmosphere. /14

Figure 5 gives the radiobrightness termperature of radiation from the system Earth-atmosphere as a function of the overal mositure content for two wave lengths, 3.2 cm (1) and 8.5 cm (2). The underlying surface here is the sea water with a temperature of 298° K. From the graphs it is obvious that the influence of the atmosphere on the radiobrightness temperature is insignificant over the entire range of possible change in the overall water content.

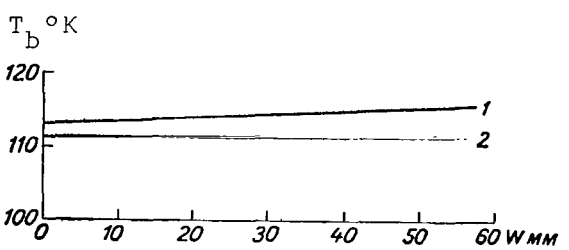

Fig. 5.

Results of the Measurements

Several results of measuring the temperature of the water surface from an airplane are given in the present collection [7,8]. In these articles, evaluations are made of the absolute measurements, which indicate that in the microwave region only those measurements of the temperature contrasts with respect to the surface having a known temperature are of interest. From the

viewpoint of determining the type of underlying surface we can look at the possible temperature heteorogeneities for the different types of surfaces, and also the temperature contrasts of the systems, ice-water and water-Earth.

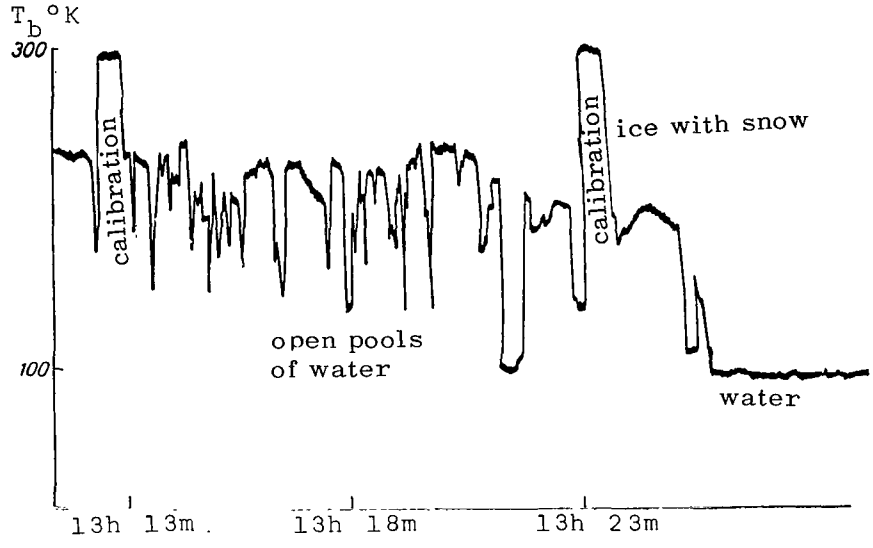

Fig. 6.

Table 4 gives the temperature heterogeneities for the various types of underlying surfaces, obtained in the Spring of 1966 and the Winter of 1967 during aircraft measurements with a radiometric /15 apparatus, operating at wave lenghts of 0.8, 1.35, 1.6 and 3.2 cm. These data for λ = 0.8 cm permit us, for example, to make the important conclusion that the temperature heterogeneities for many types of natural surfaces do not exceed 10 - 15 °, and often quite less. Thus, it is not only above the water surface that measurements can be conducted for determining the meteorological characteristics of clouds and precipitation.

As an illustration of the possible use of radiometric apparatus for determining the boundaries of the ice cover and the shore line, Figure 6 shows samples of recordings of the contrasts of radiobrightness temperature obtained from measurements from an airplane at a wave length of 3.2 cm in the region of the Barents Sea at an altitude of 8000 m. With the observation of ice with pools of open water, the radiobrightness temperature fluctuates in the range from 110 to 250° K, the lower level corresponding to the radiobrightness temperature of pure water and the upper corresponding to the temperature of ice and ice with snow. Such a large temperature contrast is found at the boundary of water-dry land, an example of the re-

cording of which, obtained in measurements from an airplane on October 8, 1966 at λ = 3.2 cm in the region of the Caspian Sea is shown on Figure 7. The observations here were carried out through cumulus clouds (8 - 10 points on the Ac scale).

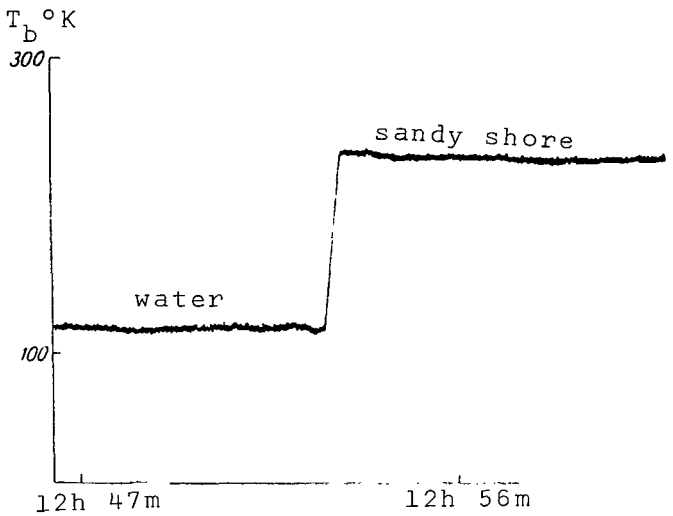

Fig. 7.

Table 4.

Character of the Underlying Surface	$\lambda = 0{,}8$ см			$\lambda = 1{,}35$ см		
	T_a min	T_a av	T_a max	T_a min	T_a av	T_a max
Desert	257	257,5	258	268	269	270
Steppe, ploughed fields	262	265	268	267	272	277
Steppe, covered with snow	250,5	254,5	261,0	249,5	255,5	260,0
Ice, covered with snow	245,5	253,0	263,0	233,0	243,0	253,0
Ice	244,5	245,5	246,5	240,0	246,0	254,0
Caspian Sea	170,0	170,5	171,0	166,0	167,0	168,0

Character of the Underlying Surface	λ = 1.60 см			λ = 3.2 см		
	T_a min	T_a av	T_a max	T_a min	T_a av	T_a max
Desert	251	256	261	245	255	266
Steppe, ploughed fields	255	258	262	257	262	267
Steppe, covered with snow	246.0	250.5	257.0	240.5	245.5	252.0
Ice, covered with snow	246.5	251.0	257.5	230.5	237.0	239.5
Ice	239.0	239.5	240.0	225.0	228.0	231.0
Caspian Sea	136.0	137.5	139.0	110.5	111.5	113.0

4. Determining the Overall Water Content, Zones of Cloud Cover and Precipitation.

As already noted, to determine the overall water content of the atmosphere we can use the results of measurements of microwave radiation in the bank of absorption of water vaper at λ ≈ 1.35 cm.

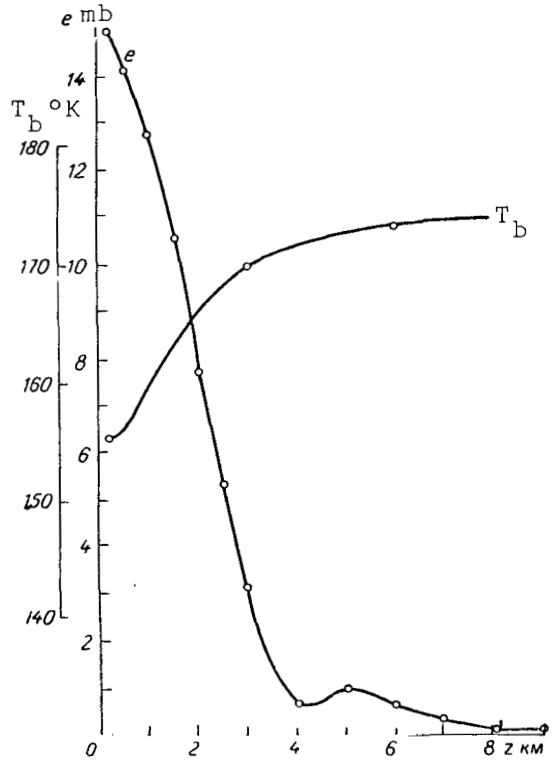

Fig. 8.

Figure 8 shows the path of the radiobrightness temperature with altitude, plotted from data of measurements in the channel λ=1.35 cm using vertical sounding of the atmosphere on October 3, 1966 in the region of the Caspian Sea.

Detailed computations and experimental data are given in the article [9] published in this collection on determining the overall water content of the atmosphere. Computations show that in the /17
measurements over a uniform water surface the dependence of the radiobrightness temperature on the overall water content is a linear one in the range from 0.5 to 3.0 cm of precipitated water.

One favorable fact also is the comparatively small influence on the radiobrightness temperature, measured at the boundary of the layer, of the profile of moisture and the temperature inside this layer. The small divergences between theory and experiment and the strong dependence of the radiobrightness temperature on moisture content in the atmosphere give a basis for using this method in satellite meteorology.

In determining the cloudcover and especially the zones of precipitation, along with absorption we are concerned with scattering; during intense precipitation it is essential to take into account multiple scattering. Detailed computations are given in [10] on the transfer of microwave radiation in clouds in [11] of from aircraft measurements of cloudcover and zones of precipitation over the water surface. The experimental data in this paper are compared with the computational results.

The results of the aircraft investigations show that the radiobrightness contrasts of precipitation during measurements over the water surface, even for precipitation with an intensity of 2 - 3 mm/hr, reach 90 - 110° K. If we allow for the fact that the greatest temperature heterogeneity of radiobrightness temperature of the underlying surface does not exceed 20 - 40°, then obviously we can also detect sufficiently intense precipitation over a variegated underlying surface.

5. Prospects for Using Microwave Technology in Meteorology.

Of greatest interest for meteorology is the use of the microwave range in solving the so-called inverse problems, i.e., determining the basic meteorological elements in the atmosphere from measurements, obtained at the upper boundary of the atmosphere from artificial Earth satellites. However, these problems can be solved just as well by using radio emission. From a certain viewpoint this range is most promising for such investigations.

First of all, absorption by water vapor and oxygen in the microwave region, as a rule, appears in the form of individual lines

or bands of comparatively simple structure. Therefore, computation of the functions of absorption, which in the IR-region are extremely complex, is rather simple here.

Secondly, the resolving power of the thermal radar apparatus by spectrum significantly exceeds the resolving power of the existing IR-temperature. For example, the line width of absorption of water vapor $\lambda = 1.35$ cm is about 6000 MHz, whereas the width of the transmission band of the radiometer may be 20 - 40 MHz. Certain difficulties are presented by the creation of radiometric apparatus with fine tuning by wave length, but they apparently can be overcome.

And finally one important advantage of microwave radiation is the possibility of sounding through clouds. This is especially significant in the regions of solid cloud cover, which are inaccessible both to the IR-apparatus and to the apparatus of the visible range.

Above we have looked at several possibilities of meteorodogical investigations using a microwave instrument. Along with this, several other prospects should be noted. This is the determination of:

(1) The profiles of temperature and pressure of the air according to the absorption in oxygen; /18
(2) The profiles of humidity from absorption in water vapor;
(3) The roughness of the sea from the brightness and polarization characteristics of the microwave radiation;
(4) The upper boundary of the clouds and the pressure at the level of the clouds from the absorption in oxygen.

In conclusion, let us add that the data from recent years have shown that clouds emit intensive microwave radiation, associated with the collision of charged drops and ice crystals. This nonthermal radiation, consequently, can be used for evaluating the phase states of the cloud and the processes of its restructuring.

REFERENCES

1. Kiegler, I.E. and L. Krawitz: Weather Radar Observations Satellites. J. Geophys. Res., Vol. 65, No. 9, 1960.
2. Stepanenko, V.D.: Radiolokatsiya v meteorologii. (Radar in Meteorology), Gidrometeoizdat, 1966.
3. Smith, R., F. Jones and R. Chesmer: Detection of Infrared Radiation. Foreign Literature Press, Moscow, 1959.
4. Shifrin, K.S.: Rasseyaniye sveta v mutnoy srede. (Scattering of Light in a Cloud Atmosphere). Gostekhizdat, 1951.
5. Shifrin, K.S. and M.M. Chernyak: Indikatrisy rassevaniva santimetrovoy radiatsii kaplyami vody. (Characteristic Curves of Scattering of Centimeter Radiation by Drops of Water)., Trudy Main Geophysical Observatory, No. 203, 1967.
6. Shifrin, K.S.: Perenos teplovoy radiatsii v oblakakh. (Transfer of Heat Radiation in Clouds), Trudy Main Geophysical Observatory, No. 46 (108), 1955.
7. Rabinovich, Yu. I., G.G. Shchukin and V.V. Melent'yev: Opredeleniye temperatury vodnoy poverkhnosti po radioizlucheniyu v satimetrovom diapazone. (Determination of the Temperature of the Water Surface from Radio Emission in the Centimeter Range), (See this Collection).
8. Rabinovich. Yu. I., G.G. Shchukin and V.G. Volkov: O vozmoshnykh pogreshnostyakh absolyutnykh exmereniy radioizlucheniya. (Possible Errors in Absolute Measurements of Radio Emission). (See this Collection).
9. Rabinovich, Yu.I.and G.G. Shchukin: Opredeleniye soderzhaniya vodyanogo para v atmosfere po ezmereniyu mikrovolnovogo izlucheniya. (Determination of the Water Vapor Content in the Atmosphere from Measuring Microwave Radiotion). (See this Collection).
10. Volchok, B.A. and M.M. Chernyak: Perenos mikrovolnovogo izlucheniya v oblakakh i osadkakh. (Transfer of Microwave Radiation in Clouds and Precipitation). (See this Collection).
11. Rabinovich, Yu.I., G.G. Shchukin and M.M. Chernyak: Radioizlucheniye oblakov i osadkov. (Radio Emission from Clouds and Precipitation). (See this Collection).

EXPERIMENTAL INVESTIGATIONS OF THE CHARACTERISTICS OF THERMAL RADIO EMISSION FROM THE SURFACE OF THE SEA

A.M. Shutko

ABSTRACT: Experimental and computational data are given on the mean values of the emission coefficients from the surface of the sea for vertical polarization in the centimeter wave length band with various intensities of swell. The computational values of the emission coefficient have been obtained for a smooth surface as well as for two-dimensional and three-dimensional statistical models of a rough sea surface. Measurements of the characteristics of radio emission from the surface of the sea were made on a two-channel radiometer at wave lengths of 0.8 and 3.37 cm. The range of the angles of sighting was from 50 - 60 to 90°.

Measurements of the characteristics of the radio emission from /19
the surface of the sea were made using a radiometric apparatus, installed on shore. The swell of the sea varied from 0 to 3 - 5 points on the scale. The surface of the sea encompassed a range of angles of sighting from 50 - 60 to 90° (in reading θ_0 from the vertical).

Figures 1 and 2 give computational and experimental data on the mean values of the emission coefficients $\overline{e}_v$ for vertical polarization at different intensities of swell in wave length bands of 3.37 and 0.8 cm, respectively. The computational values e_v were obtained for a smooth surface and for statistical models (two-dimensional and three-dimensional) with a distribution of the angles of slope ϑ near the normal [1], and with the mean square value $\sigma_\vartheta = 10°$. For the three-dimensional model of the surface the exponent of three-dimensionality ν is assumed to equal unity (ν characterizes the ratio of the mean square values σ_ϑ in the direction perpendicular to the direction of propagation of the swell, and in the direction of swell, respectively; with such a definition, $\nu \leq 1$). Computations of the emittance were carried out in approximation of geometric optics using the method described in [2] and taking into account the self-shading of the surface elements. In this approximation, the emission coefficient $e_{v,h}$ of the basic segment of the surface is determined from the reflective properties of the surface using the formula

$$e_{v,g}(\theta, \tau, \theta_0, \psi) = 1 - r_{v,g}(\theta, \tau, \theta_0, \psi) + [r_v(\theta, \tau, \theta_0, \psi) - r_g(\theta, \tau, \theta_0, \psi)] \sin^2\alpha. \quad (1)$$

Here the subscripts "v" and "h" denote the vertical and horizontal polarization, respectively; $r_{v,h}$ represents the Fresnel reflection [3] according to power; θ is the angle of slope of the surface element toward the horizon, φ is the azimuth of the normal to the surface element, θ_0, ψ are the angular coordinates of the direction of observation, α is the angle of depolarization. The signs "+" and "-" are taken in determining e_v and e_h, respectively.

In the range of waves λ = 0.8 cm, we have taken into account the influence of the illumination, created by the atmosphere, for the plane-stratified model of a cloud-free atmosphere, characterized by the dependence of the brightness temperature T_b on the zenith angle z in the form

$$T_b(\gamma, z) = (T_0 - \Delta T)(1 - e^{-\gamma \sec z}) \qquad (2)$$

/20

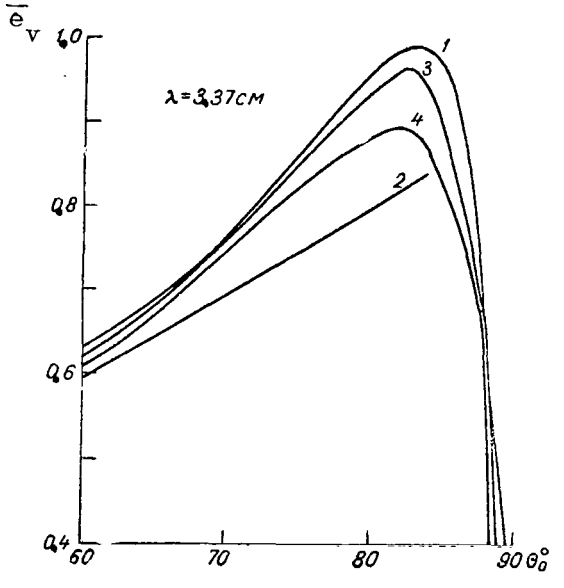

Fig. 1. Angular Dependence of the Mean Values of Emittance. The Vertical Polarization λ = 3.37 cm. 1,2: Computational Values; 3,4: Experimental Data; Swell, 0 - 3 Points on the Scale.

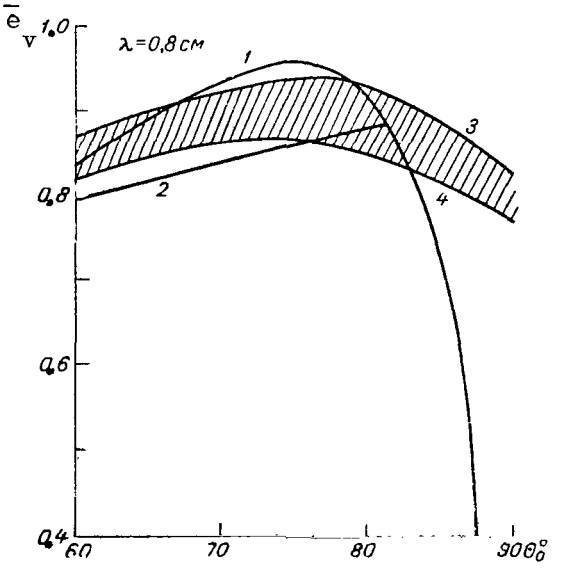

Fig. 2. Angular Dependence of the Mean Values of Emittance. The Vertical Polarization λ = 0.8 cm. 1,2: Computational Values; 3,4: Experimental Data; Swells 0 - 4 Points on the Scale.

Here T_0 is the thermodynamic temperature of the atmosphere at the surface of the Earth (sea) in degrees Kelvin, ΔT is the correction to the nonisothermicity of the atmosphere, γ is the value of absorption at the zenith, in nepers. /21

As the results of computation and the experimental data have shown, the influence of illumination on the quantity $\bar{e}_v$ for vertical polarization in the range of angles $50° < \theta_0 < 90°$ is insignificant. Thus, according to the computational data, change in γ from 0 to 0.2 nepers leads to an increase in $\bar{e}_v$ by no more than 3 - 5% in this range of angles.

As follows from the data cited, in the range of waves λ = 3.37 cm, we observe a dependence of the size of the mean value of the emission coefficient $\bar{e}_v$ for the vertical polarization on the force of the swell, especially in the region of the Brewster angle θ_0 = 80°, this being in agreement with the model representations. Increasing the swell will lead to a decrease in the emittance. The dependence of the quantity $\bar{e}_v$ in the range of waves λ = 0.8 cm is manifested more weakly and always has a unique character. The region between curves 3 and 4 on Figure 2 represents the experimental values of $\bar{e}_v$ with swell from 0 to 3 points on the scale.

The observed divergence between experimental and theoretical data, along with the errors in calibrating the apparatus and the computational method used, may be explained apparently by the change from one measurement to another of the parameters of swell and the influence on the quantity $\bar{e}_v$ of atmospheric illumination and the high-frequency components of the swell (especially in the range of millimeter radiowaves). According to [4], for example, on the surface of the sea, high-frequency gravitational (or capillary) waves exist practically independent of the force of the swell with a steepness of the slope on the order of 15 - 30°. The accuracy of the experimental data is about 10%.

The authors wishes to express his appreciation to A.Ye. Basharinov for guiding the research and for his valuable comments, as well as to M.S. Krylovaya for participating in processing the experimental data.

REFERENCES

1. Vetrovyye volny. (Wind Waves). Edited by Yu.M. Krylov. Foreign Literature Press, 1962.
2. Brekhovskikh, L.M.: Diffraktsiya voln na nerovnoy poverkhnosti. (Wave Diffraction on a Rough Surface). Zh. Eksp. i Teor. Fiz., Vol. 23, No. 3 (9), 1952.
3. Al'pert, Ya.L., V.L. Ginzburg and Ye.L. Feynberg: Rasprostraneniye radiovoln. (Propagation of Radiowaves), Gostekhizdat, 1953.
4. Shuleykin, V.V.: Fizika morya. (Physics of the Sea), AN SSSR, 1953.

THERMAL RADIATION AND REFLECTION FROM A ROUGH SEA SURFACE IN THE MICROWAVE RANGE

K.S. Shifrin and S.N. Ionina

ABSTRACT: On the basis of the distribution function of the area of the sea surface found experimentally by Cox and Munk, the following were obtained in this paper: the brightness factor for a wind velocity of 10 m/sec, zenith angles 0, 40, 70 and 80° and wave lengths 0.8, 1.35, 1.6, 3 and 8.5 cm; a simple analytical formula which relates the emission coefficient with the wind velocity and the emission coefficients for the wind velocities 0, 10 and 30 m/sec., the zenith angles 0, 40, 70 and 80° and the wave lengths 0.8, 1, 1.35, 1.6, 3, 8.5 and 10 cm.

Introduction

In studying the transfer of microwave radiation in the atmos- /22
phere we must know the character of the emission and the reflection of this radiation from real surfaces.

The surface of the sea is the largest surface on the Earth. It is uniform in structure and its form depends on a small number of parameters (mainly on the velocity and direction of the wind). These facts make it the most important and suitable factor for specific computations.

A number of authors have investigated the reflection of electromagnetic waves from rough surfaces. Let us look briefly at several of the theoretical papers on this subject.

L.M. Brekhovskikh [1] developed a method for solving problems concerning the diffraction of waves on a surface with large recurring irregularities. Included in the final form for the potential are expressions which depend on the form of the surface and the coefficient of reflection. In specific examples, we looked at the smiplest case of a uniform surface with a xonstant coefficient of reflection. We studied a sinusoidal surface and a surface representing a broken line in cross section.

The results of Brekhovskikh were generalized by Yu.P. Lysanov [2] for the case when the reflecting surface is characterized by a finite conductivity and by a complex dielectric constant. The reflection coefficient will then be a function of the angle of incidence. The surface equation was given by the periodic function. We studied a sinusoidal surface and a surface having a trochoidal

profile.

M.A. Isakovich [3] studied the scattering of waves from a statistically uneven surface with irregularities that are large in comparison with the wave length. The problem was solved in Kirchhoff approximation. The reflection coefficient here was also taken equal to unity.

F.G. Bass [4] investigated the scattering of waves on a statistically uneven surface with irregularities whose characteristic dimensions are substantially less than the wave lenght. The problem was solved using perturbation theory. The field on the surface was expanded into a series based on the amount of the small deviation from a smooth surface; and to determine the field in the entire re-/23
gion over the surface, a wave equation was used in integral form.

I.M. Fuks [5] solved the problem concerning reflection from a rough sea surface for microwave radiation. The surface of the sea was represented in the form of a small ripple on a large wave. The method of perturbation theory here is combined with Kirchhoff's method. Unfortunately, the direct use of the results both of those mentioned and of other investigations ([11]) for computing the characteristic curves of reflection from the sea is impossible. Here there are a number of reasons for this: the far reaching idealization of the shape of the surface, the limitations of the theory by the case of absolute reflection or back reflection (the problem of active location) and the complexity and awkwardness of the formulas.

The computations which were made by us below are based on a physically simple model. It seems to us that they improve the computations based on the Fresnel formulas for a smooth sea. By evaluating of the region of applicability and their accuracy we hope in the future to evaluate the range of applicability and their accuracy by comparison with more precise schemes or with experiment.

1. Model of the Sea and the Computational Method.

The purpose of this research was to compute the reflection of centimeter waves from the surface of the sea. We shall make this computation in approximation of geometric optics. As the sea surface lets us assume a rough surface consisting of a set of smooth areas, the distribution of the normals to which is described by the formula, used by Cox and Munk [7]. They studied the brightness distribution of solar glitter on the surrace of the sea. The average brightness of the sea surface in the vicinities of a given point is due to the frequency of appearance of the area required for reflection of light to the observer, and the desired function of distribution of slopes was found from this frequency. This model was used earlier by Yu. Mullamaa [6] who was concerned with the reflection of light from statistically uneven surfaces.

The conditions of applicability of our model are:

1. Diffraction at the edges of the area is ignored. This can be done if the length of the irregularities on the sea surface is much larger than the wave length of the emission. With a wind speed of 10 m/sec. (this is the mean value for the Pacific Ocean) the height of the wind waves is on the order of 2 m [8]. We know from observations that the ratio of the height of sea waves H to their length L usually lies in the range $\frac{1}{20} \leq \frac{H}{L} \leq \frac{1}{7}$. This means that L lies in the range of 14 - 40 m. Thus $L>>\lambda$ (λ is the length of the electromagnetic wave). We can ignore the influence of the ripple since Fuks [5] showed that at angles of sighting near the vertical, the intensity of the reflected signal in first approximation is determined by large-scale irregularities.

With measurements from aircraft and from artificial Earth satellites, the vertical directions are the most significant ones.

Moreover we know that approximation to geometric optics occurs more rapidly as the reflection coefficient is larger. This is immediately evident from [9] (Tables 16, 22 and 23) where the scattering of electromagnetic waves on the globe is studied. The ratio of approximate values of intensity to the precise ones for an angle of scattering of 90° for m=1.33 will be 0.14, 0.40 and 0.74, respectivly for ρ, equal to 10, 30 and 60 $\left(\rho = \frac{2\pi a}{\lambda}\right)$, whereas for $m = \infty$ even with $\rho = 10$ we have 0.95.

2. The Cox-Munk distribution function must be suitable for all/24 seas; it has been obtained for the region of Hawaiian Islands. The form of this function may be affected by salinity, temperature and other factors which we are also ignoring.

3. The effect of foam can also be ignored.

2. Goemetric Relationships and Basic Computational Formulas

Let us look at the basic geometric relationships of our problem (Fig. 1).

Let us choose a system of rectangular coordinates with the center at point o, from which the reflection is studied. The plane xoy is horizontally inclined, the y axis is opposite the direction of the wind, the z axis is directed upward. θ_1 and ϕ_1 are the polar angle and the azimuth of the direction of observation, θ' and ϕ' are the polar angle and the azimuth of the incident beam θ_n and ϕ_n are the polar angle and the azimuth of the normal to the selected area on the surface of the sea, χ is the true angle of incidence.

The distribution function has a form that differs from the ordinary normal distribution with coefficients that depend on the wind velocity,

$$P(z_{x'}, z_{y'}) = (2\pi\sigma^2)^{-1} \exp\left\{-\frac{1}{2}(\xi^2+\eta^2)\right\}\left[1-\frac{1}{2}c_{12}(\xi^2-1)\eta - \left|\frac{1}{6}c_{03}(\eta^3-3\eta)+\frac{1}{24}c_{40}(\xi^4-\right.\right.$$

$$6\xi^2+3)+\ldots(\xi^2-1)(\eta^2-1)+$$

$$\frac{1}{24}c_{01}(\eta^4-6\eta^2+3)+\ldots \qquad (1)$$

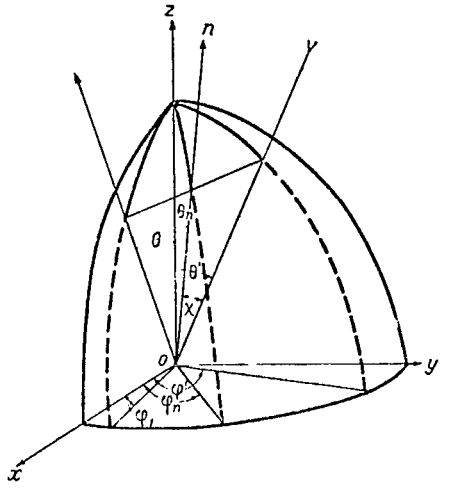

Fig. 1. Path of the Beams during Reflection (see [6] for the Relationship Between angles).

where $\xi = \frac{z_{x'}}{\sigma_x}$, $\eta = \frac{z_{y'}}{\sigma_y}$,

$$z_{x'} = \frac{\partial z}{\partial x} = \cos\varphi_n \operatorname{tg}\theta_n,$$

$$z_{y'} = \frac{\partial z}{\partial y} = \sin\varphi_n \operatorname{tg}\theta_n, \qquad (2)$$

$$\sigma_x^2 = 0{,}003 + 1{,}92\cdot 10^{-3}v,$$

$$\sigma_y^2 = 0{,}000 + 3{,}16\cdot 10^{-3}v \qquad (3)$$

(σ_x and σ_y are the mean square slopes of the area of the surface),

$$c_{21} = 0{,}01 - 0{,}0086v,$$

$$c_{03} = 0{,}04 - 0{,}033v, \qquad (4)$$

$$c_{40} = 0{,}40,$$

$$c_{22} = 0{,}12,\quad c_{04} = 0{,}23,$$

v is the wind velocity in m/sec.

Since, during observations from aircraft or from artificial Earth satellites, we do not always know the direction of the wind over the sea, we shall assume all wind directions to be equally probable and we can average $P(z_{x'}, z_{y'})$ for the direction of the wind. As a result of the averaging, the odd powers of η disappear. /25

We find

$$P(z_{x'}, z_{y'}) = (2\pi\sigma^2)^{-1}\exp\left\{-\frac{1}{2}(\xi^2+\eta^2)\right\}\left[1+\frac{1}{24}c_1(\xi^4-6\xi^2+3)+\right.$$

$$\left.+\frac{1}{4}c_2(\xi^2-1)(\eta^2-1)+\frac{1}{24}c_1(\eta^4-6\eta^2+3)+\ldots\right], \qquad (5)$$

where $\xi = \frac{z_{x'}}{\sigma}$, $\eta = \frac{z_{y'}}{\sigma}$, $\sigma^2 = \frac{\sigma_x^2+\sigma_y^2}{2}$, $\sigma^2 = 0{,}0015 + 2{,}54\cdot 10^{-3}\ v$,

$c_1 = \frac{c_{40}+c_{04}}{2}$, $c_1 = 0{,}315$, $c_2 = 0{,}12$, $c_2 = c_{22}$.

The basic formula for the intensity of reflected radiation is

$$S = \sec\theta_1 \int P(z_{x'}, z_{y'})\cos\chi\sec^4\theta_n R(\chi) S' \sin\theta_n\, d\theta_n\, d\varphi_n. \qquad (6)$$

The energy coefficients of reflection $R(\chi)$ were determined from the Fresnel formula. They depend on the true angle of incidence χ and the refractive index and the absorption coefficient n and κ. S' is the intensity of the incident current. Later on in the computations we shall assume it to be equal to unity. The integral is selected for θ_n and ϕ_n, respectively, in the range from 0 to $\frac{\pi}{2}$ and from 0 to 2π, but in such a manner that the true angle of incidence χ does not exceed $\frac{\pi}{2}$.

Let us cite the wave lengths for which the computations were made and the optical constants corresponding to them when t = 17° and the salinity is 4%.

λ cm.....	0.8	1	1.35	1.6	3	8.5	10
n.....	5.28	5.86	6.63	7.04	8.3	8.82	8.94
x.....	3.14	3.07	2.98	2.84	1.97	0.95	0.95

The dielectric constant ε and the conductivity σ depend on temperature and salinity, as well as do the optical constants n and κ:

$$n^2 = \frac{\varepsilon}{2} + \sqrt{\frac{\varepsilon^2}{4} + \left(\frac{2\pi\sigma}{\omega}\right)^2},$$
$$\kappa^2 = -\frac{\varepsilon}{2} + \sqrt{\frac{\varepsilon^2}{4} + \left(\frac{2\pi\sigma}{\omega}\right)^2} \qquad (7)$$

Thus, when the temperature varies by 5°, κ may vary by an order of magnitude of 10%, n varies less, approximately by 2%. Here the Fresnel coefficient of reflection varies by 0.7% (for normal incidence).

When the salinity (fresh water) varies from zero to 4%, κ may vary by 2 times, and n by 10%, the Fresnel coefficient of reflection by 15% (for normal incidence). Therefore for measuring the effect /26 associated with a swell, more stable values are possibly needed for the temperature and salinity.

3. Coefficients of Brightness of a Rough Sea in the Microwave Range.

We computed the coefficients of reflection $r(\theta_1, \theta, \theta'\phi')$ for the angles θ_1 from 0 to 80° and wind velocities of 10 m/sec.

From the tables for the coefficients of reflection (See the Appendix) it is obvious that the lines of equal intensity in first approximation agree with the isolines θ_n, ϕ_n. From this it is clear that they depend most strongly on the probabilities of slope of the surface elements and more slightly on the coefficients of reflection.

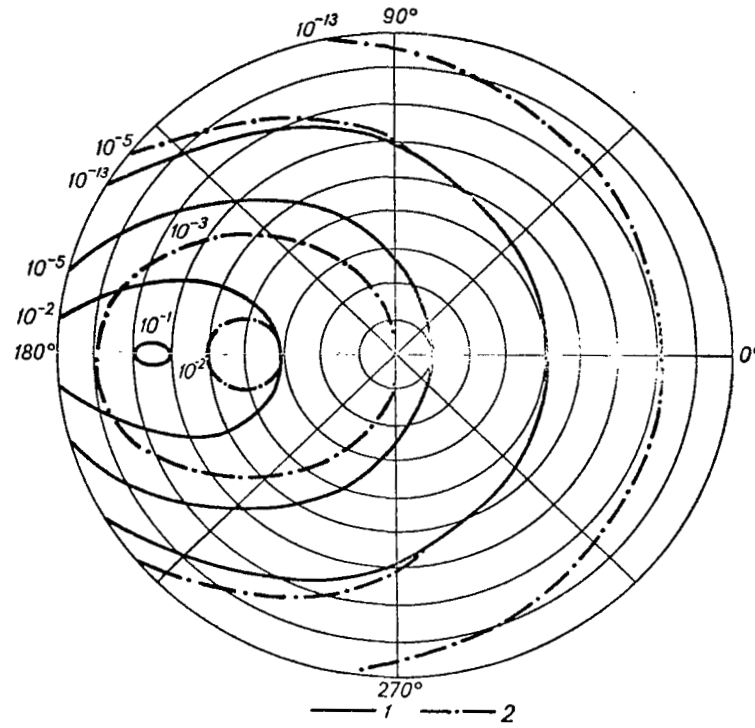

Fig. 2. Isophotes of Brightness for v = 10 m/sec, $\theta_1 = 70°$, $\phi_1 = 0°$ (1) and v = 10 m/sec, $\theta_1 = 40°$, $\phi_1 = 0°$ (2).

From comparison of Figure 2 (curves 2) and Figure 3 we make the obvious conclusion that the directionality of the reflection decreases with increase in wind velocity. The greater the velocity of the wind, the wider will be the cone of the reflected beam and the sooner will the line of equal intensity become open. Here the maximum of brightness is shifted relative to the angle of mirror reflection and the horizon becomes most vivid.

With an increase in the zenith distance θ_1, the angular dimensions of the isolines θ_n and ϕ_n decrease and this produces a decrease in ths solid angle of the reflected current.

From comparison of curves 1 and 2 on Figure 2 it is clear that/28 at larger angles of sighting the reflection from a rough surface is more directed. Quantitatively the width of the light cone ω can be defined as the greatest angular distance between points having azimuths ϕ' and 360 - ϕ' and corresponding to a brightness of $I = 0.1\ I_0$ (I_0 is the brightness at a point representing mirror reflection). Figure 4 shows how the cone is compressed with increase in the zenith distance θ_1, and when θ_1 = const the cone is expanded with increase in wind velocity.

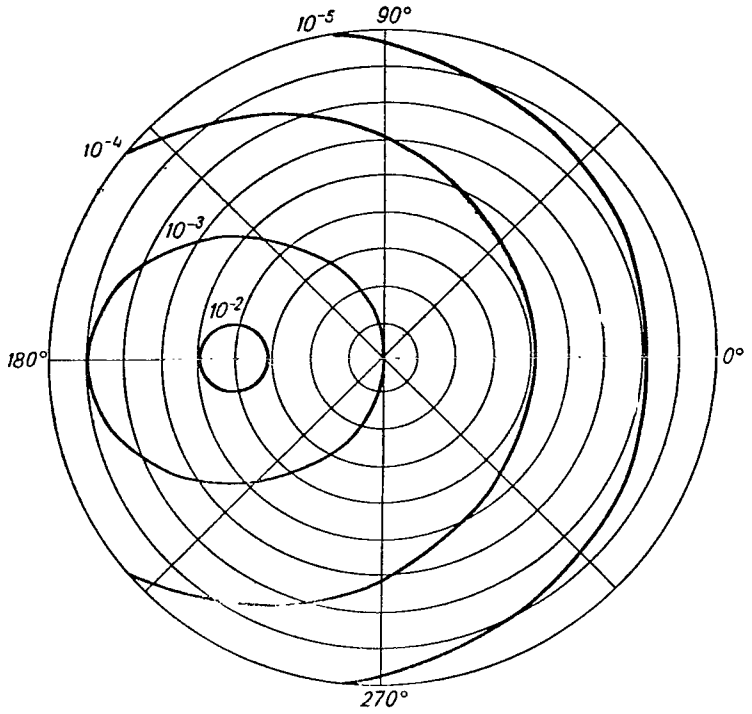

Fig. 3. Isophotes of Brightness for v = 30 m/sec., θ_1 = 40°, ϕ_1 = 0°.

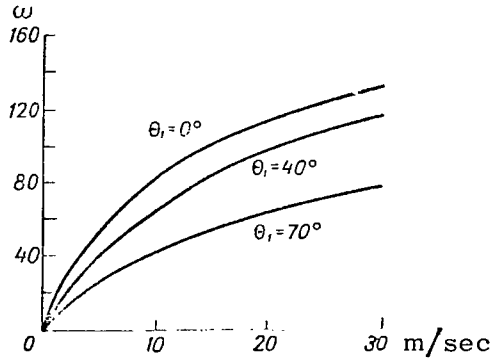

Fig. 4. Dependence of ω on Wind Velocity for Three Values of the Angles of Sighting.

4. Emission Coefficients of a Rough Sea for Centimeter Radiation

The emission coefficients of a rough sea are computed from the formula

$$I = 1 - \sec\theta_1 \int P(z_{x'}, z_{y'}) \cos\chi \sec^4\theta_n R(\chi) \sin\theta_n d\theta_n d\varphi_n. \qquad (8)$$

This integral can be easily computed by the method of steepest descents[1]:

$$I = 1 - \frac{\sec\theta_1}{2\pi\sigma^2} \int_0^{2\pi} d\varphi_n \int_0^{\frac{\pi}{2}} \exp\left\{-\frac{1}{2}\frac{\operatorname{tg}^2\theta_n}{\sigma^2}\right\} \times$$
$$\times \left[\frac{1}{24}\frac{c_1}{\sigma^4}\operatorname{tg}^4\theta_n(\cos^4\varphi_n + \sin^4\varphi_n) + \frac{1}{4}\frac{c^2}{\sigma^2}\tan^4\theta_n \sin^2\varphi_n\cos^2\varphi_n - \right.$$
$$\left. - \frac{1}{4}(c_1+c_2)\frac{\operatorname{tg}^2\theta_n}{\sigma} + \frac{1}{4}(c_1+c_2) + 1\right] \cos\chi \sec^4\theta_n R(\chi) \sin\theta_n d\theta_n.$$

Let us denote $y = \tan\theta_n$, $y_1 = \tan\theta_1$, $\frac{1}{\alpha} = 0.0015 + 2.54\cdot10^{-3}v$. Then

$$I = 1 - \frac{\tau\sec\theta_1}{2\pi} \int_0^{2\pi} d\varphi_n \int_0^{\infty} e^{-\frac{\alpha y^2}{2}} y(\cos\theta_1 + y\sin\theta_1\cos\varphi_n) \times$$
$$\times (1{,}109 - 0{,}109\alpha y^2 + 0{,}014\alpha^2 y^4) R(\chi)\, dy = 1 -$$
$$- \frac{\tau}{2\pi}\left(1{,}109 + 0{,}218\alpha\frac{d}{d\tau} + 0{,}056\alpha^2\frac{d^2}{d\tau^2}\right) \int_0^{2\pi} d\varphi_n \int_0^{\infty} e^{-\frac{\alpha y^2}{2}} y(1 +$$
$$+ yy_1\cos\varphi_n)\, k\, dy = 1 - \frac{\tau}{2\pi}\left(1{,}109 + 0{,}218\alpha\frac{d}{d\tau} + \right.$$
$$\left. + 0{,}056\alpha^2\frac{d^2}{d\tau^2}\right) \int_0^{\pi} d\varphi_n \int_0^{\infty} e^{-\frac{\alpha y^2}{2}} y\{R(\chi^+) + R(\chi^-) +$$
$$+ [R(\chi^+) - R(\chi^-)]\, yy_1\cos\varphi_n\}\, dy,$$

---

[1] We thank B.A. Bolchok who pointed out this fact to us.

where χ^+ and χ^- are determined respectively from

$$\cos\chi^+ = \cos\theta_n \cos\theta_1 + \sin\theta_n \sin\theta_1 \cos\varphi_n,$$
$$\cos\chi^- = \cos\theta_n \cos\theta_1 - \sin\theta_n \sin\theta_1 \cos\varphi_n,$$

(the angle ϕ_1 is assumed equal to zero).

Since the effective values tan θ_n and cos ϕ_n are equal respec- /29
tively to $\frac{1}{\sqrt{\alpha}}$ and $\frac{1}{\sqrt{2}}$, we find

$$I = 1 - 0{,}502\left\{\left(1 + \frac{\tan\theta_1}{\sqrt{2\alpha}}\right) R\left[\frac{\cos\theta_1 + \sqrt{\frac{1}{2\alpha}}\sin\theta_1}{\sqrt{1+\frac{1}{\alpha}}}\right] + \right.$$
$$\left. + \left(1 - \frac{\tan\theta_1}{\sqrt{2\alpha}}\right) R\left[\frac{\cos\theta_1 - \sqrt{\frac{1}{2\alpha}}\sin\theta_1}{\sqrt{1+\frac{1}{\alpha}}}\right]\right\} \qquad (9)$$

For the angle of sighting $\theta_1 = 0°$, we find

$$I = 1 - R\left[\frac{1}{\sqrt{1+\frac{1}{\alpha}}}\right] \qquad (10)$$

when, by expanding into a series over the small quantity $\frac{1}{\alpha}$, we obtain a linear dependence of the intensity of reflected radiation on the wind velocity

$$I = 1 - (R(0) + (0{,}0015 + 2{,}54 \cdot 10^{-3} v) R'(0) + \ldots).$$

For the wind velocity v = 10 m/sec., we find

$$I = 1 - 0{,}502\left\{(1 + 0{,}116\tan\theta_1) R\left[\frac{\cos\theta_1 + 0{,}116\sin\theta_1}{1{,}014}\right] + \right.$$
$$\left. + (1 - 0{,}116\tan\theta_1) R\left[\frac{\cos\theta_1 - 0{,}116\sin\theta_1}{1{,}014}\right]\right\} \qquad (11)$$

Comparison of the computations made using the method of steepest descents and numerical integration gives an error in the method of steepest descents of approximately 1%.

The computations were made for two wind velocities, 10 and 30 m/sec. The wind velocities v = 30 m/sec were taken to find the asymptotic results, since with such a velocity the Cox-Munk distribution is probably not valid. The results of the computations, found in the Table of Emission Coefficients, show that for small θ_1 with an increase in wind velocity, the I_s-component of the emission coefficient is decreased and the I_p-component is increased; the dependence of I_s and I_p on the wind velocity is linear, with small angular coefficients. Thus, for v = 10 m/sec., when $\theta_1 = 0°$, I_s drops by 1.5% and I_p increases by 1% in comparison with a smooth surface. In the region $\theta_1 = 40°$, I_s and I_p are virtually independent of the wind velocity.

For large values of θ_1, the I_s- component increases, and the I_p-component decreases with increase in wind velocity. For v = 10 m/sec, with $\theta_1 = 80°$, I_s increases by 37% and I_p drops by 10%.

Such a result is physically understandable. With small values of θ_1 when swells are in evidence, the reflected beam includes the contribution of the beam with large angles of incidence and with large values of θ_1 we have small angles of incidence. The decrease/30 in I_p near the Brewster angle can be explained by the fact that the contribution both of the small and the large angles of incidence leads near this angle to a decrease in I_p.

Thus, with an increase in wind velocity, the difference between small and large angles of observation is smoothed out, as we would expect.

Conclusions

From the results obtained we can make several conclusions.

If it is necessary to get rid of the influence of swells (in the experiments) we can use circular polarization with $\theta_1 = 0°$.

For these purposes the angle $\theta_1 = 40°$ is suitable, since the I_s-and the I_p- components for $\theta_1 = 40°$ are virtually independent of wind velocity.

If, on the other hand, we must determine the wind velocity from the character of the emission, we must make the measurements of I_s and I_p with large values of θ_1.

For $\theta_1 = 0°$ the quantities I_s and I_p for a zero wind velocity (smooth surface) may be found as $\frac{I_s + I_p}{2}$ for a rough surface. If

we know that the dependence of I_s and I_p on the wind velocity is linear, for $\theta_1 = 0°$, we can find the wind velocity from the experimental values of I_s and I_p, although it is true that the accuracy of such determinations will be very low. To increase this accuracy we must use data for large values of θ_1.

TABLE OF EMISSION COEFFICIENTS

v m/sec	λ см	$\theta_1 = 0°$		$\theta_1 = 40°$		$\theta_1 = 70°$		$\theta_1 = 80°$	
		I_s	I_p	I_s	I_p	I_s	I_p	I_s	I_p
0	0,8	0,428	0,428	0,339	0,526	0,140	0,825	0,046	0,936
10	0,8	0,421	0,431	0,335	0,529	0,153	0,797	0,086	0,894
30	0,8	0,410	0,440	0,330	0,534	0,176	0,739	0,155	0,836
0	1	0,415	0,415	0,337	0,503	0,168	0,791	0,089	0,935
10	1	0,409	0,416	0,332	0,506	0,177	0,765	0,110	0,826
30	1	0,400	0,425	0,330	0,510	0,198	0,716	0,180	0,801
0	1,35	0,396	0,396	0,321	0,482	0,159	0,773	0,084	0,937
10	1,35	0,390	0,399	0,315	0,485	0,169	0,748	0,105	0,820
30	1,35	0,382	0,405	0,315	0,490	0,188	0,700	0,172	0,750
0	1,6	0,388	0,388	0,314	0,474	0,155	0,765	0,082	0,939
10	1,6	0,381	0,390	0,310	0,476	0,163	0,741	0,110	0,821
30	1,6	0,375	0,399	0,310	0,480	0,184	0,694	0,165	0,764
0	3	0,371	0,371	0,295	0,451	0,147	0,750	0,078	0,950
10	3	0,365	0,372	0,295	0,456	0,155	0,728	0,103	0,824
30	3	0,358	0,380	0,293	0,461	0,174	0,681	0,155	0,745
0	8,5	0,365	0,365	0,294	0,417	0,144	0,743	0,076	0,949
10	8,5	0,358	0,366	0,290	0,419	0,152	0,723	0,100	0,829
30	8,5	0,351	0,374	0,289	0,455	0,171	0,678	0,155	0,738
0	10	0,362	0,362	0,291	0,443	0,143	0,738	0,075	0,922
10	10	0,355	0,363	0,286	0,445	0,150	0,715	0,090	0,817
30	10	0,348	0,370	0,285	0,450	0,169	0,666	0,154	0,729

REFERENCES

1. Brekhovskikh, L.M.: Diffraktsiya voln na nerovnoy poverkhno-/31 sti. (Diffraction of Waves on a Rough Surface)., Zh. eksper. i teor. fiz., Vol. 23, 1952.
2. Lysanov, Yu.P.: K voprosu o rasseyanii elektromagnitnykh voln na nerovnoy poverkhnosti. (The Question of Scattering of Electromagnetic Waves on a Rough Surface). Doklddy AN SSSR, Vol. 87, No. 5, 1952.
3. Isakovich, M.A.: Rasseyaniye voln ot statisticheski sherokhovatoy poverkhnosti. (Scattering of Waves from a Statistically Rough Surface)., Zh. eksper. i teor. fiz., Vol. 23, p. 305, 1952.
4. Bass, F.G. and V.G. Bocharov: K teorii rasseyaniya elektromagnitnykh voln na statisticheski nerovnoy poverkhnosti. (Theory of Scattering of Electromagnetic Waves on a Statistically Rough Surface)., Radiotekhnika i elektronika, Vol. 3, p. 180, 1958.
5. Fuks, I.M.: K teorii rasseyaniya radiovoln na vzvolnovannoy poverkhnosti morya. (Theory of Scattering of Radiowaves on a Rough Sea)., Radiofizika, Vol. 9, p. 876, 1966.
6. Mullamaa, Yu.: Diffuznoye otrazheniye i propusknaiye sveta nerovnoy poverkhnost'yu radzdela dvukh isotropnykh sred. (Diffuse Reflectance and Transmission of Light by a Rough Surface of the Boundary of Two Isotropic Media). Issledovaniya po fizike atmosfery, Vol. 3, p. 5, 1962.
7. Cox, C. and W.H. Munk: Slopes of the Sea Surface Deduced from Photographs of Sun Glitter. Bull. Scripps Inst. oceanography, Vol. 6, p. 401, 1956.
8. Davidan, I.N.: Zakonomernosti mnogoletnego raspredeleniya morskikh voln i ikh svyas' so skorost'yu vetra. (Frequency of Multi-Year Distribution of Sea Waves and Their Relationship to Wind Velocity)., Okeanologiya, Vol. 1, No. 2, 1961.
9. Shifrin, K.S.: Rasseyaniye sveta v mutnykh sredakh. (Scattering of Light in a Cloudy Atmosphere), Gostekhizdat, Moscow-Leningrad, 1951.
10. Feynberg, Ye.L.: Rasprostraneniye radiovoln vdol' zemnoy poverkhnosti. (Propagation of Radiowaves Along the Earth's Surface) , AN SSSR, Moscow, 1961
11. Rasprostraneniye UKV. (Ultrashortwave Propagation). Translation edited by B.A. Shillerov. Sovetskoye radio, 1954.

APPENDIX
Tables of Brightness Coefficients
$r_s \cdot 10^2$, $r_p \cdot 10^2$

$\theta_1 = 0$

θ	λ см									
	0,8		1,35		1,6		3,0		8,5	
	r_s	r_p	r_s	r_p	r_s	r_p	r_s	r_p	r_s	r_p
0	1,36	1,35	1,44	1,43	1,45	1,45	1,50	1,50	1,51	1,51
2	1,35	1,34	1,43	1,42	1,45	1,45	1,49	1,49	1,50	1,50
4	1,34	1,34	1,41	1,41	1,43	1,43	1,47	1,47	1,48	1,48
6	1,30	1,29	1,37	1,36	1,38	1,38	1,42	1,42	1,45	1,44
8	1,24	1,24	1,31	1,31	1,33	1,33	1,37	1,36	1,38	1,38
10	1,17	1,16	1,23	1,23	1,25	1,24	1,28	1,28	1,30	1,29
20	0,82	0,81	0,86	0,85	0,88	0,86	0,90	0,89	0,90	0,90
30	0,45	0,43	0,47	0,45	0,47	0,46	0,49	0,47	0,49	0,48
40	0,13	0,12	0,13	0,13	0,13	0,13	0,14	0,13	0,14	0,13
50	0,04	0,04	0,04	0,04	0,04	0,04	0,04	0,04	0,04	0,04
60	0,01	0,01	0,01	0,01	0,01	0,01	0,01	0,01	0,01	0,01
70	0,00	0,00	0,00	0,00	0,00	0,00	0,00	0,00	0,00	0,00
80	0,00	0,00	0,00	0,00	0,00	0,00	0,00	0,00	0,00	0,00

$\theta_1 = 40°$, $\lambda = 0,8$ см

θ′	φ′											
	0		10		20		30		40		50	
	r_s	r_p	r_s	r_p	r_s	r_p	r_s	r_p	r_s	r_p	r_s	r_p
0	0,21	0,19	0,21	0,19	0,21	0,19	0,21	0,19	0,21	0,19	0,21	0,19
10	0,05	0,05	0,05	0,05	0,05	0,05	0,06	0,05	0,07	0,07	0,08	0,07
20	0,01	0,01	0,01	0,01	0,01	0,01	0,02	0,02	0,02	0,02	0,03	0,03
30	0,00	0,00	0,00	0,00	0,00	0,00	0,00	0,00	0,00	0,00	0,01	0,00
32											0,01	0,00
34											0,00	0,00

θ	φ′											
	60		70		80		90		100		110	
	r_s	r_p	r_s	r_p	r_s	r_p	r_s	r_p	r_s	r_p	r_s	r_p
0	0,21	0,19	0,21	0,19	0,21	0,19	0,21	0,19	0,21	0,19	0,21	0,19
10	0,10	0,09	0,11	0,10	0,14	0,13	0,15	0,14	0,17	0,16	0,23	0,21
20	0,04	0,04	0,04	0,04	0,06	0,06	0,09	0,09	0,11	0,10	0,18	0,16
30	0,01	0,01	0,01	0,01	0,02	0,02	0,04	0,04	0,07	0,06	0,13	0,11
32	0,01	0,01	0,01	0,01	0,02	0,02	0,03	0,03	0,05	0,05	0,11	0,10
34	0,01	0,00	0,01	0,01	0,01	0,01	0,02	0,02	0,05	0,05	0,09	0,08
36	0,01	0,00	0,01	0,01	0,01	0,01	0,02	0,02	0,05	0,04	0,08	0,07
38	0,00	0,00	0,01	0,00	0,01	0,01	0,02	0,02	0,02	0,02	0,07	0,06
40			0,00	0,00	0,01	0,01	0,01	0,01	0,02	0,02	0,05	0,05
42					0,01	0,00	0,01	0,01	0,02	0,02	0,04	0,04
44					0,00	0,00	0,01	0,01	0,01	0,01	0,04	0,03
46							0,01	0,00	0,01	0,01	0,03	0,02
48							0,00	0,00	0,01	0,01	0,02	0,02
50									0,01	0,00	0,01	0,01
60									0,00	0,00	0,00	0,00

θ′	φ′ = 120		130		140		150		160		170	
	r_s	r_p	r_s	r_p	r_s	r_p	r_s	r_p	r_s	r_p	r_s	r_p
0	0,21	0,19	0,21	0,19	0,21	0,19	0,21	0,19	0,21	0,19	0,21	0,19
10	0,27	0,24	0,32	0,27	0,38	0,31	0,41	0,40	0,46	0,44	0,49	0,46
20	0,28	0,23	0,39	0,35	0,54	0,47	0,85	0,72	1,03	0,75	1,20	0,89
30	0,18	0,16	0,35	0,31	0,59	0,46	1,01	0,80	1,36	1,09	1,81	1,45
32	0,18	0,16	0,33	0,31	0,55	0,46	1,02	0,81	1,50	1,18	1,91	1,50
34	0,17	0,14	0,30	0,25	0,54	0,43	0,98	0,79	1,53	1,18	1,99	1,55
36	0,16	0,13	0,30	0,24	0,49	0,39	0,97	0,76	1,56	1,17	2,07	1,58
38	0,14	0,12	0,27	0,24	0,47	0,37	0,92	0,69	1,52	1,13	2,08	1,58
40	0,13	0,09	0,22	0,18	0,45	0,34	0,87	0,67	1,48	1,10	2,09	1,55
42	0,10	0,08	0,19	0,16	0,42	0,31	0,82	0,56	1,44	1,06	2,11	1,54
44	0,08	0,06	0,18	0,14	0,37	0,29	0,80	0,55	1,42	1,02	2,07	1,49
46	0,06	0,04	0,16	0,12	0,34	0,24	0,70	0,52	1,36	0,96	2,06	1,42
48	0,05	0,04	0,16	0,10	0,30	0,22	0,62	0,46	1,33	0,93	1,96	1,34
50	0,04	0,04	0,11	0,08	0,25	0,17	0,52	0,37	1,13	0,85	1,89	1,32
60	0,01	0,01	0,03	0,03	0,10	0,08	0,29	0,19	0,58	0,33	1,21	0,73
70	0,00	0,00	0,01	0,00	0,03	0,02	0,10	0,05	0,25	0,14	0,54	0,29
80			0,00	0,00	0,01	0,00	0,02	0,01	0,08	0,03	0,22	0,08
90					0,00	0,00	0,00	0,00	0,00	0,00	0,01	0,01

θ′	φ′ = 172		174		176		178		180	
	r_s	r_p	r_s	r_p	r_s	r_p	r_s	r_p	r_s	r_p
0	0,21	0,19	0,21	0,19	0,21	0,19	0,21	0,19	0,21	0,19
10	0,49	0,47	0,50	0,48	0,51	0,48	0,52	0,49	0,52	0,49
20	1,21	0,92	1,23	0,96	1,25	1,01	1,26	1,05	1,27	1,10
30	1,89	1,51	1,96	1,58	2,01	1,63	2,06	1,64	2,07	1,65
32	2,01	1,58	2,11	1,67	2,19	1,72	2,22	1,75	2,23	1,75
34	2,11	1,65	2,22	1,71	2,27	1,77	2,30	1,78	2,31	1,79
36	2,17	1,66	2,27	1,74	2,35	1,81	2,38	1,82	2,39	1,83
38	2,18	1,65	2,28	1,74	2,40	1,79	2,41	1,81	2,42	1,81
40	2,19	1,64	2,29	1,72	2,41	1,79	2,45	1,81	2,45	1,81
42	2,20	1,59	2,32	1,68	2,44	1,77	2,46	1,78	2,47	1,79
44	2,22	1,58	2,34	1,65	2,43	1,72	2,47	1,75	2,48	1,77
46	2,16	1,50	2,34	1,64	2,43	1,70	2,46	1,72	2,47	1,73
48	2,06	1,42	2,19	1,49	2,29	1,57	2,34	1,61	2,36	1,62
50	2,00	1,36	2,09	1,41	2,18	1,48	2,25	1,51	2,27	1,52
60	1,27	0,75	1,35	0,80	1,41	0,81	1,42	0,83	1,43	0,84
70	0,57	0,30	0,59	0,31	0,61	0,31	0,62	0,31	0,63	0,31
80	0,23	0,09	0,24	0,10	0,25	0,10	0,25	0,10	0,26	0,11
90	0,07	0,01	0,07	0,01	0,08	0,02	0,08	0,02	0,08	0,02

$\theta_1 = 40°$, $\lambda = 1,35$ см

θ′	φ′ = 0		10		20		30		40		50	
	r_s	r_p	r_s	r_p	r_s	r_p	r_s	r_p	r_s	r_p	r_s	r_p
0	0,21	0,19	0,21	0,19	0,21	0,19	0,21	0,19	0,21	0,19	0,21	0,19
10	0,05	0,05	0,05	0,05	0,05	0,05	0,06	0,06	0,07	0,07	0,08	0,07
20	0,01	0,01	0,01	0,01	0,01	0,01	0,02	0,02	0,02	0,02	0,03	0,03
30	0,00	0,00	0,00	0,00	0,00	0,00	0,00	0,00	0,00	0,00	0,01	0,00
32											0,01	0,00
34											0,00	0,00

θ′	φ′ = 60		70		80		90		100		110	
	r_s	r_p	r_s	r_p	r_s	r_p	r_s	r_p	r_s	r_p	r_s	r_p
0	0,21	0,19	0,21	0,19	0,21	0,19	0,21	0,19	0,21	0,19	0,21	0,19
10	0,10	0,09	0,11	0,10	0,14	0,13	0,15	0,14	0,17	0,16	0,21	0,21
20	0,04	0,04	0,04	0,04	0,06	0,06	0,09	0,09	0,11	0,10	0,18	0,16
30	0,01	0,01	0,01	0,01	0,02	0,02	0,04	0,04	0,07	0,06	0,13	0,11
32	0,01	0,01	0,01	0,01	0,02	0,02	0,03	0,03	0,05	0,05	0,11	0,10
34	0,01	0,00	0,01	0,01	0,01	0,01	0,02	0,02	0,05	0,05	0,09	0,08
36	0,01	0,00	0,01	0,01	0,01	0,01	0,02	0,02	0,05	0,04	0,08	0,07
38			0,01	0,00	0,01	0,01	0,02	0,02	0,02	0,02	0,07	0,06
40			0,00	0,00	0,01	0,01	0,01	0,01	0,02	0,02	0,05	0,05
42					0,01	0,00	0,01	0,01	0,02	0,02	0,04	0,04
44					0,00	0,00	0,01	0,01	0,01	0,01	0,04	0,03
46							0,01	0,00	0,01	0,01	0,03	0,02
48							0,00	0,00	0,01	0,01	0,02	0,02
50									0,01	0,00	0,01	0,01
60									0,00	0,00	0,00	0,00

θ′	φ′ = 120		130		140		150		160		170	
	r_s	r_p	r_s	r_p	r_s	r_p	r_s	r_p	r_s	r_p	r_s	r_p
0	0,21	0,19	0,21	0,19	0,21	0,19	0,21	0,19	0,21	0,19	0,21	0,19
10	0,28	0,24	0,33	0,28	0,40	0,32	0,43	0,42	0,48	0,46	0,52	0,48
20	0,29	0,23	0,40	0,37	0,57	0,49	0,90	0,76	1,09	0,79	1,26	0,94
30	0,18	0,16	0,36	0,32	0,62	0,48	1,07	0,84	1,43	1,15	1,91	1,53
32	0,18	0,16	0,34	0,32	0,58	0,48	1,08	0,85	1,58	1,25	2,01	1,58
34	0,17	0,14	0,31	0,26	0,57	0,46	1,03	0,83	1,61	1,25	2,10	1,64
36	0,16	0,13	0,31	0,25	0,52	0,41	1,02	0,80	1,64	1,24	2,18	1,67
38	0,14	0,12	0,28	0,25	0,49	0,39	0,97	0,73	1,60	1,19	2,19	1,67
40	0,13	0,09	0,23	0,18	0,48	0,35	0,92	0,71	1,56	1,16	2,20	1,64
42	0,10	0,08	0,20	0,16	0,44	0,32	0,87	0,59	1,52	1,12	2,22	1,63
44	0,08	0,06	0,18	0,14	0,39	0,30	0,84	0,58	1,50	1,08	2,18	1,57
46	0,06	0,04	0,16	0,12	0,35	0,25	0,74	0,55	1,43	1,01	2,17	1,50
48	0,05	0,04	0,16	0,10	0,31	0,23	0,66	0,48	1,40	0,98	2,07	1,42
50	0,04	0,04	0,11	0,08	0,26	0,17	0,55	0,39	1,19	0,90	1,99	1,39
60	0,01	0,01	0,03	0,03	0,10	0,08	0,30	0,20	0,61	0,34	1,27	0,77
70	0,00	0,00	0,01	0,00	0,03	0,02	0,10	0,05	0,26	0,14	0,57	0,30
80			0,00	0,00	0,01	0,00	0,02	0,01	0,08	0,03	0,23	0,08
90					0,00	0,00	0,00	0,00	0,00	0,00	0,01	0,01

θ′	φ′ = 172		174		176		178		180	
	r_s	r_p	r_s	r_p	r_s	r_p	r_s	r_p	r_s	r_p
0	0,21	0,19	0,21	0,19	0,21	0,19	0,21	0,19	0,21	0,19
10	0,52	0,49	0,53	0,50	0,54	0,50	0,55	0,51	0,55	0,51
20	1,27	0,97	1,30	1,01	1,32	1,07	1,33	1,11	1,34	1,16
30	1,99	1,60	2,07	1,67	2,15	1,72	2,17	1,73	2,18	1,74
32	2,12	1,67	2,22	1,76	2,31	1,81	2,34	1,85	2,35	1,85
34	2,22	1,74	2,34	1,80	2,39	1,87	2,42	1,88	2,43	1,89
36	2,29	1,75	2,39	1,84	2,48	1,91	2,51	1,92	2,52	1,93
38	2,30	1,74	2,40	1,84	2,53	1,89	2,54	1,91	2,55	1,91
40	2,31	1,73	2,41	1,81	2,54	1,89	2,58	1,91	2,58	1,91
42	2,32	1,68	2,44	1,77	2,57	1,87	2,59	1,88	2,60	1,89

θ′	φ′ 172		174		176		178		180	
	r_s	r_p	r_s	r_p	r_s	r_p	r_s	r_p	r_s	r_p
44	2.34	1.67	2.47	1.74	2.56	1.81	2.60	1.85	2.61	1.87
46	2.28	1.58	2.47	1.73	2.56	1.79	2.59	1.81	2.60	1.82
48	2.17	1.50	2.31	1.57	2.41	1.66	2.47	1.70	2.49	1.71
50	2.11	1.44	2.20	1.49	2.30	1.56	2.37	1.60	2.39	1.61
60	1.34	0.79	1.43	0.85	1.49	0.86	1.50	0.88	1.51	0.89
70	0.60	0.31	0.62	0.32	0.65	0.32	0.66	0.32	0.67	0.32
80	0.24	0.09	0.25	0.10	0.26	0.10	0.26	0.10	0.27	0.11
90	0.07	0.01	0.07	0.01	0.08	0.02	0.08	0.02	0.08	0.02

$\theta_1 = 40°$, $\lambda = 1.6$ см

θ′	φ′ 0		10		20		30		40		50	
	r_s	r_p	r_s	r_p	r_s	r_p	r_s	r_p	r_s	r_p	r_s	r_p
0	0.21	0.19	0.21	0.19	0.21	0.19	0.21	0.19	0.21	0.19	0.21	0.19
10	0.05	0.05	0.05	0.05	0.05	0.05	0.06	0.06	0.07	0.07	0.08	0.07
20	0.01	0.01	0.01	0.01	0.01	0.02	0.02	0.02	0.02	0.02	0.03	0.03
30	0.00	0.00	0.00	0.00	0.00	0.00	0.00	0.00	0.00	0.00	0.01	0.00
32											0.01	0.00
34											0.00	0.00

θ′	φ′ 60		70		80		90		100		110	
	r_s	r_p	r_s	r_p	r_s	r_p	r_s	r_p	r_s	r_p	r_s	r_p
0	0.21	0.19	0.21	0.19	0.21	0.19	0.21	0.19	0.21	0.19	0.21	0.19
10	0.10	0.09	0.11	0.10	0.14	0.13	0.15	0.14	0.17	0.16	0.24	0.21
20	0.04	0.04	0.04	0.04	0.06	0.06	0.09	0.09	0.11	0.10	0.18	0.16
30	0.01	0.01	0.01	0.01	0.02	0.02	0.04	0.04	0.07	0.06	0.13	0.11
32	0.01	0.01	0.01	0.01	0.02	0.02	0.03	0.03	0.05	0.05	0.11	0.10
34	0.01	0.00	0.01	0.01	0.01	0.01	0.02	0.02	0.05	0.05	0.09	0.08
36	0.01	0.00	0.01	0.01	0.01	0.01	0.02	0.02	0.05	0.04	0.08	0.07
38			0.01	0.00	0.01	0.01	0.02	0.02	0.02	0.02	0.07	0.06
40			0.00	0.00	0.01	0.01	0.01	0.01	0.02	0.02	0.05	0.05
42					0.00	0.00	0.01	0.01	0.02	0.02	0.04	0.04
44					0.00	0.00	0.01	0.01	0.01	0.01	0.04	0.03
46							0.01	0.00	0.01	0.01	0.03	0.02
48							0.00	0.00	0.01	0.01	0.02	0.02
50									0.01	0.00	0.01	0.01
60									0.00	0.00	0.00	0.00

θ′	φ′ 120		130		140		150		160		170	
	r_s	r_p	r_s	r_p	r_s	r_p	r_s	r_p	r_s	r_p	r_s	r_p
0	0.21	0.19	0.21	0.19	0.21	0.19	0.21	0.19	0.21	0.19	0.21	0.19
10	0.29	0.24	0.34	0.29	0.41	0.33	0.44	0.43	0.49	0.47	0.53	0.49
20	0.30	0.23	0.42	0.38	0.58	0.50	0.92	0.77	0.11	0.80	1.28	0.95

θ'	φ' 120		130		140		150		160		170	
	r_s	r_p	r_s	r_p	r_s	r_p	r_s	r_p	r_s	r_p	r_s	r_p
30	0,18	0,16	0,37	0,33	0,63	0,49	1,09	0,86	1,46	1,17	1,94	1,55
32	0,18	0,16	0,35	0,33	0,59	0,49	1,10	0,87	1,61	1,27	2,04	1,61
34	0,17	0,14	0,32	0,26	0,58	0,47	1,05	0,85	1,64	1,27	2,13	1,66
36	0,16	0,13	0,32	0,25	0,53	0,42	1,04	0,81	1,67	1,26	2,21	1,69
38	0,14	0,12	0,29	0,25	0,50	0,40	0,99	0,74	1,63	1,21	2,22	1,69
40	0,13	0,09	0,23	0,18	0,49	0,36	0,94	0,72	1,58	1,18	2,23	1,66
42	0,10	0,08	0,20	0,16	0,45	0,33	0,88	0,60	1,54	1,14	2,25	1,65
44	0,08	0,06	0,18	0,14	0,40	0,31	0,86	0,59	1,52	1,10	2,21	1,60
46	0,06	0,04	0,16	0,12	0,36	0,25	0,75	0,56	1,46	1,03	2,20	1,52
48	0,05	0,04	0,16	0,10	0,32	0,23	0,67	0,49	1,42	0,99	2,10	1,41
50	0,04	0,04	0,11	0,08	0,26	0,17	0,56	0,40	1,21	0,92	2,02	1,41
60	0,01	0,01	0,03	0,03	0,10	0,08	0,31	0,20	0,62	0,35	1,29	0,78
70	0,00	0,00	0,01	0,00	0,03	0,02	0,10	0,05	0,26	0,14	0,58	0,31
80			0,00	0,00	0,01	0,00	0,02	0,01	0,08	0,03	0,23	0,08
90							0,00	0,00	0,00	0,00	0,01	0,01

θ'	φ' 172		174		176		178		180	
	r_s	r_p	r_s	r_p	r_s	r_p	r_s	r_p	r_s	r_p
0	0,21	0,19	0,21	0,19	0,21	0,19	0,21	0,19	0,21	0,19
10	0,53	0,50	0,54	0,51	0,55	0,51	0,56	0,52	0,56	0,52
20	1,29	0,99	1,32	1,03	1,34	1,09	1,35	1,13	1,36	1,18
30	2,02	1,62	2,10	1,69	2,18	1,75	2,20	1,76	2,21	1,77
32	2,15	1,69	2,25	1,79	2,34	1,84	2,37	1,88	2,38	1,88
34	2,25	1,77	2,37	1,83	2,43	1,90	2,46	1,91	2,47	1,92
36	2,32	1,78	2,43	1,86	2,51	1,94	2,54	1,95	2,55	1,96
38	2,33	1,77	2,44	1,86	2,56	1,92	2,57	1,91	2,58	1,94
40	2,34	1,76	2,45	1,84	2,57	1,92	2,61	1,94	2,61	1,94
42	2,35	1,70	2,48	1,80	2,61	1,90	2,62	1,91	2,63	1,92
44	2,37	1,69	2,50	1,77	2,60	1,84	2,63	1,88	2,64	1,90
46	2,31	1,61	2,50	1,76	2,60	1,82	2,62	1,84	2,63	1,85
48	2,20	1,52	2,34	1,60	2,45	1,68	2,50	1,73	2,52	1,74
50	2,14	1,46	2,23	1,51	2,33	1,58	2,40	1,62	2,43	1,63
60	1,36	0,80	1,45	0,86	1,51	0,87	1,52	0,89	1,53	0,91
70	0,61	0,32	0,63	0,33	0,66	0,33	0,67	0,33	0,68	0,33
80	0,24	0,09	0,25	0,10	0,27	0,10	0,27	0,10	0,28	0,11
90	0,07	0,01	0,07	0,01	0,08	0,02	0,08	0,02	0,08	0,02

$\theta_1 = 40°$, $\lambda = 3$ см

θ'	φ' 0		10		20		30		40		50	
	r_s	r_p	r_s	r_p	r_s	r_p	r_s	r_p	r_s	r_p	r_s	r_p
0	0,22	0,20	0,22	0,20	0,22	0,20	0,22	0,20	0,22	0,20	0,22	0,20
10	0,05	0,05	0,05	0,05	0,05	0,05	0,06	0,06	0,07	0,07	0,08	0,07
20	0,01	0,01	0,01	0,01	0,01	0,01	0,02	0,02	0,02	0,02	0,03	0,03
30	0,00	0,00	0,00	0,00	0,00	0,00	0,00	0,00	0,00	0,00	0,01	0,00
32											0,01	0,00
34											0,00	0,00

θ′	φ′ = 60		70		80		90		100		110	
	r_s	r_p	r_s	r_p	r_s	r_p	r_s	r_p	r_s	r_p	r_s	r_p
0	0.22	0.20	0.22	0.20	0.22	0.20	0.22	0.20	0.22	0.20	0.22	0.20
10	0.10	0.09	0.11	0.10	0.14	0.13	0.15	0.14	0.17	0.16	0.25	0.22
20	0.04	0.04	0.04	0.04	0.06	0.06	0.09	0.09	0.11	0.10	0.19	0.16
30	0.01	0.01	0.01	0.01	0.02	0.02	0.04	0.04	0.07	0.06	0.13	0.11
32	0.01	0.01	0.01	0.01	0.02	0.02	0.03	0.03	0.05	0.05	0.11	0.10
34	0.01	0.00	0.01	0.01	0.01	0.01	0.02	0.02	0.05	0.05	0.09	0.08
36	0.01	0.00	0.01	0.01	0.01	0.01	0.02	0.02	0.05	0.04	0.08	0.07
38			0.01	0.00	0.01	0.01	0.02	0.02	0.02	0.02	0.07	0.06
40			0.00	0.00	0.01	0.01	0.01	0.01	0.02	0.02	0.05	0.05
42					0.01	0.00	0.01	0.01	0.02	0.02	0.04	0.04
44					0.00	0.00	0.01	0.01	0.01	0.01	0.04	0.03
46							0.01	0.00	0.01	0.01	0.03	0.02
48							0.00	0.00	0.01	0.01	0.02	0.02
50									0.01	0.00	0.01	0.01
60									0.00	0.00	0.00	0.00

θ′	φ′ = 120		130		140		150		160		170	
	r_s	r_p	r_s	r_p	r_s	r_p	r_s	r_p	r_s	r_p	r_s	r_p
0	0.22	0.20	0.22	0.20	0.22	0.20	0.22	0.20	0.22	0.20	0.22	0.20
10	0.30	0.25	0.35	0.30	0.42	0.34	0.45	0.44	0.50	0.48	0.54	0.50
20	0.31	0.24	0.43	0.39	0.60	0.51	0.94	0.79	1.14	0.82	1.32	0.98
30	0.19	0.16	0.38	0.34	0.65	0.50	1.11	0.88	1.49	1.19	1.99	1.60
32	0.19	0.16	0.36	0.34	0.61	0.50	1.12	0.89	1.65	1.30	2.10	1.65
34	0.17	0.14	0.33	0.27	0.60	0.48	1.08	0.87	1.69	1.30	2.19	1.71
36	0.16	0.13	0.33	0.26	0.54	0.43	1.07	0.83	1.72	1.29	2.27	1.74
38	0.14	0.12	0.30	0.26	0.51	0.41	1.01	0.76	1.68	1.24	2.28	1.74
40	0.13	0.09	0.24	0.19	0.50	0.37	0.96	0.74	1.63	1.20	2.29	1.71
42	0.10	0.08	0.21	0.16	0.46	0.34	0.90	0.62	1.59	1.17	2.31	1.70
44	0.08	0.06	0.19	0.14	0.41	0.32	0.88	0.61	1.57	1.12	2.27	1.64
46	0.06	0.04	0.16	0.12	0.37	0.26	0.77	0.57	1.49	1.06	2.26	1.57
48	0.05	0.04	0.16	0.10	0.33	0.24	0.68	0.50	1.46	1.03	2.15	1.47
50	0.04	0.04	0.11	0.08	0.27	0.18	0.57	0.41	1.24	0.94	2.07	1.46
60	0.01	0.01	0.03	0.03	0.10	0.08	0.32	0.20	0.64	0.36	1.34	0.80
70	0.00	0.00	0.01	0.00	0.03	0.02	0.10	0.05	0.27	0.15	0.60	0.32
80			0.00	0.00	0.01	0.00	0.02	0.01	0.08	0.03	0.24	0.08
90							0.00	0.00	0.00	0.00	0.01	0.01

θ′	φ′ = 172		174		176		178		180	
	r_s	r_p	r_s	r_p	r_s	r_p	r_s	r_p	r_s	r_p
0	0.22	0.20	0.22	0.20	0.22	0.20	0.22	0.20	0.22	0.20
10	0.54	0.51	0.55	0.52	0.56	0.52	0.57	0.53	0.57	0.53
20	1.33	1.01	1.36	1.06	1.38	1.11	1.39	1.16	1.40	1.20
30	2.07	1.66	2.15	1.74	2.24	1.79	2.26	1.80	2.27	1.81
32	2.21	1.74	2.31	1.83	2.40	1.89	2.43	1.92	2.44	1.92
34	2.31	1.81	2.43	1.88	2.48	1.94	2.52	1.95	2.53	1.96

θ'	φ' = 172		174		176		178		180	
	r_s	r_p	r_s	r_p	r_s	r_p	r_s	r_p	r_s	r_p
36	2,38	1,82	2,48	1,91	2,57	1,99	2,60	2,00	2,61	2,01
38	2,39	1,81	2,49	1,91	2,62	1,97	2,63	1,99	2,64	1,99
40	2,40	1,80	2,50	1,89	2,63	1,97	2,67	1,99	2,67	1,99
42	2,41	1,75	2,54	1,85	2,67	1,94	2,68	1,95	2,69	1,96
44	2,43	1,74	2,56	1,81	2,66	1,89	2,69	1,92	2,70	1,94
46	2,37	1,65	2,56	1,80	2,66	1,87	2,68	1,89	2,69	1,90
48	2,26	1,56	2,40	1,64	2,50	1,73	2,56	1,77	2,58	1,78
50	2,19	1,49	2,29	1,56	2,39	1,63	2,46	1,66	2,48	1,68
60	1,40	0,82	1,48	0,88	1,56	0,89	1,57	0,91	1,58	0,93
70	0,63	0,33	0,65	0,34	0,67	0,34	0,68	0,34	0,69	0,34
80	0,25	0,09	0,26	0,10	0,28	0,10	0,28	0,10	0,29	0,11
90	0,07	0,01	0,07	0,01	0,08	0,02	0,08	0,02	0,08	0,02

$\theta_1 = 40°$, $\lambda = 8{,}5$ см

θ'	φ' = 0		10		20		30		40		50	
	r_s	r_p	r_s	r_p	r_s	r_p	r_s	r_p	r_s	r_p	r_s	r_p
0	0,22	0,20	0,22	0,20	0,22	0,20	0,22	0,20	0,22	0,20	0,22	0,20
10	0,05	0,05	0,05	0,05	0,05	0,05	0,06	0,06	0,07	0,07	0,08	0,07
20	0,01	0,01	0,01	0,01	0,01	0,01	0,02	0,02	0,02	0,02	0,03	0,03
30	0,00	0,00	0,00	0,00	0,01	0,01	0,00	0,00	0,00	0,00	0,01	0,00
32											0,01	0,00
34											0,00	0,00

θ'	φ' = 60		70		80		90		100	
	r_s	r_p	r_s	r_p	r_s	r_p	r_s	r_p	r_s	r_p
0	0,22	0,20	0,22	0,20	0,22	0,20	0,22	0,20	0,22	0,20
10	0,10	0,09	0,11	0,10	0,14	0,13	0,15	0,14	0,17	0,16
20	0,04	0,04	0,04	0,04	0,06	0,06	0,09	0,09	0,11	0,10
30	0,01	0,01	0,01	0,01	0,02	0,02	0,04	0,04	0,07	0,06
32	0,01	0,01	0,01	0,01	0,02	0,02	0,03	0,03	0,05	0,05
34	0,01	0,00	0,01	0,01	0,01	0,01	0,02	0,02	0,05	0,05
36	0,01	0,00	0,01	0,01	0,01	0,01	0,02	0,02	0,05	0,04
38			0,01	0,00	0,01	0,01	0,02	0,02	0,02	0,02
40			0,00	0,00	0,01	0,01	0,01	0,01	0,02	0,02
42					0,01	0,00	0,01	0,01	0,02	0,02
44					0,00	0,00	0,01	0,01	0,01	0,01
46							0,01	0,00	0,01	0,01
48							0,00	0,00	0,01	0,01
50									0,01	0,00
60									0,00	0,00

θ′	φ′ = 110		120		130		140		150		160	
	r_s	r_p	r_s	r_p	r_s	r_p	r_s	r_p	r_s	r_p	r_s	r_p
0	0,22	0,20	0,22	0,20	0,22	0,20	0,22	0,20	0,22	0,20	0,22	0,20
10	0,25	0,22	0,30	0,25	0,35	0,30	0,42	0,34	0,45	0,44	0,51	0,49
20	0,19	0,16	0,31	0,24	0,43	0,39	0,61	0,52	0,95	0,80	1,15	0,83
30	0,13	0,11	0,19	0,16	0,38	0,34	0,66	0,51	1,13	0,89	1,52	1,21
32	0,11	0,10	0,19	0,16	0,36	0,34	0,62	0,51	1,14	0,90	1,68	1,32
34	0,09	0,08	0,17	0,14	0,33	0,27	0,61	0,48	1,09	0,88	1,71	1,32
36	0,08	0,07	0,16	0,13	0,33	0,26	0,55	0,43	1,08	0,84	1,74	1,31
38	0,07	0,06	0,14	0,12	0,30	0,26	0,52	0,41	1,02	0,77	1,70	1,26
40	0,05	0,05	0,13	0,09	0,24	0,19	0,50	0,37	0,97	0,75	1,65	1,22
42	0,04	0,04	0,10	0,08	0,21	0,16	0,46	0,34	0,91	0,63	1,61	1,18
44	0,04	0,03	0,08	0,06	0,19	0,14	0,41	0,32	0,89	0,62	1,59	1,14
46	0,03	0,02	0,06	0,04	0,16	0,12	0,37	0,26	0,78	0,58	1,52	1,07
48	0,02	0,02	0,05	0,04	0,16	0,10	0,33	0,24	0,69	0,51	1,49	1,04
50	0,01	0,01	0,04	0,04	0,11	0,08	0,27	0,18	0,58	0,41	1,26	0,95
60	0,00	0,00	0,01	0,01	0,03	0,03	0,10	0,08	0,32	0,20	0,65	0,36
70			0,00	0,00	0,01	0,00	0,03	0,02	0,10	0,05	0,27	0,15
80					0,00	0,00	0,01	0,00	0,02	0,01	0,08	0,03
90									0,00	0,00	0,00	0,00

θ′	φ′ = 170		172		174		176		178		180	
	r_s	r_p	r_s	r_p	r_s	r_p	r_s	r_p	r_s	r_p	r_s	r_p
0	0,22	0,20	0,22	0,20	0,22	0,20	0,22	0,20	0,22	0,20	0,22	0,20
10	0,55	0,51	0,55	0,52	0,56	0,53	0,57	0,53	0,58	0,54	0,58	0,54
20	1,34	0,99	1,35	1,02	1,38	1,07	1,40	1,13	1,41	1,17	1,42	1,22
30	2,02	1,62	2,10	1,69	2,18	1,76	2,27	1,82	2,29	1,83	2,30	1,84
32	2,13	1,68	2,24	1,76	2,35	1,86	2,44	1,91	2,47	1,95	2,48	1,95
34	2,21	1,73	2,35	1,84	2,47	1,90	2,52	1,97	2,55	1,98	2,56	1,99
36	2,30	1,76	2,42	1,85	2,52	1,94	2,61	2,02	2,64	2,03	2,65	2,04
38	2,31	1,76	2,43	1,84	2,53	1,94	2,66	2,00	2,67	2,02	2,68	2,02
40	2,32	1,73	2,44	1,83	2,54	1,91	2,67	2,00	2,72	2,02	2,72	2,02
42	2,35	1,72	2,45	1,77	2,58	1,87	2,71	1,97	2,73	1,98	2,74	1,99
44	2,30	1,66	2,47	1,76	2,60	1,84	2,70	1,91	2,74	1,95	2,75	1,97
46	2,29	1,59	2,41	1,68	2,60	1,83	2,70	1,89	2,73	1,91	2,74	1,92
48	2,18	1,50	2,29	1,59	2,44	1,66	2,54	1,75	2,60	1,79	2,62	1,80
50	2,10	1,48	2,22	1,52	2,32	1,58	2,43	1,65	2,50	1,69	2,52	1,70
60	1,36	0,81	1,42	0,83	1,51	0,89	1,58	0,90	1,59	0,92	1,60	0,94
70	0,61	0,32	0,64	0,33	0,66	0,34	0,68	0,34	0,69	0,34	0,70	0,34
80	0,24	0,08	0,25	0,09	0,26	0,10	0,28	0,10	0,28	0,10	0,29	0,11
90	0,01	0,01	0,07	0,01	0,07	0,01	0,08	0,02	0,08	0,02	0,08	0,02

$\theta_1 = 70°$, $\lambda = 0{,}8$ см

θ′	φ′ = 100		110		120		130		140		150		160	
	r_s	r_p	r_s	r_p	r_s	r_p	r_s	r_p	r_s	r_p	r_s	r_p	r_s	r_p
0	0,00	0,00	0,00	0,00	0,00	0,00	0,00	0,00	0,00	0,00	0,00	0,00	0,00	0,00
10	0,00	0,00	0,01	0,01	0,01	0,01	0,02	0,01	0,03	0,02	0,03	0,02	0,04	0,03
20			0,01	0,01	0,02	0,01	0,03	0,01	0,05	0,03	0,07	0,05	0,10	0,07
30			0,00	0,00	0,01	0,01	0,03	0,01	0,07	0,04	0,13	0,08	0,29	0,17

θ'	φ' 100		110		120		130		140		150		160	
	r_s	r_p	r_s	r_p	r_s	r_p	r_s	r_p	r_s	r_p	r_s	r_p	r_s	r_p
40					0,00	0,00	0,02	0,01	0,05	0,03	0,17	0,09	0,52	0,26
50							0,00	0,00	0,02	0,01	0,11	0,05	0,58	0,24
60									0,01	0,00	0,05	0,02	0,38	0,13
62									0,01	0,00	0,04	0,01	0,36	0,12
64									0,00	0,00	0,04	0,01	0,31	0,10
66											0,03	0,01	0,26	0,09
68											0,02	0,01	0,20	0,06
70											0,01	0,00	0,13	0,03
72											0,00	0,00	0,13	0,03
74													0,11	0,02
76													0,09	0,02
78													0,05	0,01
80													0,01	0,00

θ'	φ' 170		172		174		176		178		180	
	r_s	r_p	r_s	r_p	r_s	r_p	r_s	r_p	r_s	r_p	r_s	r_p
0	0,00	0,00	0,00	0,00	0,00	0,00	0,00	0,00	0,00	0,00	0,00	0,00
10	0,04	0,03	0,04	0,03	0,04	0,03	0,04	0,03	0,04	0,03	0,04	0,03
20	0,13	0,08	0,14	0,09	0,14	0,09	0,14	0,09	0,15	0,09	0,15	0,10
30	0,47	0,26	0,51	0,29	0,54	0,31	0,56	0,32	0,58	0,33	0,59	0,34
40	0,98	0,46	1,21	0,59	1,38	0,68	1,54	0,75	1,77	0,81	2,05	0,88
50	1,98	0,77	2,41	0,95	2,92	1,03	3,44	1,39	3,62	1,45	3,83	1,53
60	2,17	0,69	2,80	0,88	3,48	1,04	4,18	1,38	4,81	1,45	5,25	1,60
62	2,30	0,65	3,01	0,88	3,82	1,07	4,80	1,32	5,43	1,48	5,70	1,61
64	2,37	0,62	3,14	0,85	4,02	1,06	5,17	1,32	5,68	1,52	6,00	1,59
66	2,28	0,57	3,24	0,82	4,19	1,03	5,26	1,29	5,91	1,50	6,40	1,55
68	2,21	0,52	3,35	0,78	4,23	0,90	5,35	1,23	6,20	1,40	6,60	1,48
70	2,02	0,44	3,21	0,66	4,26	0,89	5,40	1,14	6,37	1,32	6,70	1,41
72	1,90	0,31	3,19	0,61	4,56	0,87	5,77	1,09	6,94	1,31	7,36	1,38
74	1,72	0,30	3,09	0,56	4,70	0,79	6,01	1,04	7,09	1,21	7,75	1,32
76	1,61	0,27	2,83	0,42	4,61	0,73	6,05	0,95	7,17	1,08	7,96	1,21
78	1,41	0,24	2,32	0,32	4,38	0,59	6,06	0,94	7,40	1,02	7,93	1,06
80	1,13	0,15	1,99	0,27	3,89	0,49	5,60	0,72	7,22	0,92	7,81	0,92
90	0,29	0,03	1,06	0,07	2,15	0,13	3,57	0,23	7,04	0,49	7,60	0,55

$\theta_1 = 70°$, $\lambda = 1{,}35$ см

θ'	φ' 100		110		120		130		140		150		160	
	r_s	r_p	r_s	r_p	r_s	r_p	r_s	r_p	r_s	r_p	r_s	r_p	r_s	r_p
0	0,00	0,00	0,00	0,00	0,00	0,00	0,00	0,00	0,00	0,00	0,00	0,00	0,00	0,00
10	0,00	0,00	0,01	0,01	0,01	0,01	0,02	0,01	0,03	0,02	0,03	0,02	0,04	0,03
20			0,01	0,01	0,02	0,01	0,03	0,01	0,05	0,03	0,07	0,06	0,10	0,08
30			0,00	0,00	0,01	0,01	0,03	0,01	0,07	0,04	0,13	0,10	0,30	0,23
40					0,00	0,00	0,02	0,01	0,05	0,03	0,17	0,12	0,53	0,32
50							0,00	0,00	0,02	0,01	0,11	0,06	0,60	0,30
60									0,01	0,00	0,05	0,02	0,39	0,17
62									0,01	0,00	0,04	0,01	0,37	0,15
64									0,00	0,00	0,04	0,01	0,32	0,12
66											0,03	0,01	0,27	0,10

θ′	φ′ = 100		110		120		130		140		150		160	
	r_s	r_p	r_s	r_p	r_s	r_p	r_s	r_p	r_s	r_p	r_s	r_p	r_s	r_p
68											0,02	0,01	0,20	0,07
70											0,01	0,00	0,13	0,05
72											0,00	0,00	0,13	0,04
74													0,11	0,03
76													0,09	0,02
78													0,05	0,01
80													0,01	0,00

θ′	φ′ = 170		172		174		176		178		180	
	r_s	r_p	r_s	r_p	r_s	r_p	r_s	r_p	r_s	r_p	r_s	r_p
0	0,00	0,00	0,00	0,00	0,00	0,00	0,00	0,00	0,00	0,00	0,00	0,00
10	0,04	0,03	0,04	0,03	0,04	0,03	0,04	0,03	0,04	0,03	0,04	0,03
20	0,13	0,10	0,15	0,11	0,15	0,11	0,15	0,11	0,16	0,11	0,16	0,11
30	0,48	0,32	0,52	0,34	0,55	0,37	0,57	0,38	0,59	0,40	0,60	0,41
40	1,01	0,66	1,26	0,69	1,43	0,84	1,59	0,93	1,83	1,02	2,13	1,09
50	2,06	0,95	2,50	1,16	3,02	1,48	3,56	1,66	3,74	1,82	3,96	1,91
60	2,25	0,85	2,90	1,15	3,60	1,46	4,32	1,67	4,96	1,89	5,11	2,06
62	2,39	0,83	3,12	1,14	3,95	1,39	4,95	1,69	5,60	1,97	5,88	2,08
64	2,46	0,79	3,25	1,12	4,15	1,39	5,33	1,71	5,86	1,97	6,18	2,09
66	2,37	0,73	3,35	1,06	4,33	1,31	5,42	1,67	6,09	1,94	6,57	2,05
68	2,29	0,66	3,46	0,98	4,37	1,29	5,52	1,60	6,37	1,84	6,77	1,96
70	2,10	0,57	3,32	0,89	4,40	1,19	5,57	1,50	6,51	1,79	6,87	1,85
72	1,97	0,51	3,29	0,83	4,71	1,15	5,95	1,47	7,11	1,75	7,53	1,85
74	1,78	0,40	3,19	0,74	4,85	1,06	6,19	1,40	7,26	1,66	7,91	1,76
76	1,67	0,35	2,93	0,62	4,76	0,94	6,23	1,28	7,34	1,56	8,12	1,63
78	1,46	0,27	2,41	0,48	4,52	0,80	6,24	1,15	7,57	1,34	8,09	1,43
80	1,17	0,22	2,07	0,35	4,02	0,68	5,78	0,96	7,89	1,28	7,97	1,23
90	0,30	0,03	1,09	0,07	2,23	0,17	3,69	0,23	7,21	0,57	7,76	0,54

$\theta_1 = 70°$, $\lambda = 1{,}6$ см

θ′	φ′ = 100		110		120		130		140		150		160	
	r_s	r_p	r_s	r_p	r_s	r_p	r_s	r_p	r_s	r_p	r_s	r_p	r_s	r_p
0	0,00	0,00	0,00	0,00	0,00	0,00	0,00	0,00	0,00	0,00	0,00	0,00	0,00	0,00
10	0,00	0,00	0,01	0,01	0,01	0,01	0,02	0,01	0,03	0,02	0,03	0,02	0,04	0,03
20			0,01	0,01	0,02	0,01	0,03	0,01	0,05	0,03	0,07	0,06	0,10	0,08
30			0,00	0,00	0,01	0,01	0,03	0,01	0,07	0,04	0,13	0,10	0,31	0,23
40					0,00	0,00	0,02	0,01	0,05	0,03	0,17	0,12	0,54	0,32
50							0,00	0,00	0,02	0,01	0,11	0,06	0,61	0,30
60									0,01	0,00	0,05	0,02	0,40	0,17
62									0,01	0,00	0,04	0,01	0,38	0,15
64									0,00	0,00	0,04	0,01	0,33	0,12
66											0,03	0,01	0,28	0,10
68											0,02	0,01	0,20	0,07
70											0,01	0,00	0,13	0,05
72											0,00	0,00	0,13	0,04
74													0,11	0,03
76													0,09	0,02
78													0,05	0,01
80													0,01	0,00

θ′	φ′ = 170		172		174		176		178		180	
	r_s	r_p	r_s	r_p	r_s	r_p	r_s	r_p	r_s	r_p	r_s	r_p
0	0,00	0,00	0,00	0,00	0,00	0,00	0,00	0,00	0,00	0,00	0,00	0,00
10	0,04	0,03	0,04	0,03	0,04	0,03	0,04	0,03	0,04	0,03	0,04	0,03
20	0,13	0,10	0,15	0,11	0,15	0,11	0,15	0,11	0,16	0,11	0,16	0,11
30	0,49	0,32	0,53	0,36	0,56	0,38	0,58	0,38	0,60	0,39	0,61	0,40
40	1,03	0,66	1,27	0,72	1,45	0,84	1,62	0,92	1,87	0,99	2,16	1,07
50	2,09	0,95	2,53	1,19	3,07	1,48	3,61	1,71	3,79	1,80	4,01	1,89
60	2,29	0,86	2,95	1,18	3,65	1,48	4,37	1,73	5,02	1,93	5,48	2,09
62	2,42	0,85	3,16	1,16	4,00	1,41	5,01	1,74	5,67	2,00	5,94	2,11
64	2,49	0,84	3,30	1,14	4,21	1,41	5,39	1,74	5,92	2,00	6,24	2,12
66	2,40	0,75	3,40	1,09	4,38	1,38	5,49	1,72	6,16	1,99	6,63	2,10
68	2,33	0,68	3,52	1,00	4,43	1,31	5,58	1,66	6,44	1,90	6,82	2,02
70	2,13	0,59	3,37	0,91	4,45	1,22	5,63	1,56	6,60	1,85	6,92	1,94
72	2,00	0,53	3,34	0,86	4,76	1,15	6,01	1,53	7,16	1,83	7,57	1,91
74	1,81	0,41	3,24	0,77	4,91	1,11	6,25	1,46	7,31	1,74	7,95	1,86
76	1,70	0,36	2,98	0,65	4,82	0,98	6,29	1,36	7,38	1,56	8,16	1,69
78	1,48	0,30	2,45	0,52	4,58	0,87	6,30	1,20	7,61	1,41	8,13	1,52
80	1,19	0,23	2,10	0,40	4,07	0,73	5,84	1,02	7,44	1,29	8,01	1,32
90	0,31	0,03	1,11	0,07	2,27	0,17	3,74	0,27	7,26	0,63	7,81	0,54

$\theta_1 = 70^\circ$, $\lambda = 3$ см

θ′	φ′ = 100		110		120		130		140		150		160	
	r_s	r_p	r_s	r_p	r_s	r_p	r_s	r_p	r_s	r_p	r_s	r_p	r_s	r_p
0	0,00	0,00	0,00	0,00	0,00	0,00	0,00	0,00	0,00	0,00	0,00	0,00	0,00	0,00
10	0,00	0,00	0,01	0,01	0,01	0,01	0,02	0,01	0,03	0,02	0,03	0,02	0,04	0,03
20			0,01	0,01	0,02	0,01	0,03	0,01	0,05	0,03	0,07	0,06	0,10	0,08
30			0,00	0,00	0,01	0,01	0,03	0,01	0,07	0,04	0,14	0,10	0,32	0,24
40					0,00	0,00	0,02	0,01	0,05	0,03	0,18	0,12	0,56	0,32
50							0,00	0,00	0,02	0,01	0,11	0,06	0,63	0,31
60									0,01	0,00	0,05	0,02	0,41	0,18
62									0,01	0,00	0,04	0,01	0,39	0,15
64									0,00	0,00	0,04	0,01	0,34	0,13
66											0,03	0,01	0,29	0,10
68											0,02	0,01	0,21	0,08
70											0,01	0,00	0,14	0,05
72											0,00	0,00	0,14	0,04
74													0,11	0,03
76													0,09	0,02
78													0,05	0,01
80													0,01	0,00

θ′	φ′ = 170		172		174		176		178		180	
	r_s	r_p	r_s	r_p	r_s	r_p	r_s	r_p	r_s	r_p	r_s	r_p
0	0,00	0,00	0,00	0,00	0,00	0,00	0,00	0,00	0,00	0,00	0,00	0,00
10	0,04	0,03	0,04	0,03	0,04	0,03	0,04	0,03	0,04	0,03	0,04	0,03
20	0,14	0,10	0,15	0,11	0,15	0,11	0,15	0,12	0,16	0,12	0,16	0,12
30	0,51	0,32	0,55	0,36	0,58	0,39	0,60	0,39	0,62	0,41	0,63	0,42
40	1,06	0,66	1,30	0,75	1,47	0,87	1,65	0,95	1,89	1,04	2,19	1,12
50	2,12	1,01	2,57	1,26	3,11	1,56	3,66	1,74	3,85	1,85	4,08	1,99

θ′	φ′ = 170		172		174		176		178		180	
	r_s	r_p	r_s	r_p	r_s	r_p	r_s	r_p	r_s	p	r_s	r_p
60	2,31	0,91	2,98	1,23	3,70	1,56	4,44	1,77	5,10	2,03	5,56	2,21
62	2,45	0,91	3,20	1,23	4,06	1,50	5,08	1,79	5,74	2,12	6,02	2,23
64	2,53	0,88	3,35	1,21	4,27	1,50	5,47	1,85	5,99	2,13	6,31	2,25
66	2,43	0,79	3,45	1,15	4,45	1,47	5,57	1,84	6,22	2,10	6,71	2,22
68	2,36	0,72	3,57	1,09	4,49	1,40	5,66	1,76	6,51	2,02	6,90	2,16
70	2,16	0,63	3,42	0,97	4,52	1,30	5,71	1,65	6,67	1,97	6,99	2,05
72	2,02	0,57	3,40	0,93	4,83	1,26	6,08	1,62	7,24	1,94	7,65	2,03
74	1,83	0,46	3,29	0,84	4,98	1,19	6,32	1,56	7,39	1,85	8,03	1,98
76	1,72	0,40	3,02	0,69	4,89	1,05	6,36	1,44	7,46	1,66	8,23	1,81
78	1,51	0,33	2,47	0,53	4,65	0,89	6,37	1,27	7,68	1,52	8,20	1,59
80	1,22	0,24	2,12	0,40	4,14	0,73	5,92	1,06	7,51	1,38	8,08	1,38
90	0,32	0,03	1,13	0,07	2,30	0,17	3,80	0,23	7,34	0,57	7,89	0,44

$\theta_1 = 70°$, $\lambda = 8{,}5$ см

θ′	φ′ = 100		110		120		130		140		150		160	
	r_s	r_p	r_s	r_p	r_s	r_p	r_s	r_p	r_s	r_p	r_s	r_p	r_s	r_p
0	0,00	0,00	0,00	0,00	0,00	0,00	0,00	0,00	0,00	0,00	0,00	0,00	0,00	0,00
10	0,00	0,00	0,01	0,01	0,01	0,01	0,02	0,01	0,03	0,02	0,03	0,02	0,04	0,03
20			0,01	0,01	0,02	0,01	0,03	0,01	0,05	0,03	0,07	0,06	0,10	0,08
30			0,00	0,00	0,01	0,01	0,03	0,01	0,07	0,04	0,14	0,10	0,32	0,25
40					0,00	0,00	0,02	0,01	0,05	0,03	0,18	0,12	0,57	0,32
50							0,00	0,00	0,02	0,01	0,11	0,06	0,61	0,31
60									0,01	0,00	0,05	0,02	0,41	0,19
62									0,01	0,00	0,01	0,01	0,39	0,16
64									0,00	0,00	0,01	0,01	0,34	0,13
66											0,03	0,01	0,29	0,11
68											0,02	0,01	0,21	0,08
70											0,01	0,00	0,14	0,05
72											0,00	0,00	0,14	0,04
74													0,11	0,03
76													0,09	0,02
78													0,05	0,01
80													0,01	0,00

θ′	φ′ = 170		172		174		176		178		180	
	r_s	r_p	r_s	r_p	r_s	r_p	r_s	r_p	r_s	r_p	r_s	r_p
0	0,00	0,00	0,00	0,00	0,00	0,00	0,00	0,00	0,00	0,00	0,00	0,00
10	0,04	0,03	0,04	0,03	0,04	0,03	0,04	0,03	0,04	0,03	0,04	0,03
20	0,14	0,10	0,15	0,11	0,15	0,11	0,15	0,12	0,16	0,12	0,16	0,12
30	0,52	0,33	0,56	0,36	0,59	0,39	0,61	0,40	0,63	0,41	0,64	0,42
40	1,07	0,68	1,31	0,75	1,49	0,87	1,67	0,97	1,91	1,07	2,21	1,14
50	2,13	1,04	2,59	1,27	3,13	1,59	3,68	1,78	3,87	1,94	4,10	2,04
60	2,33	0,93	3,01	1,25	3,72	1,58	4,46	1,80	5,12	2,07	5,58	2,26
62	2,47	0,93	3,23	1,24	4,08	1,53	5,11	1,83	5,77	2,17	6,05	2,29
64	2,55	0,88	3,37	1,23	4,29	1,53	5,50	1,88	6,04	2,18	6,35	2,31
66	2,45	0,81	3,48	1,20	4,47	1,52	5,60	1,87	6,26	2,17	6,74	2,30

θ'	φ' 170		172		174		176		178		180	
	r_s	r_p	r_s	r_p	r_s	r_p	r_s	r_p	r_s	r_p	r_s	r_p
68	2,38	0,74	3,59	1,11	4,51	1,45	5,69	1,82	6,54	2,09	6,93	2,23
70	2,18	0,65	3,44	1,01	4,54	1,33	5,74	1,71	6,71	2,04	7,03	2,13
72	2,04	0,58	3,42	0,96	4,86	1,31	6,11	1,68	7,27	2,00	7,69	2,10
74	1,85	0,50	3,31	0,85	5,00	1,23	6,36	1,60	7,41	1,90	8,06	2,04
76	1,74	0,41	3,04	0,72	4,91	1,08	6,39	1,49	7,50	1,72	8,27	1,87
78	1,52	0,35	2,49	0,55	4,67	0,92	6,40	1,31	7,72	1,57	8,24	1,64
80	1,23	0,24	2,14	0,40	4,16	0,74	5,95	1,10	7,55	1,42	8,11	1,45
90	0,32	0,03	1,15	0,07	2,32	0,17	3,82	0,23	7,37	0,57	7,92	0,44

$\theta_1 = 80°$, $\lambda = 0{,}8$ см

θ'	φ' 120		130		140		150		160		170	
	r_s	r_p	r_s	r_p	r_s	r_p	r_s	r_p	r_s	r_p	r_s	r_p
0	0,00	0,00	0,00	0,00	0,00	0,00	0,00	0,00	0,00	0,00	0,00	0,00
10	0,00	0,00	0,01	0,00	0,01	0,00	0,01	0,00	0,01	0,00	0,01	0,00
20	0,01	0,00	0,01	0,00	0,02	0,01	0,04	0,02	0,05	0,03	0,06	0,03
30			0,00	0,00	0,02	0,01	0,06	0,03	0,16	0,08	0,22	0,11
40					0,02	0,01	0,07	0,03	0,26	0,10	0,73	0,24
50					0,00	0,00	0,05	0,01	0,30	0,10	1,56	0,44
60							0,01	0,00	0,17	0,04	1,67	0,34
70							0,00	0,00	0,04	0,01	1,34	0,16
72									0,00	0,00	1,11	0,10
74											0,89	0,09
76											0,70	0,06
78											0,45	0,04
80											0,29	0,03
82											0,16	0,02
84											0,00	0,00

θ'	φ' 172		174		176		178		180	
	r_s	r_p	r_s	r_p	r_s	r_p	r_s	r_p	r_s	r_p
0	0,00	0,00	0,00	0,00	0,00	0,00	0,00	0,00	0,00	0,00
10	0,01	0,00	0,01	0,00	0,01	0,00	0,01	0,00	0,01	0,00
20	0,06	0,04	0,07	0,04	0,07	0,04	0,07	0,04	0,07	0,04
30	0,25	0,12	0,27	0,13	0,28	0,13	0,29	0,14	0,30	0,14
40	0,87	0,33	0,96	0,37	1,04	0,40	1,10	0,42	1,14	0,43
50	1,93	0,54	2,24	0,63	2,46	0,71	2,79	0,80	2,99	0,88
60	2,16	0,48	3,77	0,72	5,03	1,00	6,30	1,24	7,36	1,45
70	2,37	0,27	4,40	0,50	6,52	0,75	8,55	0,93	9,45	1,07
72	2,12	0,22	4,08	0,39	6,60	0,63	8,73	0,82	9,75	0,91
74	1,89	0,17	3,67	0,31	6,62	0,55	9,35	0,75	10,45	0,91
76	1,58	0,12	3,37	0,24	6,65	0,48	9,75	0,70	11,30	0,79
78	1,07	0,07	2,68	0,19	6,61	0,45	10,30	0,69	12,30	0,81
80	0,94	0,06	2,50	0,16	6,29	0,42	10,55	0,75	13,35	0,92
82	0,63	0,04	1,88	0,15	5,80	0,41	11,50	0,91	14,9	1,18
84	0,32	0,02	1,24	0,09	5,10	0,35	11,40	0,98	15,3	0,84
86	0,13	0,00	0,64	0,05	4,19	0,29	10,29	1,05	15,7	0,61
88	0,00	0,00	0,32	0,03	2,61	0,18	8,70	1,10	15,0	0,36
90			0,07	0,00	0,89	0,13	6,79	1,15	13,5	0,00

$\theta_1 = 80°$, $\lambda = 1{,}35$ см

θ'	φ' = 120		130		140		150		160		170	
	r_s	r_p	r_s	r_p	r_s	r_p	r_s	r_p	r_s	r_p	r_s	r_p
0	0,00	0,00	0,00	0,00	0,00	0,00	0,00	0,00	0,00	0,00	0,00	0,00
10	0,00	0,00	0,01	0,00	0,01	0,00	0,01	0,00	0,01	0,00	0,01	0,00
20	0,01	0,00	0,01	0,00	0,02	0,01	0,04	0,02	0,05	0,03	0,06	0,03
30			0,00	0,00	0,02	0,01	0,06	0,03	0,17	0,09	0,23	0,13
40					0,02	0,01	0,07	0,03	0,27	0,14	0,75	0,41
50					0,00	0,00	0,05	0,01	0,31	0,12	1,61	0,59
60							0,01	0,00	0,18	0,04	1,73	0,46
70							0,00	0,00	0,04	0,01	1,39	0,22
72									0,00	0,00	1,15	0,15
74											0,93	0,09
76											0,73	0,06
78											0,46	0,04
80											0,30	0,02
82											0,16	0,01
84											0,00	0,00

θ'	φ' = 172		174		176		178		180	
	r_s	r_p	r_s	r_p	r_s	r_p	r_s	r_p	r_s	r_p
0	0,00	0,00	0,00	0,00	0,00	0,00	0,00	0,00	0,00	0,00
10	0,01	0,00	0,01	0,00	0,01	0,00	0,01	0,00	0,01	0,00
20	0,06	0,04	0,07	0,04	0,07	0,04	0,07	0,04	0,07	0,04
30	0,26	0,14	0,28	0,15	0,29	0,16	0,30	0,17	0,31	0,18
40	0,90	0,48	0,99	0,53	1,07	0,56	1,14	0,60	1,19	0,62
50	1,99	0,72	2,31	0,85	2,53	0,97	2,87	1,08	3,08	1,16
60	2,23	0,66	3,88	1,00	5,16	1,40	6,46	1,74	7,54	2,04
70	2,44	0,41	4,44	0,73	6,68	1,07	8,73	1,35	9,63	1,55
72	2,18	0,32	4,16	0,56	6,76	0,94	8,92	1,19	9,93	1,41
74	1,95	0,27	3,78	0,48	6,78	0,82	9,53	1,15	10,64	1,29
76	1,63	0,16	3,47	0,37	6,82	0,70	9,93	0,99	11,50	1,02
78	1,11	0,13	2,76	0,27	6,77	0,62	10,49	0,87	12,52	0,99
80	0,97	0,09	2,57	0,20	6,45	0,46	10,74	0,74	13,58	0,90
82	0,65	0,06	1,94	0,14	5,95	0,37	11,71	0,76	15,14	0,95
84	0,33	0,02	1,29	0,09	5,23	0,29	11,60	0,72	15,54	0,71
86	0,13	0,00	0,66	0,05	4,32	0,22	11,50	0,68	15,94	0,48
88			0,33	0,03	2,69	0,15	8,89	0,64	15,24	0,24
90			0,07	0,00	0,93	0,07	6,96	0,60	13,74	0,00

$\theta_1 = 80°$, $\lambda = 1{,}6$ см

θ'	φ' = 120		130		140		150		160		170	
	r_s	r_p	r_s	r_p	r_s	r_p	r_s	r_p	r_s	r_p	r_s	r_p
0	0,00	0,00	0,00	0,00	0,00	0,00	0,00	0,00	0,00	0,00	0,00	0,00
10	0,00	0,00	0,01	0,00	0,01	0,00	0,01	0,00	0,01	0,00	0,01	0,00
20	0,01	0,00	0,01	0,00	0,02	0,01	0,04	0,02	0,05	0,03	0,06	0,03
30			0,00	0,00	0,02	0,01	0,06	0,03	0,17	0,09	0,23	0,14
40					0,02	0,01	0,07	0,03	0,27	0,15	0,76	0,42
50						0,00	0,05	0,01	0,31	0,13	1,64	0,60
60							0,01	0,00	0,18	0,04	1,76	0,48

θ′	φ′ 120		130		140		150		160		170	
	r_s	r_p	r_s	r_p	r_s	r_p	r_s	r_p	r_s	r_p	r_s	r_p
70							0,00	0,00	0,04	0,01	1,41	0,24
72									0,00	0,00	1,16	0,16
74											0,94	0,09
76											0,74	0,06
78											0,47	0,03
80											0,30	0,02
82											0,17	0,01
84											0,00	0,00

θ′	φ′ 172		174		176		178		180	
	r_s	r_p	r_s	r_p	r_s	r_p	r_s	r_p	r_s	r_p
0	0,00	0,00	0,00	0,00	0,00	0,00	0,00	0,00	0,00	0,00
10	0,01	0,00	0,01	0,00	0,01	0,00	0,01	0,00	0,01	0,00
20	0,06	0,04	0,07	0,04	0,07	0,04	0,07	0,04	0,07	0,05
30	0,26	0,15	0,28	0,16	0,29	0,17	0,30	0,18	0,31	0,18
40	0,91	0,48	1,00	0,55	1,09	0,58	1,15	0,62	1,20	0,64
50	2,03	0,75	2,35	0,87	2,58	1,00	2,92	1,11	3,13	1,19
60	2,27	0,68	3,93	1,07	5,23	1,45	6,54	1,80	7,63	2,10
70	2,48	0,43	4,48	0,75	6,76	1,09	8,83	1,41	9,73	1,61
72	2,23	0,34	4,21	0,57	6,84	0,96	9,01	1,29	10,04	1,47
74	1,99	0,28	3,83	0,49	6,86	0,83	9,63	1,16	10,74	1,33
76	1,66	0,16	3,52	0,37	6,89	0,70	10,01	0,99	11,61	1,07
78	1,12	0,13	2,80	0,27	6,85	0,60	10,59	0,89	12,63	1,01
80	0,98	0,09	2,62	0,20	6,53	0,46	10,85	0,74	13,71	0,90
82	0,66	0,06	1,98	0,14	6,02	0,37	11,82	0,76	15,28	0,93
84	0,33	0,02	1,30	0,09	5,30	0,29	11,72	0,71	15,68	0,70
86	0,13	0,00	0,67	0,05	4,37	0,22	11,60	0,66	16,09	0,46
88			0,33	0,03	2,73	0,15	8,98	0,61	15,38	0,23
90			0,07	0,00	0,94	0,07	7,04	0,57	13,87	0,00

$\theta_1 = 80°$, $\lambda = 3$ см

θ′	φ′ 120		130		140		150		160		170	
	r_s	r_p	r_s	r_p	r_s	r_p	r_s	r_p	r_s	r_p	r_s	r_p
0	0,00	0,00	0,00	0,00	0,00	0,00	0,00	0,00	0,00	0,00	0,00	0,00
10	0,00	0,00	0,01	0,00	0,01	0,00	0,01	0,00	0,01	0,00	0,01	0,00
20	0,01	0,00	0,01	0,00	0,02	0,01	0,04	0,02	0,05	0,03	0,06	0,03
30			0,00	0,00	0,02	0,01	0,06	0,03	0,17	0,10	0,23	0,15
40					0,02	0,01	0,07	0,03	0,28	0,16	0,77	0,45
50					0,00	0,00	0,05	0,01	0,32	0,13	1,67	0,64
60							0,01	0,00	0,18	0,04	1,78	0,51
70							0,00	0,00	0,04	0,01	1,42	0,25
72									0,00	0,00	1,17	0,17
74											0,95	0,09
76											0,75	0,06
78											0,48	0,03
80											0,31	0,02
82											0,17	0,01
84											0,00	0,00

θ′	φ′ 172		174		176		178		180	
	r_s	r_p	r_s	r_p	r_s	r_p	r_s	r_p	r_s	r_p
0	0,00	0,00	0,00	0,00	0,00	0,00	0,00	0,00	0,00	0,00
10	0,01	0,00	0,01	0,00	0,01	0,00	0,01	0,00	0,01	0,00
20	0,06	0,04	0,07	0,04	0,07	0,04	0,07	0,04	0,07	0,05
30	0,27	0,16	0,29	0,17	0,30	0,18	0,31	0,19	0,32	0,19
40	0,92	0,51	1,01	0,57	1,10	0,61	1,16	0,65	1,21	0,67
50	2,05	0,79	2,37	0,93	2,61	1,06	2,95	1,18	3,16	1,27
60	2,29	0,73	3,98	1,11	5,28	1,52	6,60	1,91	7,69	2,24
70	2,51	0,46	4,51	0,76	6,82	1,28	8,90	1,41	9,81	1,68
72	2,25	0,35	4,26	0,58	6,90	0,99	9,08	1,32	10,11	1,49
74	2,01	0,29	3,87	0,50	6,92	0,84	9,70	1,17	10,84	1,33
76	1,68	0,16	3,56	0,35	6,96	0,70	10,11	0,98	11,72	1,03
78	1,13	0,13	2,83	0,26	6,92	0,56	10,68	0,82	12,75	0,97
80	0,99	0,09	2,64	0,15	6,59	0,43	10,94	0,61	13,83	0,74
82	0,67	0,06	2,00	0,10	6,08	0,29	11,93	0,51	15,41	0,64
84	0,34	0,02	1,31	0,08	5,36	0,23	11,82	0,49	15,82	0,48
86	0,13	0,00	0,68	0,05	4,42	0,17	11,71	0,43	16,22	0,32
88	0,00	0,00	0,34	0,03	2,76	0,10	9,05	0,37	15,51	0,16
90			0,07	0,00	0,95	0,04	7,10	0,32	13,99	0,00

$\theta_1 = 80°$, $\lambda = 8{,}5$ см

θ′	φ′ 120		130		140		150		160		170	
	r_s	r_p	r_s	r_p	r_s	r_p	r_s	r_p	r_s	r_p	r_s	r_p
0	0,00	0,00	0,00	0,00	0,00	0,00	0,00	0,00	0,00	0,00	0,00	0,00
10	0,00	0,00	0,01	0,00	0,01	0,00	0,01	0,00	0,01	0,00	0,01	0,00
20	0,01	0,00	0,01	0,00	0,02	0,01	0,04	0,02	0,05	0,03	0,06	0,03
30			0,00	0,00	0,02	0,01	0,06	0,03	0,17	0,10	0,23	0,15
40	↓				0,02	0,01	0,07	0,03	0,28	0,16	0,78	0,45
50					0,00	0,00	0,05	0,01	0,32	0,14	1,68	0,65
60							0,01	0,00	0,18	0,04	1,80	0,52
70							0,00	0,00	0,04	0,01	1,43	0,26
72									0,00	0,00	1,18	0,18
74											0,95	0,09
76											0,75	0,06
78											0,48	0,03
80											0,31	0,02
82											0,17	0,01
84											0,00	0,00

θ′	φ′ 172		174		176		178		180	
	r_s	r_p	r_s	r_p	r_s	r_p	r_s	r_p	r_s	r_p
0	0,00	0,00	0,00	0,00	0,00	0,00	0,00	0,00	0,00	0,00
10	0,01	0,00	0,01	0,00	0,01	0,00	0,01	0,00	0,01	0,00
20	0,06	0,04	0,07	0,04	0,07	0,04	0,07	0,04	0,07	0,05
30	0,27	0,16	0,29	0,17	0,30	0,18	0,31	0,19	0,32	0,20

θ′	φ′ 172		174		176		178		180	
	r_s	r_p	r_s	r_p	r_s	r_p	r_s	r_p	r_s	r_p
40	0,93	0,52	1,02	0,59	1,11	0,62	1,17	0,66	1,22	0,69
50	2,06	0,81	2,39	0,95	2,62	1,09	2,97	1,21	3,18	1,30
60	2,31	0,79	3,99	1,17	5,31	1,71	6,62	1,97	7,71	2,32
70	2,53	0,47	4,53	0,80	5,85	1,35	8,93	1,46	9,84	1,75
72	2,26	0,36	4,28	0,60	6,93	1,01	9,11	1,34	10,16	1,50
74	2,02	0,30	3,89	0,51	6,95	0,85	9,74	1,18	10,88	1,33
76	1,70	0,16	3,58	0,35	6,98	0,70	10,16	0,98	11,76	1,03
78	1,14	0,13	2,85	0,26	6,94	0,55	10,72	0,83	12,79	0,97
80	1,00	0,09	2,66	0,15	6,61	0,37	10,99	0,64	13,89	0,74
82	0,67	0,06	2,01	0,10	6,11	0,27	11,97	0,49	15,47	0,56
84	0,34	0,02	1,33	0,08	5,39	0,21	11,86	0,43	15,88	0,42
86	0,13	0,00	0,69	0,05	4,44	0,15	11,75	0,37	16,28	0,28
88			0,34	0,03	2,78	0,10	9,08	0,31	15,57	0,15
90			0,07	0,00	0,95	0,04	7,13	0,25	14,04	0,00

Comments: 1. In computing the emission coefficients from Formula (8) it is necessary to convert from angles θ_n and ϕ_n to angles θ′ and θ′. Further on, in correspondence with the normalization in [6], θ′ should be taken in degrees and θ′ in radians.

2. The unfinished graphs in the tables denote zero values of the brightness coefficients.

DETERMINING THE TEMPERATURE OF THE WATER SURFACE FROM RADIO EMISSION IN THE CENTIMETER BAND

Yu. I. Rabinovich, G.G. Shchukin and V.V. Melent'yev

ABSTRACT: The possibility of aircraft measurements of the temperature of the water surface in the microwave band is discussed, the use of which will permit obtaining information on the temperature of the underlying surface even in the presence of hydrometeoric formations. The method of the measurements is studied, according to which at the present time only relative measurements can be made, using the data of ground measurements to tie in the water temperature at individual points of the route. The results of investigations are cited that were carried out in the regions of Lake Ladoga and the Caspian Sea. Comparison of the experimental data with ground measurements showed that the mean square deviation is about 2°.

Determining the temperature of the underlying surface from aircraft according to its emission is an important geophysical problem. Such investigations have been made for some time now in the infrared band of the spectrum, measurements which are strongly distorted by the effect of the atmosphere. In the presence of a cloud cover the possibility is generally eliminated of making measurements in the IR-band. /49

The use of the microwave band of the spectrum permits obtaining information concerning the temperature of the underlying surface through clouds and precipitation, the effect of which is diminished with increase in wave length. Large instrument errors of the microwave measuring apparatus may be substantially reduced even at the present time due to improvements in the apparatus and the methods of calibration.

As noted in [1], taking the problems associated with absolute calibration of the radiometric apparatus into account, at the present time we may make only relative measurements and use them for tying in the data from ground measurements of the water temperature at individual points of the route. The second limitation is due to the transition from measured radiobrightness temperatures to true temperatures, for which we must know the emission coefficient of the surface. Just as in the infrared band, the temperature can be determined only for a limited number of surfaces and mainly for a water surface, whose emission coefficients have been studied quite well as a function of the condition of the water [2].

To measure the temperature of the water surface we used a

radiometric apparatus in the three-centimeter band. First of all we made an evaluation of the possibility of using aircraft for absolute measurements of the temperature of the water surface. The fluctuation sensitivity of the radiometer is about 1.5° K. Hence, if we allow for the fact that the error in measurements is caused only by the sensitivity of the apparatus, the precision in the measurements of the temperature of the water will be no more than 3 - 4° C.

The real accuracy of the measurements in the channel λ = 3.2 cm will not exceed 3° C, since errors exist, on the one hand, due to the apparatus, i.e., the nonlinearity of the channel and errors in determining the calibration signal, and on the other hand, errors in determining the emission coefficient of the water surface, i.e., the effect of temperature and salinity.

Moreover, in measuring in the three-centimeter band further errors may arise due to the effect of the atmosphere, which can be taken into account using the results obtained in [3] and [4]. These data show that in changing the moisture content of a cloud-free atmosphere from 0 to 60 mm of precipitated water the correction to the radiobrightness temperature is from 2.5 to 5.5° K. Consequently, if no data exist on the moisture content of the atmosphere, the error will not exceed 1.5° K. With an increase in wave length up to 8 - 10 cm the effect of the atmosphere on the radiobrightness temperature drops sharply and under analogous conditions is several

/50

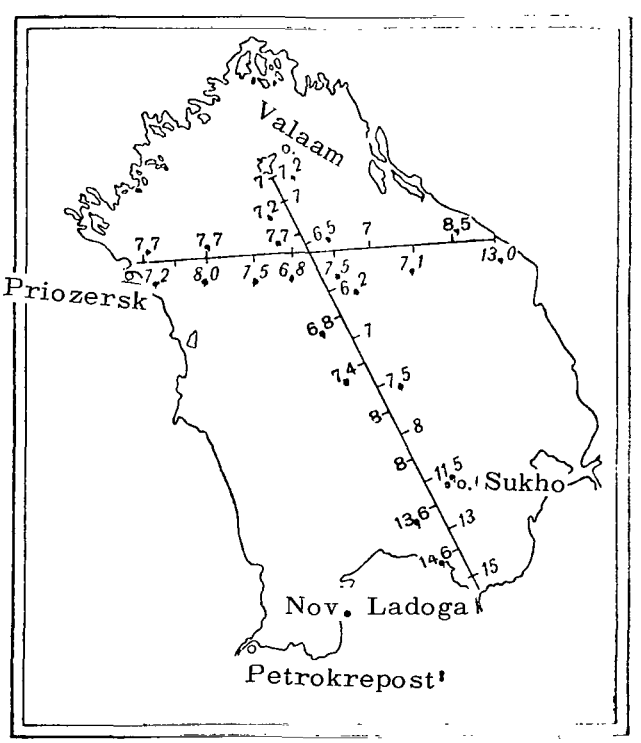

Fig. 1.

tens of degrees.

Measurements of the temperature of the water surface were made using a radiometric apparatus, installed on an IL-18 airplane, in the regions of the Caspian Sea and Lake Ladoga [5]. To make the results of the measurements absolute, we used both data from the hydrometeorological stations and special measurements of the water temperature using an infrared radiation thermometer from the Main Geophysical Observatory, installed on an IL-14 airplane. For comparison at the Caspian Sea we also used data of measurements of the temperature on cruise ships of the merchant marine.

Figure 1 shows a map of Lake Ladoga, on which are plotted the temperatures of the water obtained from data of measurements made by the IR-apparatus (italic type) and from the radiometer (regular type), operating in the three-centimeter band. The temperature drops measured on the segment Valaam-Novaya Ladoga with the two instruments differ only by 0.5°. On individual segments of the route the divergences reach 1°. These measurements were made at night in a cloud-free sky.

Similar results were obtained in the temperature mapping of Lake Ladoga, made October 10 during the day (Fig. 2). Here, no measurements by the infrared radiation thermometer were made and for comparison we used the measurements from the stations at Sukho and Valaam. /51

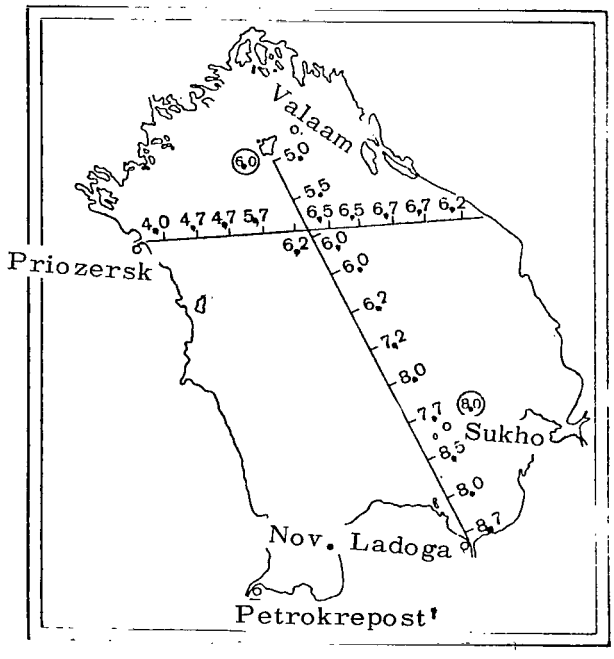

Fig. 2.

Figure 3 shows a map of the Caspian Sea, obtained by measurements for several days in the Fall of 1966. Four routes are plotted on the map; they were made for the period from September 28 to October 8, 1966. The measurements on the route Neftyanyye Kamni - Tyuleniy on October 8 were accompanied by simultaneous measurements of the water temperature by an infrared radiation thermometer from the MGO* installed on an IL-14 airplane. All the measurements were made during cloud-free or slightly cloudy weather (2 - 3 points on the Cu scale), with the exception of the flight on October 8, during which time at individual segments (to the north of the Makhachkala Traverse) the cloud cover reached 7 - 8 points.

*MGO = Main Geophysical Observatory.

To evaluate the error in the measurements we made multiple measurements of the water temperature on a segment with a constant temperature expanse near 30 km in the region of Neftyanyye Kamni. The water temperature was controlled by the data from measurements of the Hydrometeorological Service of Neftyannyę Kamni. During a period of one hour we made 20 measurements of the temperature:

Measurement	1	2	3	4	5	6	7	8	9	10
Temperature, deg.	21.6	20.8	20.2	21.3	21.0	21.0	20.8	20.2	20.8	20.5
Measurement	11	12	13	14	15	16	17	18	19	20
Temperature, deg.	21.0	20.5	20.2	21.6	22.6	21.3	21.0	20.2	22.4	20.5

Average 21.0

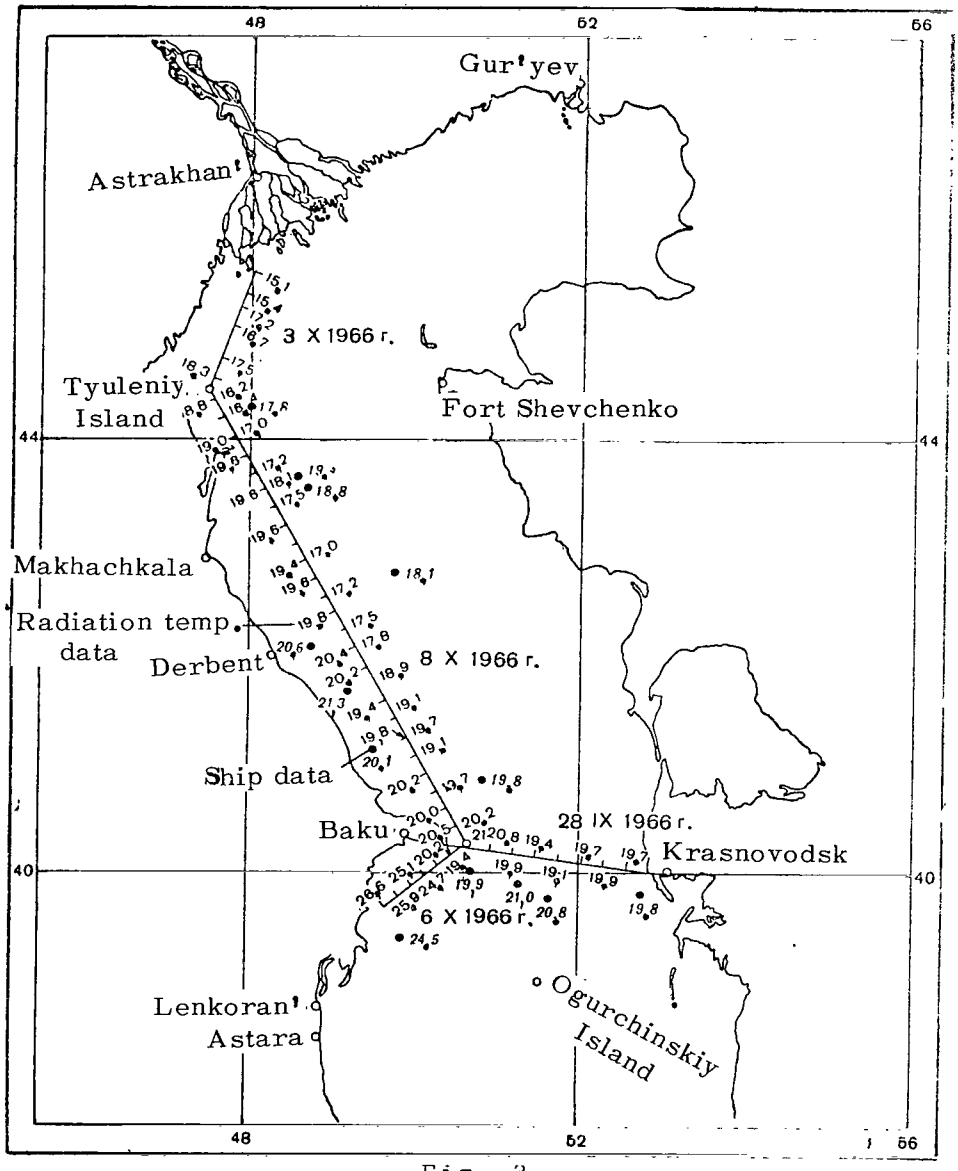

Fig. 3.

/52

The mean temperature, obtained from these measurements, practically agreed with the true temperature of the water according to the data of measurements by the Hydrometeorological Service of Neftyannye Kamni. The divergence was only 0.3°. The mean square error in the measurements with respect to the mean temperature was 0.7°. The greatest deviation from the mean value Δt_{max} = 1.6°. /53

Similar comparisons were made from the results of measurements on the route Neftyannye Kamni - Tyuleniy, which were accompanied by measurements of the water temperature by a radiation thermometer. In this case the greatest divergence between measurements Δt_{max} = 2.9°, and the mean square deviation between the 19 measurements, obtained on the route, was about 2°. The rather poor results in determining the water temperature here can be explained by the effect of the salinity of the water, which varied considerably along the route. In computing the true temperature of the water we used a constant emission coefficient along the entire route.

The obtained results show that the method of measuring the water temperature from radio emission, although it does not compete in accuracy of the absolute values with the methods of infrared technology, is still quite promising. Use of the 8 - 10 cm band permits virtually eliminating the effect of the atmosphere and carrying out measurements through clouds. However it is necessary to substantially increase the fluctuation sensitivity of the radiometer, bringing it to 0.2 - 0.5° K.

REFERENCES

1. Gurvich, A.S. and S.T. Yegorov: Opredeleniye temperatury poverkhnosti morya po yeyo teplovomu izlucheniyu. (Determining the Temperature of the Surface of the Sea from its Thermal Emission), Fizika atmosfery i okeana, Vol. 2, No. 3, 1966.
2. Shifrin, K.S. and S.N. Ionina: Teplovoye izlucheniye i otrazheniye ot volnuyushcheysya poverkhnosti morya v mikrovolnovoy oblasti. (Thermal Emission and Reflection from a Rough Sea Surface in the Microwave Band)., See this Collection.
3. Rabinovich, Yu.I. and G.G. Shchukin: Opredeleniye soderzhaniya vodyanogo para v atmosfere po izmereniyu mikrovolnovogo izlucheniya. (Determining the Amount of Water Vapor in the Atmosphere from Measuring Microwave Radiation). See this Collection.
4. Volchok, B.A. and M.M. Chernyak: Perenos mikrovolnovogo izlucheniya v oblakakh i osadkakh. (Transfer of Microwave Radiation in Clouds and Precipitation)., See this Collection.
5. Rabinovich, Yu. I., G.G. Shchukin and V.G. Volkov: O vozmozhnykh pogreshnostyakh absolyutnykh izmereniy radioizlucheniya. (Possible Errors in Absolute Measurements of Radio Emission). See this Collection.

THERMAL RADIATION FROM ICE IN THE CENTIMETER AND DECIMETER BANDS

A.A. Kurskaya, L.V. Fedorova and G.D. Yakovleva

ABSTRACT: The results of the brightness temperature of the total thermal radiation from water and a layer of uniform ice with plane interfaces at wave lengths of 3, 10 and 30 cm for vertical and horizontal polarization at angles of sighting from 10 to 90° in the temperature range of the ice surface from -5 to -30° C are discussed. The computational data are compared with the experimental data obtained during radiometric investigations of the thermal radiation from fresh and sea water in the wave bands of 3.2 and 30 cm. An analysis of the polarization properties of the thermal radiation from water and an ice layer in these wave bands is given.

1. Computational Relationships and Electrical Properties of Water and Ice.

In the radiowave band the brightness temperature of the thermal radiation of a uniform semi-infinite medium is determined by the expression /54

$$T_b = \int_0^\infty \varkappa(r)\, T(r) \exp(-\tau_r)\, dr, \qquad (1)$$

where $\kappa(r)$ is the coefficient of absorption of the electromagnetic energy in the medium, $T(r)$ is the thermodynamic temperature of the medium in degrees Kelvin, $h_2 = \frac{\cos h_1}{\sqrt{\varepsilon_2}}$, is the optical thickness of the medium and r is the length of the path of integration of the thermal radiation.

Let us look at the case of a three-layered space (Fig. 1), when a uniform ice layer of finite thickness l_2 with plane interfaces is found on the surface of the water (medium 3).

The thermal radio emission assumed in the air in this case consists of three components, representing radiation from the water, which has passed through the water/ice and ice/air interface, direct radiation from the ice layer, which has passed through the ice/air interface and finally, reradiation from the ice layer which is reflected from the ice/water interface and has passed through the ice/air interface. The thermal radiation from the water and the

reradiation from the ice along with absorption in the ice layer undergo repeated reflections at its boundaries.

As a result of the large absorption in water, a very thin layer will radiate that is directly adjacent to the ice surface, whose thermodynamic temperature may be assumed constant and equal to 273° K.

Taking the above into account, if we substitute the variable under the integral in formula (1) by $r_2 = z \operatorname{cosec} h_2$, for the brightness temperature of the total radiation from the water and the ice layer, assumed in the air at the incident angle h_1 and define it by $T_{b\,321}$, we can write the following expression:

$$T_{b321} = [1 - |R_{21}(h_1)|^2]\left\{\left[1 + \sum_{n=1}^{\infty} |R_{21}(h_1)|^{2n} |R_{23}(h_1)|^{2n} \times \right.\right.$$
$$\times \exp\left(-2n \int_0^{l_2} \varkappa_2 [T_2(z)] \operatorname{cosec} h_2 \, dz\right) [T_3(1 - |R_{23}(h_1)|^2) + |R_{23}(h_1)|^2 \times$$
$$\times \int_0^{l_2} \varkappa_2 [T_2(z)] T_2(z) \operatorname{cosec} h_2 \exp\left(-\int_0^{z} \varkappa_2 [T_2(z)] \cdot \operatorname{cosec} h_2 \, dz\right) dz\Big] +$$
$$\left. + \int_0^{l_2} \varkappa_2 [T_2(z)] T_2(z) \operatorname{cosec} h_2 \exp\left(-\int_0^{z} \varkappa_2 [T_2(z)] \operatorname{cosec} h_2 \, dz\right) dz \right\}, \quad (2)$$

/55

where T_3 is the thermodynamic temperature of the radiating layer of water, equal to 273° K, $T_2(z)$ is the thermodynamic temperature of the ice layer, which depends linearly on z, $R_{21}(h_1)$ and $R_{23}(h_1)$ are the Fresnel reflection coefficients at the ice/air and ice/water interfaces, which are determined by complex dielectric constants of the respective media, $\kappa_2[T_2(z)]$ is the absorption coefficient of the electromagnetic energy in the ice layer which depends on its temperature. The angle h_2 is related to the angle h_1 by Snellius law. In this case $\tau_r = \int_0^r \varkappa(r)\,dr$ —, since $\varepsilon_1 = 1$.

The computations of the radiobrightness temperature $T_{b\,321}$ were made on a BESM-2 computer for wave lengths 3, 10 and 30 cm at different temperatures of the ice surface in a range from -5 to -30° C. The values of the electrical parameters of the water and ice, taken from references [1-5] were used in making the computations.

Table 1 gives for the three wave lengths ε and tan δ for fresh water at a temperature of 0° C and fresh ice at a temperature of -12° C.

The temperature dependence ε of ice is apparent only at

frequencies less than 10^5 Hz, therefore in the range under analysis this value ε does not depend on temperature. In the centimeter band, tan δ for the ice decreases almost exponentially with decrease in temperature [2]. The coefficient of absorption of the electromagnetic energy in the ice layer, taking into account that tan δ of the ice with below-zero temperatures is considerably less than unity, can be computed from the formula,

$$\kappa = \frac{2\pi \tan \delta \sqrt{\varepsilon}}{\lambda} \text{ neper/m},$$

or

$$\kappa = \frac{2\pi \cdot 8.686 \tan \delta \sqrt{\varepsilon}}{\lambda} \text{ db/m}. \quad (3)$$

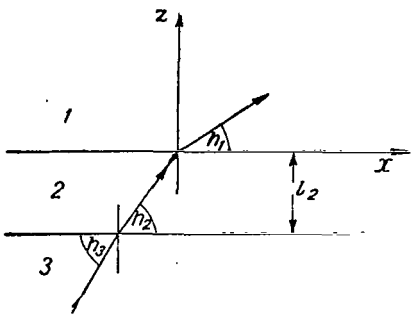

Fig. 1. Schematic of a Three-Layered Space. 1. Air ($\varepsilon_1 = 1$); 2. Ice (ε_2, $\tan_2\delta$); 3. Water (ε_3, $\tan_3\delta$).

TABLE 1: THE VALUES OF ε AND tan δ FOR FRESH WATER AND FRESH ICE

λ :	Water 0° C		Ice —12° C	
	ε	$\tan\delta \cdot 10^4$	ε	$\tan\delta \cdot 10^4$
3	40	10 000	3,1	7
10	80	4 000	3,25	9
30	90	1 100	3,4	12,5

2. Analysis of the Results of Computing $T_{b\ 321}$.

The computational results of the radiobrightness temperature, /57 carried out for the vertical and horizontal polarization with change in the incident angle h_1 from 10 to 90°, are shown on Figure 2. The total thermal radiation from the water and the ice layer is a polarized radiation. In the case of small incident angles the degree to which $T_{b\ 321}$ depends on the thickness of the ice l_2 is quite small and increases smoothly with increase in the incident angle for horizontal polarization in the range of angles from 10 to 90° and for vertical polarization - from 10 to 25°, remaining constant with any further increase in the incident angle.

With an increase in wave length the brightness temperature is lowered, especially sharply in the wave band up to 10 cm. In the decimeter band the dependence of $T_{b\ 321}$ on wave length is expressed more weakly.

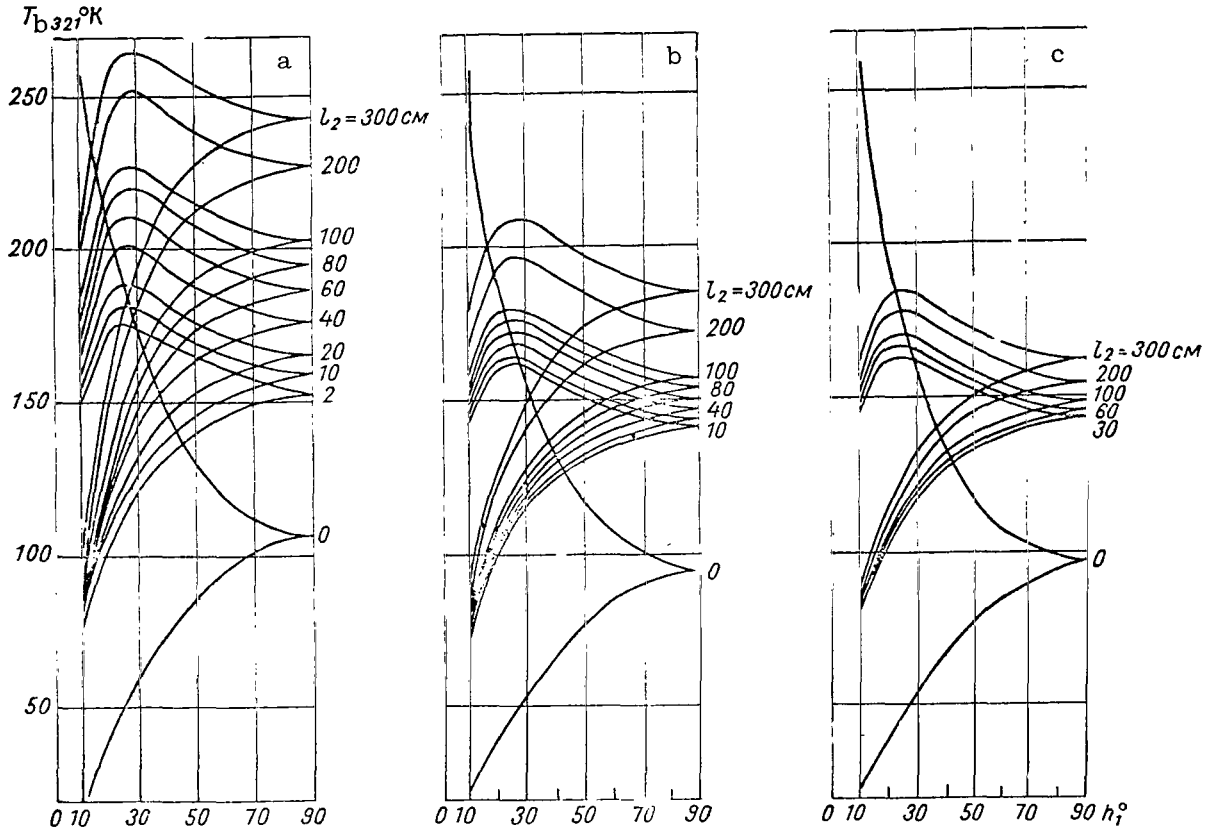

Fig. 2. Brightness Temperature $T_{b\ 321}$ as a Function of the Incident Angle h_1 For Vertical and Horizontal Polarization For Three Wave Lengths and Different Thicknesses of the Ice. a. λ = 3 cm, $t_{ice\ surf.}$ = -5° C; b. λ = 10 cm, $t_{ice\ surf.}$ = -10° C; c. λ = 30 cm, $t_{ice\ surf.}$ = -10° C.

With an ice thickness not exceeding 110 cm the greatest slope of the curve $T_{b\ 321} = f(l_2)$ occurs at a wave length of 3 cm, and rapidly decreases with increase in ice thickness in comparison with its slower increase at a wave length of 10 cm. The steepness of the curve $T_{b\ 321} = f(l_2)$ at a wave length of 30 cm is virtually constant with increase in ice thickness. Thus, with a large ice thickness (l_2 > 100 cm) the difference in the steepness of the curves depicting brightness temperature as a function of ice thickness is smoothed out at the various wave lengths.

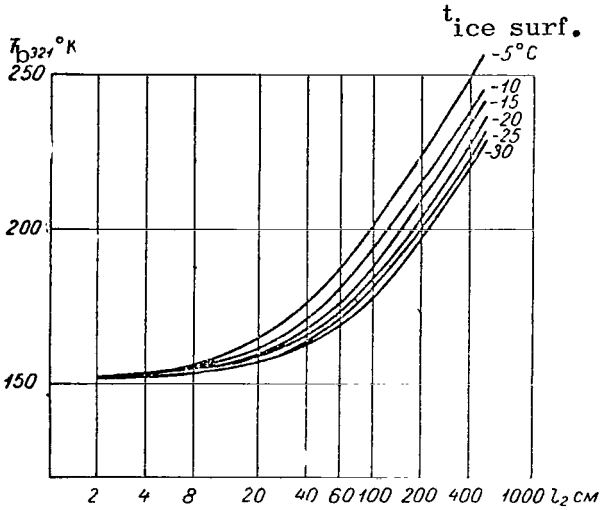

Fig. 3. Brightness Temperature $T_{b\ 321}$ as a Function of Thickness of the Ice at a 3 cm Wave Length and an Incident Angle of $h_1 = 90°$ for Different Ice Surface Temperatures.

The effect of temperature of the ice surface on brightness temperature of emission in the case of the model under study increases with increase in the ice thickness and is characterized by a decrease in $T_{b\ 321}$ with lowered surface temperature (Figs. 3 - 5).

Along with the computations of the brightness temperature of the total radiation from the water and the ice layer we made computations of the radiobrightness temperature of the thermal radiation from an open water surface at a temperature of 0° C. The computations were made from the formula,

$$T_{b31} = T_3(1 - |R_{31}(h_1)|^2), \qquad (4)$$

where T_3 is the thermodynamic temperature of the radiating layer of water, equal to 273° K, $R_{31}(h_1)$ is the Fresnel reflection coefficient at the interface water/air.

The dependence of $T_{b\ 321}$ on the incident angle h_1 for vertical and horizontal polarization for the three wave lengths is shown on Figure 2 (the case of $l_2 = 0$). /59

With horizontal polarization the formation of a comparatively thin layer of transparent ice with a thickness on the order of the wave length and any incident angle on the surface of the water is accompanied by a sudden jump in the brightness temperature which is approximately 45 - 50° K.

With vertical polarization the radiobrightness temperature of

radiation from the water which has passed through a layer of transparent ice becomes greater than the radiobrightness temperature of the radiation from an open water surface with incident angles that exceed the Brewster angle. Another distinguishing feature of the thermal radiation from the water covered with a layer of ice is its relative depolarization in comparison with radiation from an open water surface.

The degree of polarization may be characterized by the coefficient of polarization which is equal to the ratio of the difference in brightness temperatures with vertical and horizontal polarization to their sum:

$$p = \frac{T_{b\ vert} - T_{b\ horiz}}{T_{b\ vert} + T_{b\ horiz}} \qquad (5)$$

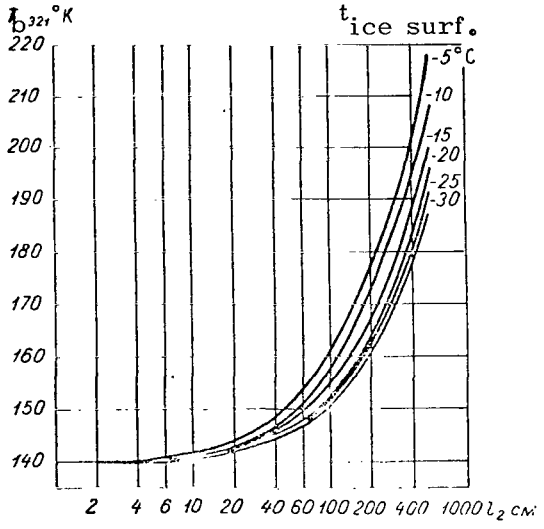

Fig. 4. Brightness Temperature $T_{b\ 321}$ as a Function of Ice Thickness at a Wave Length of 10 cm and an Incident Angle of $h_1 = 90°$ for Different Temperatures of the Ice Surface.

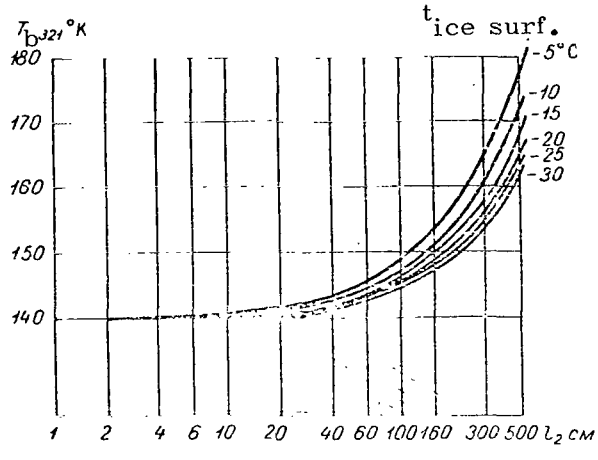

Fig. 5. Brightness Temperature $T_{b\ 321}$ as a Function of Ice Thickness at a Wave Length of 30 cm and an Incident Angle of $h_1 = 90°$ for Different Temperatures of the Ice Surface.

3. Comparison with Experimental Data

For comparison of the computational data with experimental data we used the results of radiometric investigations of the thermal radiation from fresh ice with a thickness of 70 - 90 cm on the Medvezh' Lakes in the Moscow District and sea ice with a thickness of 1.8 - 2 m in the region of Dixon Island at wave lengths of 3.2

and 30 cm.

The relative errors in measuring the brightness temperature at a wave length of 3.2 cm on the average was 13% and at a wave length of 30 cm, 20%. For the purpose of eliminating any effect from the snow cover in carrying out the measurements of the radio emission from pure ice, we removed the snow.

Typical examples of the comparison of the computation curves depicting the dependence of $T_{b\,321}$ on the incident angle h_1 with vertical and horizontal polarization with experimental data for fresh ice are shown on Figures 6 and 7. At a wave length of 3.2 cm the radio emission is substantially depolarized: the experimental values of the brightness temperatures with vertical polarization are smaller than, and with horizontal polarization are greater than, the computational values. At a wave length of 30 cm, the polarization properties of the radiation are expressed more strongly than in the centimeter band.

As is clear from Figure 8, the values of the polarization characteristics for different optical thicknesses of the ice τ_r agree sufficiently well with the computed curves, representing the model being studied with plane boundaries. Comparison of the polarization characteristics in the decimeter and centimeter bands (Figs. 9 and 10) shows that the degree of depolarization of the radiation in comparison with the computational data is increased significantly with shortening of the wave length. This can be explained obviously by the larger effect from the irregularity in the interface in the centimeter band.

Figure 11 shows two computed curves of the coefficient of polarization for a smooth and an irregular interface ice/air when $\varepsilon_2 = 3.1$. The experimental points obtained in measuring the thermal radiation from fresh ice at a wave length of 3.2 cm are similar to the computed curve for an irregular surface.

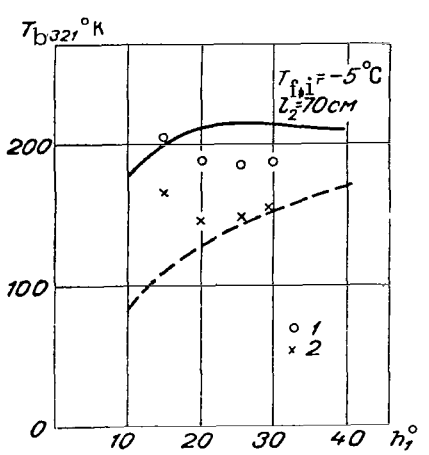

Fig. 6. Comparison of the Brightness Temperature of the Thermal Radiation from Fresh Ice with Computed Curves at a Wave Length of 3.2 cm. 1. Vertical Polarization; 2. Horizontal Polarization.

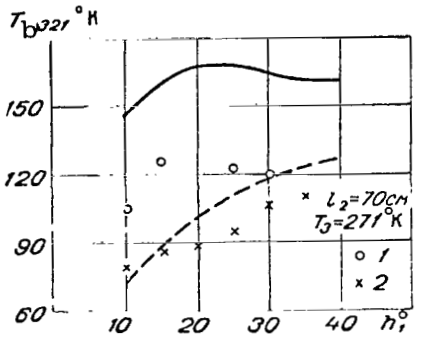

Fig. 7. Comparison of the Brightness Temperature of the Thermal Radiation from Fresh Ice with Computed Curves at a Wave Length of 30 cm. Designations are the Same as in Figure 6.

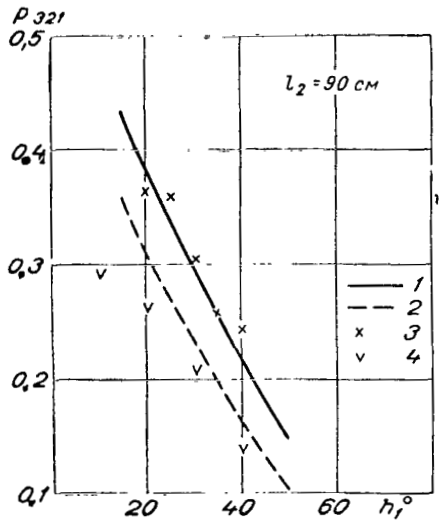

Fig. 8. Comparison of Polarization Characteristics of the Thermal Radiation from Fresh Ice with Computed Curves with Different Optical Thicknesses of the Ice at a Wave Length of 30 cm. 1. τ_r = 0.215; 2. τ_r = 0.43; 3. March 19, T_1 = -4° C; 4. March 28, T_1 = -1.5° C.

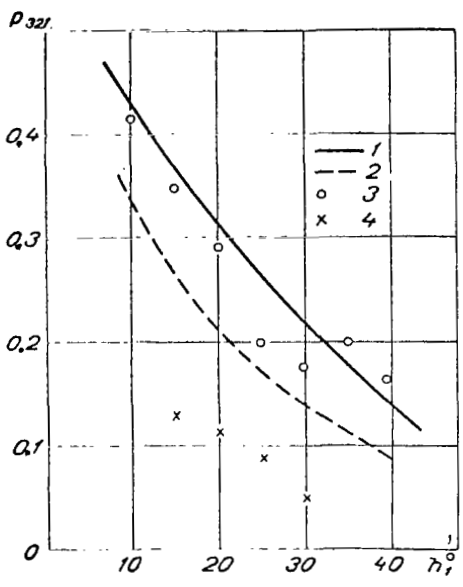

Fig. 9. Comparison of Polarization Characteristics of the Thermal Radiation from Fresh Ice with a Thickness of 70 cm with Computed Curves. 1. τ_r = 0.02; 2. ε_2 = 3.1; 3. λ = 30 cm; 4. λ = 3.2 cm.

From Figure 10 it follows that the integral absorption in a layer of sea ice is large in comparison with fresh ice. The polarization curve for sea ice lies below the polarization curve for fresh ice.

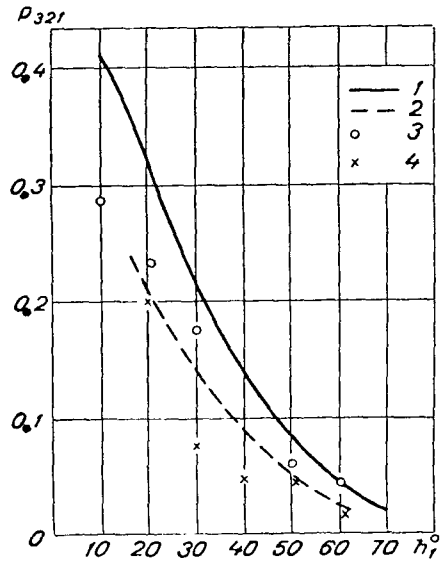

Fig. 10. Comparison of the Polarization Characteristics of Thermal Radiation from Sea Ice with Computed Curves. 1. $\tau_r = 0.04$; 2. $\varepsilon_2 = 3.1$; 3. $\lambda = 30$ cm; 4. $\lambda = 3.2$ cm.

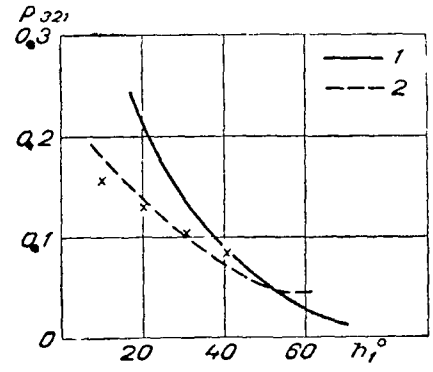

Fig. 11. Comparison of the Polarization Characteristics of Thermal Radiation from Fresh Ice with a Thickness of 90 cm at a Wave Length of 3.2 cm with Computed Curves for a Smooth (1) and a Rough (2) Interface Ice/Air when $\varepsilon_2 = 3.1$, $T_1 = 6^\circ$ C, $h_r = 40^\circ$.

REFERENCES

1. Khippel', A: Dielektriki i ikh primeneniye. (Dielectrics and their Use). Gosenergoizdat, Moscow-Leningrad, 1959.
2. Cumming, W.A.: Dielectric Properties of Ice and Snow. J. Appl. Phys., Vol. 23, Nos. 7 - 8, 1952.
3. Watt, A.D. and E.L. Maxwell: Measured Electrical Properties of Snow and Glacial Ice. J. Res. Nat. Bur. Stand., Vol. 24D, No. 4, July-August, 1960.
4. Rudakov, V.N. and V.V. Bogorodskiy: K voprosu ob izmerenii tolshchiny lednikov elektromagnitnymi metodami. (The Question of Measuring the Thickness of Glaciers by Electromagnetic Methods). Zh. Teor. Fiz., Vol. 30, No. 1, 1960.
5. Saxton, J.A. et al: Dielectric Properties of Sea Water. "Wireless Engineer", Vol. 29, No. 349, October 1952.

DETERMINING THE WATER VAPOR CONTENT IN THE ATMOSPHERE FROM MEASUREMENTS OF MICROWAVE RADIATION

Yu. I. Rabinovich and G.G. Shchukin

ABSTRACT: The transfer of microwave radiation in a cloud-free atmosphere for different models and for several real profiles of humidity and temperature is studied. The results of ground measurements of the thermal radio emission from the atmosphere in lines of absorption of water vapor $\lambda = 1.35$ cm and of aircraft measurements of the total radio emission from the system Earth-atmosphere are cited. These data are used for determining the total water vapor content in the atmosphere as a function of the meteorological conditions. A comparison of the ground and aircraft measurements is made with the theoretical computations. The mean relative error in determining the total water vapor content is found to be in the range from 11 to 16%. It is shown that with such measurements, using a radiometric apparatus installed on artificial Earth satellites, over the water surface 8 - 10 gradations can be obtained in the total water vapor content in the atmosphere in the range of its possible variation from 5 to 60 mm of precipitated water.

Introduction. Basic Methods

Determination of the total moisture content and the vertical distribution of water vapor in the atmosphere is a very real problem in satellite meteorology. At the present time methods are basically being developed for determining the integral moisture content from measurements of the spectral intensity of emitted radiation in the infrared spectral range in the bands of water vapor absorption. /62

The lines of H_2O absorption occur in the microwave spectral band. Measurements in this band have a number of advantages in comparison with the methods of IR-technology, the bases of which are the possibilities of measuring through clouds which are transparent to the radio band, and the higher sensitivity of the radio receivers.

Along with this, there are certain problems associated with allowing for the radiation from the Earth's surface, having large and highly varying reflection coefficients.

In studying microwave radiation from the atmosphere, it is convenient to use an expression for the radiobrightness temperatures, rather than for the intensities, bearing in mind the linear relationship between them, determined by the Rayleigh-Jeans formula.

The radiobrightness temperature of the anabatic radiation is related to the temperature profile and to the temperature of the underlying surface by the following relationship:

$$T_b = \varepsilon T_p \exp\left(-\int_0^h \alpha \sec\theta' \, dz\right) + \int_0^h T(z)\,\alpha \sec\theta' \exp\left(-\int_z^h \alpha \sec\theta' \, dz\right) dz + \\ + \left\{\int_0^{2\pi} d\varphi \int_0^{\frac{\pi}{2}} r(\theta, \varphi, \theta', \varphi') \sin\theta \cos\theta \, d\theta \int_0^{\infty} T(z)\,\alpha \sec\theta \exp \times \right. \\ \left. \times \left(-\int_0^z \alpha \sec\theta \, dz\right) dz \right\} \exp\left(-\int_0^h \alpha \sec\theta' \, dz\right), \qquad (1)$$

where T_p is the physical temperature of the underlying surface; $T(z)$ is the physical temperature of the atmosphere at an altitude z, α is the attentuation factor in the atmospheric gases; θ, ϕ are the angular coordinates of the incident radiation; θ', ϕ' are the angular coordinates of the departing radiation; $r(\theta, \phi, \theta', \phi')$ is the coefficient of brightness on the Earth's surface; ε is the emission coefficient of the underlying surface; h is the altitude at which the radiation receiver is placed; z is the vertical coordinate. /63

The first term of the formula describes the radiation from the underlying surface, attenuated by the layer of atmosphere and arriving at a certain altitude h above sea level.

The second term represents the radiation from the layer of atmosphere from the level of the Earth to the altitude h.

The third term describes radiation from the entire atmosphere, reflected from the underlying surface and attenuated by the layer of atmosphere from 0 to h. This formula is valid for all cases when it is not necessary to allow for scattering as is the case with the transfer of microwave radiation in a cloud-free atmosphere [1]. Moreover, the radio emission from outer space is not taken into account, since its value is negligibly small in a wave length band shorter than 10 cm [7].

Investigation of the absorption spectrum of the fundamental atmospheric gases shows that only oxygen and water vapor possess substantial absorption at wave lengths greater than 1 mm.

In the microwave band there are lines of resonance absorption of oxygen, centered near $\lambda = 0.25$ cm and $\lambda = 0.5$ cm, and the lines of water vapor shown on Table 1 [8].

TABLE 1.

Wave length, mm	Relative intensity
13.48	1
2.6 ± 0.2	$3.3 \cdot 10^{-4}$
1.63 ± 0.2	$1.9 \cdot 10^{2}$
1.3 ± 0.2	$1.4 \cdot 10^{-3}$
1.2 ± 0.2	$1.6 \cdot 10^{-4}$

Of greatest interest for measuring the water content is the line $\lambda = 1.35$ cm, which does not coincide with the lines of oxygen absorption and has an optimal absorption coefficient, which permits obtaining information concerning the amount of water vapor in the entire thickness of the atmosphere.

Thus, in computing attentuation of the microwave radiation it is necessary to take into account only the absorption in O_2 and H_2O. Consequently, the attentuation factor in formula (1) will have the form

$$\alpha = \alpha_{O_2} + \alpha_{H_2O}. \qquad (2)$$

Here we should note the important advantage of the microwave band in comparison with the infrared. In the microwave spectral band the absorption takes place in individual lines, distributed at considerable distances from one another. The line width $\lambda = 1.35$ cm comprises an order of magnitude of 0.1 cm^{-1} with a transmission band of modern radiometers of about 0.001 cm^{-1}. This permits considering the assumed radiation as monochromatic and using ordinary absorption coefficients instead of the transmission functions.

Computations of the absorption coefficients were made by Van Vleck and Weisskopf [9-11] and subsequently refined by Zhevakin and Naumov [2, 3].

Figure 1 shows a graph of the dependence of the specific absorption coefficient of water vapor on pressure and temperature, computed from the formula /64

$$\alpha_{H_2O} = 1.05 \cdot 10^{-28} \frac{N\nu^2 e^{-644/T}}{T^{5,2}} \left[\frac{\Delta\nu_p}{(\nu - \nu_0)^2 + \Delta\nu_p^2} + \frac{\Delta\nu_p}{(\nu + \nu_0)^2 + \Delta\nu_p^2} \right] + \\ + 7.6 \cdot 10^{-52} \frac{N\nu^2 \Delta\nu_p}{T^{3/2}} \text{ см}^{-1}, \qquad (3)$$

where N is the number of H_2O molecules per unit volume, ν_0 is the resonance frequency, $\Delta\nu_p$ is the half-width of the line produced by intermolecular collisions

$$\Delta\nu_r = 2{,}62 \cdot 10^9 \frac{P/760}{(T/318)^{5/8}} (1 + 0{,}0046\rho) \text{ sec}^{-1} \quad (4)$$

where P is the atmospheric pressure and ρ is the density of the H_2O per g/m^3.

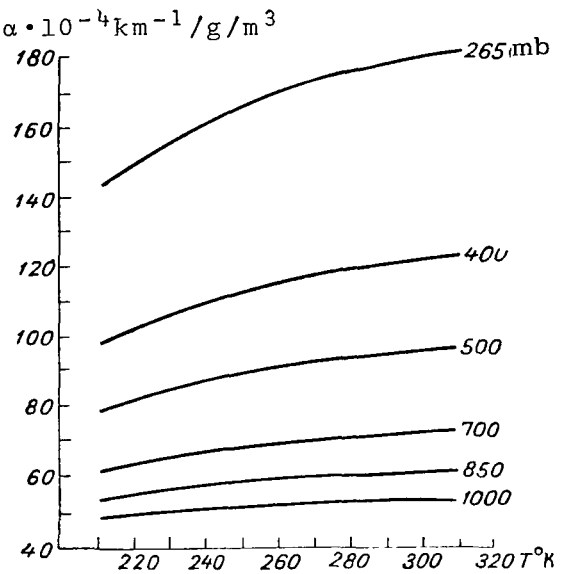

Fig. 1. Specific Absorption Coefficient of Water Vapor as a Function of Temperature and Pressure (λ = 1.35 cm).

The dependence of the absorption coefficient in oxygen is quite well known:

$$\alpha_{O_2} = \alpha_0 \left(\frac{P}{P_0}\right)^2 \left(\frac{T_0}{T}\right)^{5/2}, \quad (5)$$

where α_0 is the absorption coefficient in O_2 for standard conditions P_0 = 1013 mb, T_0 = 293° K.

1. Microwave Radiation from an Atmosphere having a Specified Structure. Analysis of the Effect of Various Factors.

In making the computations /65 of radiobrightness temperatures we used the standard distributions of temperature and moisture content.

For the temperature profile we used a model of the atmosphere which is characterized by the following data:

$$T(z) = \begin{cases} T_0 - \gamma_1 z & (0 \text{ км} \leqslant z \leqslant 11 \text{ км}) \\ T = T_{11} & (11 \text{ км} \leqslant z \leqslant 25 \text{ км}) \\ T_{11} + \gamma_2 z & (25 \text{ км} \leqslant z \leqslant 47 \text{ км}), \end{cases} \quad (6)$$

where γ_1 = 6.5°/km, γ_2 = 3.0°/km.

For the vertical distribution of the specific moisture content we used a model which was proposed by M.S. Malkevich [3]:'

$$q(z) = \begin{cases} q_0 e^{-0{,}48z} & (0 \text{ км} \leqslant z \leqslant 16 \text{ км}) \\ q_{16} e^{0{,}24(z-16)} & (16 \text{ км} \leqslant z \leqslant 31 \text{ км}). \end{cases} \quad (7)$$

By numerical integration of equation (1) the atmosphere was

divided into layers having a thickness of 0.5 km for the first 3 km, a thickness of 1 km up to 11 km, and a thickness of 5 km up to 31 km.

The data required for the computations on the emission coefficients of the water surface under various conditions were taken from [5].

From equation (1) and the formulas for the profiles of the meteorological elements and emission coefficients we programmed a "Ural-4" digital computer and made the computations.

Table 2 gives the original parameters, according to which we made the computations: T_p is the physical temperature of the underlying surface, ρ_0 is the absolute moisture content, U_0, P_0 and T_0 represent the relative moisture content, the atmospheric pressure and the temperature of the air on the Earth's surface, respectively.

TABLE 2.

Salinity of the water, 0/00	T_p °K	T_0 °K	U_0 %	P_0 mb	ρ_0 g/m^3
40	298	288	0, 20, 40, 60, 80, 100	1013	
		293	0, 20, 40, 60, 80, 100	1013	
		298	0, 20, 40, 60, 80, 100	1013	
		303	0, 20, 40, 60, 80, 100	1013	
	273	273	60, 80	1013	
		278	60, 80	1013	
0	283	278	60, 80	1013	
		283	60, 80	1013	
		288	60, 80	1013	
	293	288	60, 80	1013	
		293	60, 80	1013	
		298	60, 80	1013	
40	298	288		1013	7,5; 15
		293			7,5; 15
		298			7,5; 15
		303			7,5; 15
		298		1100	15
		298		900	15

Moreover, we made computations for the real profiles of the meteorological elements obtained during ground and aircraft measurements. The computational results are presented in the form of a summary graph (Fig. 2), where the radiobrightness temperature T_b is given as a function of the amount of precipitated water W in the entire thickness of the atmosphere. /66

In order for it to be easy to trace the dependence of the radiobrightness temperature on the various factors, we can look

individually at the three terms in equation (1). Figure 3 shows the dependences of the components of the radiobrightness temperature for various conditions. Figure 3a shows the radiobrightness temperature of the water surface (when T_p = 208° K, salinity 40 0/00), attenuated by the effect of the thickness of the atmosphere with temperatures at the Earth's surface T_0 equal to 288, 293, 298 and 303° K, as a function of the total water content. From the graph it is obvious that the effect of the temperature of the air is virtually nonexistent.

Figures 3b and 3c show the dependences of the radiation from the atmosphere and the back radiation from the atmosphere, reflected from the surface of the water, on the water content. These graphs in comparison with Figure 3a have an inverse dependence on water content. Moreover, here the air temperature already exerts an influence.

If we look at the computational results obtained, we can evaluate the influence of the individual factors on the accuracy of the measurement of the total water content.

Salinity of the Water. Change in the salinity of the water from 0 to 40 0/00 gives on the average an increase in the radiobrightness temperatures up to 3° K. This is illustrated in Table 3.

TABLE 3.

U_0%	T_p °K	T_0 °K	T_b (0‰) °K	T_b (40‰) °K	ΔT_b°
60	298	288	145,7	148,7	3
80	298	288	153,2	156,2	3

Here we look at two cases which differ in the water content. Both of them give an increase in the radiobrightness temperature by 3° during transition from fresh water to sea water.

Temperature of the Air on the Surface of the Water. The influence of the air temperature can be seen in the data of Table 4, in which the changes in radiobrightness temperatures are shown for various amounts of water content for two air temperatures (T_0 = 288° K and T_0 = 303° K) over the water surface (T_p = 298° K, salinity 40 0/00). With the largest water content which makes sense under these conditions, the greatest change in the radiobrightness temperature is 3.2° K.

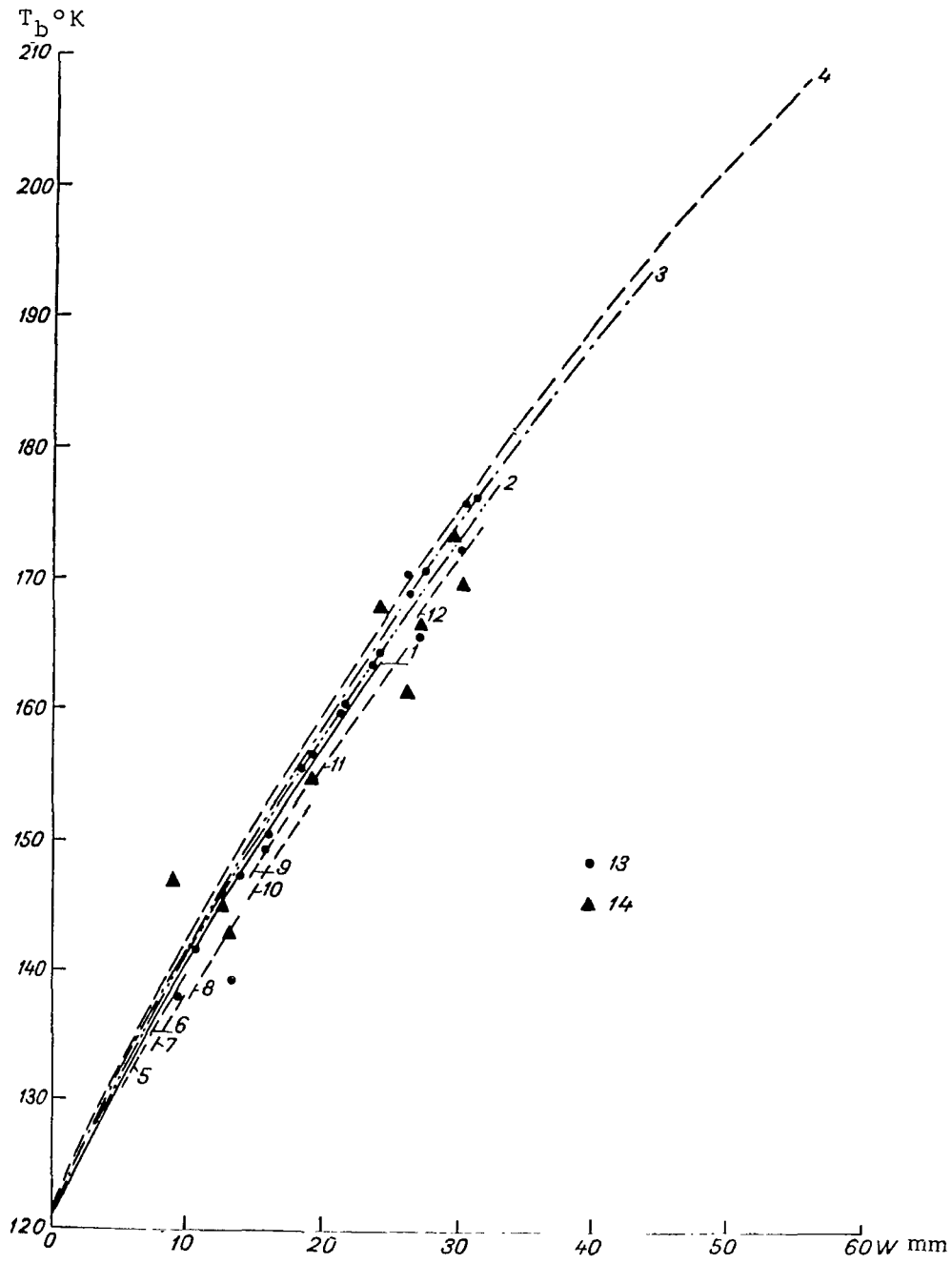

Fig. 2. Radio Emission from the System Earth-Atmosphere (λ = 1.35 cm) Sea Water (T_p = 298° K, 40 0/00): 1. T_0 = 288° K; 2. T_0 = 293°K; 3. T_0 = 298° K; 4. T_0 = 303° K; Fresh Water (T_p = 273° K, 0 0/00): 5. T_0 = 273° K; 6. T_0 = 278° K; Fresh Water (T_p = 283° K, 0 0/00): 7. T_0 = 278° K; 8. T_0 = 283° K; 9. T_0 = 288° K; Fresh Water (T_p = 293° K, 0 0/00): 10. T_0 = 288° K; 11. T_0 = 293° K; 12. T_0 = 298° K; 13. T_b For Real Profiles; 14. Experimental Data T_b. /67

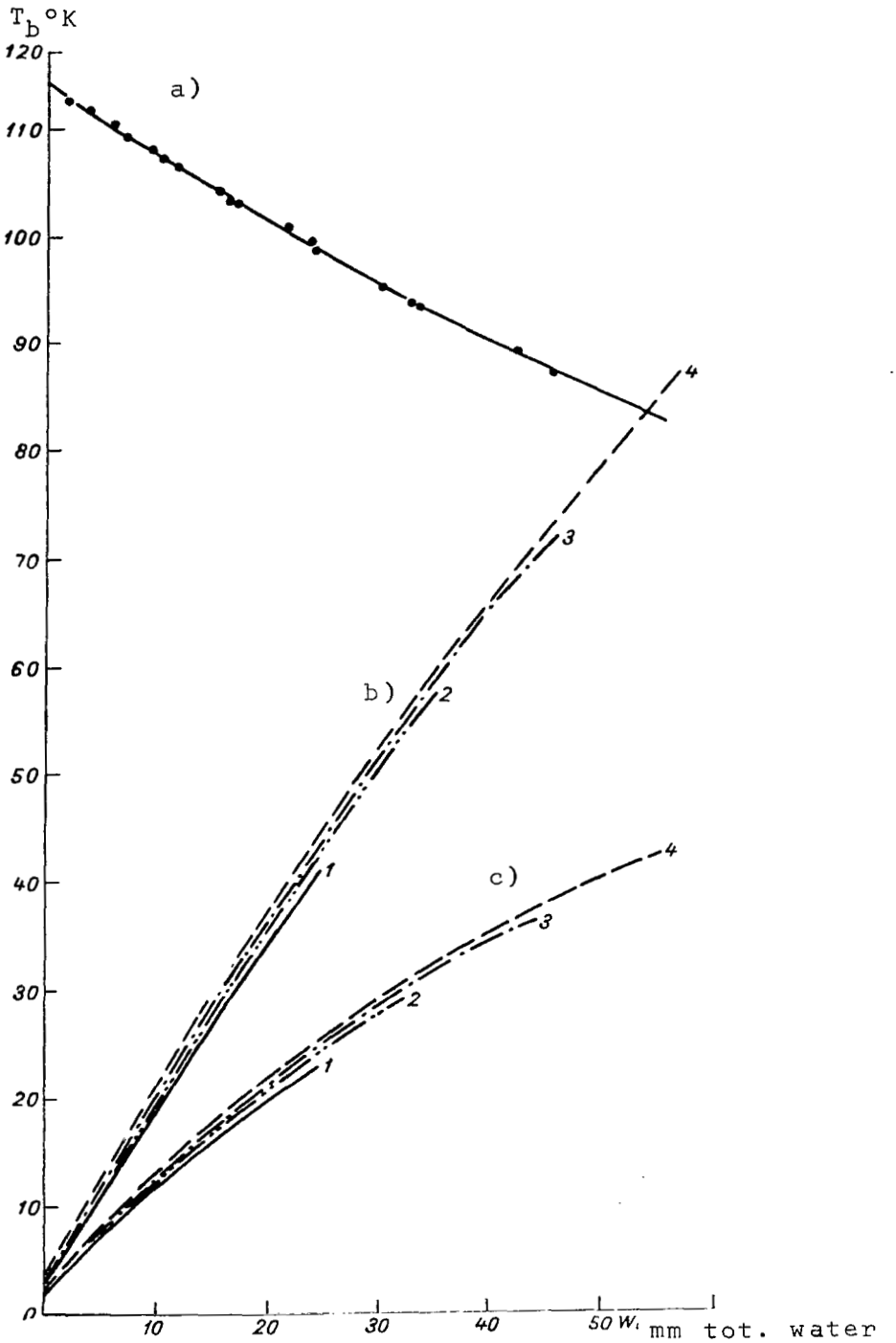

Fig. 3. Components of Radio Emission from the System Earth-Atmosphere as a Function of Total Water Vapor Content. 1. T = 288° K; 2. T = 293° K; 3. T = 298° K; 4. T = 303° K. /68

TABLE 4.

W mm	T_b (T_0 = 288 °K)	T_b (T_0 = 303 °K)	ΔT_b°
5	131.7	132.3	0.6
10	140.6	142.4	1.8
15	149.5	151.3	1.8
20	157.8	160.0	2.2
24	164.0	167.2	3.2

Temperature of the Water Surface. Change in temperature of the fresh water by 10° C leads to a error in measuring the radiobrightness temperature that does not exceed 2° K. This is obvious from the computational data shown on Table 5. /69

TABLE 5.

U_0 %	T_0 = 278 °K		T_0 = 288 °K	
	T_p = 273 °K	T_p = 283 °K	T_p = 283 °K	T_p = 293 °K
60	135.1	133.6	147.3	145.6
80	139.6	138.2	154.7	153.2

Atmospheric Pressure on the Earth's Surface. Change in P_0 from 1100 to 900 mb leads to a drop in the values of T_b by 6° K. For real changes in P_0 consisting of about 60 - 100 mb, ΔT_b will be 2 - 3° K.

Comparison with Real Profiles of the Meteorological Elements. We computed the values of the radiobrightness temperatures from the profiles of the H_2O obtained during measurements at Voyeykovo, over Lake Ladoga and the Caspian Sea for Summer and Fall. The maximal divergence between T_b, computed from the real and the standard profiles of the meteorological elements, does not exceed 4° K.

These dimensions characterize the influence of individual factors on the radiobrightness temperature. However this does not mean that all of them must be summed in determining the error. Moreover, evaluation of the possible accuracy of the measurements can be made from the graph (Fig. 2) plotted from the results of theoretical calculations. This graph encompasses a wide spectrum of the various meteorological conditions characterizing the state of the atmosphere and the water surface, and from this we can approximately evaluate the amount of the error in determining the total moisture content if we know only the radiobrightness temperature of the water surface. This error is determined by the width of the family of individual functions $T_b = f(W)$. The results of

this evaluation are shown on Table 6.

TABLE 6.

Variation range of Moisture Content, mm...	0-10	10-25	25-55
Absolute error, mm of precipitated water	2.5	3.5	4.5

2. Aircraft Measurements and Their Analysis

Experimental proof of the dependence of radio emission from the underlying surface and the atmosphere on the total moisture content was carried out by measurements from an IL-18 airplane. The method of the measurements and the instruments used in these flights are described in detail in [6].

The flights were made over the Caspian Sea and Lake Ladoga in the Summer and Fall of 1966 in a cloud-free sky. Moreover, in the Fall of 1965 at Voyeykovo at the observatory base, measurements were made of the radiobrightness temperatures of the sky at the zenith using the same instruments that were used under ground conditions.

Vertical sounding of the atmosphere up to altitudes of 9 - 10 km were made with simultaneous measurements of the profile of temperature, moisture and pressure using an electrometeograph over the segments of the water surface chosen that are uniform in temperature. In this case we can compare the computational and the experimental values of the radiobrightness temperatures as well as determine the moisture content of the atmosphere from measuring the radiobrightness temperature by using the theoretical computations (Fig. 2). /70

In determining the total moisture content W_b from the graphs in Figure 2 the took the average climatic data as the data for the fresh or sea water temperatures.

The results of the measurements and their comparison with the theoretical computations are shown on Table 7.

TABLE 7.

Date	Region	T_b°K Experimental	T_b°K Theoretical	$\lvert\Delta T_b^\circ\rvert$	W_b mm	W mm	$\frac{\Delta W}{W}$ %
1966							
June 11	Lake Ladoga	154.8	156.8	2.0	19.0	19.2	1.0
June 13	"	142.9	139.4	3.5	13.0	13.3	2.3
June 17	"	144.8	145.8	1.0	14.0	12.6	11.0
June 20	"	173.5	173.3	0.2	30.8	29.4	4.8
June 23	"	167.0	164.8	2.2	27.5	24.1	14.1
June 28	Caspian Sea	170.0	173.0	3.0	27.4	29.9	8.4
Oct. 3	"	167.0	166.0	1.0	25.4	26.9	5.6
Oct. 6	"	161.7	170.9	9.2	22.0	26.0	15.4

If we analyze the results of the comparison, we can note completely satisfactory agreement between the results of the computations and the experiment. The greatest relative error in determining the overall moisture content is no more than 16%, and the average for all cases of measurements is 10%.

3. Ground Measurements and Their Analysis

It is of interest to study the data as well which were obtained during the ground measurements where, for comparison, we can use the theoretical computations made according to formula (1). The program for the computations was set up in such a way that as the intermediate result, we had the radiobrightness temperature of the sky as

$$T_{bs} = \int_0^\infty T(z)\,\alpha \sec\theta \exp\left(-\int_0^z \alpha \sec\theta\, dz\right) dz. \qquad (8)$$

The computational results from formula (8) are shown in the form of a graph giving the radiobrightness temperature as a function of the total moisture content of the atmosphere for various air temperatures on the surface of the Earth (Table 2). From these data we made the evaluations of the influence of the various factors which were similarly satisfied for measurements from above. Without stopping to examine the influence of each of them, we can show that the scatter in values of the total water content determined from the ground measurements is less than in the previous case and is characterized by the data in Table 8.

TABLE 8. /71

Variation range of moisture content, mm of precipitated water	0 - 10	10-25	25-55
Absolute error, mm of precipitated water	1.0	2.5	3.5

For practical utilization of the computational results we may propose a correlation equation between the total moisture content in centimeters of precipitated water and the radiobrightness temperature of the sky

$$W = 0{,}056T_b - 0{,}16. \qquad (9)$$

These results were proven by comparison with the data from /72
ground measurements of the radiobrightness temperatures of the sky, the results of which are shown on Table 9.

The data from the total moisture content of the entire thickness of the atmosphere $W_{r/s}$ were obtained from the results of radio

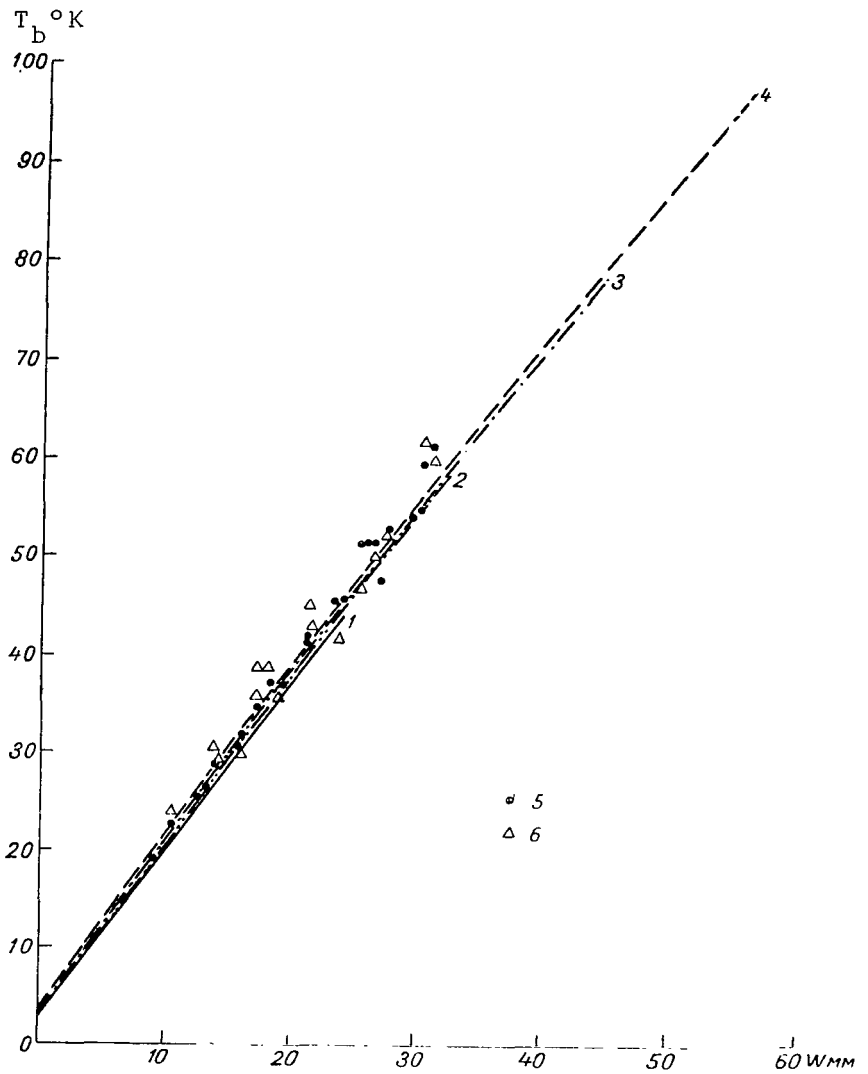

Fig. 4. Radio Emission from a Cloud-Free Sky. 1. T_0 = 288° K; 2. T_0 = 293° K; 3. T_0 = 298° K; 4. T_0 = 303° K; 5. $T_{b\ s}$ for real profiles; 6. Experimental Data $T_{b\ s}$.

TABLE 9.

Date	T_{bs} °K Exper.	T_{bs} °K Theor.	ΔT_b °	W_b mm	$W_{r/s}$ mm	$\frac{\Delta W}{W_{r/s}}$ %	W_a mm	$\frac{\Delta W}{W_a}$ %
1965								
Aug. 7	49.9	51.4	1.5	24.8	22.25	6.9	23.5	5.5
Aug. 9	29.0	28.6	0.4	15.0	13.84	8.6	13.0	15.3
Sept. 9	42.5	41.9	0.6	23.2	21.40	8.4	19.8	17.1
Sept. 9	38.8	45.3	6.5	21.2	23.40	9.4	17.9	18.4
Sept. 10	60.0	61.2	1.2	34.0	31.00	9.7	28.5	19.2
Sept. 11	46.80	53.10	6.3	26.0	27.3	4.8	21.9	18.7
Sept. 16	30.0	31.8	1.8	15.8	16.0	13.0	13.5	17.0
Sept. 18	35.8	34.8	1.0	19.2	17.2	12.0	16.4	17.0
Sept. 25	35.0	41.4	6.4	18.8	21.2	11.0	16.0	17.5
Oct. 2	16.5	22.7	6.2	8.1	10.6	23.6	6.8	19.1

sounding of the Voyeyokovo Meteorological Station.

If we analyze the results of the comparison, we can see that in this case we observe fully satisfactory agreement of the results of the computations and the experiment. The error in determining $T_{b\ s}$ from the computations does not exceed 6° K. On the one hand, this characterizes the accuracy of the measurements assured by the measuring instruments and on the other hand confirms the correct choice of the theoretical plan and model of the atmosphere.

The greatest relative error in determining the total moisture content from the ground measurements of the radiobrightness temperature of the sky at the zenith does not exceed 24%, and the mean is 11%. Moreover, by comparing the total moisture content W_b, determined from the graph on Figure 4, and W_a determined from the approximation formula, we can see that the mean relative error in using the formula does not exceed 16%.

Conclusions

The obtained theoretical and experimental data fully confirm the possibility of determining the total moisture content of a cloud-free atmosphere from measuring the radio emission from the underlying surface and the atmosphere in the absorption band of the water vapor λ = 1.35 cm.

If we use a radiometric instrument analogous to that with which we obtained the experimental data discussed above, we can make our measurements of the total moisture content of the atmosphere from an artificial Earth satellite over the underlying water surface with 8 - 10 gradations in the variation range of moisture content from 5 to 60 mm of precipitated water. Here it is sufficient to use the value of the water temperature (for the oceans) according to the mean climatological data. If we take into account the small dependence of the measurement results on the temperature of the underlying surface, we may assume that we can measure the moisture content over a uniform expanse of ground formations with a slightly lesser accuracy (4 - 5 gradations).

REFERENCES

1. Shifrin, K.S.: Rasseyaniye sveta v mutnoy srede. (Scattering of Light in a Cloudy Atmosphere)., Gostekhizdat, 1951. /73
2. Zhevakin, S.A. and A.P. Naumov: O koeffitsiente pogloshcheniya elektromagnitnykh voln vodynymi parami v diapazone 10 - 2 cm. (The Absorption Coefficient of Electromagnetic Waves by Water Vapors in the range of 10 - 2 cm). Izv. VUZ, ser. Radiofizika, Vol. 6, No. 4, 1963.
3. Zhevakin, S.A. and A.P. Naumov: Pogloshcheniye santimetrovykh i millimetrovykh radiovoln atmosfernymi parami vody. (Absorption of Centimeter and Millimeter Radio Waves by Atmospheric Water Vapors)., Radiotekhnika i elektronika, Vol. 9, No. 8, 1964.

4. Malkevich, M.S., Yu. V. Samsonov and L.I. Koprova: Vodyanoy par v stratosfere. (Water Vapor in the Stratosphere)., Ukr. Fiz. Zh., Vol. 80, No. 1, 1963.
5. Shifrin, K.S. and S.N. Ionina: Teplovoye izlucheniye i otrazheniye ot volnuyushcheysya poverkhnosti morya v mikrovolnovoy oblasti. (Thermal Radiation and Reflection from a Rough Sea Surface in the Microwave Band). See this Collection.
6. Shifrin, K.S., Yu. I. Rabinovich and G.G. Shchukin: Issledovaniye polya mikrovolnovogo izlucheniya v atmosfere. (Investigation of the Field of Microwave Radiation in the Atmosphere). See this Collection.
7. Hogg, D.C.: Effective Antenna Temperatures Due to Oxygen and Water Vapor in the Atmosphere., J. Appl. Optics, Vol. 30, No. 9., 1959.
8. Rogers, T.F.: Absolute Intensity of Water Vapor Absorption at Microwave Frequencies. Phys. Rev. Vol. 93, No. 1, 1954.
9. Van Vleck, I.H.: Absorption of Microwaves by Water Vapor. Phys. Rev., Vol. 71, pp. 425 - 432, 1947.
10. Van Vleck, I.H.: The Absorption of Microwaves by Oxygen. Phys. Rev., Vol. 71, pp. 413 - 424, 1947.
11. Van Vleck, I.H. and V.F. Weisskopf: On the Shape of Collision Broadened Lines. Rev. Modern Physics, Vol. 17, pp. 227 - 236, 1945.

ABSORPTION AND SCATTERING OF MICROWAVES IN PRECIPITATION

K.S. Shifrin and M.M. Chernyak

ABSTRACT: The results of computations in the absorption coefficient and the natural thermal radiation are given for individual drops from clouds and precipitation, and for the unit volume. For small drops there is a curious anomalous effect, i.e., with heating the thermal radiation from these systems drops. The characteristic curves of scattering from individual drops and for the unit volume in the microwave band are also computed for the various spectra of particles. These data are necessary for accurate computations of the transfer of microwave radiation in hydrometeors.

Scattering and attenuation of radio waves by drops from clouds /74
and precipitation are of great interest for radiometeorology and radioastronomy. Solution to a number of problems requires knowledge of the attenuation factors, scattering coefficients and the characteristic curves of scattering of microradiowaves by precipitation of different intensities and different temperatures. For this purpose we made calculations of the attenuation factors and the scattering coefficients and the characteristic curves of individual drops of water for temperatures of -10.0, 0 + 10.0, 20.0° C and wave lengths of 0.8, 1.35, 1.6, 2.5, 3.2, 4.0, 5.6 and 8.5 cm. The results of these computations were examined in [1]. In the present paper we cite data on the absorption coefficients, their dependence on temperature and dimensions of the drops. We look at the influence of the width of the spectrum of drop distribution according to the form of the characteristic curves of scattering and the possibility of approximating it in a series of Legendre polynomials. We give the numerical data of the expansion coefficients for precipitation of various intensities.

1. Reference Formulas for the Computations.

As we know [2], the absorption coefficient of a particle is equal to the difference between the attenuation factor and the scattering coefficient, which can be computed from the following formulas:

$$k = \frac{2\pi a^2}{\rho^2} \sum_{l=1}^{\infty} \operatorname{Im}(-1)^l l(l+1)(c_l - b_l), \qquad (1)$$

$$k_{\text{r}} = \frac{2\pi a^2}{\rho^2} \sum_{l=1}^{\infty} \frac{l^2 (l+1)^2}{2l+1} (|c_l|^2 + |b_l|^2), \tag{2}$$

$$k_{\text{p}} = k - k_{\text{r}}. \tag{3}$$

The coefficients c_1 and b_1 are expressed through the Bessel and Hankel functions from the arguments ρ and $m\rho$, where $m = n - i\kappa$ is the complex refractive index. The values of m for the wave lengths and temperatures given above are computed from the Debye formulas given in [1].

Very often it is more convenient to operate, rather than with the coefficients, with the effective factors of attenuation, scattering and absorption which are related to the respective coefficients by the following equations:

$$K = \frac{k}{\pi a^2}, \quad K_{\text{r}} = \frac{k_{\text{r}}}{\pi a^2}, \quad K_{\text{p}} = \frac{k_{\text{p}}}{\pi a^2}.$$

When $\rho = \frac{2\pi a}{\lambda} \ll 1$ and $|m|\rho \gg 1$, formulas (1) and (2) convert /75 to the following:

$$K = \frac{8\pi a}{\lambda} \operatorname{Im}\left(-\frac{m^2-1}{m^2+2}\right), \tag{4}$$

$$K_{\text{r}} = \frac{128\pi^4 a^4}{3\lambda^4} \left|\frac{m^2-1}{m^2+2}\right|^2, \tag{5}$$

$$K_{\text{p}} = K - K_{\text{r}}. \tag{6}$$

The basic mass of the cloud drops, whose dimensions do not exceed 100 μ, for $\lambda \geq 0.8$ cm, may be presumed "small", and the computations of K, K_r are made from formulas (4) and (5). Here, since the radius of the drop a is small, $K \gg K_r$ and the effective factor of absorption K_p practically coincides with K. For drops from precipitation, the computations must be made from the complete formulas (1) and (2).

The normalized characteristic curves of scattering for a drop of water is computed from the formula

$$f(\beta, m, \rho) = \frac{i_1 + i_2}{2\pi\rho^2 K_{\text{r}}}, \tag{7}$$

where β is the angle of scattering, and functions i_1 and i_2 are related to the amplitudes of the partial waves c_1, b_1 and the

angular functions $Q_1(\cos\beta)$ and $S_1(\cos\beta)$ by the following relationships [2]:

$$i_1 = \left| \sum_{l=1}^{\infty} (c_l Q_l + b_l S_l) \right|^2, \tag{8}$$

$$i_2 = \left| \sum_{l=1}^{\infty} (c_l S_l + b_l Q_l) \right|^2. \tag{9}$$

Per unit volume of precipitations the normalized characteristic curves of scattering and the absorption coefficient are determined by the following relationships:

$$F(\beta, m, \rho) = \frac{\int_0^{\infty} a^2 K_r(m, \rho) f(\beta, m, \rho) N(a)\, da}{\int_0^{\infty} a^2 K_r(m, \rho) N(a)\, da}, \tag{10}$$

$$\gamma_p = \pi \int_0^{\infty} a^2 K_r(m, \rho) N(a)\, da, \tag{11}$$

where N(a) is the distribution density of the drops by size.

As the distribution function of the drops by size we used the Marshal-Palmer distribution for precipitations

$$N(a) = N_0 e^{-xa}, \tag{12}$$

where $N_0 = 8 \cdot 10^{-2}$ cm^{-4}, $x = 82P^{-0.21}$ cm^{-1}, P is the intensity of the precipitations in mm/hr. The number of drops per cm^3, the radii of which lie in the range from a to a + da, will be equal to N(a)da.

2. Effective Factor of Absorption as a Function of Drop Size and of Temperature

The results from computing the effective factor of absorption /76 are illustrated by the graph on Figure 1, along the abscissa axis of which are plotted the diameters of the drops in millimeters.

On the figure we can see the dependence of K_p on the refractive index m and its imaginary part. If we compare these curves with the analogous curves with small absorption, we can then see that in this latter case there are clearly expressed diffraction maxima whose

values drop in proportion to increase in ρ. With increase in the imaginary part of the refractive index the diffraction maxima are attenuated and a part of them generally disappears. In the centimeter band K_p has only one weakly expressed diffraction maximum. It is weakly expressed for the effective factor of attenuation K. In proportion to the increase in the particle the dependence of the effective factor of absorption on the refractive index disappears since K and K_T cease to depend on it [2].

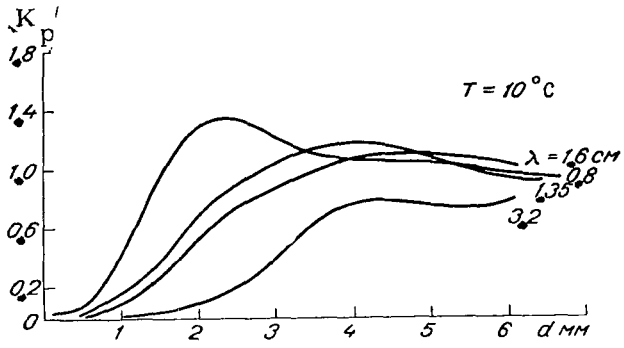

Fig. 1. Effective Factor of Absorption as a Function of Drop Size.

Figure 2 shows the temperature dependence of the effective factor of absorption on

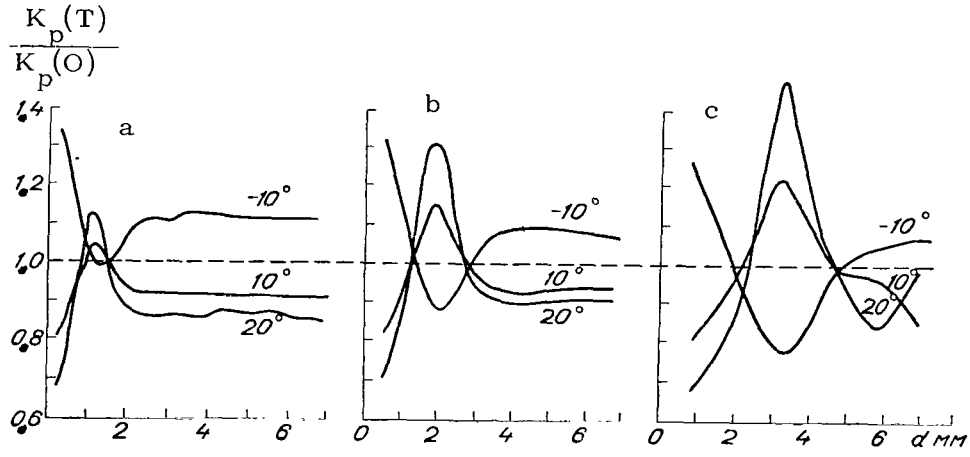

Fig. 2. Temperature Dependence of the Effective Factor of Absorption on Drop Diameter.

drop diameter for wave lengths 0.8 cm (a), 1.6 cm (b) and 3.2 cm (c). Along the ordinate axis is plotted the ratio of the effective factor of absorption at the temperature shown on the graph, to its value at 0° C, and along the abscissa axis is plotted the diameter of the drops. As we can see, K_p, especially for λ = 0.8 cm, at below-zero temperatures exceeds the respective value for above-zero temperatures. The effective factor of absorption for $\lambda \leq 3.2$ cm and particles with a $\geq$ 2.5 mm at a temperature of -10° C remains larger here than at temperatures of 10 and 20° C. Qualitatively such a dependence for K_p can be understood by comparing the temperature dependence of n and κ. /7

With a decrease in the temperature, n and κ are decreased.

The rate of decrease of n is greater than that of κ. This means that with a decrease in temperature the reflection of the radiation from the surface of the drop will be decreased. More energy will enter it and since κ varied little, the greater incident energy will be the absorption energy. The increase in absorption with drop in temperature leads to the intensity of the natural thermal radiation from a small particle increasing with decrease in the temperature.

Table 1 shows for illustration of this effect, the values of the brightness of radiation B of a drop with a radius of 10 μ. From the table it is clear that with an increase in temperature the radiation from the drops decreases. This anomalous dependence of radiation on temperature can be explained in the following manner.

TABLE 1

T °C	$B \cdot 10^{18}$ W/m^2 Hz		
	$\lambda = 0{,}62$ см	$\lambda = 1{,}24$ см	$\lambda = 3{,}2$ см
20	9,86	0,63	0,015
10	11,82	0,80	0,019
−8	16,77	1,26	0,034

The effect of temperature on $k_p = k_p(T)$ and the Planck function $B^* = B^*(T)$ is contradictory. For small drops the drop in k_p with increase in T is so high that it surpasses the increase in $B^*(T)$ such that on the whole the radiation from the drop decreases. For large drops k_p depends little on T and the path of the radiation with change in T is determined by the path of the function $B^*(T)$.

TABLE 2

P mm/hr	$\lambda = 0{,}8$ см		$\lambda = 1{,}35$ см		$\lambda = 1{,}6$ см		$\lambda = 3{,}2$ см	
	λS	γ_p км$^{-1}$	λS	γ_p км$^{-1}$	λS	γ_p км$^{-1}$	λS	γ_p км$^{-1}$
2	0,31	0,1302	0,14	0,0525	0,11	0,0377	0,05	0,0052
3	0,33	0,1910	0,17	0,0806	0,13	0,0588	0,05	0,0092
5	0,36	0,3061	0,20	0,1371	0,16	1,1021	0,06	0,0187
12	0,40	0,6546	0,26	0,3271	0,21	0,2514	0,07	0,0595
16	0,42	0,8289	0,28	0,4298	0,23	0,3527	0,08	0,0855
20	0,43	0,9907	0,30	0,5286	0,24	0,4135	0,08	0,1126
25	0,44	1,1905	0,31	0,6545	0,26	0,5162	0,09	0,1496
30	0,45	1,3557	0,32	0,7616	0,27	0,6043	0,09	0,1827
36	0,46	1,5779	0,33	0,9097	0,29	0,7266	0,10	0,2310
40	0,46	1,7032	0,34	0,9944	0,29	0,7973	0,10	0,2600
90	0,49	3,1042	0,39	2,0061	0,35	1,6568	0,13	0,6502

The absorption coefficients per unit volume of precipitations γ_p of different intensities were computed from formula (1) at a temperature of 10° C and are shown on Table 2. Moreover, in the same table, for each wave length, is shown the value of the /78

probability of survival of the photon per unit volume of precipitations

$$\lambda_S = \frac{\gamma_S}{\gamma},$$

where γ_S is the scattering coefficient, γ is the attenuation factor. The least probability of survival is at λ = 3.2 cm, the greatest at λ = 0.8 cm; generally the value of λ_S does not exceed 0.50.

3. Polydisperse Characteristic Curves.

The polydisperse characteristic curves of scattering $F(\beta)$ were computed for distribution (12) according to formula (10) for the intensities of precipitation and wave lengths shown on Table 3. Figure 3 shows the characteristic curves of scattering for wave lengths 0.8 and 3.2 cm and for two intensities of precipitation (6 and 32 mm/hr). The values of the characteristic curves of scattering for the individual drops of water at various temperatures are given in [3].

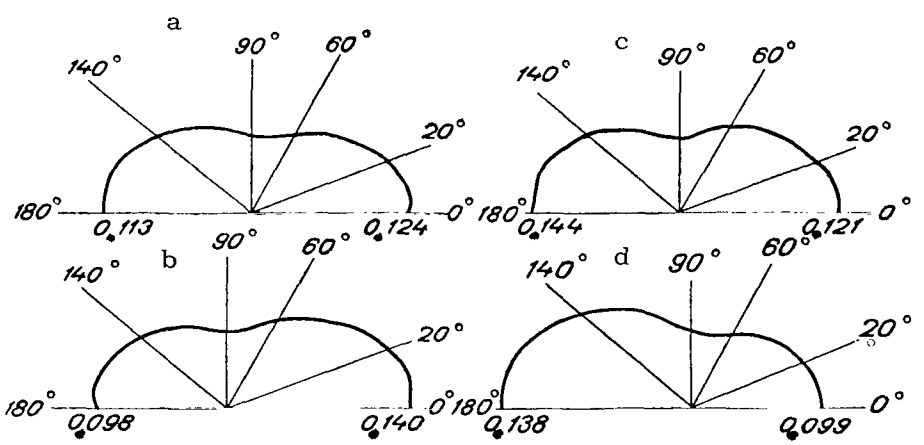

Fig. 3. Characteristic Curves of Scattering Per Unit Volume of Precipitation. a: P = 6 mm/hr, λ = 0.8 cm; b: P = 32 mm/hr, λ = 0.8 cm; c: P = 6 mm/hr, λ = 3.2 cm; d: P = 32 mm/hr, λ = 3.2 cm.

From the data in Table 3 it is obvious that for λ = 0.8 cm with an increase in intensity of precipitation and consequently with an increase in the number of large drops the forward scattering is increased (β = 0°). As far as the wave lengths of 1.35 and 1.6 cm are concerned the back scattering (β = 180°) predominates for all intensities of precipitation, but with an increase in intensity there is a slight tendency to increase the amount of energy scattered forward. At a wave length of $\lambda \geq 2$ cm the back scattering increases with increase in the intensity of precipitation.

TABLE 3

P mm/hr	λ см	$F(\beta)$ 0°	10°	20°	30°	40°	50°	60°	70°	80°	90°	100°
5	0.8	0.1237	0.1213	0.1148	0.1050	0.0936	0.0822	0.0722	0.0650	0.0610	0.0606	0.0635
	1.35	0.1062	0.1044	0.0994	0.0918	0.0829	0.0740	0.0662	0.0609	0.0588	0.0602	0.0650
	1.6	0.1067	0.1049	0.1000	0.0925	0.0835	0.0745	0.0667	0.0612	0.0589	0.0601	0.0648
	3.2	0.1224	0.1206	0.1150	0.1068	0.0966	0.0858	0.0671	0.0613	0.0590	0.0602	0.0647
8	0.8	0.1256	0.1232	0.1163	0.1062	0.0945	0.0827	0.0726	0.0652	0.0612	0.0607	0.0634
	1.35	0.1052	0.1034	0.0984	0.0908	0.0819	0.0731	0.0656	0.0605	0.0587	0.0604	0.0655
	1.6	0.1047	0.1029	0.0980	0.0905	0.0818	0.0730	0.0655	0.0604	0.0585	0.0602	0.0654
	3.2	0.1172	0.1154	0.1101	0.1022	0.0925	0.0823	0.0728	0.0653	0.0606	0.0593	0.0616
12	0.8	0.1289	0.1263	0.1190	0.1083	0.0959	0.0837	0.0732	0.0656	0.0614	0.0607	0.0632
	1.35	0.1049	0.1031	0.0980	0.0904	0.0815	0.0727	0.0653	0.0604	0.0587	0.0606	0.0658
	1.6	0.1036	0.1018	0.0968	0.0894	0.0807	0.0721	0.0648	0.0600	0.0584	0.0604	0.0658
	3.2	0.1119	0.1102	0.1052	0.0976	0.0884	0.0789	0.0702	0.0635	0.0598	0.0595	0.0628
20	0.8	0.1342	0.1313	0.1233	0.1116	0.0983	0.0853	0.0742	0.0662	0.0617	0.0607	0.0628
	1.35	0.1051	0.1033	0.0981	0.0904	0.0814	0.0725	0.0652	0.0604	0.0588	0.0608	0.0662
	1.6	0.1030	0.1012	0.0962	0.0887	0.0800	0.0714	0.0642	0.0597	0.0584	0.0606	0.0663
	3.2	0.1051	0.1035	0.0988	0.0917	0.0832	0.0744	0.0667	0.0612	0.0587	0.0597	0.0642
30	0.8	0.1394	0.1363	0.1275	0.1148	0.1005	0.0867	0.0751	0.0668	0.0620	0.0607	0.0623
	1.35	0.1058	0.1039	0.0986	0.0907	0.0816	0.0727	0.0653	0.0605	0.0591	0.0611	0.0664
	1.6	0.1031	0.1013	0.0962	0.0886	0.0798	0.0712	0.0641	0.0596	0.0585	0.0608	0.0666
	3.2	0.1001	0.0985	0.0940	0.0872	0.0792	0.0711	0.0641	0.0594	0.0578	0.0598	0.0652
90	0.8	0.1593	0.1550	0.1432	0.1264	0.1083	0.0915	0.0779	0.0683	0.0625	0.0601	0.0603
	1.35	0.1095	0.1074	0.1017	0.0932	0.0836	0.0742	0.0666	0.0617	0.0601	0.0620	0.0669
	1.6	0.1050	0.1031	0.0977	0.0898	0.0807	0.0718	0.0646	0.0602	0.0591	0.0615	0.0671
	3.2	0.0884	0.0869	0.0829	0.0769	0.0700	0.0633	0.0581	0.0553	0.0558	0.0599	0.0675

TABLE 3

P mm/hr	λ см	$F(\beta)$ 110°	120°	130°	140°	150°	160°	170°	180°	ω_1	ω_2	q
5	0,8	0,0691	0,0766	0,0851	0,0936	0,1014	0,1075	0,1121	0,1127	0,0001	0,0153	1,09
	1,35	0,0728	0,0828	0,0939	0,1050	0,1150	0,1230	0,1281	0,1298	—0,0096	0,0154	0,81
	1,6	0,0726	0,0826	0,0939	0,1053	0,1169	0,1237	0,1289	0,1301	—0,0095	0,0157	0,81
	3,2	0,0719	0,0808	0,0904	0,0994	0,1067	0,1115	0,1132	0,1132	0,0027	0,0157	1,08
8	0,8	0,0688	0,0760	0,0842	0,0924	0,0999	0,1057	0,1105	0,1108	0,0010	0,0152	1,13
	1,35	0,0735	0,0836	0,0948	0,1058	0,1158	0,1236	0,1286	0,1304	—0,0105	0,0152	0,81
	1,6	0,0736	0,0839	0,0954	0,1068	0,1180	0,1254	0,1305	0,1323	—0,0109	0,0156	0,80
	3,2	0,0671	0,0752	0,0850	0,0953	0,1049	0,1126	0,1176	0,1194	—0,0012	0,0157	0,98
12	0,8	0,0682	0,0750	0,0827	0,0904	0,0974	0,1030	0,1080	0,1077	0,0025	0,0152	1,19
	1,35	0,0739	0,0840	0,0951	0,1061	0,1159	0,1236	0,1286	0,1303	—0,0106	0,0152	0,80
	1,6	0,0742	0,0847	0,0962	0,1076	0,1184	0,1263	0,1311	0,1329	—0,0117	0,0155	0,78
	3,2	0,0693	0,0783	0,0889	0,0998	0,1099	0,1180	0,1233	0,1251	—0,0049	0,0157	0,89
20	0,8	0,0672	0,0733	0,0803	0,0874	0,0938	0,0989	0,1044	0,1033	0,0049	0,0153	1,30
	1,35	0,0742	0,0842	0,0951	0,1059	0,1154	0,1229	0,1277	0,1294	—0,0106	0,0150	0,81
	1,6	0,0748	0,0853	0,0967	0,1080	0,1184	0,1267	0,1310	0,1327	—0,0122	0,0153	0,77
	3,2	0,0719	0,0821	0,0937	0,1054	0,1161	0,1247	0,1303	0,1322	—0,0097	0,0157	0,79
30	0,8	0,0662	0,0717	0,0781	0,0846	0,0905	0,0952	0,1011	0,0993	0,0072	0,0154	1,40
	1,35	0,0744	0,0842	0,0948	0,1053	0,1146	0,1219	0,1265	0,1281	—0,0102	0,0148	0,82
	1,6	0,0751	0,0855	0,0968	0,1078	0,1179	0,1267	0,1303	0,1320	—0,0122	0,0152	0,78
	3,2	0,0739	0,0849	0,0971	0,1095	0,1207	0,1296	0,1354	0,1374	—0,0132	0,0157	0,73
90	0,8	0,0625	0,0661	0,0706	0,0754	0,0799	0,0835	0,0908	0,0868	0,0148	0,0161	1,83
	1,35	0,0742	0,0832	0,0928	0,1022	0,1105	0,1170	0,1211	0,1225	—0,0080	0,0143	0,89
	1,6	0,0753	0,0851	0,0957	0,1060	0,1151	0,1265	0,1267	0,1282	—0,0111	0,0148	0,82
	3,2	0,0782	0,0910	0,1049	0,1186	0,1309	0,1406	0,1468	0,1489	—0,0211	0,0157	0,59

As the computations showed, the characteristic curves of scattering of a polydiverse volume can be represented, with an error that does not exceed 10%, in the form of a segment of a series of Legendre polynomials with three terms of expansion:

$$F(\beta)=\frac{1}{4\pi}[c_0+3c_1P_1(\cos\beta)+5c_2P_2(\cos\beta)], \qquad (13)$$

and $c_0 = 1$.

Table 3 gives the values of the coefficients of this expansion /81
$\omega_1 = \frac{c_1}{2\pi}$ $\omega_2 = \frac{c_2}{2\pi}$. The coefficient ω_1 with change in the intensity of precipitation varies more strongly than does ω_2. This is quite clear from the data in Table 3.

For a rough estimation of the angular distribution of the scattered radiation we can use the ratio of the integral scattering to the leading (with respect to the direction of propagation of the radiation) hemisphere

$$\Gamma_1=2\pi\int_0^{\frac{\pi}{2}}F(\beta)\sin\beta\,d\beta \qquad (14)$$

and to the trailing hemisphere

$$\Gamma_2=2\pi\int_{\frac{\pi}{2}}^{\pi}F(\beta)\sin\beta\,d\beta. \qquad (15)$$

If we substitute (13) into (14) and (15) we find the following values for Γ_1 and Γ_2:

$$\Gamma_1=\pi\left[\frac{c_0}{2\pi}+1{,}5\omega_1\right], \qquad (16)$$

$$\Gamma_2=\pi\left[\frac{c_0}{2\pi}-1{,}5\omega_1\right]. \qquad (17)$$

If we know Γ_1 and Γ_2 we can find the coefficient of asymmetry of scattering

$$q=\frac{\Gamma_1}{\Gamma_2}=\frac{\omega_0+1{,}5\omega_1}{\omega_0-1{,}5\omega_1},$$

where $\omega_0 = \frac{c_0}{2\pi}$.

The values of q for the different wave lengths and intensities of precipitation are shown on Table 4. From the values of q it is clear that for a wave length of 0.8 cm the scattering to the leading hemisphere is greater than to the trailing hemisphere and is increased in proportion to the increase in intensity of precipitation. When λ is equal to 1.35, 1.6 and 3.2 cm, the scattering to the trailing hemisphere is greater than to the leading hemisphere.

TABLE 4.

P mm/hr	q			
	$\lambda = 0{,}8$ см	$\lambda = 1{,}35$ см	$\lambda = 1{,}6$ см	$\lambda = 3{,}2$ см
3	1,04	0,86	0,87	1,08
5	1,00	0,84	0,84	0,92
8	1,04	0,83	0,82	0,92
10	1,04	0,82	0,81	0,92
15	1,08	0,82	0,80	0,89
20	1,08	0,82	0,80	0,85
25	1,12	0,82	0,80	0,79
30	1,17	0,83	0,80	0,75

Of great interest is the explanation of the effect of the width of the spectrum of the distribution of particles by size on the characteristic curves of scattering and the value of the coefficient of asymmetry q in precipitations of different intensity. For this purpose we computed the characteristic curves of scattering for which, as the distribution function N(a), we used the gamma-distribution /82

$$N(a) = Aa^{\alpha}e^{-\sigma a}.$$

The values of α were assumed equal to 1, 2, 3. The computations were made for intensities of precipitation from 0.25 to 100 mm/hr.

The values of the coefficient of asymmetry of scattering for several intensities of precipitation are shown on Table 5. The relative width of the spectrum $\Delta\varepsilon$ is related to α by the simple formula [4]

$$\Delta\varepsilon = \frac{2{,}48}{\sqrt{\alpha}}.$$

Thus, for the cases being studied it was equal to 2.48, 1.76 and 1.43.

TABLE 5

P mm/hr	λ = 0.8 см			λ = 1.35 см			λ = 1.6 см			λ = 3.2 см		
	α = 1	α = 2	α = 3	α = 1	α = 2	α = 3	α = 1	α = 2	α = 3	α = 1	α = 2	α = 3
3	1.01	1.04	1.05	0.83	0.82	0.80	0.82	0.79	0.77	1.06	0.96	0.87
5	1.04	1.10	1.21	0.82	0.80	0.82	0.80	0.79	0.77	0.96	0.87	0.79
8	1.08	1.19	1.32	0.82	0.82	0.83	0.79	0.79	0.79	0.92	0.79	0.72
10	1.10	1.24	1.37	0.82	0.82	0.84	0.79	0.79	0.80	0.84	0.76	0.68
16	1.19	1.32	1.54	0.82	0.84	0.87	0.79	0.80	0.82	0.77	0.69	0.64
20	1.21	1.37	1.65	0.89	0.84	0.89	0.80	0.80	0.83	0.75	0.67	0.62
25	1.25	1.46	1.72	0.98	0.86	0.91	0.80	0.82	0.83	0.72	0.66	0.61
36	1.34	1.58	1.91	0.85	0.89	0.94	—	—	—	0.68	0.62	0.58
50	1.41	1.69	2.06	0.84	0.92	0.97	—	—	—	0.65	0.61	0.57
90	1.58	1.95	2.42	0.91	0.96	0.96	—	—	—	0.62	0.58	0.55

From analysis of the characteristic curves and the coefficients of asymmetry we can make the following conclusions.

When λ = 0.8 cm the scattering to the leading hemisphere is greater than to the trailing hemisphere; with a decrease in the width of the spectrum it is increased. The respective values of the coefficients of asymmetry for the gamma-distribution are greater than for the Marshal-Palmer distribution. The scattering of the energy of wave lengths 1.35 and 1.6 cm to the leading hemisphere increases with decrease in the width of the spectrum of the particles. For precipitations of average intensity, scattering to the trailing hemisphere is the predominant one. Especially interesting is the distribution of scattered energy from the 3.2 cm wave length. Here the back scattering is increased, with increase in the intensity of precipitations and with a decrease in the width of the spectrum of the particles, much more rapidly than it is decreased for wave lengths 1.35 and 1.6 cm.

REFERENCES

1. Shifrin, K.S. and M.M. Chernyak: Oslableniye i rasseyaniye santimetrovogo izlucheniya kaplyami osadkov. (Attenuation and Scattering of Centimeter Radiation by Drops from Precipitations). Trudy Main Geophysical Observatory, No. 203, 1957.
2. Shifrin, K.S.: Rasseyaniye sveta v mutnoy srede. (Scattering of Light in a Cloudy Atmosphere)., Gostekhizdat, 1951.
3. Shifrin, K.S. and M.M. Chernyak: Indikatrisy rasseyaniya santimetrovoy radiatsii kaplyami vody. (Characteristic Curves of Scattering of Centimeter Radiation by Drops of Water). Trudy Main Geophysical Observatory, No. 203, 1967.
4. Shifrin, K.S.: K teorii mikrostruktury. (The Theory of the Microstructure)., Trudy Main Geophysical Observatory, No. 109, 1961.

TRANSFER OF MICROWAVE RADIATION IN CLOUDS AND PRECIPITATION

B.A. Volchok and M.M. Chernyak

ABSTRACT: A precise calculation has been made of the transfer of microwave radiation in a plane layer of clouds and precipitation. The brightness of the emitted radiation is examined as a function of the optical thickness of the layer, the probability of photon survival, the characteristic curves of scattering and of the reflecting properties of the underlying surface. The error which occurs with various simplified approaches is evaluated.

1. Formulation of the Problem and Method of Solving It.

Let us look at a plane parallel layer with an optical thickness τ_0 (Fig. 1). No radiation is externally incident on the upper boundary of the layer ($\tau = 0$), but radiation with an intensity of $I_\tau(\mu, \phi)$ is incident on the lower boundary ($\tau = \tau_0$); the reflection coefficient of the underlying surface is equal to R. /83

To determine the intensity of radiation $I(\tau, \mu, \phi)$ on the optical depth τ in the direction determined by the angles $\vartheta = \arccos \mu$ and ϕ, let us use the transfer equation in the following form [1]:

$$\mu \frac{\partial I(\tau, \mu, \varphi)}{\partial \tau} + I(\tau, \mu, \varphi) = \int_0^{2\pi} d\varphi' \int_{-1}^{1} F(\varkappa, \tau) I(\tau, \mu', \varphi') d\mu' + S(\tau, \mu, \varphi) \quad (1)$$

Where τ is the optical thickness, ϕ is the azimuth, $\vartheta = \arccos \mu$ is the angle between the direction of the beam and the normal to the layer, $I(\tau, \mu, \phi)$ is the intensity of the radiation

$$\varkappa = \mu\mu' + \sqrt{1-\mu^2}\sqrt{1-\mu'^2}\cos(\varphi' - \varphi),$$

$S(\tau, \mu, \phi)$ is a function of the natural radiation from the layer, $F(\varkappa, \tau)$ is the characteristic curve of scattering.

The boundary conditions according to the above, assume the following form:

$$I(0, \mu, \varphi) = 0 \quad \text{when } \mu > 0,$$
$$I(\tau_0, \mu, \varphi) = I_\tau(\mu, \varphi) + \int_0^{2\pi} d\varphi' \int_0^{1} R(\varkappa) I(\tau, \mu', \varphi') d\mu' \quad \text{when } \mu < 0, \quad (2)$$

where $R(\kappa)$ is the reflection coefficient of the underlying surface.

We will assume that the characteristic curves of scattering $F(\kappa, \tau)$ are independent of the optical thickness and, just as the reflection coefficient, can be represented in the form of an expansion of Legendre polynomials:

$$F(\varkappa) = \frac{\lambda}{2\pi} \sum_{\nu=0}^{\infty} \frac{2\nu+1}{2} \omega_\nu P_\nu(\varkappa), \tag{3}$$

$$R(\varkappa) = \frac{1}{2\pi} \sum_{\nu=0}^{\infty} \frac{2\nu+1}{2} r_\nu P_\nu(\varkappa), \tag{4}$$

where $\lambda = \frac{K_r}{K_{att}}$ is the probability of photon survival, K_r is the coefficient of scattering per unit volume, K_{att} is the attenuation factor. /84

In [4] it was shown that for centimeter radiation, the characteristic curves of scattering can be represented by three terms of expansion by Legengre polynomials. There also are shown the values of ω_ν for precipitations of different intensity.

If we assume that the functions I_τ, S may be represented by a trigonometric series of the type

$$\frac{1}{2} C_0(\mu) + \sum_{m=1}^{\infty} C_m(\mu) \cos m\varphi,$$

we will seek the function $I(\tau, \mu, \phi)$ in the form of a series

$$I(\tau, \mu, \varphi) = \frac{1}{2} I_0(\tau, \mu) + \sum_{m=1}^{\infty} I_m(\tau, \mu) \cos m\varphi. \tag{5}$$

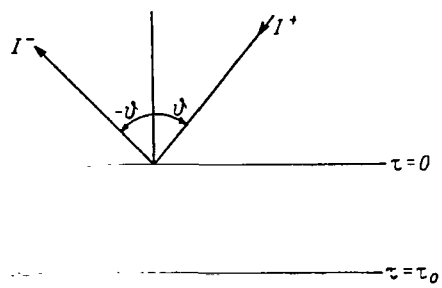

Fig. 1. Schematic of the Reflection of Beams from a Plane Parallel Layer.

Then for each function $I_m(\tau, \mu)$ we will have the following boundary problem:

$$\mu \frac{\partial I_m(\tau, \mu)}{\partial \tau} + I_m(\tau, \mu) = \int_{-1}^{1} I_m(\tau, \mu') F_m(\varkappa) d\mu' + S_m(\tau, \mu) \qquad (6)$$

with the boundary conditions

$$I_m(0, \mu) = 0 \quad \text{when } \mu > 0,$$
$$I_m(\tau_0, \mu) = I_{\tau m}(\mu) + \int_0^1 R_m(\varkappa) I_m(\tau, \mu') d\mu' \quad \text{when } \mu < 0. \qquad (7)$$

Solution to equation (6) with the boundary conditions (7) can be found by the finite-difference method described in reference [2].

Computations were made on an M-20 computer for the various values of $F(\varkappa)$ and λ, borrowed from [3], in which case the value of λ varied from 0.1 to 0.5. The optical thickness τ varied from 0.5 to 3. Since, for wave lengths less than 10 cm, the reflection from the majority of ground underlying surfaces has a diffuse character, the computations were made with a diffuse coefficient of reflection, whose value varied from 0 to 1. Since, in the centimeter band, the Planck function of radiation has a rather simple form:

$$B = \frac{2kT}{\lambda_0^2},$$

where k is the Botlzmann constant, T is the temperature in degrees Kelvin, λ_0 is the wave length, then in equation (1) it is easy to convert from values of the intensity of radiation to the brightness temperature. In the tables given below the brightness temperatures are given in degrees Kelvin, and I^+ and I^- are the brightness temperatures respectively of the katabatic and the anabatic radiations. T_s and T_c denote the temperatures of the underlying surface and the atmosphere. /85

2. Analysis of the Computational Results.

The results of calculations for an absolutely black underlying surface, bounding the layer from below, are given in the Appendix (Table 1). Table 2 of the Appendix gives the values of the brightness temperatures only for the anabatic radiation. B ω_1, ω_2 we denote the coefficients of expansion of the characteristic curves in a series for the Legendre polynomials. The characteristic curves of scattering which correspond to them are shown in

Table 3 of the Appendix and are illustrated in Figure 2. The spherical characteristic curves of scattering correspond to the values $\omega_1 = 0$, $\omega_2 = 0$. Figure 3 illustrates the brightness temperature as a function of the angle ν, when $R = 0$. The same values of the numbers refer to the anabatic and the katabatic radiations which corresponds to it.

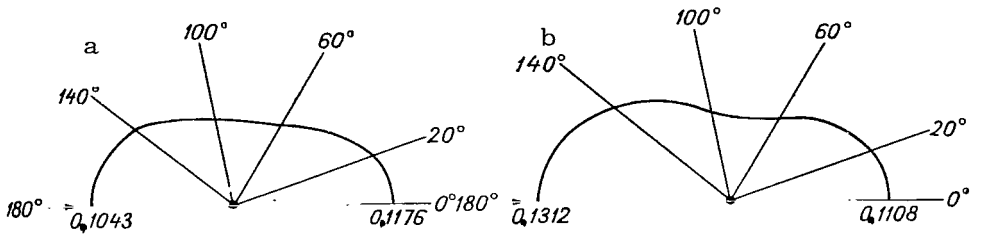

Fig. 2. Characteristic Curves of Scattering per Unit Volume of Precipitation. a: $\lambda_0 = 0.9$ cm, P = 23 mm/hr; b: $\lambda_0 = 3$ cm, P = 35 mm/hr.

As is obvious from the tables, the angular structure of the field of the brightness temperature when $\lambda = 0.4$ and $\lambda = 0.1$ with large values of τ is expressed more weakly than with small optical thicknesses. The increase in brightness temperature in the katabatic radiation with increase in the angle of incidence basically occurs due to the increase in the natural radiation from the atmosphere. In the anabatic radiation the decrease in brightness temperature with an increase in the angle ϑ is due to the increase in absorption and scattering of the transmitted radiation.

Comparison of the fields of the brightness temperatures, computed for the various characteristic curves, shows that these differences are insignificant. The brightness temperatures for the anabatic radiation when $\tau_0 = 3$ and $\tau_0 = 0.5$ differ less than by 3° K. For large angles the values of the brightness temperatures coincide. The brightness temperatures differ slightly also which correspond to the spherical and the nonspherical characteristic curves of scattering. The difference in temperatures does not exceed 2% both when $\lambda = 0.4$ and when $\lambda = 0.1$ for all values of the examined optical thicknesses. This is explained by the fact that with large values of λ the frequency of scattering is high and consequently the form of the characteristic curves of scattering has no substantial influence on the angular structure of the field of the brightness temperature. With a decrease in the value of λ the contribution of the scattered radiation is also decreased. The basic role is begun to be played by the absorption and the natural radiation from the atmosphere, which, being satisfied by the isotropic radiation from the underlying surface, also leads to a weak manifestitation of the angular structure of the field of the radiation. This is especially well seen from the Tables of Brightness Temperatures when $\lambda = 0.1$, where most strongly expressed is the decrease in the difference in the temperatures for the small and large angles. For the anabatic radiation when $\tau_0 = 3$, it does not /86

not exceed 7° K, and when $\tau_0 = 0.5$ it does not exceed 20° K. Apparently the role of the characteristic curves of scattering will be high where $\lambda > 0.1$, the simple scattering will be predominant and the underlying surface is a mirror surface.

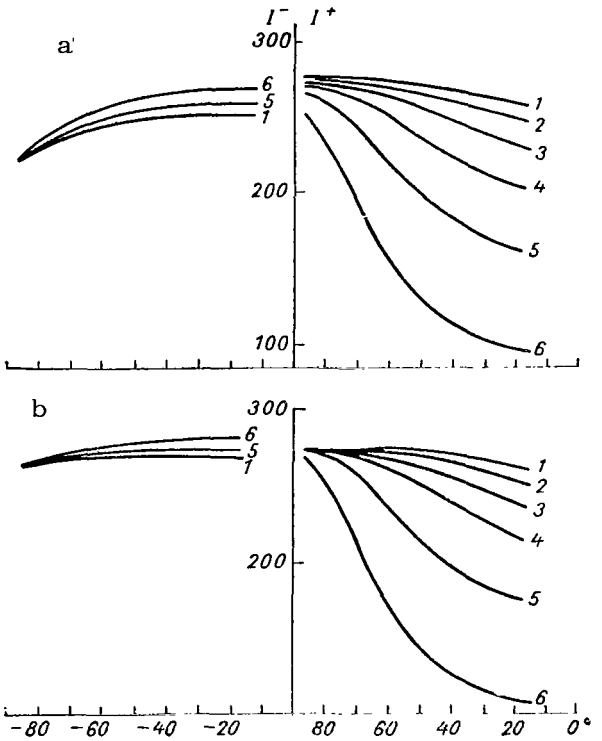

Fig. 3. Brightness Temperature of the Anabatic and Katabatic Radiation as a Function of the Angle of Sighting when R = 0, T_0 = 291° K, T_c = 275° K. a: $\omega_1 = -0.0426$, $\omega_2 = 0.1040$, $\lambda S = 0.4$. b: $\omega_1 = -0.0961$, $\omega_2 = 0.1012$, $\lambda_S = 0.1$. 1. $\tau = 3$; 2. $\tau = 2.5$; 3. $\tau = 2$; 4. $\tau = 1.5$; 5. $\tau = 1$; 6. $\tau = 0.5$.

With an increase in λ and the temperature constant of the atmosphere and the underlying surface, the brightness temperature of the anabatic radiation is decreased; the difference in temperatures is smaller as the optical thickness is smaller. Thus, for example, with an increase in λ from 0.1 to 0.5 for $\vartheta = -17°40'$ the brightness temperatures differ by 11.4% ($\tau_0 = 3$) and by 6.2% ($\tau_0 = 0.5$) and for $\vartheta = -87°20'$ the brightness temperatures differ by 17.5% ($\tau_0 = 3$) and by 11.7% ($\tau_0 = 0.5$). With an increase in the temperature of the underlying surface by 160°K and a variable temperature of the atmosphere, the increase in the brightness temperature of the anabatic radiation is small. When $\tau_0 = 0.5$ this increase amounts to 3.5% ($\vartheta = -17°40'$) and when $\tau_0 = 3$ it is lacking. For the katabatic radiation the increase in brightness temperature comprises tens of degrees.

The numerical values of the brightness temperatures in the presence from below of a diffuse reflecting surface are shown on Table 4 of the Appendix and are illustrated on Figure 4, where along the ordinate axis is plotted the ratio of the brightness temperature to the temperature of the atmosphere. The computations were made for spherical characteristic curves of scattering, for the temperature of the underlying surface for the values of λ and R equal to 291° K. /87

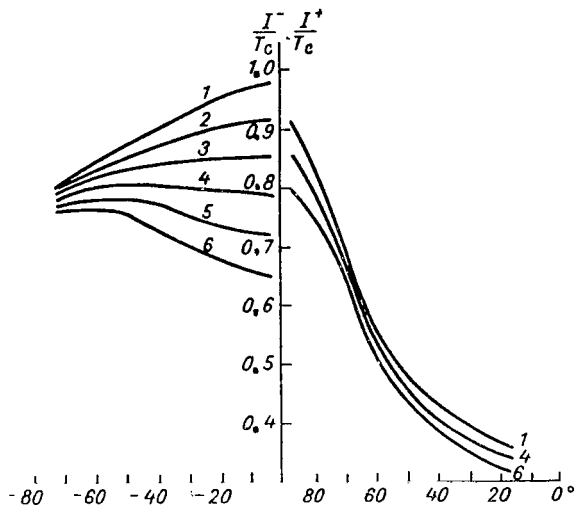

Fig. 4. Brightness Temperature of the Anabatic and Katabatic Radiation as a Function of the Angle of Sighting for a Diffusely Reflecting Underlying Surface when T_c = 275° K, λ_s = 0.4, τ_0 = 0.5. 1. R_0 = 0; 2. R_0 = 0.2; 3. R_0 = 0.4; 4. R_0 = 0.6; 5. R_0 = 0.8; 6. R_0 = 1.

Since, with increase in the reflection coefficient, the natural radiation from the underlying surface is decreased, then it is obvious that with an increase in R the brightness temperatures which correspond to the anabatic and katabatic radiation, must be decreased and the smaller the optical thickness of the layer the more strongly expressed will be the change in the brightness temperature. When λ = 0.1 the change in R from 0 to 1 produces a decrease in I^- for ν = -17°40' by 0.33% (τ_0 = 3) and by 37.6% (τ_0 = 0.5). For ν = -87°40' and τ_0 = 3 the differences in the brightness temperatures are lacking, and when τ_0 = 0.5 it becomes less than 1%. With an increase in λ the difference in the brightness temperatures is increased. Thus, when λ = 0.4 for ν = -17°40' the brightness temperatures differ from the respective values when λ = 0.1 by 0.6% (τ_0 = 3) and by 50.6% (τ_0 = 0.5). Thus, we can virtually ignore the effect from the bottom with diffuse reflection for the optical thicknesses $\tau_0 \geq 3$ and $0.1 \leq \lambda \leq 0.4$ on the value of the brightness temperature. When $\tau_0 < 3$ the effect of the underlying surface must be taken into account. This is seen especially well for τ_0 = 0.5 and λ = 0.4. Even when R = 0.8 - 1.0 the usual character of the dependence of I^- on varies. As is obvious from Figure 4, when $0.8 \leq R \leq 1.0$ the brightness temperature increases along with the increase in . This can be explained in the following way. Since R is high, the basic contribution to radiation incident on the lower boundary of the layer is carried

by the intensity of the katabatic radiation reflected by the surface, and this latter is small for small angles of incidence and is increased in proportion to the increase in angular distance. But since the scattering in the medium is high, the illumination of the reflecting surface is then found to have an insignificant influence on the anabatic current of radiation. The natural radiation from the atmosphere begins to predominate and it grows with increase in the angular distance from the normal, which produces an increase in I^-. /88

Now let us look at the problem of the contribution of the scattered radiation to the intensity of the anabatic and katabatic radiation. Table 5 of the Appendix gives the values of the brightness temperatures in degrees Kelvin without taking into account the scattered radiation when $\lambda = 0.1$ and $\lambda = 0.4$ and an absolutely black underlying surface. In this case the transfer equation has the following solution:

$$I^- = Ie^{-\tau \sec \vartheta} + (1-\lambda)S\left(1 - e^{-\tau \sec \vartheta}\right),$$

$$I^+ = (1-\lambda)S\left(1 - e^{-\tau \sec \vartheta}\right).$$

Comparison of the data from Table 5 with the data from Tables 1 and 2 shows that the brightness temperatures when $\lambda = 0.4$ and ϑ 17°40' differ by 48% ($\tau_0 = 3$) and by 12.5% ($\tau_0 = 0.5$), but when $\vartheta = -87°20'$ it is by 32% ($\tau_0 = 3$) and by 35% ($\tau_0 = 0.5$). When $\lambda = 0.1$ and $\vartheta = -17°40'$ the brightness temperatures differ by 8.7% ($\tau_0 = 3$) and by 4% ($\tau_0 = 0.5$). Therefore, when $\tau_0 < 0.5$ and $\lambda \leq 0.1$, we are justified in ignoring the multiple scattering, but when $\lambda > 0.1$ and $\tau_0 > 0.5$ it must be taken into account. Since in precipitations the mean intensity for wave lenghts less than 3.2 cm, $\lambda \geq 0.2$ and an optical thickness of $\tau_0 > 1$, it is necessary to take into account the multiple scattering. In [4] are given data about λ for precipitations of various intensity and for wave lengths of the microwave band.

The basic conclusions which can be made from the above are the following.

1. With large optical thicknesses the angular structure of the field in the katabatic radiation is expressed more strongly than in the anabatic.

2. The increase in the probability of photon survival λ leads to an increase in the brightness temperature of the anabatic radiation. The effect of λ is greater as the optical thickness becomes larger. For the katabatic radiation a decrease in brightness temperature is observed with optical thickness greater than 1.5 and

$\vartheta < 76°$. For angles greater than 76°, and $\tau_0 \geq 1.5$ with an increase in λ the brightness temperature is increased.

3. The extent of the characteristic curves of scattering and their deviation from the spherical has substantial influence on the angular structure of the field of radiation of microradio waves. The effect of the form of the characteristic curves is smaller as the optical thickness τ_0 is greater.

4. For an optical thickness of $\tau_0 \geq 3$ and $0.1 \leq \lambda \leq 0.4$ the influence of the diffusely reflecting underslying surface on the value of the brightness temperature is very small. With small optical thicknesses the effect of the reflecting properties of the underlying surface becomes significant.

5. We are justified in ignoring the contribution of scattering to the intensity of radiation when $\tau_0 \leq 0.5$ and $\lambda \leq 0.1$. The error here does not exceed 4%. When $\lambda > 0.1$ and $\tau > 0.5$ the contribution of the scattering must be taken into account.

The computations, the results of which are given in the present article, were made on an M-20 computer by A.I. Kostinaya using a program written by L.P. Bass under the direction of T.A. Germogenova. We would like to express our appreciation to the above colleagues and to Prof. K.S. Shifrin for assistance and constant interest in the research.

REFERENCES

1. Sobolev, V.V.: Perenos luchistoy energii v atmosferakh zvezd/89 i planet. (Transfer of Radiant Energy in the Atmospheres of Stars and Planets)., Gostekhizdat, 1956.
2. Germogenova, T.A.: O kharaktere resheniya unravneniya perenosa dlya ploskoxstnogo sloya. (The Character of Solving Transfer Equations for a Plane Layer)., Zh. vych. matem. i matem. fiz., Vol. 1, No. 6, 1961.
3. Shifrin, K.S. and M.M. Chernyak: Indikatrisy rasseyaniya santimetrovoy radiatsii kaplyami vody. (Characteristic Curves of Scattering of Centimeter Radiation by Drops of Water)., Trudy Main Geophysical Observatory, No. 203, 1967.
4. Shifrin, K.S. and M.M. Chernyak: Pogloshcheniye i rasseyaniye mikrovoln v osadkakh. (Absorption and Scattering of Microwaves in Precipitations)., See this Collection.

Table 1

	ϑ	$\tau_0=3$		$\tau_0=2{,}5$		$\tau_0=2$		$\tau_0=1{,}5$		$\tau_0=1$		$\tau_0=0{,}5$		Comment
		$\tau=0$	$\tau=3$	$\tau=0$	$\tau=2{,}5$	$\tau=0$	$\tau=2$	$\tau=0$	$\tau=1{,}5$	$\tau=0$	$\tau=1$	$\tau=0$	$\tau=0{,}5$	
I^+	17°40′	0	263,3	0	254,6	0	240,1	0	215,9	0	175,7	0	109,1	$T_S=291°$ K
	39 40	0	269,7	0	264,1	0	253,6	0	233,9	0	196,9	0	127,9	$T_C=275°$ K
	60	0	274,8	0	273,2	0	269,4	0	259,7	0	234,6	0	169,5	$\lambda=0{,}1$
	76 40	0	275,7	0	275,5	0	275,0	0	273,8	0	269,0	0	238,8	$\omega_1=0{,}028$
	87 20	0	275,0	0	273,8	0	270,6	0	262,2	0	239,3	0	175,9	$\omega_2=0{,}079$
I^-	—17 40	271,5	291,0	272,0	291,0	272,8	291,0	274,2	291,0	276,7	291,0	281,3	291,0	
	—39 40	270,4	291,0	270,7	291,0	271,3	291,0	272,5	291,0	274,8	291,0	279,6	291,0	
	—60	268,6	291,0	268,6	291,0	268,9	291,0	269,4	291,0	271,0	291,0	275,6	291,0	
	—76 40	266,0	291,0	266,0	291,0	266,0	291,0	266,1	291,0	266,4	291,0	268,5	291,0	
	—87 20	268,3	291,0	268,4	291,0	268,6	291,0	269,1	291,0	270,5	291,0	275,0	291,0	
I^+	17 40	0	263,3	0	254,7	0	240,4	0	216,5	0	176,5	0	100,0	$T_S=291°$ K
	39 40	0	269,7	0	264,3	0	253,9	0	234,5	0	197,8	0	128,8	$T_C=275°$ K
	60	0	274,9	0	273,5	0	269,8	0	260,3	0	235,6	0	170,6	$\lambda=0{,}1$
	76 40	0	275,9	0	275,7	0	275,3	0	274,3	0	269,8	0	240,0	$\omega_1=-0{,}096$
	87 20	0	276,1	0	276,0	0	275,3	0	275,2	0	274,1	0	271,4	$\omega_2=0{,}101$
I^-	—17 40	270,5	291,0	271,0	291,0	271,8	291,0	273,3	291,0	275,9	291,0	280,7	291,0	
	—39 40	269,8	291,0	270,1	291,0	270,7	291,0	271,9	291,0	274,2	291,0	279,1	291,0	
	—60	268,5	291,0	268,6	291,0	268,7	291,0	269,4	291,0	271,0	291,0	275,5	291,0	
	—76 40	266,5	291,0	266,6	291,0	266,6	291,0	266,6	291,0	267,0	291,0	269,0	291,0	
	—87 20	263,4	291,0	263,4	291,0	263,4	291,0	263,4	291,0	263,5	291,0	263,7	291,0	
I^+	17 40	0	263,2	0	254,6	0	240,2	0	216,2	0	176,2	0	109,6	$T_S=291°$ K
	39 40	0	269,6	0	264,1	0	253,7	0	234,2	0	197,4	0	129,4	$T_c=275°$ K
	60	0	274,8	0	273,3	0	269,6	0	260,0	0	235,1	0	170,1	$\lambda=0{,}1$
	76 40	0	275,8	0	275,6	0	275,2	0	274,0	0	269,4	0	239,5	$\omega_1=0$
	87 20	0	279,1	0	275,9	0	275,6	0	275,0	0	273,9	0	271,1	$\omega_2=0$

	—17 40	271.6	291.0	272.1	291.0	273.0	291.0	274.4	291.0	276.8	291.0	281.4	291.0	
	—39 40	270.6	291.0	270.9	291.0	271.5	291.0	272.7	291.0	275.0	291.0	279.6	291.0	
I^-	—60	269.0	291.0	269.2	291.0	269.3	291.0	270.0	291.0	271.5	291.0	276.0	291.0	
	—76 40	266.7	291.0	266.7	291.0	266.7	291.0	266.8	291.0	267.1	291.0	269.2	291.0	
	—87 20	263.3	291.0	263.3	291.0	263.4	291.0	263.4	291.0	263.5	291.0	263.7	291.0	
	17 40	0	262.9	0	254.3	0	240.0	0	216.0	0	175.9	0	109.4	$T_S = 275°$ K
	39 40	0	263.3	0	263.8	0	253.4	0	233.9	0	197.1	0	128.2	$T_c = 275°$ K
I^+	60	0	274.4	0	272.9	0	269.2	0	259.6	0	234.8	0	169.8	$\lambda = 0.1$
	76 40	0	275.3	0	275.1	0	274.7	0	273.5	0	268.9	0	239.1	$\omega_1 = 0$
	87 20	0	275.4	0	275.2	0	274.9	0	274.3	0	273.2	0	270.4	$\omega_2 = 0$
	—17 40	270.9	275.0	270.9	275.0	270.9	275.0	270.9	275.0	271.1	275.0	271.8	275.0	
	—39 40	270.3	275.0	270.3	275.0	270.3	275.0	270.3	275.0	270.4	275.0	271.2	275.0	
I^-	—60	269.0	275.0	269.0	275.0	269.0	275.0	269.0	275.0	269.1	275.0	269.8	275.0	
	—76 40	266.7	275.0	266.7	275.0	266.7	275.0	266.7	275.0	266.7	275.0	267.1	275.0	
	—87 20	263.3	275.0	263.3	275.0	263.3	275.0	263.3	275.0	263.3	275.0	263.4	275.0	
	17 40	0	258.8	0	248.2	0	231.3	0	204.5	0	162.5	0	97.5	$T_S = 291°$ K
	39 40	0	266.3	0	258.8	0	245.7	0	222.8	0	183.1	0	114.8	$T_c = 275°$ K
I^+	60	0	273.2	0	270.1	0	263.6	0	250.1	0	220.4	0	153.4	$\lambda = 0.4$
	76 40	0	275.7	0	274.5	0	272.2	0	267.7	0	257.1	0	218.8	$\omega_1 = 0.028$
	87 20	0	277.0	0	276.1	0	274.5	0	271.6	0	266.0	0	254.2	$\omega_2 = 0.079$
	—17 40	252.5	291.0	253.2	291.0	254.5	291.0	256.7	291.0	260.9	291.0	269.8	291.0	
	—39 40	249.6	291.0	250.1	291.0	251.0	291.0	252.9	291.0	256.9	291.0	266.1	291.0	
I^-	—60	243.7	291.0	243.9	291.0	244.4	291.0	245.5	291.0	248.4	291.0	257.5	291.0	
	—76 40	233.9	291.0	234.0	291.0	234.1	291.0	234.5	291.0	235.6	291.0	240.8	291.0	
	—87 20	220.4	291.0	220.4	291.0	220.5	291.0	220.8	291.0	231.3	291.0	222.9	291.0	
	17 40	0	258.6	0	247.9	0	230.9	0	204.0	0	161.9	0	97.1	$T_S = 291°$ K
	39 40	0	266.2	0	258.6	0	245.4	0	222.4	0	182.7	0	114.4	$T_c = 275°$ K
I^+	60	0	273.1	0	260.0	0	263.5	0	249.8	0	220.1	0	153.0	$\lambda = 0.4$
	76 40	0	275.7	0	274.4	0	272.1	0	267.6	0	256.9	0	235.5	$\omega_1 = 0.048$
	87 20	0	276.9	0	276.0	0	274.4	0	271.5	0	266.0	0	254.0	$\omega_2 = 0.081$

	ϑ	$\tau_0=3$		$\tau_0=2,5$		$\tau_0=2$		$\tau_0=1,5$		$\tau_0=1$		$\tau_0=0,5$		Comment
		$\tau=0$	$\tau=3$	$\tau=0$	$\tau=2,5$	$\tau=0$	$\tau=2$	$\tau=0$	$\tau=1,5$	$\tau=0$	$\tau=1$	$\tau=0$	$\tau=0,5$	
I^-	—17°40′	253,1	291,0	253,9	291,0	255,1	291,0	257,9	291,0	261,5	291,0	270,3	291,0	
	—39 40	250,2	291,0	250,7	291,0	251,6	291,0	253,5	291,0	257,4	291,0	266,5	291,0	
	—60	244,2	291,0	244,4	291,0	244,9	291,0	246,0	291,0	248,9	291,0	257,8	291,0	
	—76 40	234,2	291,0	234,4	291,0	234,4	291,0	234,8	291,0	235,9	291,0	241,1	291,0	
	—87 20	220,5	291,0	220,6	291,0	220,7	291,0	220,9	291,0	221,5	291,0	223,0	291,0	
I^+	17°40′	0	259,5	0	249,1	0	232,4	0	205,9	0	164,1	0	99,1	$T_S=291°$ K
	39 40	0	266,9	0	259,6	0	246,7	0	224,1	0	184,7	0	116,3	$T_C=275°$ K
	60	0	273,6	0	270,6	0	264,4	0	251,1	0	221,8	0	154,7	$\lambda=0,4$
	76 40	0	275,9	0	274,7	0	272,6	0	268,3	0	258,0	0	219,8	$\omega_1=0,043$
	87 20	0	277,1	0	276,2	0	274,7	0	271,9	0	266,5	0	254,9	$\omega_2=0,104$
I^-	—17°40′	250,0	291,0	250,7	291,0	251,9	291,0	254,2	291,0	258,6	291,0	268,0	291,0	
	—39 40	247,4	291,0	247,9	291,0	248,8	291,0	250,7	291,0	254,8	291,0	264,4	291,0	
	—60	242,2	291,0	242,4	291,0	242,8	291,0	243,9	291,0	246,8	291,0	256,1	291,0	
	—76 40	233,2	291,0	233,1	291,0	233,2	291,0	233,6	291,0	234,6	291,0	239,9	291,0	
	—87 20	220,0	291,0	220,0	291,0	220,1	291,0	220,4	291,0	220,9	291,0	222,5	291,0	
I^+	17 40	0	259,5	0	249,1	0	232,4	0	205,8	0	163,9	0	98,6	$T_S=291°$ K
	39 40	0	266,7	0	259,3	0	246,4	0	223,7	0	184,1	0	115,7	$T_C=275°$ K
	60	0	273,3	0	270,2	0	263,6	0	250,4	0	220,8	0	153,8	$\lambda=0,4$
	76 40	0	275,7	0	274,4	0	272,7	0	267,5	0	256,8	0	218,6	$\omega_1=0$
	87 20	0	276,6	0	276,0	0	274,3	0	271,5	0	265,5	0	253,5	$\omega_2=0$
I^-	—17 40	252,5	291,0	253,2	291,0	254,3	291,0	256,5	291,0	260,7	291,0	269,5	291,0	
	—39 40	249,2	291,0	249,6	291,0	250,6	291,0	252,4	291,0	256,4	291,0	265,6	291,0	
	—60	242,9	291,0	243,1	291,0	243,5	291,0	244,8	291,0	247,0	291,0	256,8	291,0	
	—76 40	233,0	291,0	233,1	291,0	233,2	291,0	233,6	291,0	234,7	291,0	240,0	291,0	
	—87 20	219,9	291,0	220,1	291,0	220,1	291,0	220,4	291,0	220,9	291,0	222,6	291,0	

I^+	17 40	0	167,5	0	161,5	0	151,4	0	134,6	0	106,3	0	59,0	$T_S = 275°$ K
	39 40	0	172,6	0	169,2	0	173,7	0	150,4	0	127,0	0	82,9	$T_c = 291°$ K
	60	0	176,1	0	175,3	0	173,1	0	167,3	0	151,9	0	110,6	$\lambda = 0,4$
	76 40	0	177,0	0	176,9	0	176,8	0	176,5	0	174,3	0	156,6	$\omega_1 = 0,028$
	87 20	0	177,4	0	177,4	0	177,4	0	177,3	0	177,2	0	177,0	$\omega_2 = 0,079$
I^-	—17 40	182,8	275,0	185,8	275,0	190,8	275,0	199,2	275,0	213,3	275,0	236,6	275,0	
	—39 40	180,3	275,0	182,2	275,0	185,8	275,0	192,6	275,0	205,4	275,0	230,7	275,0	
	—60	178,1	275,0	178,5	275,0	179,8	275,0	192,9	275,0	191,5	275,0	214,2	275,0	
	—76 40	177,2	275,0	177,2	275,0	177,2	275,0	177,4	275,0	178,6	275,0	188,5	275,0	
	—87 20	176,4	275,0	176,4	275,0	176,4	275,0	176,4	275,0	176,5	275,0	176,6	275,0	
I^+	17 40	0	158,6	0	153,5	0	144,9	0	130,6	0	106,5	0	66,4	$T_S = 275°$ K
	39 40	0	162,7	0	159,4	0	153,3	0	141,7	0	119,7	0	78,2	$T_c = 275°$ K
	60	0	166,0	0	165,2	0	163,1	0	157,7	0	143,2	0	104,3	$\lambda = 0,4$
	76 40	0	166,9	0	166,8	0	166,7	0	166,4	0	164,3	0	147,5	$\omega_1 = 0,028$
	87 20	0	167,3	0	167,3	0	167,3	0	167,3	0	167,2	0	166,9	$\omega_2 = 0,079$
I^-	—17 40	173,0	275,0	176,3	275,0	181,9	275,0	191,2	275,0	206,7	275,0	232,5	275,0	
	—39 40	170,3	275,0	172,4	275,0	176,4	275,0	183,9	275,0	198,0	275,0	224,8	275,0	
	—60	167,9	275,0	168,4	275,0	169,8	275,0	173,3	275,0	182,7	275,0	207,8	275,0	
	—76 40	167,0	275,0	167,0	275,0	167,1	275,0	167,3	275,0	168,6	275,0	179,5	275,0	
	—87 20	166,3	275,0	166,3	275,0	166,3	275,0	166,3	275,0	166,4	275,0	166,0	275,0	
I^+	17 40	0	167,4	0	161,4	0	151,3	0	134,4	0	106,2	0	58,9	$T_S = 291°$ K
	39 40	0	172,5	0	163,1	0	162,6	0	150,3	0	127,0	0	82,9	$T_c = 291°$ K
	60	0	176,0	0	175,2	0	173,0	0	167,2	0	151,8	0	110,6	$\lambda = 0,4$
	76 40	0	177,0	0	176,9	0	176,8	0	176,5	0	174,3	0	156,5	$\omega_1 = 0,028$
	87 20	0	177,5	0	177,5	0	177,4	0	177,4	0	177,3	0	177,0	$\omega_2 = 0,079$
I^-	—17 40	183,5	291,0	187,0	291,0	192,8	291,0	202,0	291,0	219,0	291,0	246,2	291,0	
	—39 40	180,6	291,0	182,8	291,0	187,0	291,0	194,9	291,0	209,9	291,0	238,1	291,0	
	—60	179,1	291,0	179,7	291,0	180,1	291,0	183,8	291,0	193,7	291,0	220,2	291,0	
	—76 40	177,2	291,0	177,2	291,0	177,2	291,0	177,5	291,0	178,8	291,0	190,3	291,0	
	—87 20	176,4	291,0	176,4	291,0	176,4	291,0	179,4	291,0	179,5	291,0	176,7	291,0	

Table 2

	ϑ	$\tau_0 = 3$	$\tau_0 = 2{,}5$	$\tau_0 = 2$	$\tau_0 = 1{,}5$	$\tau_0 = 1$	$\tau_0 = 0{,}5$	Comment
	−17°40′	271,5	272,0	272,8	274,2	276,7	281,3	$T_S = 291°$ K
	−39 40	270,4	270,7	271,3	272,5	274,8	279,6	$T_c = 275°$ K
I^-	−60	268,6	268,6	268,9	269,4	271,0	275,6	$\lambda = 0{,}1$
	−76 40	266,0	266,0	266,0	266,1	266,4	268,5	$\omega_1 = 0{,}028$
	−87 20	268,3	268,4	268,6	269,1	270,5	275,0	$\omega_2 = 0{,}079$
	−17 40	270,5	271,0	271,8	273,3	275,9	280,7	$T_S = 291°$ K
	−39 40	269,8	270,1	270,7	271,9	274,2	279,1	$T_c = 275°$ K
I^-	−60	268,5	268,6	268,8	269,4	271,0	275,5	$\lambda = 0{,}1$
	−76 40	266,5	266,6	266,6	266,6	267,0	269,0	$\omega_1 = 0{,}096$
	−87 20	263,4	263,4	263,4	263,4	263,5	263,7	$\omega_2 = 0{,}101$
	−17 40	271,6	272,1	273,0	274,4	276,8	281,4	$T_S = 291°$ K
	−39 40	270,6	270,9	271,5	272,7	275,0	279,6	$T_c = 275°$ K
I^-	−60	269,0	269,2	269,3	270,0	271,5	276,0	$\lambda = 0{,}1$
	−76 40	266,7	266,7	266,7	266,8	267,1	269,2	$\omega_1 = 0$
	−87 20	263,3	263,3	263,4	263,4	263,5	263,7	$\omega_2 = 0$
	−17 40	270,9	270,9	270,9	270,9	271,1	271,8	$T_S = 275°$ K
	−39 40	270,3	270,3	270,3	270,3	270,4	271,2	$T_c = 275°$ K
I^-	−60	269,0	269,0	269,0	269,0	269,1	269,8	$\lambda = 0{,}1$
	−76 40	266,7	266,7	266,7	266,7	266,7	267,1	$\omega_1 = 0$
	−87 20	263,3	263,3	263,3	263,3	263,3	263,4	$\omega_2 = 0$
	−17 40	252,5	253,2	254,5	256,7	260,9	269,8	$T_S = 291°$ K
	−39 40	249,6	250,1	251,0	252,9	256,9	266,1	$T_c = 275°$ K
I^-	−60	243,7	243,9	244,4	245,5	248,4	257,5	$\lambda = 0{,}4$
	−76 40	233,9	234,0	234,1	234,5	235,6	240,8	$\omega_1 = 0{,}028$
	−87 20	220,4	220,4	220,5	220,8	221,3	222,9	$\omega_2 = 0{,}079$
	−17 40	250,0	250,7	251,9	254,2	258,6	268,0	$T_S = 291°$ K
	−39 40	247,4	247,9	248,8	250,7	254,8	264,4	$T_c = 275°$ K
I^-	−60	242,2	242,4	242,8	243,9	246,8	256,1	$\lambda = 0{,}4$
	−76 40	233,0	233,1	232,2	236,6	234,6	239,9	$\omega_1 = 0{,}043$
	−87 20	220,0	220,0	220,1	220,4	220,9	222,5	$\omega_2 = 0{,}104$
	−17 40	252,5	253,2	254,3	256,5	260,7	269,5	$T_S = 291°$ K
	−39 40	249,2	249,2	250,6	252,4	256,4	265,6	$T_c = 275°$ K
I^-	−60	242,9	243,1	243,5	244,8	247,0	256,8	$\lambda = 0{,}4$
	−76 40	233,0	233,1	233,2	233,6	234,7	256,8	$\omega_1 = 0$
	−87 20	219,9	220,2	220,1	220,4	220,9	222,6	$\omega_2 = 0$
	−17 40	173,0	176,3	181,9	191,2	206,7	232,5	$T_S = 275°$ K
	−39 40	170,3	172,4	176,4	183,9	198,0	224,8	$T_c = 275°$ K
I^-	−60	167,9	168,4	169,8	173,3	182,7	207,8	$\lambda = 0{,}4$
	−76 40	167,0	167,0	167,1	167,3	168,6	179,5	$\omega_1 = 0{,}028$
	−87 20	166,3	166,3	166,3	166,3	166,4	166,6	$\omega_2 = 0{,}079$
	−17 40	271,4	271,8	272,2	272,7	272,6	268,2	$T_S = 291°$ K
	−39 40	270,6	270,8	271,1	271,6	271,6	267,5	$T_c = 275°$ K
I^-	−60	269,0	269,1	269,2	269,6	269,7	267,5	$\lambda = 0{,}1$
	−76 40	266,7	266,7	266,7	267,7	266,8	266,3	$R = 0{,}2$
	−87 20	263,3	263,4	263,4	263,4	263,4	263,3	$\omega_1 = \omega_2 = 0$

	ϑ	$\tau_0 = 3$	$\tau_0 = 2{,}5$	$\tau_0 = 2$	$\tau_0 = 1{,}5$	$\tau_0 = 1$	$\tau_0 = 0{,}5$	Comment
	−17°40′	271,1	271,1	270,8	269,5	263,8	241,3	$T_{\blacksquare} = 291°$ K
	−39 40	270,4	270,4	270,2	269,3	264,8	244,1	$T_c = 275°$ K
I^-	−60	269,0	269,0	269,0	268,6	266,1	250,4	$\lambda = 0{,}4$
	−76 40	266,7	266,7	266,7	266,6	266,3	260,4	$R = 0{,}6$
	−87 20	263,3	263,3	263,3	263,3	263,2	262,4	$\omega_1 = \omega_2 = 0$
	−17 40	252,2	252,7	253,3	254,1	254,7	253,0	$T_{\blacksquare} = 291°$ K
	−39 40	249,0	249,3	249,8	250,6	251,4	250,7	$T_c = 275°$ K
I^-	−60	242,8	243,0	243,2	243,7	244,6	245,3	$\lambda = 0{,}4$
	−76 40	233,0	233,0	233,3	233,3	233,7	234,5	$R = 0{,}2$
	−87 20	219,9	220,0	220,0	220,1	220,3	220,3	$\omega_1 = \omega_2 = 0$
	−17 40	251,7	251,6	251,7	248,9	241,7	217,6	$T_S = 291°$ K
	−39 40	248,7	248,7	248,3	246,7	240,8	218,7	$T_c = 275°$ K
I^-	−60	242,7	242,7	242,6	241,8	238,1	220,9	$\lambda = 0{,}4$
	−76 40	233,1	232,9	222,8	232,5	239,3	222,8	$R = 0{,}6$
	−87 20	219,9	219,9	219,8	220,0	218,8	215,4	$\omega_1 = \omega_2 = 0$

Table 3

P mm/hr	λ_0 см	F (ϰ) 0°	10°	20°	30°	40°	50°	60°
23	0,9	0,1176	0,1161	0,1096	0,0974	0,0867	0,0769	0,0689
35	3,0	0,1108	0,1097	0,1073	0,0965	0,0855	0,0802	0,0704
100	3,0	0,0969	0,0959	0,0935	0,0847	0,0754	0,0706	0,0634

P mm/hr	λ_0 см	F (ϰ) 70°	80°	90°	100°	110°	120°	130°
23	0,9	0,0638	0,0614	0,0621	0,0650	0,0726	0,0770	0,0843
35	3,0	0,0625	0,0610	0,0612	0,0645	0,0721	0,0818	0,0934
100	3,0	0,0579	0,0585	0,0611	0,0671	0,0768	0,0884	0,1017

P mm/hr	λ_0 см	F (ϰ) 140°	150°	160°	170°	180°	ω_1	ω_2
23	0,9	0,0891	0,0949	0,0999	0,1031	0,1043	0,028	0,079
35	3,0	0,1027	0,1153	0,1239	0,1297	0,1312	−0,043	0,104
100	3,0	0,1146	0,1262	0,1350	0,1412	0,1429	−0,096	0,101

Table 4

	ϑ	$\tau_0=3$		$\tau_0=2{,}5$		$\tau_0=2$		$\tau_0=1{,}5$		$\tau_0=1$		$\tau_0=0{,}5$		Comment
		$\tau=0$	$\tau=3$	$\tau=0$	$\tau=2{,}5$	$\tau=0$	$\tau=2$	$\tau=0$	$\tau=1{,}5$	$\tau=0$	$\tau=1$	$\tau=0$	$\tau=0{,}5$	
I^+	17°40′	0	259,1	0	248,7	0	231,8	0	205,1	0	162,8	0	97,2	$T_S=291°$ K
	39 40	0	266,3	0	258,8	0	245,8	0	222,8	0	182,8	0	113,9	$T_c=275°$ K
	60	0	272,9	0	269,6	0	263,1	0	249,3	0	219,1	0	151,4	$\lambda=0{,}4$
	76 40	0	277,8	0	273,7	0	271,1	0	268,0	0	254,6	0	215,0	$R=0{,}2$
	87 20	0	276,1	0	275,0	0	273,3	0	269,4	0	262,6	0	248,5	$\omega_1=\omega_2=0$
I^-	—17 40	252,2	286,9	252,7	286,0	253,3	284,5	254,1	281,6	254,7	276,3	253,0	265,3	
	—39 40	249,0	286,9	249,3	286,0	249,8	284,5	250,1	281,6	251,4	276,3	250,7	265,3	
	—60	242,8	286,9	243,0	286,0	243,2	284,5	243,7	281,6	244,6	276,3	245,3	265,3	
	—76 40	233,0	286,9	233,0	286,0	233,3	284,5	233,3	281,6	233,7	276,3	234,5	265,3	
	—87 20	219,9	286,9	220,0	286,0	220,0	284,5	220,1	281,6	220,3	276,3	220,3	265,3	
I^+	17 40	0	258,4	0	247,7	0	230,7	0	203,4	0	160,4	0	94,0	$T_S=291°$ K
	39 40	0	265,5	0	257,8	0	244,4	0	220,9	0	180,1	0	110,2	$T_c=275°$ K
	60	0	271,8	0	268,4	0	261,4	0	246,9	0	215,6	0	146,4	$\lambda=0{,}4$
	76 40	0	273,7	0	272,0	0	268,9	0	263,0	0	250,8	0	207,3	$R=0{,}6$
	87 20	0	274,3	0	272,8	0	270,2	0	265,3	0	256,3	0	237,8	$\omega_1=\omega_2=0$
I^-	—17 40	251,7	278,1	251,6	275,3	251,0	270,3	248,9	261,3	241,7	244,5	217,6	210,6	
	—39 40	248,7	278,1	248,7	275,3	248,3	270,3	246,7	261,3	240,8	244,5	218,7	210,6	
	—60	242,7	278,1	242,7	275,3	242,6	270,3	241,8	261,3	238,1	244,5	220,9	210,6	
	—76 40	233,1	278,1	232,9	275,3	232,8	270,3	232,5	261,3	239,3	244,5	222,8	210,6	
	—87 20	219,9	278,1	219,9	275,3	219,8	270,3	220,5	261,3	218,8	244,5	215,4	210,6	
I^+	17 40	0	258,0	0	247,2	0	230,0	0	202,5	0	159,1	0	92,3	$T_S=291°$ K
	39 40	0	265,0	0	257,3	0	243,7	0	219,9	0	178,6	0	108,2	$T_c=275°$ K
	60	0	271,3	0	267,7	0	260,5	0	245,7	0	213,7	0	143,6	$\lambda=0{,}4$
	76 40	0	273,3	0	277,8	0	267,8	0	261,3	0	247,2	0	203,2	$R=0{,}8$
	87 20	0	273,4	0	271,7	0	268,6	0	263,1	0	252,9	0	232,0	$\omega_1=\omega_2=0$
I^-	—17 40	251,4	273,3	251,0	269,4	249,8	262,7	246,1	250,4	234,7	227,4	198,7	181,2	
	—39 40	248,5	273,3	248,3	269,4	247,5	262,7	244,6	250,4	235,0	227,4	201,6	181,2	
	—60	242,7	273,3	242,6	269,4	242,2	262,7	240,7	250,4	234,6	227,4	207,8	181,2	
	—76 40	232,9	273,3	232,1	269,4	232,7	262,7	232,1	250,4	229,9	227,4	217,1	181,2	
	—87 20	219,9	273,3	219,8	269,4	219,6	262,7	219,3	250,4	218,0	227,4	212,8	181,2	

	17 40	0	263,0	0	254,4	0	240,0	0	215,9	0	175,6	0	108,8	$T_S = 291°$ K
	39 40	0	269,4	0	263,9	0	253,4	0	233,8	0	196,8	0	127,4	$T_c = 275°$ K
I^+	60	0	274,6	0	273,0	0	269,2	0	259,5	0	234,3	0	168,8	$\lambda = 0,1$
	76 40	0	275,5	0	275,2	0	274,6	0	273,3	0	268,2	0	237,5	$R = 0,6$
	87 20	0	275,6	0	275,3	0	274,9	0	274,0	0	272,3	0	268,1	$\omega_1 = \omega_2 = 0$
	—17 40	271,1	279,8	271,1	278,0	270,8	274,8	269,5	268,3	263,8	255,0	241,3	224,4	
	—39 40	270,4	279,8	270,4	278,0	270,2	274,8	269,3	268,3	264,8	255,0	244,1	224,4	
I^-	—60	269,0	279,8	269,0	278,0	269,0	274,8	268,6	268,3	266,1	255,0	250,4	224,4	
	—76 40	266,7	279,8	266,7	278,0	266,7	274,8	266,6	268,3	266,3	255,0	260,4	224,4	
	—87 20	263,3	279,8	263,3	278,0	263,3	274,8	263,3	268,3	263,2	255,0	262,4	224,0	
	17 40	0	262,9	0	254,3	0	239,9	0	215,7	0	175,4	0	108,5	$T_S = 291$ K
	39 40	0	269,3	0	263,8	0	253,3	0	233,6	0	196,6	0	127,1	$T_c = 275°$ K
I^+	60	0	274,5	0	272,9	0	269,1	0	259,3	0	234,0	0	168,4	$\lambda = 0,1$
	76 40	0	275,3	0	275,0	0	274,5	0	273,1	0	267,8	0	236,8	$R = 0,8$
	87 20	0	275,4	0	275,1	0	274,7	0	273,7	0	271,7	0	267,1	$\omega_1 = \omega_2 = 0$
	—17 40	270,9	275,9	270,8	273,6	270,1	269,2	267,8	260,6	259,4	242,7	227,6	201,8	
	—39 40	270,3	275,9	270,2	273,6	269,8	269,2	268,1	260,6	261,3	242,7	232,0	201,8	
I^-	—60	269,0	275,9	269,0	273,0	268,8	269,2	268,1	260,0	264,3	242,7	241,7	201,8	
	—76 40	267,8	275,9	266,7	273,6	266,7	269,2	266,6	260,6	265,9	242,7	257,4	201,8	
	—87 20	263,3	275,9	263,3	273,6	263,3	269,2	263,3	260,6	263,1	242,7	262,0	201,8	
	17 40	0	262,8	0	254,2	0	239,8	0	215,6	0	175,2	0	108,2	$T_S = 291°$ K
	39 40	0	269,3	0	263,7	0	253,2	0	233,5	0	196,3	0	126,5	$T_c = 275°$ K
I^+	60	0	274,4	0	272,8	0	268,9	0	259,1	0	233,7	0	167,9	$\lambda = 0,1$
	76 40	0	275,2	0	274,9	0	274,3	0	272,8	0	267,5	0	236,1	$R = 1,0$
	87 20	0	275,2	0	274,9	0	274,4	0	273,4	0	271,2	0	266,1	$\omega_1 = \omega_2 = 0$
	—17 40	270,7	272,1	270,4	269,2	269,4	263,6	266,1	252,8	254,9	230,4	213,9	178,9	
	—39 40	270,2	272,1	270,0	269,2	269,4	263,6	266,9	252,8	257,7	230,4	219,8	178,9	
I^-	—60	268,9	272,1	268,9	269,2	268,7	263,6	267,7	252,8	262,5	230,4	233,0	178,9	
	—76 40	266,7	272,1	266,7	269,2	266,6	263,6	266,5	252,8	265,6	230,4	254,3	178,9	
	—87 20	263,3	272,1	263,3	269,2	263,3	263,6	263,2	252,8	263,0	230,4	261,6	178,9	
	17 40	0	257,5	0	246,7	0	229,3	0	201,5	0	157,7	0	90,6	$T_S = 291°$ K
	39 40	0	264,5	0	256,7	0	242,9	0	218,8	0	177,0	0	106,1	$T_c = 275°$ K
I^+	60	0	270,6	0	267,0	0	259,6	0	244,3	0	211,7	0	140,8	$\lambda = 0,4$
	76 40	0	272,2	0	270,2	0	266,5	0	259,6	0	255,7	0	199,0	$R = 1,0$
	87 20	0	272,4	0	270,4	0	267,0	0	260,8	0	249,2	0	226,0	$\omega_1 = \omega_2 = 0$

	ϑ	$\tau_0=3$		$\tau_0=2{,}5$		$\tau_0=2$		$\tau_0=1{,}5$		$\tau_0=1$		$\tau_0=0{,}5$		Comment
		$\tau=0$	$\tau=3$	$\tau=0$	$\tau=2{,}5$	$\tau=0$	$\tau=2$	$\tau=0$	$\tau=1{,}5$	$\tau=0$	$\tau=1$	$\tau=0$	$\tau=0{,}5$	
	−17°40′	251,1	268,2	250,4	263,3	248,5	254,5	243,1	238,7	227,3	209,3	179,0	150,6	
	−39 40	248,3	268,2	247,9	263,3	246,6	254,5	242,4	238,7	228,9	209,3	183,7	150,6	
I^-	−60	242,6	268,2	242,4	263,3	241,8	254,5	239,6	238,7	231,0	209,3	194,1	150,6	
	−76 40	232,8	268,2	272,8	263,3	232,5	254,5	231,7	238,7	228,6	209,3	210,0	150,6	
	−87 20	219,8	268,2	219,8	263,3	219,6	254,5	219,1	238,7	217,2	209,3	210,0	150,6	
	17 40	0	263,1	0	254,5	0	240,2	0	216,1	0	176,0	0	109,3	$T_S=291°$ K
	39 40	0	269,5	0	264,0	0	253,6	0	234,0	0	197,2	0	128,1	$T_c=275°$ K
I^+	60	0	274,7	0	273,2	0	269,5	0	259,6	0	234,9	0	169,7	$\lambda=0{,}1$
	76 40	0	275,7	0	275,5	0	275,0	0	273,8	0	269,0	0	238,9	$R=0{,}2$
	87 20	0	275,9	0	275,7	0	275,4	0	274,7	0	273,3	0	270,1	$\omega_1=0$ · $\omega_2=0$
	−17 40	271,4	287,3	271,8	286,7	272,2	285,6	272,7	283,5	272,6	279,1	268,2	269,0	
	−39 40	270,6	287,3	270,8	286,7	271,1	285,6	271,6	283,5	271,6	279,1	268,0	269,0	
I^-	−60	269,0	287,3	269,1	286,7	269,2	285,6	269,6	283,5	269,7	279,1	267,5	269,0	
	−76 40	266,7	287,3	266,7	286,7	266,7	285,6	266,7	283,5	266,8	279,1	266,3	269,0	
	−87 20	263,3	287,3	263,4	286,7	263,4	285,6	263,4	283,5	263,4	279,1	263,3	269,0	
	17 40	0	263,0	0	254,5	0	240,1	0	216,0	0	175,8	0	109,1	$T_S=291°$ K
	39 40	0	269,5	0	263,9	0	253,5	0	233,9	0	197,0	0	127,8	$T_c=275°$ K
I^+	60	0	274,7	0	273,1	0	263,9	0	259,6	0	234,6	0	169,3	$\lambda=0{,}1$
	76 40	0	275,6	0	277,3	0	274,8	0	273,5	0	268,6	0	238,2	$R=0{,}4$
	87 20	0	275,7	0	275,5	0	275,1	0	274,4	0	272,8	0	269,1	$\omega_1=0$ $\omega_2=0$
	−17 40	271,3	283,6	271,4	282,4	271,5	280,2	271,1	276,0	268,2	267,1	254,8	246,8	
	−39 40	270,5	283,6	270,6	282,4	270,7	280,2	270,4	276,0	268,2	267,1	256,1	246,8	
I^-	−60	269,0	283,6	269,0	282,4	269,1	280,2	269,0	276,0	267,9	267,1	259,0	246,8	
	−76 40	266,7	283,6	266,6	282,4	266,7	280,2	266,7	276,0	266,1	267,1	268,3	246,8	
	−87 20	263,3	283,6	263,3	282,4	263,3	280,2	263,3	276,0	263,3	267,1	268,8	246,8	

Table 5

	ϑ	$\tau_0=3$		$\tau_0=2,5$		$\tau_0=2$		$\tau_0=1,5$		$\tau_0=1$		$\tau_0=0,5$		Comment
		$\tau=0$	$\tau=3$	$\tau=0$	$\tau=2,5$	$\tau=0$	$\tau=2$	$\tau=0$	$\tau=1,5$	$\tau=0$	$\tau=1$	$\tau=0$	$\tau=0,5$	
I^+	17°40′	0	236,9	0	229,4	0	217,1	0	196,3	0	160,9	0	101,0	$T_S=291°$ K
	39 40	0	242,6	0	237,8	0	229,2	0	212,1	0	180,0	0	118,1	$T_c=275°$ K
	60	0	247,0	0	245,8	0	243,0	0	235,1	0	214,1	0	156,4	$\lambda=0,1$
	76 40	0	247,5	0	247,5	0	247,5	0	247,0	0	244,3	0	219,0	$\omega_1=0$
	87 20	0	247,5	0	247,5	0	247,5	0	247,5	0	247,5	0	247,5	$\omega_2=0$
I^-	—17 40	249,4	291,0	250,6	291,0	252,9	291,0	256,5	291,0	262,7	291,0	273,3	291,0	
	—39 40	248,4	291,0	249,1	291,0	250,7	291,0	253,7	291,0	259,4	291,0	270,3	291,0	
	—60	247,6	291,0	247,8	291,0	248,2	291,0	249,7	291,0	253,4	291,0	263,5	291,0	
	—76 40	247,5	291,0	247,5	291,0	247,6	291,0	247,6	291,0	248,1	291,0	252,5	291,0	
	—87 20	247,5	291,0	247,5	291,0	247,5	291,0	247,5	291,0	247,5	291,0	247,5	291,0	
I^+	17 40	0	157,9	0	153,0	0	144,7	0	130,8	0	107,3	0	67,3	$T_S=291°$ K
	39 40	0	161,7	0	158,6	0	152,8	0	141,4	0	120,0	0	78,7	$T_c=275°$ K
	60	0	164,7	0	163,8	0	162,0	0	156,8	0	142,7	0	104,3	$\lambda=0,4$
	76 40	0	165,0	0	165,0	0	165,0	0	164,7	0	162,9	0	146,0	$\omega_1=0$
	87 20	0	165,0	0	165,0	0	165,0	0	165,0	0	165,0	0	165,0	$\omega_2=0$
I^-	—17 40	170,0	291,0	174,2	291,0	180,5	291,0	191,0	291,0	209,1	291,0	239,6	291,0	
	—39 40	166,8	291,0	169,9	291,0	174,3	291,0	183,0	291,0	199,4	291,0	230,9	291,0	
	—60	165,3	291,0	165,8	291,0	167,2	291,0	171,4	291,0	182,0	291,0	211,4	291,0	
	—76 40	165,0	291,0	165,0	291,0	165,1	291,0	165,3	291,0	166,7	291,0	179,5	291,0	
	—87 20	165,0	291,0	165,0	291,0	165,0	291,0	165,0	291,0	165,0	291,0	165,0	291,0	

INVESTIGATION OF RADIO EMISSION AND ABSORPTION OF A CLOUDY ATMOSPHERE IN THE MILLIMETER AND CENTIMETER WAVE BANDS

A.Ye. Basharinov and B.G. Kutuza

ABSTRACT: The influence of the temperature changes in the Debye parameters on the UHF-spectrum of absorption and radio emission from clouds is studies. A method of simultaneous measurements of the absorption of radio emission from a cloudy atmosphere in the microwave band is described. Experimental data on the spectrum of radiobrightness temperatures and the value of the absorption in stratiform and cumuloform clouds are cited. According to the measurement data of the absorptions at waves of 0.41, 0.82 and 1.6 cm of radio emission from the Sun the value of the relaxation time of a molcule of water is determined, the value of which, at a temperature of -10° C, was $2.5 \cdot 10^{-12}$ sec. According to the results of the spectral variations in the total absorption and the radio-brightness temperature of the atmosphere, evaluations were obtained for the integral water content of the clouds and of the total moisture content of the atmosphere.

1

The radioastronomical methods of investigating the atmosphere, /100 developed in references [1-4] relative to a free atmosphere, may also be used for investigating hydrometeors.

The purpose of the present paper is to investigate, by radio-astronomical methods, the spectrum of the microwave absorptions as a function of the properties of atmospheric cloud formations.

Let us look at the relationships which characterize the radio transparency and the emittance of a cloudy atmosphere in the UHF-band.

The radiobrightness temperature of the natural radiation from the atmosphere under conditions of a local thermodynamic equilibrium, without taking into account the processes of scattering, is determined in the form [5]

$$T_b = \int_0^a T(\Gamma) e^{-\Gamma} d\Gamma, \qquad (1)$$

where $\Gamma_a = \sec z \int_0^{\infty} \varkappa_a(H)\,dH$ is the total absorption in the atmosphere in the direction of the zenith angle z, $\Gamma = \sec z \int_0^{H_1} \varkappa_a(H)\,dH$ is the absorption in the layer of the atmosphere at an altitude of H_1 (0 - H_1), T(Γ) is the absolute temperature as a function f the absorption.

The integral relationship (1) for the brightness temperature may be represented also in the form

$$T_b = (T_0 - \Delta T) \ldots e^{-\tau_a} \qquad (2)$$

where ΔT is the correction for nonisothermicity of the atmosphere comprising from 5 - 30° K at different wave lengths.

The total absorption in a cloudy atmosphere is comprised of absorption in oxygen, water vapor and in water drops. The absorption coefficient in oxygen and water vapor for wave lengths of λ> 0.2 cm outside the regions of resonance of oxygen has the form [2]

$$\varkappa_a = \frac{\gamma_{11} P^2}{T^{5/2}} \ldots \frac{\gamma_{21} P}{T^{3/2}} \rho_h = \frac{\gamma_{22} P}{T^2} \rho_h e^{-\frac{280}{T}}, \qquad (3)$$

where α_{11}, α_{21}, α_{22} are constants for a given wave, P is the pressure, T is the temperature, ρ_h is the absolute humidity. /101

Absorption in liquid clouds under conditions of Rayleigh scattering may be represented by the following expression

$$\tau_{cl} \int_0^l \frac{8.2}{\lambda} \operatorname{Im}\left(\frac{\varepsilon_c - 1}{\varepsilon_c + 2}\right) w_l\,dl, \qquad (4)$$

where λ is the wave length, ω_ℓ is the water content of the clouds in g/m^3, ε_c is the complex dielectric onstant of the water, ℓ is the length of the beam in the cloud.

For an isothermic cloud the absorption is proportional to its integral water content W (the amount of water in a liquid state, included in a column of air with a base of 1 m^2, the direction of which coincides with the electrix axis of the antenna). Here

$$W = \int_0^l w_l\,dl. \qquad (5)$$

The frequency dependence of the dielectric constant of water in the radio band is determined by the Debye formula

$$\varepsilon_c = \frac{\varepsilon_0 - \varepsilon_\infty}{1 + i\frac{\Delta\lambda}{\lambda}} + \varepsilon_\infty, \qquad (6)$$

where $\Delta\lambda = 2\pi c\tau_p \frac{\varepsilon_0 + 2}{\varepsilon_\infty + 2}$, τ_r is the relaxation time of the molecules of water, ε_0 is the dielectric constant of the water at frequencies $\omega << \frac{1}{\tau_r}$, $\varepsilon\infty$ is the dielectric constant of the water at frequencies $\omega >> \frac{1}{\tau_r}$.

The frequency dependence of the complex dielectric constant of the water is manifested in the spectral dependence of the absorption coefficient in the clouds. The dielectric properties of the water drops were investigated by a number of authors under laboratory conditions (see, for example, [6-9]).

According to the data of Kerr [6], the values ε_0 and ε_∞ coincide with the results given in [7], and the value $\Delta\lambda$ differs slightly from that given in [7]. The largest discrepancy is found for a temperature of 40° C. At a temperature of 0 - 10° C the values differ little among themselves. Table 1 gives the results of both papers.

TABLE 1.

Temperature, °C	ε_0	ε_∞	$\Delta\lambda$ [7] cm	$\Delta\lambda$ [6] cm
0	88	5.5	3.34	3.59
10	84	5.5	2.39	2.24
20	80	5.5	1.80	1.52
30	76.5	5.5	1.39	1.12
40	73	5.5	1.12	0.859

Lane and Saxton [9] measured the values of the refractive index of the water at wave lengths of 0.62, 1.24, and 3.21 cm at temperatures above the melting point of ice and determined the imaginary part of the refactive index of water at wave lengths of 0.62 and 1.24 cm at a temperature of -8° C. /102

These investigations show that the Debye formulas can be used in the extire millimeter and centimeter band. From Table 1 it is

clear that the parameters ε_0 and $\Delta\lambda$ depend on temperature. The temperature. The temperature dependence is expressed most strongly on the parameter $\Delta\lambda$ due to change in the relaxation time of the molecules of water.

At a temperature above the melting point of ice the experimental values of τ_r, taken from [6] and [7], may be represented within 5% accuracy by a temperature dependence of the following type:

$$\tau_r = e^{a\left(\frac{273}{T} - b\right)} 10^{-12} \text{ sec}, \tag{7}$$

where a and b are constants, T is the absolute temperature of water in degrees Kelvin.

The values of the constants a and b from the results of references [6] and [7] are the following: for [6] a = 10.5, b = 0.96; for [7] a = 7.6, b = 0.95.

In the clouds the drops of water are mostly found in a supercooled state, i.e., at a temperature below the melting point of ice. In studying the spectra of the clouds we shall assume that at temperatures below the melting point of ice the parameter remains constant, the parameter ε_∞ remains constant and the parameter ε_0 may be found by linear extrapolation of the values when T > 273° K; for τ_r the relationship in [7] is satisfied with the constants a = 9 and b = 0.95.

The spectrum of absorption in a liquid cloud is determined by $\operatorname{Im}\left(\frac{\varepsilon_c - 1}{\varepsilon_c + 2}\right)$. On Figure 1 is plotted $\operatorname{Im}\left(\frac{\varepsilon_c - 1}{\varepsilon_c + 2}\right)$ as a function of y, where $y = \frac{2\pi c \tau_r}{\lambda} \frac{\varepsilon_0 + 2}{\varepsilon_\infty + 2}$

Curves 1 and 2 on Figure 1 correspond to values of ε_0 at temperatures of 20 and -10° C. We can see that the difference between the curves consists only of the fact that they are shifted relative to y.

With values of y < 2 we find a linear dependence $\operatorname{Im}\left(\frac{\varepsilon_c - 1}{\varepsilon_c + 2}\right)$ on y. When τ_r = const we have $\operatorname{Im}\left(\frac{\varepsilon_c - 1}{\varepsilon_c - 2}\right) \sim \frac{1}{\lambda}$ and $\Gamma c\ell \approx \frac{1}{\lambda 2}$. The condition y > 0.8 cm with a temperature of 20° C and in the wave band λ> 2.5 cm with a temperature of -10° C.

With an increase in y in the range of 2 < y < 10 the slope of the curves is decreased. Here the form of the spectrum in the short-wave band deviates strongly from the quadratic function.

The maximum $\mathrm{Im}\left(\frac{\varepsilon_c - 1}{\varepsilon_c + 2}\right)$ occurs when the values of y = 10-14. In the region of the maximum $\mathrm{Im}\left(\frac{\varepsilon_c - 1}{\varepsilon_c + 2}\right)$ the derivative $\frac{\partial \mathrm{Im}\left(\frac{\varepsilon_c - 1}{\varepsilon_c + 2}\right)}{\partial \tau_r}$ has a value near zero, which leads to a decrease in the temperature dependence of the absorption. With a temperature of $t_{c\ell}$ = -10° C the maximum $\mathrm{Im}\left(\frac{\varepsilon_c - 1}{\varepsilon_c + 2}\right)$ is near the wave length λ = 0.4 cm; at a temperature of $t_{c\ell}$ = 10° C, it is near the wave length λ = 0.2 cm.

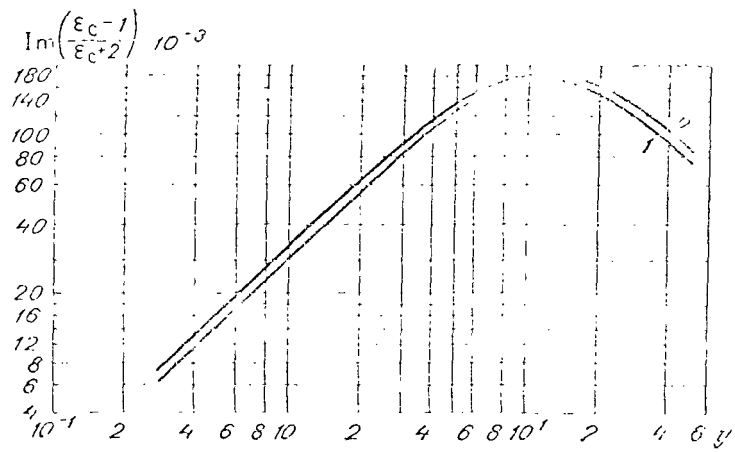

Fig. 1. Temperature Factor of the Absorption Coefficient in a Cloud as a Function of the Parameter y. /103

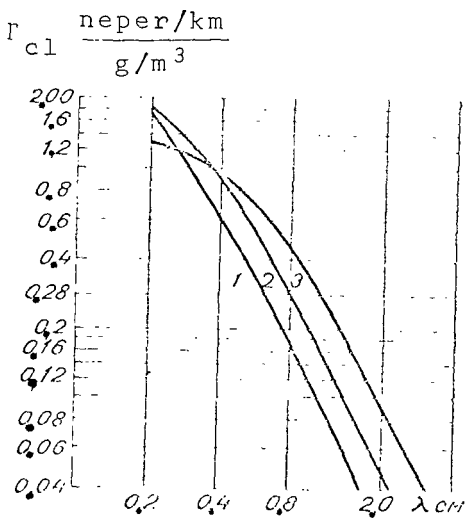

Fig. 2. Spectra of Absorption in a Cloud for Various Values of the Temperature. 1. $t_{c\ell}$ = 20° C; 2. $t_{c\ell}$ = 0° C; 3. $t_{c\ell}$ = 20° C.

Figure 2 gives the spectra of absorption in clouds for temperature values of 20, 0 and -20°C. From the graphs in Figure 2 it is clear that the temperature of cloud has quite a strong influence on the spectrum of absorption. For example, at a temperature of -20° C the absorption in the clouds, taking into account the extrapolation, significantly deviates from the function $\approx \frac{1}{\lambda^2}$ in the millimeter wave band[1].

3

The experimental investigations of the radiation and absorption of a cloudy atmosphere were begun by us in 1962 - 1963 at wave lengths of 0.4 and 0.8 cm in the region of Leningrad. These investigations were then continued on an RT-22 radiotelescope at the Lebedev Physics Institute [12].

At the time of the radiometric measurements of the atmosphere we regularly made observations of temperature, pressure and the absolute moisture content on the surface of the Earth; in cloudy weather we noted the form and the altitude of the lower boundary of the cloud from [13]. We made four flights for aircraft-sounding from the Vnukovo airport, located at a distance of 60 km from the RT-22.

The measurements were made at the following wave lengths: 0.4, 0.8, 1.6, 3.3 and 10 cm. The concise characteristics applicable to the RT-22 radiometric instrument are shown on Table 2.

In Table 2, $\sqrt{\delta T^2}$ is the fluctuation sensitivity of the radiometer, τ_t is the time constant of the emitter, Δf is the frequency band transmitted by the radiometer, θ is the width of the directional diagram for the level 0.5. The electric axes of the antenna at the indicated wave lengths were set up with the aid of a special radiator, aligned in focus of the 22-meter mirror.

The calibration measurements of the antenna parameters were made by a combined determination of the radio transparency and the radiobrightness temperature of the atmosphere simultaneously on several wave lengths. This permitted determining the antenna parameters with an accuracy no less than 10% in mean square error.

---

[1] Because of the smallness of the imaginary part of the dielectric constant of ice the absorption in crystalline clouds regardless of the form of the crystals is more than two orders of magnitude smaller than in drop supercooled clouds, having a temperature and water content identical to them. If we take into account that the water content of the crystalline clouds is less than the liquid clouds and does not exceed 0.7 g/m^3 [11] then it is obvious that we can ignore the absorption in them.

Table 2

Type of Radiometer	Wave length, cm	$\sqrt{\delta T^2}$	τ_t sec.	Δf MHz	θ ang. min.
Superheterodyne	0.41	3÷4	8	30	2.0
Superheterodyne	0.82	0.8	4	30	2.0
Superheterodyne	1.57	0.8	5	60	3.5
Parametric	3.34	0.1	5	60	5.9
Superheterodyne	3.34	0.1	5	60	5.9
Parametric of Direct Amplification	10.3	0.05	2	200	18.0

The radiometric measurements of the clouds were made on the RT-22 from May 1964 to June 1965 under various meteorlogical conditions. The registration of the clouds was made with a stationary antenna or with rotation of it by azimuth. In the presence of a solid uniform cloud cover or storm we used the vertical cross sections of the atmosphere. /105

The signal/noise ratio, determined by the brightness temperature of radiation from the cloud relative to the level of the clear sky and the fluctuation sensitivity of the radiometer was not the same at the various wave lengths. The largest signal/noise ratio was obtained at a wave length of 0.82 cm. At this wave length we recorded the radiation from clouds of the lower level and the vertical development, with the exception of thin, translucent stratus and cumulus clouds. At all wave lengths we confidently recorded the large cumulus clouds Cu cong and the individual average cumulus clouds Cu med.

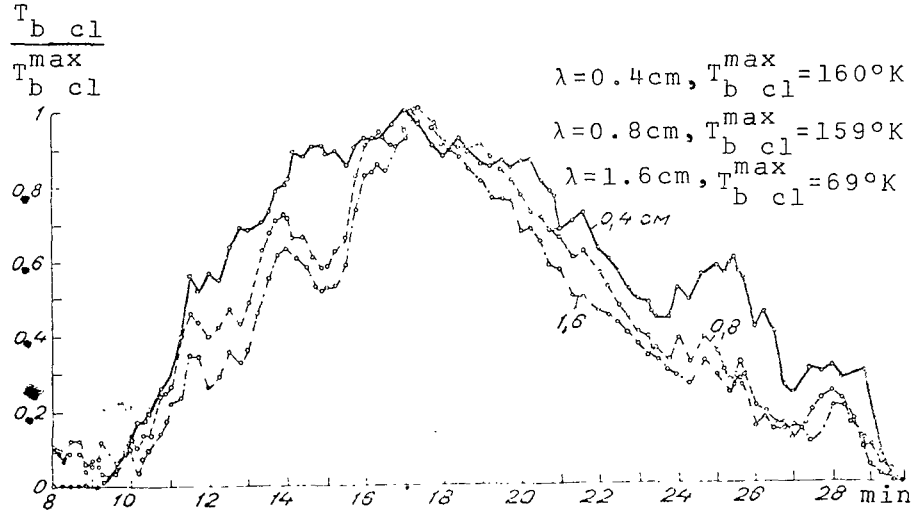

Fig. 3. Relative Variations of the Brightness Temperature of the Cloud at Wave Lengths of 0.4, 0.8 and 1.6 cm. The Brightness Temperature of a Cloud-Free Sky at λ = 0.4 cm was 100° K, at λ = 0.8 cm, 38° K, at λ = 1.6 cm, 22° K. The zenith angle is 60°.

Table 3

Type of Clouds	t_{cl} °C	z	$\lambda = 0{,}41$ см		$\lambda = 0{,}82$ см		$\lambda = 1{,}6$ см		$\lambda = 3{,}3$ см		$\lambda = 10{,}0$ см	
			$\bar{T}_{b\,cl}$	$T^{max}_{b\,cl}$	$\bar{T}_{b\,cl}$	$T^{max}_{b\,cl}$	$\bar{T}_{b\,cl}$	$T^{max}_{b\,cl}$	$\bar{T}_{b\,cl}$	$T^{max}_{b\,cl}$	$\bar{T}_{b\,cl}$	$T^{max}_{b\,cl}$
Cu hum.	0–5	60	–	–	4	10	—	—	—	—	—	—
Cu med.	0–5	60	50	130	30	120	10	40	2,5	11,0	0,3	1,3
Cu cong.	0–5	60	90	160	70	162	25	67	7,0	20,0	1,0[1]	2,5[1]
St, Sc Winter	-10	0	20[1]	35[1]	12	20	4	7	0,9[1]	1,5[1]	0,1[1]	0,2[1]
St, Sc Summer	5	0	35[1]	70[1]	15	35	5	11	1,0	2,5	0,1[1]	0,3[1]

[1] The data were obtained by using the results of measurements at wavelengths of λ = 0.82 cm and λ = 1.6 cm.

Table 4

Type of Clouds	t_{cl} °C	z	$\lambda = 0{,}41$ см		$\lambda = 0{,}82$ см		$\lambda = 1{,}6$ см		$\lambda = 3{,}3$ см		$\lambda = 10{,}0$ см	
			$\bar{\Gamma}_{cl}$	Γ^{max}_{cl}	$\bar{\Gamma}_{cl}$	Γ^{max}_{cl}	$\bar{\Gamma}_{cl}$	Γ^{max}_{cl}	$\bar{\Gamma}_{cl}$	Γ^{max}_{cl}	$\bar{\Gamma}_{cl}$	Γ^{max}_{cl}
Cu hum.	0–5	60	–		0,01	0,01	—	—	—	—	—	—
Cu med.	0–5	60	0,1	2,6	0,14	0,73	0,04	0,21	0,009	0,012	0,0011	0,0048
Cu cong.	0–5	60	1,1	3,3	0,40	1,21	0,12	0,35	0,026	0,075	0,0036	0,0091
St, Sc Winter	—10	0	0,13	0,24	0,05	0,09	0,015	0,026	0,0034	0,006	0,0004	0,0008
St, Sc Summer	5	0	0,20	0,46	0,06	0,14	0,019	0,040	0,0036	0,009	0,0004	0,0011

Figure 3 shows as an example the curves of measuring the brightness temperature of the atmosphere, obtained in measuring the radiation from a large cumulus cloud at wave lengths of 0.41, 0.82 and 1.6 cm on September 3, 1964. The intervals of averaging the brightness temperatures T_{bcl} are found in the range from 5 - 20 sec. For convenience of comparison the curves are normalized to the respective maximal values of T_{bcl}^{max}. From Figure 3 it is clear that the curves of the relative change in T_{bcl} are not the same for the various wave lengths. This fact is due to the disruption in the proportionality between T_{bcl} and w in the millimeter wave band, which to a large degree appears at a wave length of 0.41 cm.

As a result of interpreting the recordings of the radiation from various types of clouds we obtained average and maximal values of T_{bcl}, which are shown on Table 3. At wave lengths of 0.4, 3.3 and 10 cm for the individual types of clouds there were fewer measurements made than at wave lengths of 0.8 and 1.6 cm. In this case the data are cited from the results of measurements at wave lengths of 0.8 and 1.6 cm taking the spectral dependence of the radiation into account.

The random error of an individual measurement of the brightness temperature of the cloud, determined mainly by the fluctuation threshold and the stability of the amplification factor of the receiver, depended little on the intensity of radiation from the cloud and did not exceed 10% of the measured value for developed cumulus clouds.

Absorption in clouds was determined with measurements of the /107
brightness temperature of the atmosphere and from observations of the radiation emission from the Sun by tracking the position of the center of its disk.

The data on absorption, obtained from measuring the natural radio emission, involve a wide class of clouds. The absolute temperature of the cloud was determined from the materials of aircraft sounding of the atmosphere, and also was evaluated from the temperature at the surface of the Earth and the average altitude of the clouds. In this latter case the sub-cloud temperature gradient was chosen according to [11]. The accuracy of the estimation was assumed equal to $\pm 4^{\circ}$ C. Table 4 gives the values of the average and the maximal absorptions in the clouds, obtained for measurements of the brightness temperatures.

The measurements of the absorption from radio emission of the Sun permitted obtaining a higher accuracy, thus making it possible to use these measurements for determining the characteristics of the dielectric constant of the water drops.

4

The experimental investigation of the effect of temperature on the spectrum of the relative absorptions in the cloud was carried out from the solar radio emission for wave lengths of 0.41, 0.82 and 1.6 cm. During these measurements the cloud temperature varied in a range from +3 to -13°, which permitted obtaining experimental data on the temperature dependence of the dielectric constant of the water drops in the region of supercooling.

The measurements showed that with a decrease in temperature a decrease is observed in the absorption ratio $\frac{\Gamma_{cl}(0.4)}{\Gamma_{cl}(0.8)}$, $\frac{\Gamma_{cl}(0.8)}{\Gamma_{cl}(1.6)}$ and an increase in the relaxation constant τ_r. Figure 4 shows the values of $\frac{\Gamma_{cl}(0.4)}{\Gamma_{cl}(0.8)}$ and $\frac{\Gamma_{cl}(0.8)}{\Gamma_{cl}(1.6)}$, measured in tracking the center of the solar disk. There also are shown the temperature dependences of the ratios of absorptions in the cloud at these wave lengths, obtained at temperatures below the melting point of ice by extrapolation from values of ε_0, and τ_r measured at temperatures of $T_{cl} \geq 273°$ K. Table 5 shows the values of the relaxation time of water molecules obtained during eight observational measurements.

TABLE 5

Observations	1	2	3	4	5	6	7	8
t_{cl} °C	12.5	-8	-7	-4	-2.5	2	2	3
$\tau_r \cdot 10^{-12}$ sec	2.60	2.20	2.07	1.91	1.67	1.75	1.27	1.20

From Figure 4 it is clear that the measured values of the ratios of the absorptions $\frac{\Gamma_{cl}(0.4)}{\Gamma_{cl}(0.8)}$ and $\frac{\Gamma_{cl}(0.8)}{\Gamma_{cl}(1.6)}$ within the limits of error agree with the computational curves. Here the experimental points lie near curve 2, representing the extrapolation of data from [6] rather than near curve 1, representing the extrapolation of data from [7], although the experimental errors do not permit making a confident choice between those in [6] and those in [7]. /108

5

The data from the spectral measurements of the total absorption and brightness temperature of a cloudy atmosphere were interpreted to obtain estimations of the integral water content of the clouds and the total moisture content of the atmosphere. As follows from [3] and [4], the total absorption of a cloudy atmosphere depends on the total moisture content of the atmosphere and the integral water content of the clouds. Evaluations of the possibility of combined determinations of the total moisture content and the integral water content from data of radiometric observations at several wave lengths show that the measurement accuracy of these

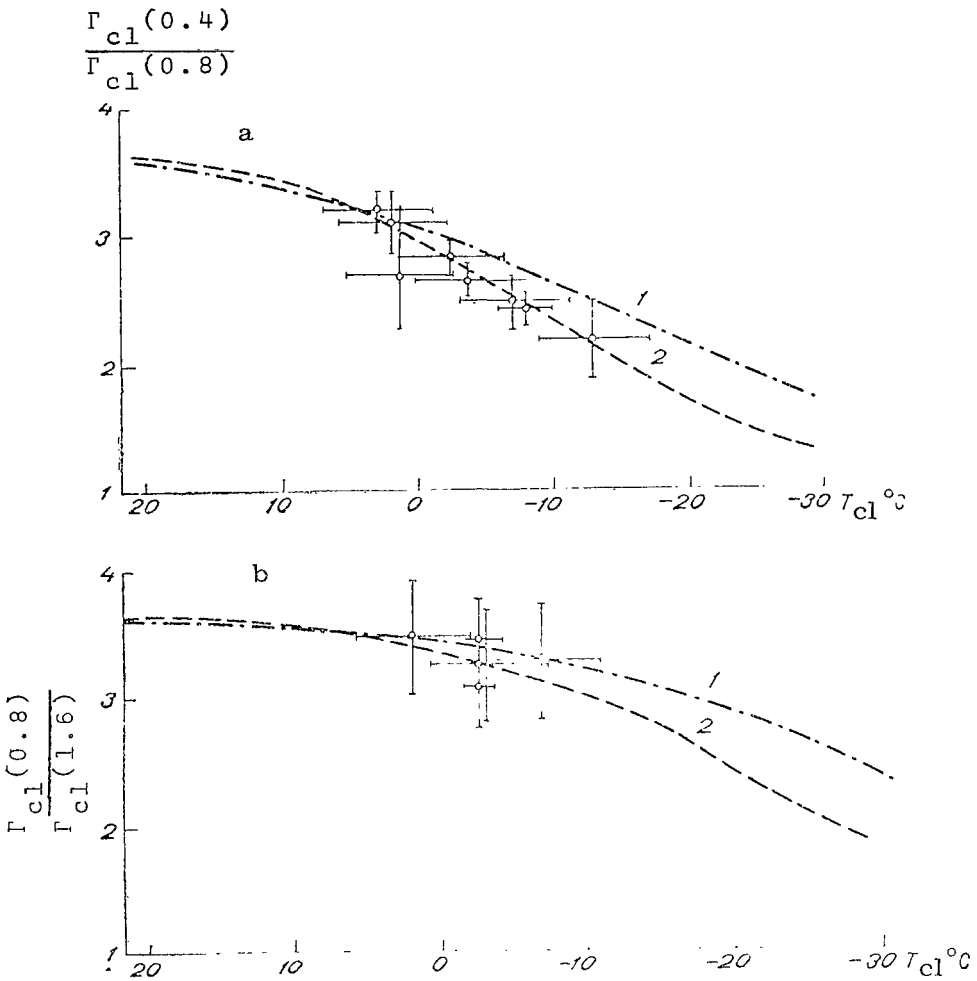

Fig. 4. Relative Absorptions in a Cloud at Wave Lengths of 0.4, 0.8 and 1.6 cm as a Function of its Temperature. a. 0.4 and 0.8 cm; b. 0.8 and 1.6 cm.

values, taking into account the real sensitivity of the radiometric receivers, is about 10%.

As an example, in Table 6 are shown the results of interpreting one group of measurements ($z = 80°$), carried out on September 3, 1964. In the first two lines of the table are shown the values of the total moisture content R and water content W, obtained from /109 measurements of the radiobrightness temperatures at wave lengths of 0.82 and 1.6 cm, in the third and fourth lines are the values of the intergal water content of the clouds obtained from measurements respectively of wave lengths 3.3 and 0.82 cm using the data on total moisture content of the atmosphere.

The average value of the integral moisture content is 18.7. 10^3 g/m^2 with a mean square error of the individual measurement

of $\pm$ 1.5·10^3 g/m^2. The aircraft sounding of the atmosphere carried out during the same hours gives a similar result: R = 17.7·10^3 g/m^2. From the data in Table 6 it is clear that the difference between the values of the integral water content, found from measuring the absorption at wave lengths of 0.82 - 1.6 cm and at a wave length of 3.3 cm, does not exceed 20%. The divergence between the values of the integral water content, shown in the second and fourth lines, is considerably smaller.

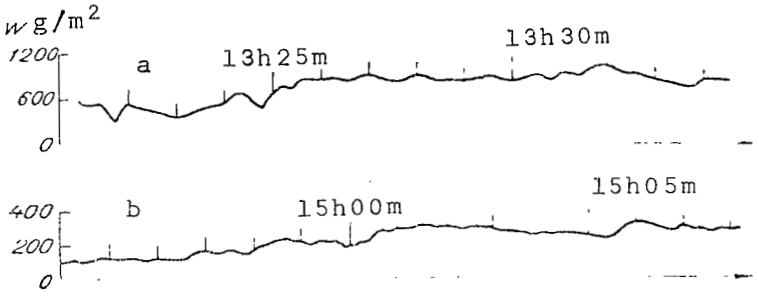

Fig. 5. Realization of Time Variations in the Integral Water Content in Stratocumulus Clouds. a. December 18, 1964, sec z = 5.5; b. May 18, 1965, sec z = 1.48.

Table 6

Time, hr. min	14 20	14 21	14 22	14 23	14 24	14 25	14 26	14 27	14 28	14 29	14 30
R kg/m^2	17,9	18,5	18,9	21,6	17,0	16,8	17,4	17,6	19,7	17,9	18,5
W g/m^2	0	0	0	0	730	1020	1060	1270	1710	1680	1760
$W_{3,3}$ g/m^2							1060	1160	1560	1570	1860
$W_{0,8}$ g/m^2	0	0	80	110	720	1010	1900	1350	1730	1710	1750

Time, hr. min	14 31	14 32	14 33	14 34	14 35	14 36	14 37	14 38	14 39	14 40
R kg/m^2	17,2	17,4	17,4	18,9	21,9	21,6	19,7	19,5	18,1	17,6
W g/m^2	1710	1560	1250	1150	770	210	260	150	110	190
$W_{3,3}$ g/m^2	1900	1730	1460	1300						
$W_{0,8}$ g/m^2	1710	1450	1340	1260	900	410	250	200	130	160

The scatter in experimental values of the total moisture content determined using a combination of 0.82 - 1.6 cm wave lengths, is decreased with increase in the zenith angle up to 85°. The mean square error of evaluating the integral water content depends little on the zenith angle and is 30 - 40 g/m^2, which corresponds /110 to a 10% accuracy in measuring W in the central part of the cumulus cloud.

An example of realizing the time variations of the integral water content in non-transparent stratocumulus clouds obtained during observations of the solar radio emission is shown on Figure 5.

The difference in the average values of the integral water content of the stratocumulus clouds when z = 0° for a single session of observations did not exceed by more than 2 - 3 times the mean seasonal water reserves of stratocumulus clouds given in the work by V.Ye. Minervin [14] for Moscow. For maximal values of W(0) the difference exceeded the water reserves given in [14] by 5 - 6 times.

These experimental data show that measurements of the radio transparency of the atmosphere by radioastronomical methods at several wave lengths permit determining the integral values of the moisture content and the water content with an accuracy no less than 10 - 20%.

REFERENCES

1. Zhevakin, S.A., V.S. Troitskiy and N.M. Tseytlin: Radioizlucheniye atmosfery i issledovaniye pogloshcheniya santimetrovykh voln. (Radio Emission from the Atmosphere and Investigation of the Absorption of Centimeter Waves)., Izv. VUZ, ser. Radiofizika, Vol. 1, No. 2, p. 19, 1958.
2. Zhevakin, S.A. and V.S. Troitskiy: Pogloshcheniye santimetrovykh voln v sloistoy atmosfere. Absorption of Centimeter Waves in a Stratified Atmosphere)., Radiotekhnika i elektronika, Vol. 4, No. 1, 1959.
3. Salomonovich, A.Ye. and O.M. Atayev: Teplovoye izlucheniye i pogloshcheniye v zemnoy atmosfere radiovoln 8-mm diapazona. (Thermal Radiation and Absorption in the Earth's Atmosphere of Radio Waves of the 8-mm Band). Izv. VUZ, ser. Radiofizika, Vol. 3, No. 4, p. 606, 1960.
4. Nicoll, G.R.: The Measurement of Thermal and Similar Radiations at Millimeter Wave Lengths. Proc. I.E.E.E. B 104, No. 17, p. 519, 1957.
5. Kondrat'yev, K.Ya.: Luchistiy teploobmen v atmosfere. (Radiant Heat Transfer in the Atmosphere). Gidrometeoizdat, 1956.
6. Kerr, D.E.: Propagation of Short Radio Waves. MIT Radiation Laboratory Series, 13, New York, 1951.
7. Collie, C.H., J.B. Hasted and Ritson: Dielectric Properties of H_2O and D_2O. Proc. Phys. Soc., Vol. 60, No. 338, p. 2, 1948.
8. Buchanan, T.I. and M.A. Balance: Methods for Measurement of Permittivity in the Microwave Region. Proc. Inst. Electr. Eng., Vol. 99, No. 58, p. 111, March 1961.
9. Lane, I.A. and I.A. Saxton: Dielectric Dispersion in Pure Polar Liquids at Very High Radio Frequencies. Proc. Roy. Soc., Ser. A., Vol. 213, No. 1114, p. 400, 1952.
10. Minervin, V.Ye.: Vodnost' kristallicheskikh oblakov. (Water Content of Crystalline Clouds)., Trudy Central Aerological Observatory, No. 64, 1965.
11. Borovikov, A.M. I.I. Gayvoronskiy, Ye.G. Zak, V.V. Kostarev, I.P. Mazin, V.Ye. Minervin, A.Kh. Khrgian and S.M. Shmeter: Fizika oblakov. (Physics of Clouds). Gidrometeoizdat, 1961.

12. Kalachev, P.D. and A.Ye. Salomonovich: Radioteleskop FIAN SSSR s 22-metrovym parabolicheskim reflektorom. (Radio Telescope of the Physics Institute, Academy of Sciences, USSR with a 22-Meter Parabolic Reflector)., Radiotekhnika i elektronika, Vol. 6, No. 3, 1961.
13. Atlas oblakov. (Atlas of Clouds), Gidrometeoizdat, Leningrad. 1957.
14. Minervin, V.Ye.: Vodozapasy oblakov. (Water Reserves of Clouds)., Trudy Central Aerological Observatory, No. 64, 1965.

EXPERIMENTAL INVESTIGATIONS OF ATTENUATION AND RADIO EMISSION FROM RAIN IN THE UHF-BAND

B.G. Kutuza

ABSTRACT: The results of simultaneous measurements by radiometric methods of attenuation and radiation from the atmosphere, containing rain precipitation at wave lengths of 0.41, 0.82, 1.6 and 3.3 cm, are cited. The dependence of attenuation of radio emission in rain on the dimensions of the drops is confirmed experimentally. Based on the data of attenuation in rain at different wave lengths, the effective diameters of the drops and the integral water content of the rain are evaluated.

1

Measurements have been made by a number of authors [1-3] of attenuation in rain of millimeter and centimeter waves. The method of the measurements in these papers differed little and resulted in the following. The attenuation was determined between the source and receiver, placed at the ends of an open line of sight, with simultaneous measurement of the intensity and other meteorological parameters of the rain. Here, as a rule, the attenuation in the rain was measured at individual wave lengths. /111

In the present paper we investigated the attenuation and radio emission from the rain by radioastronomical methods. A brief description of the method of radiometric measurements on the RT-22 were given in [5].

2

Observations of radio emission and attenuation from rain were made in the course of two periods, September, 1964 and June, 1965. In the first case the rainfall in each observation was due to the passage of a frontal cloud cover. In June, 1965 the precipitations were due to cumulonimbus clouds. The intensity of the rain varied in a range from 0.5 to 65 mm/hr. Four observations were made in September, and in June, eight were made. Each observation continued for 1 - 2 hours.

Natural radiation from the atmosphere was received with a fixed antenna at wave lengths of 0.82, 1.6 and 3.3 cm. In the observations of solar radio emission, 0.41, 0.82 and 1.6 cm waves were used.

The radiometric observations were accompanied by recordings of the rain intensity. For this purpose we used a Tret'yakov

precipitation gauge, which was set up on an open area near the RT-22. The exposure time of the precipitation gauge as a function of rain intensity was chosen from 3 to 15 minutes.

Figure 1 shows examples of recording the brightness temperature of the atmosphere at three wave lengths during the time of rainfall from nimbostratus clouds on September 10, 1964. The antenna was set up counter to the movement of the clouds so that its axis was placed in the plane of the velocity vector. The zenith angle was 75°. Therefore reception of radiation from the rain was begun prior to the appearance of the rain in the radiotelescope. On Figure 1 the steep decline in the recording at the /112
3.3 cm wave length is due to the onset of rain at the site of reception. When the rain drops fell on the antenna horn, directed to the zenith and covered with a polyethylene film, a sharp change occured in the antenna temperature. On two other wave lengths this was not expressed since the circuit of the antenna was hooked up to a matched load, and the face of the exciter[1] was protected from rain drops on the reception channel horn.

Table 1

λ_1 cm	0.82	1.6	3.3
T_b^{max} °K	269	184	40.5
$\bar{T}_b$ °K	252	149	37
$T_{b\ c\ s}$ °K	74	54	12

Table 1 gives values of the average T_b and the maximal T_b^{max} brightness temperatures of the atmosphere, obtained as a result of interpreting the two observational periods during rain fall. The data refer to a zenith angle of $z = 75°$. The values of $\bar{T}_b$ have been averaged for 50 minutes. The maximal brightness temperatures were observed during a period of 4 minutes. The intensity of the rain was approximately 5 mm/hr.[2]

From Table 1 it is obvious that the brightness temperatures, at wave lengths of 1.6 and 3.3 cm during the time of rain, are

---

[1] The effect of rain on the parameters of the antenna was not investigated especially. However conditions arose sufficiently often when the rain drops appeared earlier in the zone of the antenna beam than at the reception site. Here no deviations were noted on the millimeter waves at the moment of incidence of the rain drops on the antenna.

[2] During this period of observations no measurement of rain intensity was made.

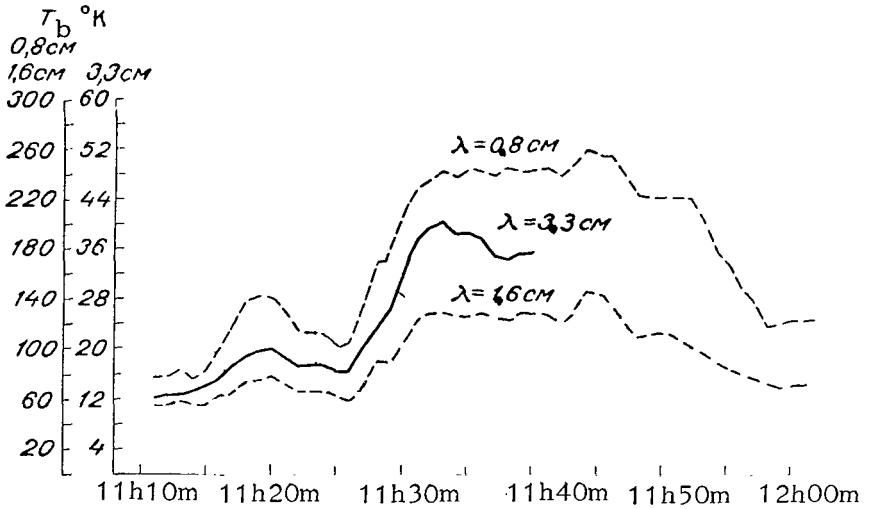

Fig. 1. Variations in Brightness Temperature of the Atmosphere at Wave Lengths of 0.82, 1.6 and 3.3 cm at the Time of Rain.

significantly higher than with radiation from cumulus congestus clouds, which among all clouds do not produce precipitation and have the highest integral water content. As a result of the large optical depth at the 0.82 cm wave length ($\tau \approx 3$) the brightness temperature becomes near the thermodynamic temperature of the rain. /113

3

The measurements of attenuation in rain were conducted by tracking the center of the solar disk. Figure 2 shows graphs which indicate the changes in attenuation in the atmosphere at 0.41, 0.82 and 1.6 cm wave lengths during the time of rainfall from nimbostratus clouds on September 10, 1964. The zenith angle of the Sun in this period of time varied from 59 to 64°. The experimental points were plotted at an interval of 15 seconds. On Figure 2 it is obvisou how the increase in attenuation in rain takes place. On the curves we can see individual scatters and a large drop following the first rise. The optical depth at the 0.41 cm wave length reaches 4.7 nepers; at the 0.82 cm wave length, it is 2.4 nepers, and at the 1.6 cm wave length it is 0.8 neper.

In June, 1965 simultaneous measurements were made of attenuation in rain and its intensity. Figure 3 shows the experimental values of the optical depth of the rain τ_r at the 0.82 cm wave length as a function of its intensity. The values of τ_r were obtained after subtraction from the total attenuation of absorption in the oxygen and the water vapor. They were averaged for the exposure time of the precipitation gauge and reduced to $z = 0°$. The approximation curve, plotted from the available points, has a knee with values of the rain intensity greater than 10 mm/hr. Analogous functions $\tau_r = f(I)$ were obtained for the 0.41 and 1.6 cm wave lengths.

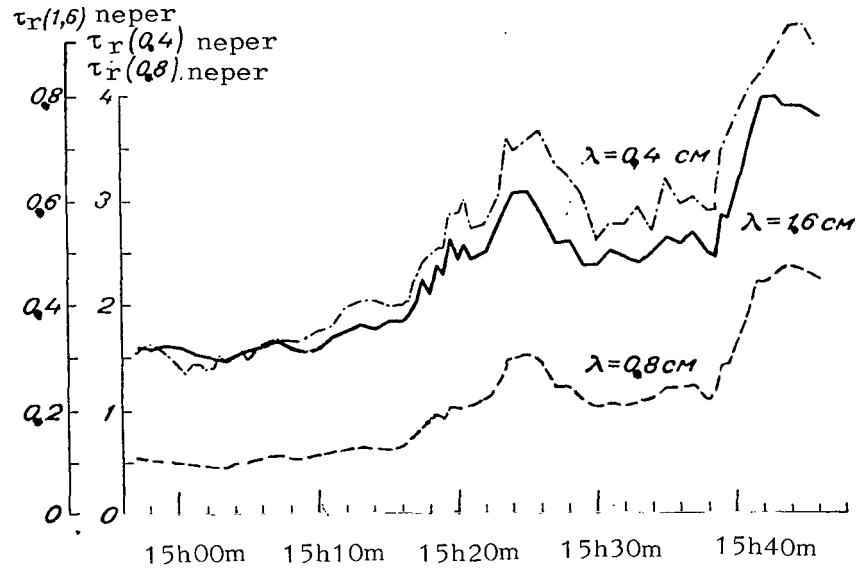

Fig. 2. Time Variations in Attenuation in the Atmosphere at 0.41, 0.82 and 1.6 cm Wave Lengths During Rain.

The maximal values of attenuation in the atmosphere during rain, observed on June 21, 1965, with a rain intensity of 65 mm/hr at the 0.41 cm wave length, were 6.5 nepers; at the 0.82 cm wave length, 6.0 nepers, and at the 1.6 cm wave length, 2.8 nepers (with a zenith angle z = 40°). Under these conditions the signal from the Sun at the 0.41 and 0.82 cm wave lengths decreased by approximately 500 times. /11

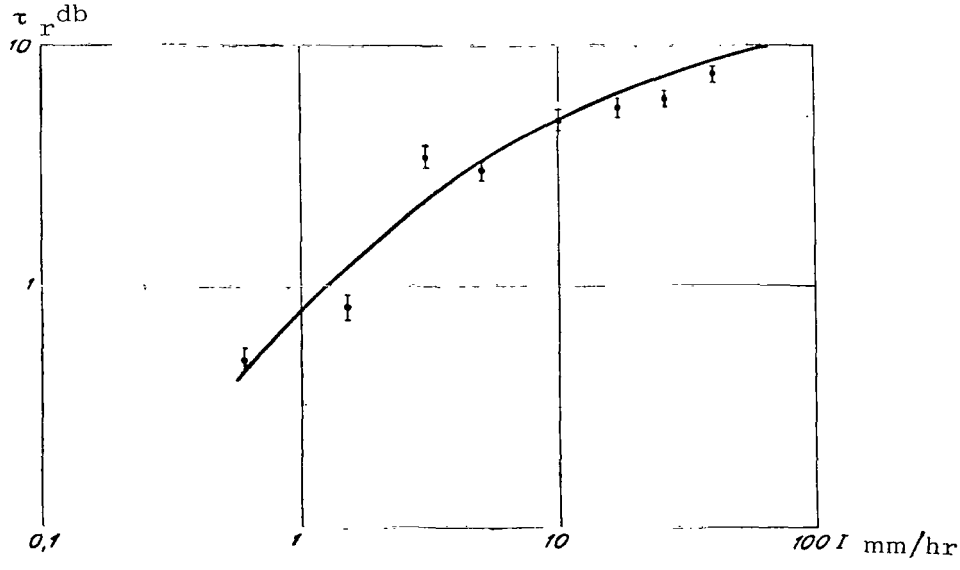

Fig. 3. Attenuation in Rain at the 0.82 cm Wave Length as a Function of its Intensity.

When $\tau < 2$ nepers the measurement error was determined by the stability of the amplification factor of the receiver and, in absolute value, did not exceed 0.4 neper at the three wave lengths. For larger values of the optical depth the intensity of the signal from the Sun was found to be near the fluctuation threshold of the receiver's sensitivity, as a result of which the absolute measurement error of τ_r increased.

4

In individual observations on the 0.82 cm wave length, measurements were made of the attenuation in rain for the horizontal and vertical polarizations. Change in the plane of polarization was accomplished using a ferrite polarizer. The calibration measurements were made during observations of solar radio emission for two polarizations in cloud-free weather. Table 2 shows the results of interpreting the difference in attenuation in rain for the vertical and the horizontal polarizations. The zenith angle for these measurements was 30°; the average values for the rain intensity were 2.5 mm/hr and the attenuation for the vertical polarization was 1.7 nepers.

Table 2

Session . .	1	2	3	4	5	6	7
Time hr.min.sec.	17 06 30	17 07 05	17 07 30	17 08 10	17 08 30	17 08 55	17 09 05
$\frac{\tau_r^{\rightarrow} - \tau_r^{\uparrow}}{\tau_r^{\uparrow}}$ %	5,8	4,0	2,9	4,2	5,4	2,2	7,3

According to references [4,5], the difference in attenuation in rain for the vertical and horizontal polarizations with an intensity of 2.5 mm/hr at the 0.86 cm wave length is about 10%. The smaller values of $\tau_r^{\rightarrow} - \tau_r^{\uparrow} \,/\, \tau_r^{\uparrow}$ in Table 2 may be assumed as being due to scatter in the zenith anges of the observations. /115

5

Simultaneous measurements of the value of the attentation during precipitations at the 0.41, 0.82 and 1.6 cm wave lengths made it possible to determine the ratio of the coefficients $\frac{\tau_r(0.4)}{\tau_r(0.8)}$ and $\frac{\tau_r(0.8)}{\tau_r(1.6)}$. The values of τ_r were found from the difference in the total attenuation in the atmosphere and the absorption in oxygen and water vapor. With moderate and heavy rain, the amount of attenuation in the atmosphere for the oxygen and water vapor was quite small. No distinction was made between the components of attenuation in clouds and in rain.

The first measurements of the ratios of the attenuation factors were made for precipitations, which fell from nimbostratus clouds. Figure 4 shows experimental values of $\tau_r(0.4)$ and $\tau_r(0.8)$

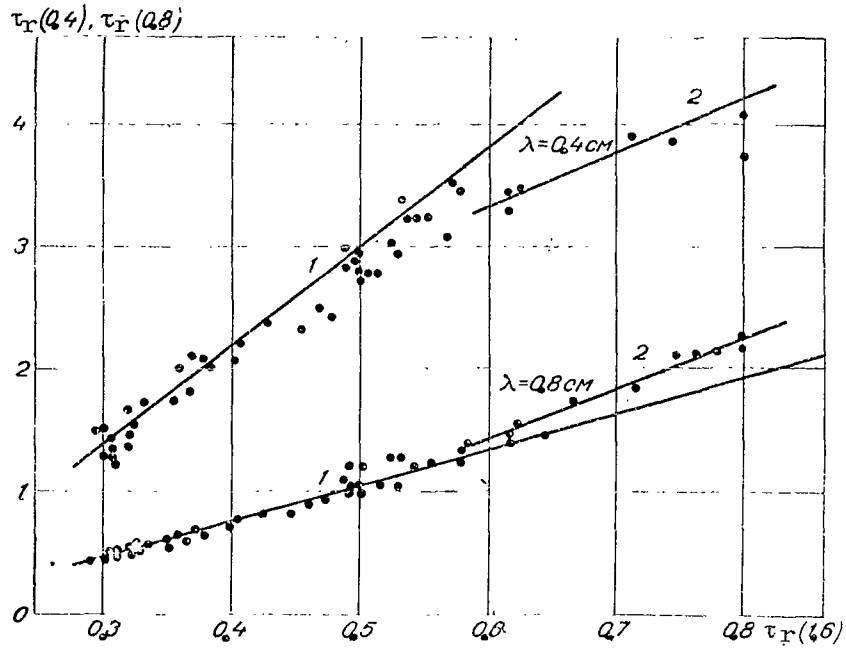

Fig. 4. Attenuations in the Atmosphere at the 0.41 and 0.82 cm Wave Lengths as a Function of Attenuation at the 1.6 cm Wave Length on September 10, 1964.

as a function of attenuation at the 1.6 cm wave length. On the right-hand side of the figure we see points that were obtained during measurements in rain. The lines have been plotted which approximate the experimental values of attenuation during these periods, when (1) there was no rain at the site of reception and (2) when there was. The slope of the lines permits us to judge the ratios of the attenuation factors. In the absence of rain /116

$\frac{\tau_r(0.4)}{\tau_r(0.8)} = 2.8$ and $\frac{\tau_r(0.8)}{\tau_r(1.6)} = 3.20$, which corresponds to the spectral characteristics of attenuation in a cloud at a temperature of 8° C. The lines which characterize time variations in attenuation during rainfall have another slope. Here the ratio $\frac{\tau_r(0.4)}{\tau_r(0.8)}$ is decreased and assumes a value of 1.6, but the ratio $\frac{\tau_r(0.8)}{\tau_r(1.6)}$ is increased up to 3.8.

During observations of precipitations which fall from cumulonimbus clouds, we noted that in the process of rainfall the ratio of the attenuation factors varies. Figure 5 shows the values of the ratios of the attenuation factors $\frac{\tau_r(0.4)}{\tau_r(0.8)}$ and $\frac{\tau_r(0.8)}{\tau_r(1.6)}$ during the passage of a storm front on June 21, 1965. Along the abscissa axis is plotted the time figured from the beginning of the appearance of rain at the measurement site. There also are given the values of the rain intensity measured by the precipitation gauge. The

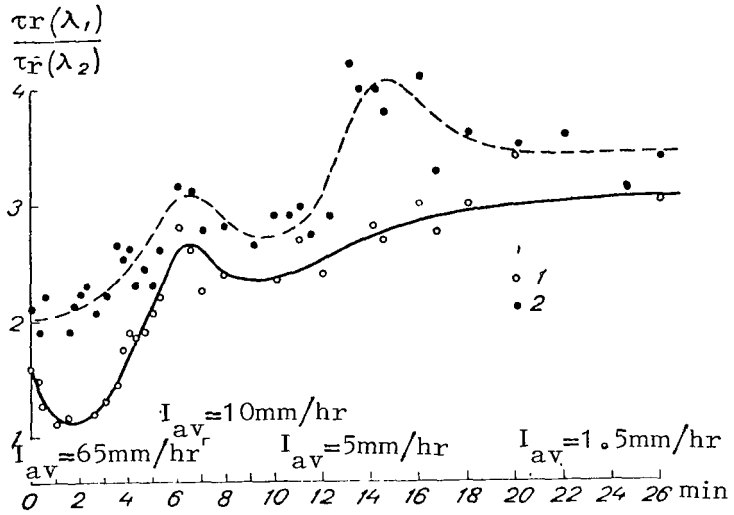

Fig. 5. Time Variations of Relative Attenuations in the Atmosphere at the 0.41, 0.82 and 1.6 cm Wave Lengths During the Passage of a Storm Front. 1. $\frac{\tau_r(0.4)}{\tau_r(0.8)}$; 2. $\frac{\tau_r(0.8)}{\tau_r(1.6)}$.

antenna was set up counter to the movement of the storm. In the initial period of the storm we noted an intense precipitation. The relative attenuation at the 0.41 and 0.82 cm wave lengths in this case was 1.2, and at the 0.82 and 1.6 cm wave lengths, it was 2.04. Then the ratios of the attenuations of both pairs of wave lengths began to increase. Figure 5 shows the rise in the curve of the ratio $\frac{\tau_r(0.8)}{\tau_r(1.6)}$ with a rain intensity of 5.0 mm/hr.

6

The difference in the UHF-spectrum of attenuation in rain and /117
the spectrum of attenuation in a cloud cover is due to the larger dimensions of the drops and the appearance of resonance effects [6,7]. Figures 6 and 7 give the computational functions of the relative attenuations of the 0.41, 0.82, 1.6 and 3.3 cm wave lengths for a range of diameters from 0.6 to 4 mm. In the computations (Fig. 6) it was assumed that in rain the distribution of drops by dimensions corresponds to the distribution cited in [8]. Multiple scattering [7] was taken into account for the case of a one-dimensional atmosphere [9]. The dotted line shows analogous curves with a constant drop diameter, without taking multiple scattering into account.

If we compare the measured values of the relative attenuations in rain at the above wave lengths with the computational curves[3],

[3] Computation of the effective factors of attenuation, absorption

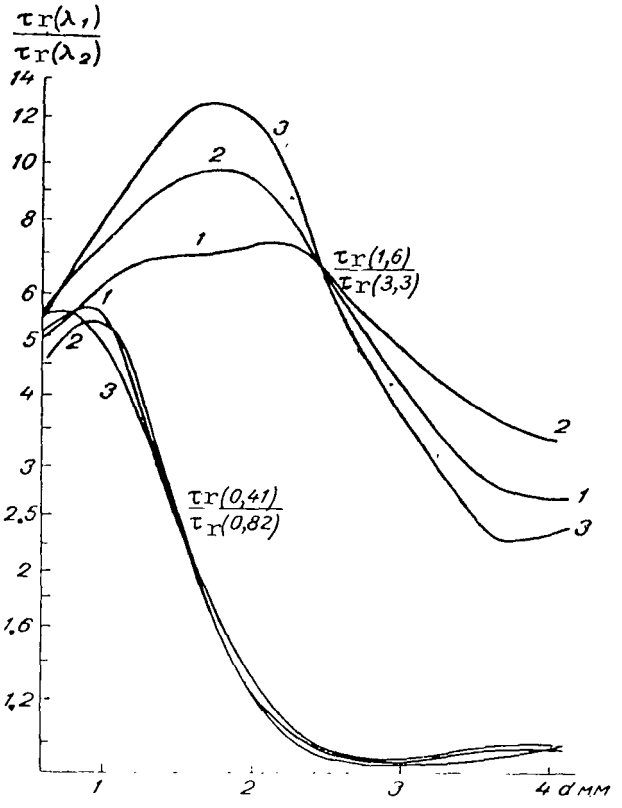

Fig. 6. Relative Attenuations of the 0.41, 0.82, 1.6 and 3.3 cm Wave Lengths in Rain as a Function of the Effective Diameter of the Drops. (Mondisperse Atmosphere). 1. ± 10° C; 2. 0° C; 3. -20° C.

we can estimate the effective values of the drop diameters. With a ratio of attenuations in rain $\frac{\tau_r(0.4)}{\tau_r(0.8)}$ and $\frac{\tau_r(0.8)}{\tau_r(1.6)}$ (see Fig. 4) the effective dimensions of the drops enter the resonance region of the 0.82 cm wave length and their diameter lies in the range from 1.6 to 2.0 mm. The values of the relative attenuations for the initial period of the storm (Fig. 5) correspond to the average dimensions of the drop diameters (3.4 - 3.8 mm). The time variation in the relative spectrum of the three wave lengths permits judging as to the decrease in the average dimensions of the drops. /118

7

The measurement results of the attenuations at three waves

footnote #3 cont.

and scattering of water drops according to the Mie formulas was made by I.Ya. Gushchina on a BESM-2 computer.

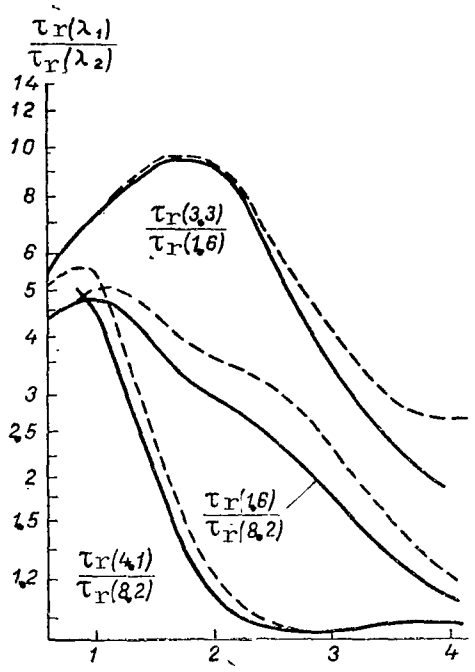

Fig. 7. Relative Attenuations of the 0.41, 0.82, 1.6 and 3.3 cm Wave Lengths in Rain with Identical Drop Dimensions as a Function of Drop Diameter, Taking Multiple Scattering into Account (One-Dimensional Atmosphere).

lengths were used for evaluating the integral water content, contained in an atmospheric column during rainfall. For evaluation of the integral water content we used a model which allows for the distribution of drops by dimensions. Here it was assumed that the drop distribution by dimensions [8] is valid in the entire path of the wave propagation.

The integral water content was computed for two variants: allowing for single scattering and multiple scattering (a one-dimensional atmosphere). The effective diameter of the drops was found from the ratio $\frac{\tau_r(\lambda_1)}{\tau_r(\lambda_2)}$ for two combinations of wave lengths: 0.41 and 0.82 cm and 0.82 and 1.6 cm.

Table 3 gives the results of interpreting a single session of measurements of storm rain on June 21, 1965. The observations were conducted at a zenith angle of $z = 40°$. Here M_1 is the integral water content, obtained from measurements at the 0.41 and 0.82 /119 cm wave lengths; M_2 is the integral water content obtained using measurements at the 0.82 and 1.6 cm wave lengths; M_1' and M_2' are the same, but allowing for multiple scattering. $W_{0.8}$ is the integral water content of the cloud cover at which this attenuation would be observed at the 0.82 cm wave length.

From Table 3 it is clear that the divergence between values of the integral water content determined from the different combinations of waves, on the average is 10 - 15%. The values of M, obtained by allowing for multiple scattering, are found to be greater by approximately 50% in comparison with those which allow only for single scattering. If we compare $W_{0.8}$ with the other values of the integral water content corresponding to one and the same moment of time we find that the average cross section of attenuation of the rain drops exceeds the cross section of attenuation of the cloud cover by 4 - 7 times. On the assumption that the clouds and the rain have one and the same integral water content, the error in determining M is approximately 20%. The values of the integral water content of a heavy rain and cumulus congestus clouds give comparible results. The difference in attenuation is due apparently to the large cross section of attenuation of the raindrops.

Table 3

Time hr.min.sec.	15 24 00	15 25 30	15 26 40	15 28 00	15 29 15	15 31 00
$\tau_r(0,4)$ neper	4,92	5,40	5,00	4,18	3,34	3,73
$\tau_r(0,8)$ neper	3,10	5,29	4,58	2,17	1,52	1,66
$\tau_r(1,6)$ neper	1,47	2,70	2,23	0,83	0,58	0,60
M_1 kg/m^2 . . .	2,3	4,8	4,1	1,7	1,3	1,4
M_2 kg/m^2 . . .	2,4	4,3	3,6	1,6	1,1	1,3
M_1' kg/m^2 . . .	3,5	7,5	6,6	2,4	1,7	1,9
M_2' kg/m^2 . . .	3,7	6,5	5,6	2,5	1,7	1,9
$W_{0,8}$ kg/m^2 . .	16,5	26,6	22,9	10,5	7,6	8,3
I mm/hr . . .		65			10	

Time hr.min.sec.	15 34 00	15 36 15	15 37 30	15 42 00	15 44 00
$\tau_r(0,4)$ neper	3,43	3,42	2,73	2,50	2,04
$\tau_r(0,8)$ neper	1,46	1,30	1,00	0,83	0,69
$\tau_r(1,6)$ neper	0,50	0,45	0,25	0,20	0,19
M_1 kg/m^2 . . .	1,3	1,30	1,0	0,9	0,7
M_2 kg/m^2 . . .	1,1	1,0	1,0	0,9	0,6
M_1' kg/m^2 . . .	1,7	1,6	1,3	1,1	0,9
M_2' kg/m^2 . . .	1,7	1,5	1,4	1,2	0,8
$W_{0,8}$ kg/m^2 . .	7,3	6,5	5,0	4,2	3,5
I mm/hr			5		

For a more precise determination of the integral water content and the possibilities of distinguishing the contribution of the components of total attenuation in rain and in clouds, we must allow for the distribution function of the drops by size, which requires additional investigations.

REFERENCES /120

1. Rasprostraneniye ul'trakorotkikh voln. (Propagation of Ultrashort Waves). Translated from the English by B.A. Shillerov. Sovietskoye radio, 1954.
2. Usikov, A.Ya., V.L. German and I.Kh. Vakser: Experimental'noye i teoreticheskoye issledovaniye pogloshcheniya i rasseyaniya millimetrovykh voln v osadkakh. (Experimental and Theoretical Investigation of Absorption and Scattering of the Millimeter Waves in Precipitation)., Ukrainskiy fizicheskiy zhurnal, Vol. 6, No. 5, 1961.
3. Okamura, S., K. Funakawa, H. Uda, I. Kato and T. Oguchi: Effect of Polarization on the Attenuation by Rain at Millimeter-Wave Lengths. J. Radio Res. Labs. (Tokyo), Vol. 8, No. 36, March 1961.
4. Oguchi, T.: Attenuation of Electromagnetic Waves Due to Rain with Distorted Raindrops. J. Radio Res. Labs. (Tokyo), Vol. 7, No. 33, September 1960.

5. Basharinov, A.Ye. and B.G. Kutuza: Issledovaniye radioizlucheniya i pogloshcheniya atmosfery v millimetrovom i santimetrovom diapazonakh voln. (Investigation of Radio Emission and Absorption of the Atmosphere in the Millimeter and Centimeter Wave Lengths). See this Collection.
6. Shifrin, K.S.: Rasseyaniye sveta v mutnoy srede. (Scattering of Light in a Cloudy Atmosphere)., Gostekhizdat, 1951.
7. van de Hulst, G.: Rasseyaniye sveta malymi chastitsami. (Scattering of Light by Small Particles)., Foreign Literature Press, Moscow, 1961.
8. Best, A.C.: The Size Distribution of Raindrops. Q.J. Roy, Met. Soc., Vol. 76, No. 327, 1950.
9. Sobolev, V.V.: Perenos luchistoy energii v atmosferakh zvezd i planet. (Transfer of Radiant Energy in the Atmospheres of Stars and Planets)., Gostekhizdat, 1956.

CONTRASTS IN RADIOBRIGHTNESS TEMPERATURES DURING OBSERVATIONS OF CLOUDS AND PRECIPITATIONS

V.D. Stepanenko

ABSTRACT: A method of computing the radiobrightness temperatures and precipitations in the centimeter wave length band is described. Values of the radiobrightness temperatures and contrasts of rain-free clouds of different types with various glancing angles for the horizontal polarization. The results of computations of radiobrightness temperatures and contrasts of rains of different intensity and snowfalls over the basic types of underlying surfaces at various glancing angles for the horizontal and vertical polarizations are cited. The values of the brightness temperatures and contrasts of clouds and precipitations during observations from Earth are computed. The results of measurements of radio emission from the atmosphere and atmospheric condensations by a radiometer from Earth are cited, and a comparison is made between experiment and computational data.

The possibilities of detecting clouds and precipitations by means of passive radar depend on the radiobrightness temperatures and contrasts of these temperatures both in scanning these meterological targets on the background of land and water surfaces from aircraft, and with radiometric observations from the Earth. /121

Following references [2,3], the intensity of thermal radiation from the atmosphere, found at a temperature of T_{av} and characterized by the absorption coefficient α, will be

$$I_f = \frac{2k}{\lambda^2} T_{av}\left[1 - \exp\left(-\int_0^\infty \alpha\, dl\right)\right] + I_s \exp\left(-\int_0^\infty \alpha\, dl\right), \qquad (1)$$

where k is the Boltzmann constant, λ is the wave length of the radiation.

The first term in formula (1) describes natural radiation from the atmosphere and the second - the cosmic radio emission.

The value $\int_0^\infty \alpha dl = \Gamma$ characterizes the total absorption of radio waves in the atmosphere at an angle δ.

If we express the intensity of the thermal radio emission

through the temperature, formula (1) can be written in the form

$$T_b(\delta) = T_{av}(1 - e^{-\Gamma(\delta)}) + T_b e^{-\Gamma(\delta)}. \quad (2)$$

Since at $\lambda \leq 10$ cm the quantity T_b does not exceed fractions of degrees [2], then

$$T_b(\delta) = T_{av}[1 - e^{-\Gamma(\delta)}]. \quad (3)$$

In reference [2] the authors assume $\Gamma(\delta)$ to be a small quantity; therefore the brightness temperature of the sky, because of radiation from the atmosphere, is defined as

$$T_b(\delta) = T_{av}\Gamma(\delta). \quad (4)$$

This same formula (4) has been recommended for use in computing the radiobrightness temperature of clouds and precipitations. However, our computations showed that at $\lambda \leq 3$ cm it is necessary to use formula (3) rather than formula (4), since this latter (in the case of determining $T_b(\delta)$ of the clouds and precipitations even at $\lambda = 3$ cm) may give an error on the order of 200%.

In the general case, with computation of the thermal radio emis- /122
sion from bodies, it is necessary to take into account the reflection from the part of the energy of radiation from atmosphere 2 of the interface of the atmospheres 1 - 2, which are determined by the reflection coefficent (in size)

$$R_2^2 = \left(\frac{E_{2\,ref}}{E_{2\,inc}}\right)^2.$$

where $E_{2\,inc}$ and $E_{2\,ref}$ are the values of the complex amplitudes of incident and reflected waves on the surface of the atmospheres.

As a result, the radiobrightness temperature of atmosphere 2 on its upper boundary is determined by the expression

$$T_{b2} = T_{2av}(1 - R_2^2)(1 - e^{-\Gamma}). \quad (5)$$

For gases of the atmosphere, cloud cover and the majority of precipitations, R^2 is a small value, therefore the coputational formula for these atmospheres is expression (3).

The absorption coefficient of the underlying surface in the band of centimeter and millimeter wave lengths is high, and the thermal radio emission is formed in the thin surface layer. In this case, $e^{-\Gamma} \approx 0$ and $T_{b2} = T_2 \text{ av } (1-R_2^2)$.

If the interface of the atmospheres is a plane surface, i.e., for the irregularities h_s, the criterion of Rayleigh irregularities $h_s \leq \frac{\lambda}{16 \cos \delta} = h_{max}$ is satisfied, then for the vertical and horizontal components of the field of thermal radio emission propagating in uniform atmosphere 1, the reflection coefficients R^2 will differ from the interface of atmospheres 1 - 2.

In the works of various authors [5,8,11], theoretical and experimental values are given for the reflection coefficients of different surfaces. Here the reflection coefficients for water and other surfaces are computed by assuming these surfaces to be smooth. Unfortunately, in the literature there are very little experimental data concerning the values of R^2 for rough water and other uneven surfaces.

In installing the radiometer on the aircraft its antenna will use the energy of thermal radio emission from the underlying surface and a cloud-free atmosphere or an atmosphere with clouds and precipitations.

The difference between the energy of the thermal radio emission, used by the antenna from the underlying surface and the cloud-free atmosphere and the energy used by the antenna in the presence of a cloud cover and precipitations, determines the radiobrightness contrast of the zones of clouds and precipitations.

The energy of the thermal radio emission, used by the antenna directed toward the Earth, in the case of a cloud-free atmosphere, can be expressed through the radiobrightness temperature in the following manner: /123

$$T_b = T(1-R^2)e^{-\Gamma_a} + \overline{T}(1-e^{-\Gamma_a}) + \overline{T}(1-e^{-\Gamma_a})R^2 e^{-\Gamma_a}, \qquad (6)$$

where T is the absolute temperature of the underlying surface, Γ_a is the absorption coefficient of the radio waves by atmospheric gases.

The third term on the right-hand side of equation (6) determines the part of the energy of thermal radiation from the atmosphere which, having been cut off from the underlying surface, is incident on the antenna of the radiometer. Let us denote it as the illumination (Fig. 1).

For clouds without precipitation we have the following relationship:

$$T_b = T(1-R^2)e^{-(\Gamma_1+\Gamma_2+\Gamma_3)} + \overline{T}_1(1-e^{-\Gamma_1})\left[e^{-(\Gamma_2+\Gamma_3)} + R^2 e^{-(\Gamma_1+\Gamma_2+\Gamma_3)}\right] + \quad (7)$$
$$+\overline{T}_2(1-e^{-\Gamma_2})\left[e^{-\Gamma_3} + R^2 e^{-(2\Gamma_1+\Gamma_2+\Gamma_3)}\right] + \overline{T}_3(1-e^{-\Gamma_3})\left[1+R^2 e^{-(2\Gamma_1+2\Gamma_2+\Gamma_3)}\right],$$

where Γ_1, Γ_2, Γ_3 are the absorption coefficients in atmospheric gases and clouds for each layer, T_1, T_2, T_3 are the average temperatures of the layers.

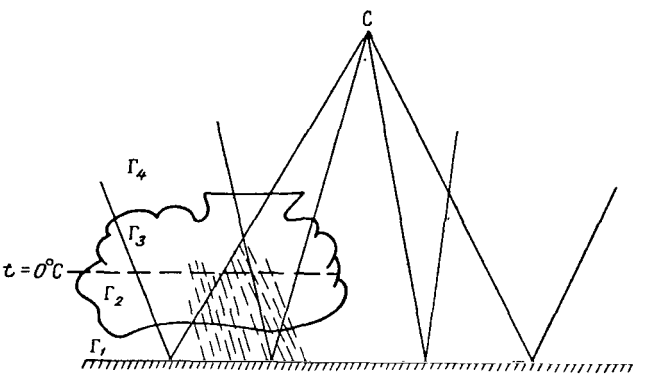

Fig. 1. Diagram, Depicting the Detection of Clouds and Precipitations from an On-Board Radio Thermal Locator.

In the presence of rainfall, according to Figure 1, we will have the following expression for the radiobrightness temperature:

$$T_b = T(1-R^2)e^{-\left(\Gamma_1'+\Gamma_2'+\Gamma_3+\Gamma_4\right)} + \overline{T}_1\left(1-e^{-\Gamma_1'}\right)\times$$
$$\times\left[e^{-(\Gamma_2+\Gamma_3+\Gamma_4)} + R^2 e^{-\left(\Gamma_1'+\Gamma_2'+\Gamma_3+\Gamma_4\right)}\right] + \overline{T}_2(1-e^{-\Gamma_2})\times$$
$$\times\left[e^{-(\Gamma_3+\Gamma_4)} + R^2 e^{-(2\Gamma_1+\Gamma_2+\Gamma_3+\Gamma_4)}\right] + \overline{T}_3(1-e^{-\Gamma_3})\times$$
$$\times\left[e^{-\Gamma_4} + R^2 e^{-\left(2\Gamma_1'+2\Gamma_2'+\Gamma_3+\Gamma_4\right)}\right] + \overline{T}_4(1-e^{-\Gamma_4})\times$$
$$\times\left[1+R^2 e^{-\left(2\Gamma_1'+2\Gamma_2'+2\Gamma_3+\Gamma_4\right)}\right]. \quad (8)$$

In formulas (7) and (8) it is assumed that the illumination is due to a solid cloud cover or a zone of clouds that are identical in their characteristics with the cloud cover and precipitation occupying the unrefracted part of the main lobe of the radiation

pattern of the antenna. Under real conditions, especially for small angles of δ, this may sometimes not be satisfied.

The difference between equations (7), (8) and (6) or between equations (8) and (7) will give a value of the contrast of the radiobrightness temperatures ΔT_b of the zone of clouds and precipitation over various underlying surfaces.

Included in these equations are the absorption coefficients of the radio waves in atmospheric gases, clouds and precipitations. For atmospheric gases they can be computed from the well-known formulas in [5]. The absorption coefficients for clouds without precipitation and light rains [1,4,6] can also be computed easily since in these cases the parameter $\frac{2\pi a}{\lambda} < 1$ (where a is the radius of the particle) and the attenuation of the radio waves as a result of the small scattering occurs practically due to their absorption. However, for large rain drops, the contribution of scattering becomes significant. As a result of this, equation (1) must be solved by allowing for scattering which, generally speaking, involves considerably difficulty. /124

Although there are several approximate methods for solving the transfer equation, allowing for scattering, their use is a special problem that is outside the framework of our article. However, in order to approximately know the limits of applicability of equation (8),we made computations involved with an accurate determination of the effective areas of scattering Q_s and the effective areas of attenuation Q_t, of 1 m^3 of different rains with typical distributions of drops according to the precise Mie formulas. The number of drops N per 1 m^3 was assumed equal to 500. The precise values of Q_s and Q_t for drops of a given size were taken from references [4,5].

From analysis of Table 1 we can make a number of important practical conclusions. For $\lambda \geq 2$ cm up to very heavy rains (I = 20 mm/hr), $Q_s << Q_t$. This permits a sufficiently accurate determination, using formula (8), of the value of the radiobrightness temperatures in almost the entire centimeter wave band. For $\lambda < 2$ cm, in particular when $\lambda = 0.8$ cm, Q_s becomes comparable with Q_t for almost all rains. At wave lengths of $\lambda = 1.2 - 1.6$ cm we can ignore the scattering for drizzling and light rains without any large errors.

Now, if we know the limits of applicability of equations (6), (7) and (8) we can more reliably interpret the values of T_b and ΔT_b computed below, not only for the clouds, but also for zones of precipitation. Such computations were made under the condition that these atmospheric condensations are localized over the various underlying surfaces.

TABLE 1: VALUES OF THE EFFECTIVE AREAS OF ATTENUATION Q_t AND THE TOTAL SCATTERING Q_s (mm^2/m^3) FOR VARIOUS RAINS.

λ см	Intensity of Rain, mm/hr					
	$I = 0.25$			$I = 1$		
	Q_t	Q_s	$\frac{Q_s}{Q_t}$	Q_t	Q_s	$\frac{Q_s}{Q_t}$
0.8	$7.8 \cdot 10^{-3}$	$2.16 \cdot 10^{-3}$	0.28	$3.99 \cdot 10^{-2}$	$1.63 \cdot 10^{-2}$	0.41
1.2	$1.97 \cdot 10^{-3}$	$2.72 \cdot 10^{-4}$	0.14	$1.03 \cdot 10^{-2}$	$2.25 \cdot 10^{-3}$	0.22
1.6	$1.0 \cdot 10^{-3}$	$4.5 \cdot 10^{-5}$	$4.5 \cdot 10^{-2}$	$4.3 \cdot 10^{-3}$	$2.1 \cdot 10^{-4}$	$4.9 \cdot 10^{-4}$
2.0	$4.3 \cdot 10^{-4}$	$1.1 \cdot 10^{-5}$	$2.5 \cdot 10^{-2}$	$2.1 \cdot 10^{-3}$	$1.13 \cdot 10^{-4}$	$5.8 \cdot 10^{-1}$
3.0	$9.89 \cdot 10^{-5}$	$1.1 \cdot 10^{-7}$	$1.1 \cdot 10^{-3}$	$4.9 \cdot 10^{-4}$	$3.9 \cdot 10^{-6}$	$7.9 \cdot 10^{-3}$

λ см	Intensity of Rain, mm/hr					
	$I = 5$			$I = 20$		
	Q_t	Q_s	$\frac{Q_s}{Q_t}$	Q_t	Q_s	$\frac{Q_s}{Q_t}$
0.8	$18.97 \cdot 10^{-2}$	$10.13 \cdot 10^{-2}$	0.53	$81.14 \cdot 10^{-2}$	$48.81 \cdot 10^{-2}$	0.60
1.2	$5.71 \cdot 10^{-2}$	$2.15 \cdot 10^{-2}$	0.38	$27.21 \cdot 10^{-2}$	$13.81 \cdot 10^{-2}$	0.49
1.6	$2.44 \cdot 10^{-2}$	$5.59 \cdot 10^{-3}$	0.23	$12.55 \cdot 10^{-2}$	$4.31 \cdot 10^{-2}$	0.34
2.0	$1.15 \cdot 10^{-2}$	$1.6 \cdot 10^{-3}$	0.14	$5.98 \cdot 10^{-2}$	$1.06 \cdot 10^{-2}$	0.19
3.0	$2.81 \cdot 10^{-3}$	$1.1 \cdot 10^{-4}$	$3.9 \cdot 10^{-2}$	$1.95 \cdot 10^{-2}$	$1.74 \cdot 10^{-3}$	0.09

In the computations, pertaining to a water surface, the water temperature T was assumed equal to 290° K. The distribution of air temperature with altitude corresponded to the standard. The distribution of water content in the air was chosen after A.A. Khvostikov. For clouds without precipitation, such as stratus and stratocumulus clouds, their thickness was assumed equal to $\Delta H = 0.5$ km and the mean water content $\bar{W} = 0.1$ g/m^3; for altocumulus and altostratus clouds $\Delta H = 0.6$ km and $\bar{W} = 0.17$ g/m^3; for cumulus and cumulus congestus clouds, $\Delta H = 1.5$ km and $\bar{W} = 0.2$ g/m^3. The space factor of the radiation pattern of the antenna for the particles from clouds and precipitation $K_s = 1$ for the first and second types of clouds and $K_s = 0.5$ for cumulus clouds. /125

In the presence of a light rain (I = 1 mm/hr) the thickness of the clouds $\Delta H = 7$ km, the thickness of the band of rain $\Delta H_r = 3$ km and the water content of the clouds $\bar{W} = 0.2$ g/m^3. For moderate rain (I = 5 mm/hr) $\Delta H = 8$ km, $\Delta H_r = 4$ km, $\bar{W} = 0.3$ g/m^3. Finally, for a heavy rain (I = 20 mm/hr), $\Delta H = 9$ km, $\Delta H_r = 5$ km, $W_r = 1$ g/m^3. The lower edge of the rain clouds was assumed to be at an altitude of 0.5 km.

The computations of the radiobrightness temperatures and their contrasts were made for different frequencies, glancing angles, and the horizontal and vertical components of the field of thermal radio emission.

Tables 2 and 3 show the results of computing T_b and ΔT_b, when the clouds and the precipitations are located over a water surface.

Let us note that ΔT_b was computed as the difference between equation (7) or (8) and equation (6).

From analysis of Tables 2 and 3 it is clear that in the wave length bands being studied, the quantities ΔT_b of clouds without precipitation, distributed over a water surface, are small and rarely exceed $\pm$ 10°. Another picture is observed in the presence of zones of precipitation. In these cases the values of ΔT_b are always positive and often exceed 100°. The quantity ΔT_b depends little on the type of polarization, however the frequency dependence is great as is the dependence on the glancing angle, which varies in the various types of polarization. It is interesting to note that ΔT_b for heavy rains at λ = 3 cm is greater than at λ = 0.8 cm and λ = 1.3 cm. At λ = 10 cm, as a result of weak absorption in the clouds and precipitations, ΔT_b does not exceed 12° even for heavy rains.

TABLE 2: CONTRASTS IN RADIOBRIGHTNESS TEMPERATURE (°K) DURING OBSERVATIONS OF RAIN-FREE CLOUDS OVER WATER (HORIZONTAL POLARIZATION).

λ cm	Clouds: Stratus, Stratocumulus			Altocumulus, Altostratus			Cumulus Cumulus congestus		
	Glancing angle, deg.								
	90	60	30	90	60	30	90	60	30
0.8	2	1	—8	2	4	—14	5	7	—31
1.3	10	10	—34	3	—10	—37	0	4	—78
3	—6	0	1	—6	0	0	0	6	—14

TABLE 3: CONTRASTS IN RADIOBRIGHTNESS TEMPERATURES OF VARIOUS RAINS (°K) FALLING OVER WATER /126

λ cm	Intensity of rain, mm/hr	Horizontal Polarization			Vertical Polarization		
		Glancing angle, deg.					
		90	60	30	90	60	30
0.8	1	58	67	98	72	61	35
1.3		29	30	15	30	24	20
3		18	9	20	8	9	8
10		2	2	7	2	2	2
0.8	5	103	115	134	128	109	43
1.3		73	76	64	56	81	37
3		26	32	95	110	25	37
10		1	0	3	7	7	1
0.8	20	101	110	126	128	96	28
1.3		104	102	138	110	78	42
3		102	121	174	110	101	55
10		4	7	12	5	5	2

The values of ΔT_b for the various rains falling over dry land, at λ = 1 cm are shown on Table 4. The values of the reflection coefficients R, that are necessary for the computations, were taken from reference [11]. The computed values of ΔT_b of the rains falling over a coniferous forest are shown on Table 5.

TABLE 4: CONTRASTS OF ΔT_b (°K) OF VARIOUS RAINS, FALLING OVER DRY LAND (λ = 1 cm).

Intensity of Rain, mm/hr	Horizontal Polarization			Vertical Polarization		
	Glancing Angle, Deg.					
	90	60	30	90	60	30
1	17	24	63	18	12	—7
5	26	36	81	29	15	—17
20	27	36	81	30	13	—15

TABLE 5: CONTRASTS OF ΔT_b (°K) OF VARIOUS RAINS FALLING OVER A CONIFEROUS FOREST.

Intensity of Rain, mm/hr	Glancing Angle, Deg.		
	90	60	30
1	—1	—1	—5
5	—5	—7	—15
20	—74	—89	—162

The values of ΔT_b of rains falling over dry land, at λ = 1 cm /127 are slightly smaller than over a water surface (λ = 1.3 cm). This is explained mainly by the large influence of the natural radio emission from dry land in comparison with the radiation from water.

It is interesting to note that for rains falling over a coniferous forest ($R^2 \approx 0$) at λ = 3 cm, the values of $\Delta T_b < 0$, i.e., the zones of rain surveyed from above are characterized by values of ΔT_b which do not exceed 1 - 2° K.

Computations of the contrasts of ΔT_b over snow and ice (Tables 6 and 7) were made for conditions that are characteristic of winter time in our hemisphere. The temperature of the underlying surface was assumed equal to 268° K. Absorption in clouds was determined by taking the temperature correction into account [1].

TABLE 6: CONTRASTS OF ΔT_b (°K) OF SNOW FALLING OVER A SNOW SURFACE (λ = 1 cm).

Intensity of Snowfall, mm/hr	Horizontal Polarization			Vertical Polarization		
	Glancing Angle, deg.					
	90	60	30	90	60	30
0.1	1	2	11	1	1	0
1	2	4	15	2	2	—2
5	10	14	50	10	5	—10

TABLE 7: CONTRASTS OF ΔT_b (°K) OF SNOW FALLING OVER ICE ON SEA WATER (λ = 1 cm).

Intensity of Snowfall, mm/hr	Horizontal Polarization			Vertical Polarization		
	Glancing Angle, deg.					
	90	60	30	90	60	30
0.1	13	16	26	14	13	11
1	19	22	39	19	16	15
5	92	128	138	90	78	51

With a snowfall intensity of I = 0.1 mm/hr, with conversion into water, the vertical expanse of the cloud cover was assumed equal to ΔH = 2 km, and the mean water content of the dropping liquid phase of the cloud $\bar{W}$ = 0.1 g/m^3; the vertical expanse of the zone of snowfall ΔH_{sn} = 1.5 km.

With I = 1 mm/hr, ΔH = 3 km, $\bar{W}$ = 0.1 g/m^3, ΔH_{sn} = 2.5 km. When I = 5 mm/hr, ΔH = 4 km, $\bar{W}$ = 0.5 g/m^3, ΔH_{sn} = 3.5 km.

Since we can ignore attenuation in solid precipitations in determining the overall absorption, the natural radio emission from winter clouds and precipitations then is due to the dropping liquid phase, i.e., to the water content of the winter clouds.

During observations of the zones of snow falling over an underlying surface of snow, the contrasts in ΔT_b are smaller than for the zones of rain. This is due to the smaller absorption of the radio waves by the winter clouds and precipitations, which is not compensated by the slightly larger natural radio emission from the

Earth's surface, that is free of snow during the warm half of the year. However the contrasts in ΔT_b in the observations of snowfall over ice on a water surface, in value, approach that of ΔT_b over clear water. The reason for this is the small natural radio emission from ice on a water surface, and the increase in absorption of the radio waves in the liquid dropping clouds with lowering of temperature. /128

The sparsity of experimental data on the reflection coefficients $R(\delta,\lambda)$ from a water surface with different roughness, and also from other underlying surfaces, limits the universality of the obtained results.

In those cases when the observations are made from the Earth, the values of the radiobrightness temperatures of a cloud-free atmosphere, and in the presence of clouds without precipitation and a rain cloud cover, may be respectively computed using the following formulas:

$$T_b = \overline{T}\left(1 - e^{-\Gamma_a}\right), \tag{9}$$

$$T_b = \overline{T}\left(1 - e^{-\Gamma_1}\right) + \overline{T}_2\left(1 - e^{-\Gamma_2}\right)e^{-\Gamma_1} + \overline{T}_3\left(1 - e^{-\Gamma_3}\right)e^{-(\Gamma_1+\Gamma_2)}, \tag{10}$$

$$T_{ib} = \overline{T}_1\left(1 - e^{-\Gamma_1}\right) + \overline{T}_2\left(1 - e^{-\Gamma_2}\right)e^{-\Gamma_1'} + \overline{T}_3\left(1 - e^{-\Gamma_3}\right)e^{-\left(\Gamma_1+\Gamma_2'\right)} + \overline{T}_4\left(1 - e^{-\Gamma_4}\right)e^{-\left(\Gamma_1'+\Gamma_2+\Gamma_3\right)}. \tag{11}$$

The designations in these formulas are the same as in equations (6) - (8). The computations (Table 8) were made under the atmospheric conditions taken earlier for λ = 0.8 cm (numerator) and λ = 3 cm (denominator).

The possibility of detecting clouds and precipitations with the aid of radiometers depends not only on the contrast in ΔT_b, but also on the sensitivity of the receiver, the scanning time of the basic area and the space factor K_s. /129

Since it is of practical interest to study the energy of the thermal radio emission received by the antenna of the radiometer, it is then characterized by the antenna temperature T_{ant}

$$T_{ant} = T_b(1 - \beta_s)\eta K_s + T_\delta \beta_s \eta + T_0(1 - \eta), \tag{12}$$

where T_b is the brightness temperature in the direction of the major lobe of the radiation pattern, β_s is the scattering coefficient of the antenna, η is the efficiency of the antenna, T_δ is the average brightness temperature of the radiation incident on the side lobes, T_0 is the temperature of the antenna.

Usually $\beta \approx 0.2 - 0.3$ and $\eta \approx 0.8$. If the observations are

TABLE 8: COMPUTATIONAL VALUES OF T_b AND ΔT_b (°K) OF CLOUDS AND PRECIPITATIONS DURING OBSERVATIONS FROM THE EARTH.

Type of Cloud Cover and Intensity of the Rain	Angle of elevation of the antenna, Deg.							
	90		60		30		10	
Stratus	29/3	5/0	34/3	5/0	55/5	8/0	133/17	18/1
Cumulostratus	28/3	3/0	32/3	4/0	54/5	7/0	127/16	13/0
Altocumulus	27/3	3/0	31/3	2/0	49/5	2/0	123/17	8/1
Cumulus congestus	99/11	74/8	110/12	82/9	161/18	114/13	252/58	137/42
I = 1 mm/hr	120/12	95/9	133/14	105/10	187/23	140/18	262/65	147/49
I = 5 mm/hr	224/30	199/27	234/34	206/30	264/56	217/51	273/135	158/129
I = 20 mm/hr	273/132	248/129	273/146	245/143	273/200	226/195	273/214	158/198

carried out from a satellite at altitudes on the order of several hundreds of kilometers, then in first approximation in formula (12) we can drop the second and third terms. Then, when $K_s = 1$, $T_{ant} = 0.56\ T_b$ and $\Delta T_{ant} = 0.56\ \Delta T_b$.

In reference [9] it was shown that the most frequently encountered value of K_s of the zones of precipitations for an area with a radius of 50 km is about 0.3 - 0.4, and for an area with a radius of 25 km, it is 0.6. Then, respectively, $\Delta T_{ant} = 0.2\ \Delta T_b$ and $\Delta T_{ant} = -.4\ \Delta T_b$.

If the change in the antenna temperature, produced by ΔT_b of the clouds and the precipitations, exceeds the sensitivity of the radiometer receiver, these atmospheric condensations will be detected.

The possibilities of detection depend also on the scanning time of the basic area because the signal may be assumed steady, if this time is equal to 2 - 3 τ (here τ is the time constant of the receiver).

Finally, detection of clouds and precipitations will depend substantially on the value of the space factor K_s. Let us illustrate this in the following example. Let us look at the case when $K_s = 1$ and when $K_s < 1$. For simplicity we shall assume that the radio emission from the underlying surface is attentuated only by clouds. The contribution of the radiobrightness temperature of atmospheric gases to T_{ant} in the formulas will not be

taken into account, since it will be the same for any value of K_s.

In the first case ($K_s = 1$)

$$T_{ant} = (T_{bE} e^{-\Gamma cl} + T_{b\,cl})(1 - \beta_s)\eta, \quad (13)$$

where $T_{b\,E}$ is the brightness temperature of the Earth, $T_{b\,cl}$ is the brightness temperature of the clouds.

In the second case ($0 < K_s < 1$)

$$T_{ant} = [T_{bE}(1 - K_s - K_s e^{-\Gamma cl}) + T_{b\,cl} K_s](1 - \beta_s)\eta. \quad (14)$$

From expressions (13) and (14) it is clear that the contribution of the radiation to T_{ant} is directly proportional to K_s, which can never be said about the influence of radiation from the underlying surface.

Let us take $e^{-\Gamma cl} = 0.5$. This represents an absorption of the electromagnetic energy at $\lambda = 1.3$ cm in rain with an intensity of 5 mm/hr with $\delta = 90°$.

We will assume $K_s = 0.35$. Then $T_{b\,E} e^{-\Gamma cl} \approx T_{b\,E}(1 - K_s - K_s e^{-\Gamma cl})$, i.e., almost the same amount of energy is received from the underlying surface in both cases and difference in the values of T_{ant} will be determined by the variation in the value of the natural radio emission from the cloud cover. Under these conditions the contrast in ΔT_{ant} of these atmospheric condensations on a background of the underlying surface comprises about 20% of that previously computed (see Table 3).

In other cases the variation in T_{ant} is not proportional to K_s and may be determined from formulas (13) and (14). /130

At the present time some experimental data have been compiled on the natural thermal radio emission from a clear atmosphere and in the presence of clouds and precipitations [10]. However the size of this material is considerably smaller than was obtained by using the methods of active radar in meteorological targets. No results of such experimental determinations from aircraft of radio emission from the atmosphere and atmospheric condensations, as far as we know, have been obtained.

The author, in conjunction with N.F. Pavlov and I.V. Korol'kov, using a manufactured model of a 3-cm radiometer, in July 1964 began measurements of the T_b of the atmosphere from the Earth. The measurements were made in conjunction with the MRL-1 Meteorological Radio Station which was used to search for zones of precipitations and to obtain their radar characteristics. The radiometer had an antenna with a 736 mm parabolic reflector. The fluctu-

TABLE 9: RADIOBRIGHTNESS TEMPERATURE OF THE ATMOSPHERE IN DIFFERENT WEATHER (λ = 3 cm)

Date	Time hr. min.	δ°	T_b°K	Existence of Precipitations and Clouds
1964				
June 14	15 10-17 00	0	214	Heavy steady rain
		3	200	
		5	139	
		10	95	
June 23	17 00-17 55	2	58	Cloud-free
		10	14	
		45	6	
Aug. 5	17 20-18 40	0	113	Cumulus and cumulus congestus
		0	141	cloud cover, 5 points on the scale
		0	149	
		3	79	
		10	3	
		20	0	
Aug. 7	12 00-14 00	0	141	Cumulus and cumulus congestus
		0	82	cloud cover, 5 points on the scale
		3	78	
		3	83	
		3	146	
		3	75	
		3	69	
		3	45	
		0	130	
		0	141	
Aug. 18	18 30-19 05	0	113	Cloud-free
		0	103	
		1	81	
		10	18	
Aug. 12	15 40	0	187	Light steady rain
		0	182	
		0	206	
	16 00	0	133	Rain ceased, cloud cover of 10
		0	155	points on the scale
		0	110	

ation sensitivity of the receiver with τ = 64 sec was about 1.5°. /131

As a result of measurements of the antenna temperature of the atmosphere in different weather, we determined the brightness

temperatures T_b. In this case we used the familiar approximation equation

$$T_b(\delta) = \frac{T_{ant}(\delta) - T_0(1-\eta)}{\eta} \qquad (15)$$

The experimentally found values of T_b are given in Table 9. Analysis of the table shows that the values of T_b in the presence of clouds and precipitations are greater than the values of T_b in clear or slightly cloudy weather. On the average, of all the measurements the contrast of the radiobrightness temperatures ΔT_b of heavy rain was about 80 - 110° K with δ = 0 -10°. In light rain and an angle of elevation of the antenna δ = 0°, $\Delta T \approx 75°$ K. One case should be mentioned (August 7, 1964), when a negative contrast (ΔT = -80° K) of an individual cumulonimbus cloud was observed with δ = 0°.

Comparison of the computational and experimental data shows generally that they have a satisfactory agreement. It also follows here to emphasize again the necessity of making further systematic measurements of T_b and ΔT_b of the atmosphere both from the Earth and, in particular, from aircraft.

REFERENCES

1. Battan, L.D.: Radiolokatsionnaya meteorologiya. (Radar Meteorology). Gidrometeoizdat, Leningrad, 1962.
2. Troitskiy, V.S., S.A. Zhevakin and N.M. Tseytlin: Radioizlucheniye atmosfery i issledovaniye pogloshcheniya santimetrovykh voln. (Radio Emission from the Atmosphere and Investigation of Absorption of Centimeter Waves)., Izv. VUZ, ser. Radiofizika, Vol. 1, No. 2, 1958.
3. Nikolayev, A.G. and S.V. Pertsov: Radioteplolokatsiya. Passivnaya radiolokatsiya. (Radio Thermal Location. Passive Radar)., Sovietskoye Radio, 1964.
4. Stepanenko, V.D.: Radiolokatsiya v meteorologii. (Radar in Meteorology)., Gidrometeoizdat, 1966.
5. Rasprostraneniye ul'trakorotkikh radiovoln. (Propagation of Ultrashort Radio Waves)., Translated from the English by B.A. Shillerov. Sovietskoye radio, 1954.
6. Shifrin, K.S.: Rasseyaniye sveta v mutnoy srede. (Scattering of Light in a Cloudy Atmosphere)., Gostekhizdat, 1951.
7. Zhevakin, S.A. and V.S. Troitskiy: Pogloshcheniye santimetrovykh voln v sloistoy atmosfere. (Absorption of Centimeter Waves in a Stratified Atmosphere)., Radiotekhnika i elektronika, No. 1, 1959.
8. Taylor, R.: Izmereniya radiolokatsionnykh otrazheniy ot zemnoy poverkhnosti na chastotakh 10; 15,5 i 35 Ggts. (Measurements of Radar Reflections from the Earth's Surface at Frequencies of 10, 15.5 and 35 GHz). Zarubezhaaya radiotekhnika, No. 3 1956.
9. Stepanenko, V.D.: Nekotoryye geometricheskiye kharakteristiki oblakov i osadkov po radiolokatsionnym nablyudeniyam. (Several Geometric Characteristics of Clouds and Precipitations from Radar Observations)., See this Collection.
10. Orhaug, T.: The Effect of Atmospheric Radiation in the Microwave Region. Publ. Nat. Radio Astronom., Vol. 1, No. 4, 1962.
11. Solov'yev, N.P.: Otrazhayushchiye svoystva zemnykh pokrovov. (Reflecting Properties of the Earth's Mantle)., Trudy Riga Institute of Civil Engineers, No. 27, 1963.

SEVERAL GEOMETRIC CHARACTERISTICS OF CLOUDS AND PRECIPITATIONS BASED ON RADAR OBSERVATIONS

V.D. Stepanenko

ABSTRACT: Experimental data are presented on the basic geometric characteristics of clouds and precipitations: the horizontal cross sections and the vertical dimensions obtained with the aid of the MRL-1 meteorological radar station.

For a number of radiometeorological and other problems it is necessary to have knowledge of the geometric characteristics of clouds and precipitations such as their horizontal cross sections and vertical dimensions. /132

We know that steady precipitations occupy areas in tens, thousands and hundreds of thousands of square kilometers, and that cloud bursts involve several hundred or thousands of square kilometers. However, as was noted in references [1,3,4], the cross sections of radio echoes often occur in a smaller area of the precipitation bands, especially in detection by nonmeteorological radar stations which are characterized by a small potential.

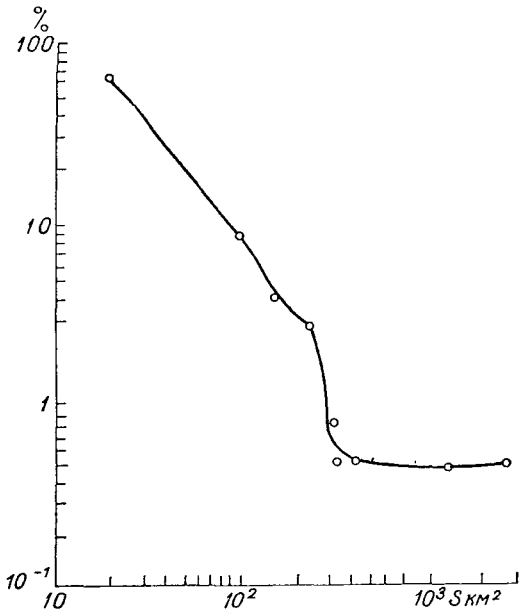

Fig. 1. Frequency of Radio Echo Cross Sections from Precipitations.

For a radar station such as the MRL-1 and other high-potential radar stations the precipitations which are determined by pluviographs in the range from 50 - 70 km from the radar station, are represented on the screens of these stations without substantial cross-sectional distortions [2].

Radio echoes from the precipitation bands, located at large distances from the radar station (as a result of the curvature of the Earth, attenuation of the radiowaves and radiation from overhead and weakly reflecting parts of the precipitations) as a rule, are smaller than their real geometric dimensions.

Figure 1 shows the distribution of cross sections of 282 precipitation sources in the range of 100 km, obtained with the aid of the above radar stations over

the territory of the European USSR in the warm half of the year. From this figure it is clear that in approximately 80% of the cases the cross section of the radio echoes from precipitation sources does not exceed 60 km^2, although individual sources are observed with a dimension of 2500 km^2 and more.

It is interesting to look at the statistical data, concerning /133 the degree of closure of the plan position indicator deflectors at the radar stations, from recordings of the precipitation bands at various ranges.

Since in a range from 0 - 50 km, the radar stations detect all precipitations, the ratio of the cross section occupied by the precipitations S_0 to the cross section of a circle with a radius of 50 km then represents a cross sectional space factor of the radiation pattern K_s in detecting the precipitations from aircraft, when the basic cross section on the surface of the Earth has a radius of 50 km.

Some idea of the degree of closure of the plan position indicator deflectors can be found from Tables 1 and 2. In them are shown the frequencies in percents of the ratios of cross sections occupied by the cross sections S_0 to the cross sections of a circle S_c or cross sections of rings, whose radii are shown in the tables.

TABLE 1

R км	S_0/S_c										Average	No. of Days with Observations
	0,04—0,1	>0,1—0,2	>0,2—0,3	>0,3—0,4	>0,4—0,5	>0,5—0,6	>0,6—0,7	>0,7—0,8	>0,8—0,9	>0,9—1		
0—50	40,7	22,7	13,7	4,64	4,54	4,54	4,54	—	—	4,64	0,24	22
>50—100	47,0	34,5	3,0	15,5	—	-	-	—	—	—	0,12	32

TABLE 2

R км	S_0/S_c					No. of Days with Observations
	≤ 0,04	>0,04—0,08	>0,08—0,12	>0,12—0,16	Average	
100—150	64	20	8	8	0,042	25

The quantity S_0 was determined by summation of all cross sections of radio echoes from individual precipitation sources, which are found in the selected ranges.

As it would be expected, the largest value of the degree of deflector closure is observed in a radius of 50 km where the mea value $\frac{S_0}{S_c} = 0.24$. The smallest value of the examined cases for the

degree of closure is observed in a radius of 100 - 150 km, where $\frac{S_0}{S_c} = 0.042$.

The cross sections occupied by atmospheric condensations in the vertical plane may be obtained by analyzing Figures 2 and 3. The curves on these figures have been plotted as results of the radar observations using the MRL-1, operating in a program of vertical scanning of the antenna. To decrease the errors due to the influence of the range and the reflectivity z on the geometric dimensions of the clouds we interpreted the case when clouds without precipitations were located $R \leq 16$ km from the MRL-1 and the rainfall was at $R \leq 50$ km.

As we know it is the radio echoes from cumulonimbus clouds /134
which have the greatest thickness. Most often their thickness is on the order of 5 - 8 km. The thickness of the radio echoes from nimbostratus clouds is slightly smaller. The maximum of frequency for them is at $\Delta H = 4 - 5$ km.

Radio echoes from clouds without precipitation are characterized usually by double-peaked frequency curves of their thicknesses. Here the first maximum represents a thickness of 1 km and the second approximately 2 km.

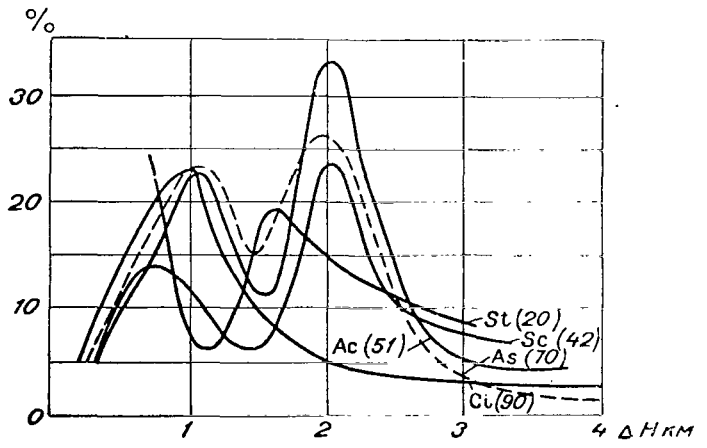

Fig. 2. Frequency of Thicknesses of Radio Echoes from Rain-Free Clouds.

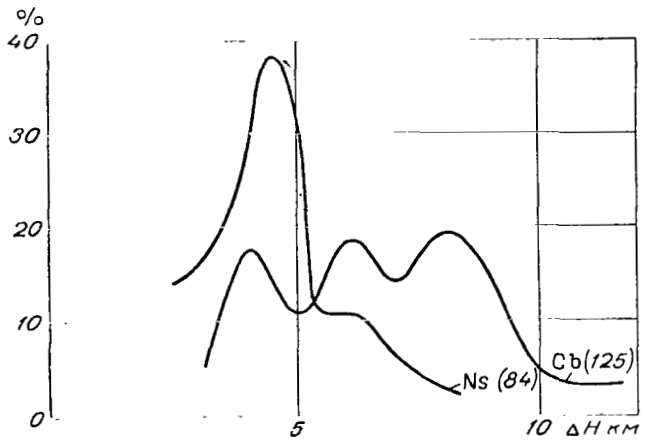

Fig. 3. Frequency of Thicknesses of Radio Echoes from Rain Clouds.

REFERENCES

1. Battan, A.D.: Radiolokatsionnaya meteorologiya. (Radar Meteorology), Gidrometeoizdat, Leningrad, 1962.
2. Brylev, G.B. and Ye.M. Sal'man: O predel'noy dal'nosti radiolokatsionnogo obnaruzheniya livnevykh osadkov. (The Maximum Range of Radar Observation of Cloudbursts)., Trudy Main Geophysical Observatory, No. 159, 1964.
3. Stepanenko, V.D.: Radiolokatsiya v meteorologiya. (Radar in Meteorology), Gidrometeoizdat., 1966.
4. Atlas, D. and H. Banks: The Interpretation of Microwave Radiation from Rainfall. Met., Vol. 8, No. 3, 1953.

THE STRUCTURE OF PRECIPITATION FIELDS IN THE UKRAINE

Zh.D. Alibegova

ABSTRACT: Several results of investigating the character of the spottiness of precipitation fields which occur on the territory of the Experimental Meteorological Proving Ground in the Ikraine are cited. The expanse and the cross sections of individual sources of precipitation fields are computed. Analysis showed that the greatest frequency occurs for sources having an expanse up to 6 km (88% of all cases). The average expanse of the spot along the major axis is 6 km with a maximum value equal to 22 km. Most probable are the sources of precipitations having a cross section up to 20 km^2 (about 83% of all cases). Sources with a cross section from 20 to 30 km^2 comprise about 5%, and on the cross section of the other gradations there are altogether several percents of the total number of cases of precipitation sources.

Data on the spatial structure of precipitation regions, the most probably cross sections and forms of precipitation sources, the frequency of precipitations of one or another intensity by gradations have great practical application; therefore, knowledge of the characteristics of the statistical structure of precipitations in these or other regions is of considerable value to us. /135

The expanse of the precipitation bands of different intensity is of interest in solving problems of determining these bands with the aid of radiometric instruments.

In the 1920's, I.I. Kasatkin was concerned with the study of regions of isochronal precipitation over the territory of Moscow and its environs [4]; however, the greatest interest in the problem of investigating the structure of the precipitation field began to appear with the appearance of new observational methods (radar, aircraft, satellite).

A number of papers have appeared on studying the character of the spottiness of the precipitation field in Valday and in the Ukraine, in regions which are most thickly equipped with meteorological stations and posts [3,5,6].

There exist some data on the structure of the precipitation field in the Northwest part of the European USSR and in the Asiatic USSR [1,2,7,8]; however, the majority of the above papers have

been involved in the study only of the structure of cloudbursts.

The accuracy of the observations of precipitation bands depends on the sensitivity of the measuring instruments and also on the sizes of the bands and the intensity of the precipitation in these precipitation bands.

Which characteristics of the structure of the precipitation field will be determined by the measurement instruments and which characteristics will be found from the field of its influence? What distortions will be obtained at different scales of averaging by cross section? These are the questions which are of interest to us.

In the present paper in which we give several preliminary results of investigating the spottiness of the precipitation field in the Ukraine, we used pluviographic recordings of the path of the rains determined by the stations and posts of the Experimental Meteorological Proving Ground.

As has been noted, previous investigations on the character of the spottiness in these of other regions of the USSR were made basically either by using radar methods (in this case, in view of the limited resolving power of the measuring instruments, virtually no information was obtained on the precipitations of small intensity), or the characteristics of the precipitations were averaged for long periods of time. We made an attempt to investigate the /136 spottiness of the precipitation field at 15-minute intervals of time. Moreover, as certain of our computations showed, we can never ignore rains of small intensity.

Computation of the frequency of precipitations of various intensity by gradiations for several points of the European USSR (in percents of the time of precipitation of all rains for the summer season) showed that the greatest frequency was for cloudbursts, and for low-intensity precipitations. In 90-95% of the time for all precipitations in the North-west part of the European USSR, their intensity was 0 - 3 mm/hr. In Moscow the frequency of precipitations with an intensity of 0 - 3 mm/hr was 86% and in Poltavo, 81%.

In themselves these values are large, but the difference between them is high. This is explained by the fact that in Moscow (center of the European USSR) and in Poltavo (Ukraine) the frequency of precipitations with an intensity of 3.1 - 10 mm/hr is high (12 - 13% versus 5% in the North-west part of the European USSR).

As far as the intensity of precipitations greater than 10 mm/hr is concerned, in the North-west their frequency is only 1 - 2%, although it is true that in the South of the European USSR their frequency increases to 6 - 7%, i.e., in the Ukraine the number of cloudbursts is high.

The low-intensity precipitations also make a significant contribution to the overall total of all precipitations. Thus, in Leningrad, for the warm half of the year, about 300 mm of precipitation fall with an intensity of 0 - 3 mm/hr and about 150 mm with an intensity of 3.1 - 10 mm/hr.

In Moscow the contribution of low-intensity precipitations is also high (190 mm versus 100 mm of precipitations with an intensity of 3.1 - 10 mm/hr). In Poltavo the number of cloudbursts is high and thus the contribution which they make to the total precipitations is also. Here about 130 mm of precipitation fall with an intensity up to 3 mm/hr and about 100 mm with an intensity of 3.1 - 10 mm/hr and higher.

The region of the Experimental Meteorological Proving Ground which we selected for studying the character of the spottiness of the precipitation field is due first of all to the significant number of networks of stations and posts and secondly because the spottiness in regions such as Crimean Steppes, the Ukraine, the Urals and the Northern Caucasian Steppes is expressed most strongly, the precipitation sources are small and the correlation bonds between the values of the precipitations at the various points drop rapidly.

We charted the individual moments of rains occuring in the Ukraine and found 497 sources (taking into account those sources whose reality was confirmed by pluviographic recording of the path of the rain wven though this occured only at a single station) and 197 spots, whose reality was confirmed directly by two or more stations.

TABLE 1: FREQUENCY OF SPOTS OF DIFFERENT EXPANSE BY GRADIATIONS (% OF THE TOTAL NUMBER OF CASES)

	≤3 km	3.1-6 km	6.1-10 km	10.1-15 km	>15 km	Number of cases
Reality of spot confirmed by even one station	22	49	22	6	1	497
Reality of spot confirmed by two or more points	68	20	9	2	1	197

As we can see from Table 1, the greatest frequency is for pre-/137
cipitation sources with an expanse up to 6 km (88% of all cases), and for sources with an expanse greater than 10 km, it is only several percent of the sources which occur.

The average expanse of the spot along the major axis is 6 km with a maximal value equal to 22 km.

Unfortunately, we must mention that all computations have been made without reference to origin of the precipitations. In the future a study will be made of the spottiness of the precipitation field taking into account the origin of the precipitations, the physico-geographical conditions of the region and the synoptic situation.

In addition to the expanse of the precipitation sources, we also computed the cross sections, simultaneously encompassed by rain, The cross sections were computed from the formula $S = \pi ab$, where a and b are the major and minor semiaxes of the precipitation sources.

The shape of the spots was assumed to be elliptical, since in charting the individual moments of rains at 15-minute intervals, basically the shape of the precipitation sources had the form of a slightly elongated ellipse.

Analysis of Table 2 shows that sources with a cross section up to 20 km^2 (about 83% of all cases) are the most frequently encountered ones, and the maximum (64.5%) is for sources with a cross section up to 10 km^2. Spots of precipitations with a cross section from 20 to 30 km^2 comprise about 5% of all spots, and for cross sections of other gradations only several percents of the total number of cases involve sources of precipitation.

TABLE 2: FREQUENCY OF PRECIPITATION SOURCES OF DIFFERENT CROSS SECTION

Cross section, km^2	<10	10-20	20-30	30-40	40-50	50-100	>100
Frequency, % of all cases of precipitation sources	64.5	19.8	5.1	2.5	2.1	3.5	2.5

The mean cross section of the spots was on the order of 15 km^2 with a minimal value of 3 km^2 and a maximal value of 276 km^2.

The computations which we made permit us to make the following conclusion.

For the territory of the Ukraine and regions which are similar to it in physico-geographical conditions, comparatively small precipitation sources are characteristic. Most probable are spots with an expanse up to 6 km and a cross section up to 20 km^2

REFERENCES

1. Anchugova, R.A. and T.I. Morozova: O vremennoy i prostranstvennoy izmenchivosti livnevykh osadkov po dannym radiolokatsionnykh nablyudeniy. (Time and Space Variations in Cloudbursts Based on Data from Radar Observations). Trudy Main Geophysical Observatory, No. 186, 1966.
2. Bogomazova, Z.P. and Z.P. Petrova: Issledovaniye vydayushchikhsya dozhdey Severo-Zapadnogo rayona ETS i ikh zavisimosti ot ploshchadi rasprostraneniye. (Investigation of Rainfall in the North-West Region of the European USSR and its Dependence on the Cross Section of Propagation)., Trudy Mining and Geological Instiute, No. 1 (55), 1947.
3. Bogomazova, Z.P. and Z.P. Petrova: Issledovaniye vydayushchikhsya dozhdey no territorii USSR, ikh khoda i rasprostraneniye po ploshchadi. (Investigation of Rainfall in the Territory of the UkrSSR, its Path and Propagation by Cross Section). Trudy Mining and Geological Instiute, No. 6 (60), 1948.
4. Kasatkin, I.I.: Klassifikatsiya dozhdey. (Classification of Rains)., Met. vestnik, No. 3, 1925.
5. Muchnik, V.M.: Obnaruzheniye groz radiolokatorom po dannym o maksimal'noy intensivnosti dozhdey. (Detection of Thunderstroms by Radar from Data on Maximal Rain Intensity). Meteorologiya i gidrologiya, No. 10, 1963.
6. Muchnik, V.M.: Nekotoryye radiolokatsionnyye khrakteristiki livney i groz. (Several Radar Charcateristics of Showers and Thunderstorms)., Trudy Central Aerological Observatory No. 20, 1958.
7. Petrova, Z.P.: Livni na Aziatskoy territorii SSSR. (Showers on the Azian Part of the USSR)., Trudy Mining and Geological Institute, No. 1(55), 1947.
8. Sal'man, Ye.M.: Radiolokatsionnyye issledovaniya struktury livney i groz. (Radar Investigation of the Structure of Showers and Thunderstorms)., Trudy Main Geophysical Observatory, No. 72, 1957.

POSSIBLE ERRORS IN ABSOLUTE MEASUREMENTS OF RADIO EMISSION

Yu.I. Rabinovich, G.G. Shchukin and V.G. Volkov

ABSTRACT: A detailed study is given of the influence of various factors on the accuracy of determining the radiobrightness temperature and an estimation of the total error in measuring the radio emission from a water surface, using an aircraft radiometric instrument at the λ = 3.2 cm band. Methods of calibrating the radiometric instrument and reproducing the radiobrightness temperature based on the known antenna temperature are examined. It is shown that the greatest accuracy in measurements may be attained by calibrating the instrument according to the natural microwave radiation from a uniform water surface.

One of the important problems in thermal radar measurements is/138 that of evaluating the accuracy of determining the radiobrightness temperature of the received radiation. This accuracy depends on a number of factors including especially the parameters of the antenna-feeder circuit and the characteristics of the receiver. Moreover, the methods used to calibrate the instruments and to make the measurements and the interpretations have considerable influence.

The purpose of the present article is to make a detailed study of the influence of these factors on the accuracy of reproducing the radiobrightness temperature and evaluate the total error in applying it to measurements of radio emission from a water surface using aircraft radiometric instruments in the λ = 3.2 cm band. The sensitivity of the radiometer is 1.5° K with a time constant of τ = 1 sec.

Determination of the radiobrightness temperature of the surface to be investigated using hhe thermal radar instrument can be conditionally divided into two operations: determination of the antenna temperature and the conversion from antenna temperature to radiobrightness temperature. The errors which creep into the measurement process can also be conveniently studied in such a sewuence. Generally the following sources of error exert an influence on the accuracy of measuring the radiobrightness temperature:

(1) Accuracy of determining losses in the antenna-feeder circuit;

(2) Accuracy of determining the scattering coefficient of the antenna;

(3) Accuracy of maintaining and determining a zero level for the radiometer;

(4) Accuracy of determining the temperature of the exciter during calibration;

(5) Errors in recording measurable values and taking the readings from the tape of the recording instruments.

1. Determination of Antenna Temperature

The antenna temperature of the radio emission at the input of the receiver T_γ is associated with the temperature at the output of the antenna T_a by the following equation:

$$T_\gamma = T_a(1-\gamma) + T_0\gamma, \qquad (1)$$

where γ are losses in the antenna-feeder circuit.

Consequently, in order to determine the antenna temperature it is necessary to know the losses in the antenna-feeder circuit. These losses can be accounted for by two methods: (a) preliminary mea- /139 surements of the losses in the antenna-feeder circuit and then taking them into account; or (b) by eliminating the influence of the losses in the antenna-feeder circuit by calibrating the instrument directly at the input of the antenna exciter.

It is more convenient to use the second method, since the first requires a high measurement precision. At the present time the measurement precision of losses in the centimeter band is ± 0.1 db, which represents an error in the determining the radiobrightness temperature of approximately ± 7° (when T_0 = 300° K).

If the second method is used, determination of the value of the radiobrightness temperature is reduced to comparing the useful signal at the input of the reciever with the signal from some standard source. Since the useful signal enters the receiver through the antenna-feeder circuit, the standard signal must also pass through this circuit.

In the described instrument, in the measurement process of the radiobrightness temperatures, a periodic calibration is automatically made for the zero point of the scale, i.e., the point at which the antenna temperature is equal to the temperature of the "cold" standard, by eliminating modulation from the commutator and hooking up a matched load with a temperature T_0 to the input of the receiver. It is obvious that in the absence of modulation, i.e., when the coefficient of modulation is equal to zero, $T_a = T_0$.

To calibrate the height of the scale at the effective point,

noises from a GSh type gas-discharge tube are connected through the directional coupler to the input of the channel. In this case at the antenna input the temperature rises to the value ΔT, and the voltage at the output of the radiometer is increased to a value ΔE. The height of the scale S will then be

$$S = \frac{\Delta E}{\Delta T} \text{ V/deg.} \qquad (2)$$

If we assume that the scale of the radiometer is linear, then the zero point and the height will determine the entire scale. The value of the calibrated signal T_c will be practically constant in time, however as a function of the amplification factor there will correspond to it different readings expressed in units of length of the scale of the output instrument. A sample of the recordings of antenna temperature is shown on Figure 1. Obviously the antenna temperature is determined by the following equation:

$$T_a = T_0 - T_c \frac{l}{k}. \qquad (3)$$

Hence the calibration signal will be

$$T_c = \frac{T_0 - T_a}{l} k, \qquad (4)$$

where $\frac{T_0 - T_a}{l}$ is the height of the scale of the recording instrument in deg/mm, T_0 is the temperature of the "cold" standard, l is the linear segment of the scale, representing the difference in temperatures $T_0 - T_a$, k is the segment of the scale representing the increase in the signal from the "hot" GSh standard.

The instrument can be calibrated, i.e., the value of the calibration signal T_c can be determined, before installing the instrument on the aircraft. The radio emission from the atmosphere is used for this purpose. The antenna, along with the waveguide circuit, is placed into a metal shield and directed to the zenith with a known radio brightness temperature. The dimensions of the shield are chosen in such a way that reception is guaranteed of radiation /140 at an angle corresponding to the main lobe of the radiation pattern of the antenna, by screening the effect of the back and side lobes. The aperture of the shield must comprise no more than 60-80° in the range of which the radiobrightness temperature of a cloud-free atmosphere may be assumed constant in the 3-cm band [4]. Thus, using the metal shield and by directing the back and side lobes of the antenna system to the region of the sky with a known radiobrightness temperature we can calibrate the radiometer and assume that it is reduced to the input of the exciter. Figure 2 shows the radiation

pattern of an antenna with a shield and without. Simultaneously with the calibration of the instrument it is necessary to determine the meteorological characteristics of the atmosphere for computing the radiobrightness temperature of a cloud-free sky.

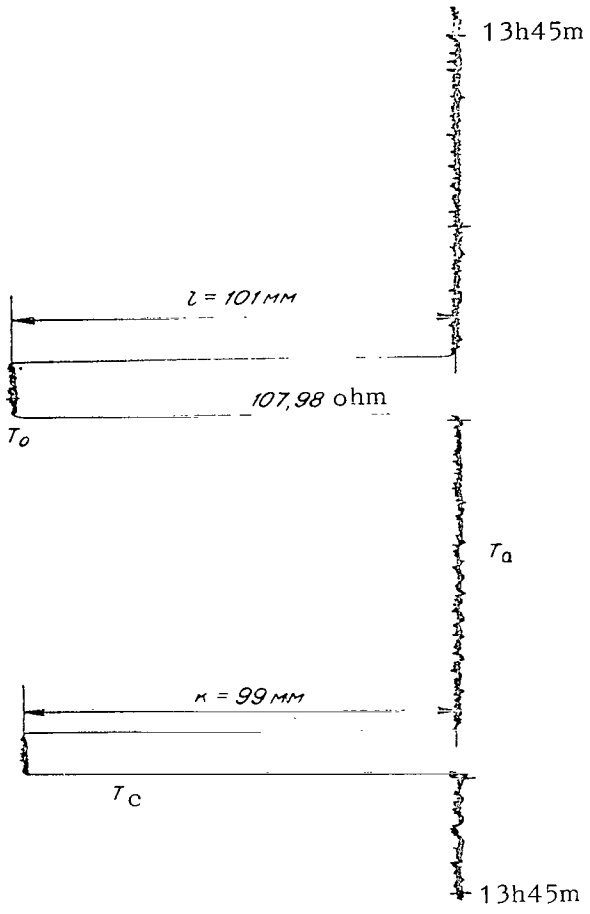

Fig. 1. Sample of Recording of Antenna Temperature. Caspian Sea, December 29, 1966.

A second method which is feasible under ground conditions is to calibrate the radiometric instrument by the nitrogen load. In this case, the matched load at the temperature of liquid nitrogen is connected directly to the exciting horn of the antenna. To make the calibration it is necessary to have a precise measurement of the losses in the feeder circuits, connecting the standard load to the antenna exciter. /141

The radiobrightness temperature of the radiation, fed to the input of the exciter can be computed from the formula

$$T'_{ni} = T_{ni}\eta + T_{at}(1-\eta), \quad (5)$$

where T'_{ni} is the radiobrightness temperature of the nitrogen load, T_{at} is the temperature of the surrounding atmosphere, η is the efficiency of the feeder circuit, T_{ni} is the temperature of the nitrogen, taking into account the losses which occur in the matched load. When the standing water ratio is equal to unity, this temperature is equal to the physical temperature of nitrogen 77° K.

For the ground experiment, computation of the calibration signal is made from Formula (4) in which $T_a = T'_{ni}$. In the case of aircraft measurements, it is necessary to again consider the losses in the radio-transparent deflector

$$T'_c = \frac{T_c}{\eta_1} \quad (6)$$

where η_1 is the efficiency of the deflector, T_c' is the value of the calibration signal taking losses in the deflector into account.

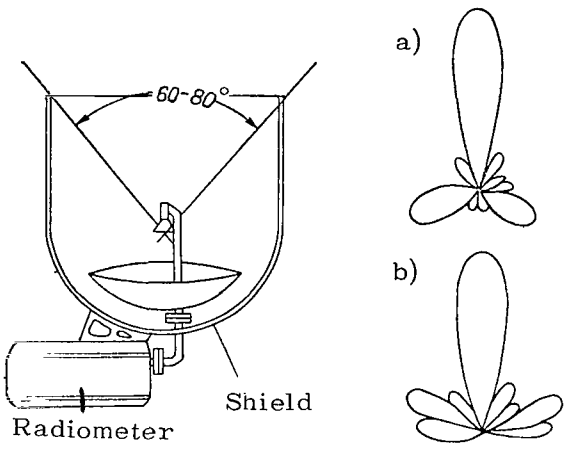

Fig. 2. Structure of the Antenna Radiation Pattern. a - without Shield; b - with Shield.

A third method used in aircraft conditions is the determination of T_c from the radio emission of a water surface. To do so, several flights are made over a uniform water surface with a known physical temperature at a minimally attainable altitude (100 m). To make the calibration it is necessary to know the value of the radiobrightness temperature of the water surface which is determined from computational data. Using the computations the radio emission of the atmosphere is also determined. The obtained computational value of the radiobrightness temperature of the water surface, allowing for back radiation from the atmosphere, is taken equal to the antenna temperature. Further computation of the value of the calibration signal can be made using Formula (4).

Let us look at the advantages and disadvantages of these methods of calibrating the radiometric instrument.

Calibration from the nitrogen load is of greatest interest, /142 since it permits determining the calibration signal by a completely independent method. However, in measuring the absolute values of the radiobrightness temperature from a water surface a large error is introduced into the antenna temperature determined from T_c. This is caused by the low accuracy of the radio engineering measurements of the losses in the supplementary circuit, connecting the nitrogen load to the exciter; the measurement precision, as noted above, does not exceed ±0.1 db.

The methods used to calibrate from radio emission of the atmosphere or a water surface have a high accuracy, which is determined only by the errors in the computational methods.

The errors in determining the antenna temperature can be estimated by using the basic Equation (3). After taking the logarithm of it and determining the differential by converting to finite increments, we obtain an expression for the relative error in determining the antenna temperature

$$\frac{\Delta T_a}{T_a} = \frac{\frac{\Delta T_0}{T_0}\frac{1}{T_C\frac{l}{k}} + \frac{\Delta T_C}{T_C}\frac{1}{T_0} + \frac{1}{T_0}\left(\frac{\Delta l}{l} + \frac{\Delta k}{k}\right)}{\frac{1}{T_C\frac{l}{k}} - \frac{1}{T_0}}, \quad (7)$$

where $\frac{\Delta T_0}{T_0}$ is the relative error in determining the temperature of the "cold" standard, $\frac{\Delta T_C}{T_C}$ is the relative error in determining the value of the calibration signal, $\frac{\Delta l}{l}$, $\frac{\Delta k}{k}$ are the relative errors in determining the linear dimensions of the scale of the recording instrument, corresponding to the difference in temperatures T_0-T_a and the increase in the "hot" standard T_C.

With respect to the fact that the linear dimensions of l and k were chosen as practically the same (Fig. 2) and bearing in mind that the errors in Δl and Δk, determined by the accuracy in taking the readings from the tape of the recording instrument, are equal (about 1 mm), expression (7) takes the form

$$\frac{\Delta T_a}{T_a} = \frac{\frac{\Delta T_0}{T_0}\frac{1}{T_C} + \frac{\Delta T_C}{T_C}\frac{1}{T_0} + \frac{\Delta l}{l}\frac{2}{T_0}}{\frac{1}{T_C} - \frac{1}{T_0}}. \quad (8)$$

The error in determining the temperature of the "hot" standard using a standard resistance thermometer is 0.4 $\pm$ 0.2°.

The value of the calibration signal is determined, according to [1], from the formula

$$T_C = \frac{c}{\alpha}(T_e - T_0), \quad (9)$$

where T_e is the electron temperature of the discharge, comprising approximately 15,000-20,000° K, c is the coupling coefficient of the gas-discharge tube with the noise generator, α is the attenuation factor of the attenuator (ratio of incident power to emitting).

Since $T_e >> T_0$ and the value of T_0 during flight varies only in the range from 20 to 25° K, we may assume the value T_C to be constant in time. Consequently, the error in determining T_C is de- /143 termined only by the accuracy of the method used to calibrate the instrument.

In determining T_C from the radio emission of the water surface a considerable error may arise in allowing for the emission coefficient from the water surface, since there are not sufficient reliable data available for the various temperatures and salinity of the water. The scatter of data in the emission coefficient is about

0.005 which leads to an error in determining the antenna temperature of about 1.5°.

We can also determine T_c from atmospheric radiation, because here in the various states of a cloud-free atmosphere the radiobrightness temperature of the zenith region of the sky varies in a range from 3-5° K. However, since in this case the antenna temperature itself is small, the errors in the measurements will increase.

Taking the above into account we can evaluate the relative error in determining the antenna temperature as a function of the method used to calibrate the instrument by the following values (Table 1):

TABLE 1

Calibration Method	Relative Error, %
From the nitrogen load	10.0
From the radio emission of the atmosphere	7.0
From the radio emission of the water surface	5.0

2. Determination of the Radiobrightness Temperature from a Known Antenna Temperature

In the aircraft radiometer the pencil-beam antenna is of mirror type. In addition to the basic lobe, the radiation pattern has side lobes, therefore the antenna temperature at a given radiobrightness temperature of the investigated surface and background will represent the total radiation received not only from the region of the main lobe of the pattern but also from a wider zone, in the general case comprising an angle of 4π ster.

With a known radiation pattern[1] $F(\theta,\phi)$ and brightness distribution $T_b(\theta,\phi)$ the antenna temperature is determined by the following equation:

$$T_a(\theta_0, \varphi_0) = \frac{S_{ef}}{\lambda^2}\int_{4\pi}\int T_b(\theta, \varphi) F(\theta - \theta_0, \varphi - \varphi_0)\sin\theta\, d\theta\, d\varphi, \qquad (10)$$

where S_{ef} is the reception cross section of the antenna, θ_0, ϕ_0 is the direction of the maximum of the radiation pattern of the antenna.

However, in practice the brightness distribution $T_b(\theta,\phi)$ is unknown, and the radiation pattern $F(\theta-\theta_0, \phi-\phi_0)$ is known with a

[1] On the strength of reciprocity theory [1], the radiation pattern of the antenna at reception is identical to the pattern at the transmitter.

known confidence, since it is plotted only in two planes, and the level of the long-range side radiation is often found to be lower than the sensitivity of the instrument. Therefore, the important characteristic of the antenna is the evaluation of the integral current of side scattering to a certain solid angle. Usually for evaluation of this value we introduce the scattering coefficient /144

$\beta_\Omega = \frac{P_{side}}{P_0}$, equal to the ratio of the power of P_{side} radiated by the antenna outside the solid angle Ω of the main lobe of the radiation pattern to the entire radiation with a power of P_0. Obviously the relationship between the coefficient β_Ω and the radiation pattern of the antenna $F(\theta,\phi)$ has the form

$$\beta_\Omega = 1 - \frac{\int\int_\Omega F(\theta, \varphi) \sin\theta \, d\theta \, d\varphi}{\int\int_{4\pi} F(\theta, \varphi) \sin\theta \, d\theta \, d\varphi}. \qquad (11)$$

With a strictly given function $F(\theta,\phi)$ the amount of power scattered outside the solid angle of the main lobe is uniquely figured according to expression (10). Then for the measured microwave radiation with a radiobrightness temperature T_b located on a uniform background with a radiobrightness temperature T_g, the antenna temperature will be equal to

$$T_a = T_b(1-\beta) + T_g\beta. \qquad (12)$$

However, in practice, it is impossible to compute the precise determination of the function of the radiation pattern for all angles over the entire sphere. Nevertheless we can, after analyzing the basic factors influencing the distribution of the scattered energy in space for typical antennas, and without knowing in detail the radiation patterns, estimate the value of the power scattered outside the effective angle.

Let us look at the basic factors influencing the distribution of emitted power in the wave band of the mirror antenna:

(a) The type of amplitude distribution in the antenna aperture for a given wave length λ;

(b) Radiation of the exciter of the antenna mirror outside the angle of irradiation of the mirror aperture;

(c) Radiation of the diffraction currents near the edge of the mirror;

(d) Scattering of the radiation in the design elements of the antenna and structure of the antenna carrier.

The size of the antenna aperture and the type of the amplitude distribution in the aperture determine the spatial distribution of the basic amount of irradiated power at the solid angle near the normal to the antenna. Computation of this distribution is made by integrating for the aperture; therefore, ususlly the distribution of the obtained field is called an aperture distribution. Let us figure what part of the irradiated power is included in the solid angle of the investigated surface, formed by the cone θ, which represents the angle between the normal to the aperture of the antenna and the direction to the boundary of the investigated surface, if the center does not lie on the normal:

$$G(\Omega) = \frac{\int_0^{\theta} F(\theta) \sin\theta \, d\theta}{\int_0^{\pi} F(\theta) \sin\theta \, d\theta}. \qquad (13)$$

In the case of extended surfaces, which occur with measurements of the water temperature $G(\Omega) = 1$.

The amplitude distributions in the aperture of the mirror antennas depend on the radiation pattern of the irradiating instrument. With irradiation of the mirror a part of the irradiated power is scattered outside the solid angle, which occupies the mirror of the relative phase center of the exciter. The current of radiation scattered by the horn, unlike the aperture scattering, is concentrated /145 in a rather large solid angle, adjacent to the back hemisphere.

A more complex problem is that of evaluating radiation from the mirror due to diffraction currents on the illuminated and the shaded parts of the mirror, irradiated by the spherical front. We can approximately evaluate the value of the edge currents, if we sum the radiation from the exciter at the solid angle, which is equal to the cross section of the diffraction currents scaled to the square of the distance to the exciter.

The scattering of the electromagnetic energy on the structural elements, incident in the current of radiation (exciter, supports, face of the carrier, etc.) may be high. The power scattered on the structural elements is concentrated in wide solid angles near the direction of the mirror reflection of the beams from the structural elements. Most often these angles pertain to the front hemisphere of the antenna.

This analysis of the individual factors which influence the scattering of energy permits evaluating the radiobrightness temperatures from a known antenna temperature.

For an antenna located below an airplane, when all scattering in the rear is converted to the front hemisphere in the case of the

investigated extended surface, for which $\Omega >> \Omega_{gl}$, we obtain the following expression:

$$T_a = (1 - \beta_0) T_b + T_g \beta_0. \quad (14)$$

Thus, the coefficient $G(\Omega)$ represents the characteristics of the directed radiation, but β_0 characterizes the undirected radiation of the antenna system.

As shown above, in our case $G(\Omega) = 1$ and the value of β_0 is determined by the scattering of the exciter and diffraction on the edges of the mirror.

It is possible to experimentally determine the scattering outside the main lobe of the radiation pattern by using hhe method of artificial sources of radiation, which was described in detail in [2]. As such a source we used a disk of the absorbing material, black rubber with notches, the emission coefficient of which is approximately 0.96 - 0.98 (Fig. 3). The angular dimensions of the "black" disk were chosen equal to the angular dimensions of the main lobe of the radiation pattern of the antenna to decrease the diffraction correction. To eliminate the effect of radiation from the Earth's surface we used the metal shield described above.

The measurements were made in the following sequence: (a) by computation we determined the radiobrightness temperature of the atmosphere T_d in the direction to the source and made a recording of the antenna temperature T_1 at the scale of the recording instrument

$$T_1 = T_d (1 - \beta) + T_g \beta. \quad (15)$$

The background was the atmospheric radiation received at the side lobes of the radiation pattern of the antenna; (b) we set up an artificial source and made the recordings of the antenna temperature T_2 on this same background

$$T_2 = T_D (1 - \beta) + T_g \beta. \quad (16)$$

To decrease the mean square error we made a series of such measurements.

From the obtained formulas it is easy to determine the coefficient of scattering /146

$$\beta = 1 - \frac{T_2 - T_1}{T_D - T_d}, \quad (17)$$

where T_D is the radiobrightness temperature of the "black" disk $T_2 - T_1$ is the difference in antenna temperatures with the disk and without, determined from the tape of the self-recorder using the calibration signal T_c of the noise generator.

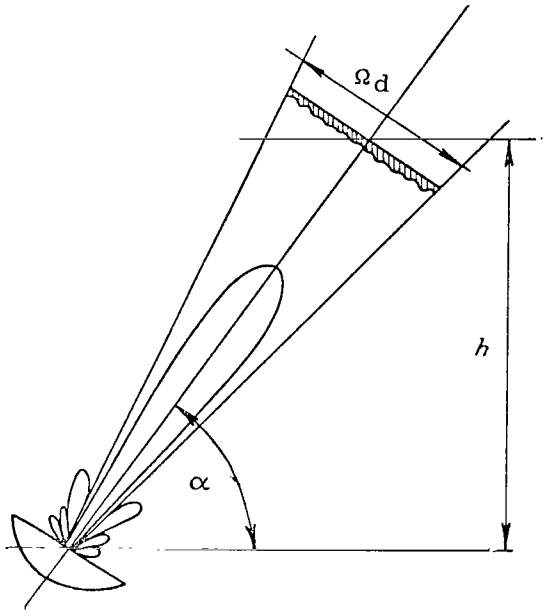

Fig. 3. Schematic of the Measurements of the Scattering Coefficient of the Antenna.

As a result of the measurements we obtained the average value of the scattering coefficient as 0.22.

Under aircraft conditions we proved the values of the measured scattering coefficient of the antenna. To do so the flight was carried out according to the following method. In the region of the Caspian Sea, a flight was made over a sandy island, and the altitude H and the flight velocity v in determining β were chosen based on the equation

$$\Delta x = \theta H + 3v\tau \qquad (18)$$

and

$$v \leqslant \frac{\Delta x}{3\tau},$$

where θ is the width of the radiation pattern of the antenna, τ is the time constant and Δχ is the size of the island.

The scattering coefficient was computed from the formula

$$\beta = 1 - \frac{T_2 - T_1}{T_i - T_w}, \qquad (19)$$

where $T_2 = T_i (1 - \beta) + T_g\beta$, $T_1 + T_w (1 - \beta) + T_g\beta$; T_i and T_w are the computed values of the radiobrightness temperatures of the sandy island and the sea water.

The obtained data of β is found to be in the range from 0.14 to 0.23. Hence it is obvious that the measurement method of the scattering coefficient of the antenna in the aircraft conditions has one significant disadvantage: the value of β is fully determined by the values of the emission coefficients of the water surface and the sandy surface of the island, which are known with low accuracy. This leads to significant errors in determining β. Moreover, under real /147

conditions, the choice of suitable objects (islands) is difficult for measuring β (located completely in the main lobe of the radiation pattern of the antenna).

Let us look at the contribution of each component of the radiation pattern.

In the first side lobes approximately 5 - 8% of scattered energy is concentrated; the diffraction of the edges of the mirror of the antenna is 2 - 4%, and the scattering on the exciter is equal to approximately 8 - 10%. Since the antenna has a linear polarization, we may assume that half of the nondirected irradiated power possesses a horizontal polarization and half a vertical. Consequently, about 14% of the scattered power belongs to the radiobrightness temperature which is practically equal to T_b of the investigated surface.

Evaluation of the error in determining the radiobrightness temperature can be made, proceeding from the basic equation (12). Converting it, we obtain an expression for the radiobrightness temperature

$$T_b = \frac{T_a - T_g\beta}{1-\beta}. \qquad (20)$$

After determining the differential of the logarithm of this expression and converting to finite increments, we obtain the following formula for the relative error in determining the radiobrightness temperature

$$\frac{\Delta T_b}{T_b} = \frac{\frac{\Delta T_a}{T_a}\frac{1}{T_g\beta} + \frac{\Delta T_g}{T_g}\frac{1}{T_a} + \frac{\Delta\beta}{\beta}\frac{1}{T_a}}{\frac{1}{T_g\beta} - \frac{1}{T_a}} + \frac{\frac{\Delta\beta}{\beta}}{\frac{1}{\beta}-1}, \qquad (21)$$

where $\frac{\Delta T_g}{T_g}$ is the relative error in determining the radiobrightness temperature of the background, $\frac{\Delta\beta}{\beta}$ is the relative error in determin- the scattering coefficient of the antenna.

The relative error in determining the antenna temperature determined in the previous paragraph is included in formula (21).

As a result of the computations we obtained the following values of the relative error in determining the radiobrightness temperature of the water surface (Table 2):

TABLE 2

Calibration Method	$\Delta T_b/T_b$%
From the nitrogen load	15.5
From the radio emission of the atmosphere	11
From the radio emission of the water surface	9

The obtained result shows that even with the best method of /148
calibration for the radio emission of the water surface (fresh water with a known temperature) the error is approximately 9%, which with a radiobrightness temperature of the water at about 110° K, gives an absolute error of 10°. This means that the available methods of calibrating the instrument and the determining the basic characteristics of the instrument (sensitivity, scattering coefficient of the antenna and losses in the antenna-feeder circuit) do not permit determining the radiobrightness temperature and from it, the temperature of the water surface with any rational degree of accuracy. Significantly better results are given by relative measurements in the process of which the results are tied in at individual segments of the measurements to the real temperature of the water determined from independent infrared or maritime measurements. The evaluations of the errors obtained in this case on the experimental data are given in [3] and confirm the possiblity of using radiometric instruments the temperature mapping of the water surfaces, although the accuracy of the thermal radar measurements are still not as good as the infrared measurements.

REFERENCES

1. Kuz'min, A.D. and A.Ye. Salomonovich: Radioastronomicheskiye metody izmereniy parametrov antenn. (Radioastronomical Methods of Measuring the Parameters of Antennas)., Sovietskoye radio, 1964.
2. Tseytlin, N.M.: Primeneniye metodov radioastronomii v antennoy tekhnike. (Using the Methods of Radioastronomy in Antenna Technology), Sovietskoye radio, 1966.
3. Rabinovich, Yu.I., G.G. Shchukin and V.V. Melent'yev: Opredeleniye temperatury vodnoy poverkhnosti po radioizlicheniyu v santimetrovom diapazone. (Determination of the Temperature of the Water Surface from Radio Emission in the Centimeter Band)., See this collection.
4. Hogg, D.C.: Effective Antenna Temperatures Due to Oxygen and Water Vapor in the Atmosphere. J. Appl. Optics, Vol. 30, No. 9, 1959.

RADIO EMISSION FROM CLOUDS AND PRECIPITATIONS

Yu. I. Rabinovich, G.G. Shchukin and M.M. Chernyak

ABSTRACT: The radio emission from clouds and precipitations in the microwave band gives substantial contrast in comparison with the radiation from a clear atmosphere, which can be easily detected. In this respect, this article investigates the methods of aircraft measurements of radio contrasts of cloud cover and precipitations over a water surface. A comparison is made of the experimental data of radio emission and theoretical computations for two wave lengths: 0.8 and 3.2 cm.

Determination of the characteristics of large cloud formations /149 and the detection of precipitation bands based on their radio emission is a unique possible method of solving this problem using satellite meteorology. This is especially important for detecting precipitations and determining their intensity over water areas of the Earth which are poorly known in meteorology. Knowledge of the location of bands of cloud cover and precipitations and their movements with time yields considerable data for predicting weather on a global scale [1].

The radio emission from clouds and precipitations in the microwave band gives a substantial contrast in comparison with radiation from a clear atmosphere, which may be easily detected. In real cases of cloud formations and precipitations the optical thickness τ is less than 0.5 and the probability of photon survival $\lambda < 0.1$. Under these conditions, as shown in [2], we can ignore the contribution of multiple scattering and the radiation transfer equation will have the following form:

$$I(\tau, \theta) = I_0 e^{-\tau \sec \theta} + B(1 - e^{-\tau \sec \theta}) + B_1(1 - e^{-\tau \sec \theta}) e^{-\tau \sec \theta}. \quad (1)$$

Converting from intensities to radiobrightness temperatures, we find

$$T_b = (1 - R) T_s e^{-\tau \sec \theta} + T(1 - e^{-\tau \sec \theta}) + RT(1 - e^{-\tau \sec \theta}) e^{-\tau \sec \theta}, \quad (2)$$

where T_s is the temperature of the underlying surface, T is the temperature of the atmosphere in which the transfer of radiation occurs, τ is the optical thickness of the layer, θ is the angle between the normal to the layer and the direction of sighting, R is the reflection coefficient of the underlying surface.

Since the stratiform clouds and the precipitations of low intensity have optical thicknesses τ, which do not exceed 0.2, and $\lambda \approx 0.02 - 0.04$, the computations of the transfer of microwave radiation may be done from formula (2). Tables 1 and 2 give the computational data on the contrasts of cloud cover and precipitation on a background of a water surface. The computations were made for the real meteorlogical characteristics of the atmosphere and the underlying surface, which were obtained in experimental flights. For comparison of the computations with the measurements we used the results of four flights in which the radiobrightness temperature of the clouds and precipitations was measured. In the comparisons we computed and experimentally determined the increase in radiobrightness temperature due to cloud cover and precipitations with respect to the radiobrightness temperature of the underlying surface with a cloud-free sky /150

$$\Delta T_b = T_{b\ cl} - T_{b\ atm}. \qquad (3)$$

TABLE 1: RADIOBRIGHTNESS CONTRAST OF PRECIPITATIONS

October 12, 1966	December 26, 1966
Baltic Sea	Sea of Azov
Type of Cloud Cover: 10 b Ns	10 b Frnb
$H_{l.b.}$ = 200 m, $H_{u.b.}$ = 1800 m	$H_{l.b.}$ = 250 m, $H_{u.b.}$ = 350 m
10 b As	10 b Ns
$H_{l.b.}$ = 400 m, $H_{u.b.}$ = 5200 m	$H_{l.b.}$ = 350 m, $H_{u.b.}$ = 3850 m
$T_{l.b.}$ = 254° K, $T_{u.b.}$ = 251.6°K	$T_{l.b.}$ = 282° K, $T_{u.b.}$ = 257.2°K
Precipitations: intensity 1 mm/hr	Intensity 1.5 - 2 mm/hr
T water = 278° K	T Water = 283° K

Wave length, cm	ΔT_b deg.		ΔT_b deg	
	Theoretical	Experimental	Theoretical	Experimental
0.8	43.0	41.5	96.6	105.0
3.2	4.0	9.0	5.0	15.0

Let us briefly look at the method used to measure cloud cover and precipitations for which we used the radiometric instrument of the 0.8 and 3.2 cm bands described in [4].

The flights were conducted in regions where the boundary of the cloud cover passed. Thus, over one and the same underlying surface we made measurements both in a cloud-free sky, in cloud cover and in precipitations. The water surface of the lakes and seas served as the underlying surface. By taking into account the small variability in the water temperature at some distance from the shore, using this method we can obtain the values of the increase in radiobrightness temperature due to the clouds and

TABLE 2: RADIOBRIGHTNESS CONTRAST OF CLOUD COVER

October 10, 1966	December 26, 1966
Lake Oneiga	Sea of Azov
Type of Cloud Cover: 10 b Sc	10 b Sc
$H_{l.b.}$ = 110 m, $H_{u.b.}$ = 3000 m	$H_{l.b.}$ = 650 m, $H_{u.b.}$ = 2200 m
$T_{l.b.}$ = 267.7° K, $T_{u.b.}$ = 256.1°K	$T_{l.b.}$ = 277.3°K, $T_{u.b.}$ = 269°K
T water = 279° K	T water = 283° K

Wave length, cm	ΔT_b deg.		ΔT_b deg	
	Theoretical	Experimental	Theoretical	Experimental
0.8	24.5	26.0	13.0	15.0
3.2	2.5	2.0	2.0	4.0

precipitations. To determine the altitude of the upper and lower edges of the cloud cover and the distribution of temperature and moisture content with altitude before the beginning and end of the measurements, we made a vertical sounding of the atmosphere. More- /151
over, detection of the heavy cloud cover and the precipitation bands were made using aircraft navigation radar.

On the basis of the aircraft measurements of radio emission of clouds and precipitations made in 1967, Table 3 has been compiled which contains the increase in ΔT_b due to different types of cloud cover and precipitations.

TABLE 3:

Type of Cloud Cover	Intensity of Precipitations mm/hr	ΔT_b deg	
		λ = 0.8 cm	λ = 3.2 cm
Ci,Cs	-	2-5	0.0
Cu cong.	-	15-45	2.5-7.0
Sc	-	26.0	2.0
As,Ac	-	15.0	4.0
Cu	-	7-12	2-4
Frnb,Ns,Ac	1	55.0	6.0
St fr.,As,Ac	1.5-2	100.0	20.0
Ns,As,Ac	2-3	110.0	45.0

As is obvious from Table 3, the maximum values of ΔT_b were obtained for large nimbostratus clouds and the minimum values for clouds of the upper level. With an increase in the intensity of precipitations the radiobrightness contrast ΔT_b also increases.

It is interesting to compare the results of aircraft measurements of the bands of cloud cover and precipitation of different intensity with the computations made on the basis of meteorological measurements on Earth and from aircraft. Comparison was made for four cases, of which two include precipitations, and two, cloud cover. The results of the comparison are given in Tables 1 and 2. Here also are shown the meteorological characteristics of the atmosphere, the cloud cover and the precipitations according to aircraft measurements: $H_{u.b.}$ is the altitude of the upper boundary of the cloud cover, $H_{l.b.}$ is the altitude of the lower boundary, $T_{u.b.}$ and $T_{l.b.}$ are the temperature at the upper and the lower boundary of the cloud cover, respectively.

Comparison of the theoretical and the experimental data showed a good agreement between them. The divergence, as a rule, does not exceed 20% in the $\lambda = 0.8$ cm band.

Analysis of the obtained data shows that even for precipitations of low intensity, up to 2 mm/hr, in the 0.8 cm band the contrasts reach 70-90°. This means that there is a real possibility for detecting bands of precipitations of moderate intensity, not only over a uniform water surface but also over a natural underlying surface of dry land, in which the fluctuations in radiobrightness temperature are usually 20 - 40° [3].

In studying the experimental and theoretical data it is obvious that for detection of bands of cloud cover and precipitation it is feasible to use measurements in two wave lengths: 0.8 and 3.2 cm. On the channel $\lambda = 0.8$ cm the greatest radiobrightness contrast is obtained and the range $\lambda = 3.2$ cm is necessary for determining the type and the temperature of the underlying sufrace and also of precipitations in the presence of a multilevel cloud cover.

REFERENCES

1. Bashirinov, A.Ye., S.T. Yegorov, M.A. Kolosov and B.G. Kutuza: Author's Certificate No. 27927 of May 23, 1964. /152
2. Volchok, B.A. and M.M. Chernyak: Perenos mikrovolnovogo izlucheniya v oblakakh i osadkakh. (Transfer of Microwave Radiation in Clouds and Precipitations)., See this Collection.
3. Shifrin, K.S., Yu. I. Rabinovich and G.G. Shchukin: Issledovaniye polya mikrovolnovogo izlucheniya v atmosfere. (Investigation of the Field of Microwave Radiation in the Atmosphere)., See this Collection.
4. Rabinovich, Yu. I., G.G. Shchukin and V.G. Volkov: O vozmozhnykh pogreshnostyakh absolyutnykh izmereniy radioizlucheniya. (Possible Errors in Absolute Measurements of Radio Emission). See this Collection.

FEATURES OF THE METHOD OF ULTRAHIGH FREQUENCY RADIOMETRIC PROBING OF THE ATMOSPHERE FROM AIRCRAFT

A.Ye. Basharinov, S.T. Yegorov, M.A. Kolosov and B.G. Kutuza

ABSTRACT: Models of forming a radiating current of UHF radiation from a heterogeneous atmosphere are studied. The relationships which characterize the dependences of the spectrum of radiobrightness temperatures on the value of the integral moisture content and water content in the atmosphere are given. The obtained evaluations of the sensitivity of the radiometric method show that the minimal recordable variations in the integral moisture content are 0.2 - 0.5 g/cm^2 and the minimal recordable variations in water reserve of the clouds are (1-3) 10^{-2} g/cm^2.

1

Probing of the atmosphere by the method of receiving atmospheric radiothermal radiation is a further development of ground investigations of the radiothermal emission from the atmosphere. /153

Beginning with the work of Dicke and Beringer [1], at the present time (see, for example, the summary [2]) a large number of investigations have been made on the radio emission from a free atmosphere.

In a number of papers there are results cited on the observations of radiothermal radiation of hydrometeors ([3-5] and articles in this collection and others).

In [7] it was proposed to use the results of the radiometric observations of UHF radiation from the atmosphere using aircraft for detection of regions of rain formations.

The discussion of the method of radiometric UHF probes given in [8] and the articles of the present collection show the feasibility of further theoretical and experimental investigations of this method.

Below we give several models of the spectrum of UHF radiation from a heterogeneous atmosphere and evaluations of the sensitivity of the method to determing the moisture content and the water content.

2

Radiometric detection of the hydrometeors and determination

of the moisture content and water content in the atmosphere with observations from aircraft is based on measuring the spectrum of intensity of the emitted UHF current of thermal radiation from the atmosphere.

The current of emitted thermal radiation in the UHF band consists of a circect current of radiation from the layer of the atmosphere, an atentuated current of radiation from the underlying surface and a current of back radiation from the atmosphere reflected by the underlying surface.

The radiobrightness temperature of radiation depends on the state of the atmosphere and is a function of the integral absorption in the direction of the sighting.

Without taking into account the effects of scattering, let us write an equation for the radio brightness with vertical sounding in the form /154

$$T_b(\lambda) = T_0[1 - R(\lambda)]\, e^{-\int_0^H \gamma_\lambda(h)\,dh} + \int_0^H T(h)\,\gamma_\lambda(h)\, e^{-\int_h^H \gamma_\lambda(l)\,dl}\,dh + \\ + R(\lambda)\, e^{-\int_0^H \gamma_\lambda(h)\,dh} \int_0^H T(h)\,\gamma_\lambda(h)\, e^{-\int_0^h \gamma_\lambda(l)\,dl}\,dh, \qquad (1)$$

where H is the altitude of the instrument over the surface of the Earth, T_0 is the temperature of the underlying surface, $R(\lambda)$ is the reflection coefficient of the surface, $\gamma_\lambda(h)$ is the linear absorption coefficient of the atmosphere.

Determination of the altitude profiles of the temperature and absorption in the atmosphere from the results of measuring the spectrum of radiobrightness temperatures $T_b(\lambda)$ is a rather complicated problem.

Introduction of the integral parameters permits expressing the radio brightness through the mean temperature T* and the integral absorption τ,

$$T_b(\lambda) = T_0(1-R)e^{-\tau(\lambda)} + T_1^*(1 - e^{-\tau(\lambda)}) + T_2^* R e^{-\tau(\lambda)}(1 - e^{-\tau(\lambda)}), \qquad (2)$$

where

$$T_1^*(\lambda) = \frac{\int_0^H T(h)\,\gamma_\lambda(h)\, e^{-\int_h^H \gamma_\lambda(l)\,dl}\,dh}{\int_0^H \gamma_\lambda(h)\, e^{-\int_h^H \gamma_\lambda(l)\,dl}\,dh},$$

$$T_2^*(\lambda) = \frac{\int_0^H T(h)\,\gamma_\lambda(h)\,e^{-\int_0^h \gamma_\lambda(l)\,dl}\,dh}{\int_0^H \gamma_\lambda(h)\,e^{-\int_0^h \gamma_\lambda(l)\,dl}\,dh},$$

$$\tau(\lambda) = \int_0^H \gamma_\lambda(h)\,dh.$$

With a known temperature of the underlying surface, the values of the mean temperatures $T_1^*(\lambda)$ and $T_2^*(\lambda)$ are computed from the data of the atmospheric models.

In the centimeter band of radio waves the basic absorbing layer is located at altitudes up to 3 km, and in first approximation it may be assumed that $T_1^*(\lambda) \approx T_2^*(\lambda) \approx T_0 - \Delta T$.

As is obvious from (2) the derivative of the value of the integral absorption in the layer is increased with increase in the reflectivity of the underlying surface.

With flights over the Earth's mantle with a small reflectivity /155
$R \approx 0.1$ (sands, plant covers, etc.) the radio brightness in the absence of precipitations depends little on the condition of the atmosphere.

In the case of flights over a water surface having a reflectivity of $R \approx 0.4 - 0.5$, the radio brightness depends sharply on the condition of the atmosphere.

Simultaneous measurements of the radio brightness temperatures at several points of the spectrum permit determining the values of the integral absorptions $\tau(\lambda_i)$ and evaluating the contribution of the absorption components in oxygen, water vapors and hydrometeors.

Let us write the integral absorption in the form of a sum of components:

$$\tau(\lambda) = \int_0^H \gamma_\lambda(h)\,dh = \int_0^H \gamma_{k\lambda}(h)\,dh + \int_0^H k_\rho(\lambda, T)\,\rho(h)\,dh + \int_0^H k_w(\lambda, T)\,w(h)\,dh + \int_0^H k_r(\lambda, T)\,w_r(h)\,dh. \quad (3)$$

In (3) the values $k\rho(\lambda, T)$, $k_w(\lambda, T)$, $k_r(\lambda, T)$ represent, respectively the linear absorption coefficients in water vapors, in a finely dropping atmosphere and in rainfalls with a single

specific content of the absorbing agent.[1]

Let us introduce the weighting factors:

$$k_\rho^*(\lambda, T_0) = \frac{\int_0^H k_\rho(\lambda, T)\,\rho(h)\,dh}{\int_0^H \rho(h)\,dh},$$

$$k_w^*(\lambda, T_0) = \frac{\int_0^H k_w(\lambda, T)\,w(h)\,dh}{\int_0^H w(h)\,dh},$$

$$k_r^*(\lambda, T_0) = \frac{\int_0^H k_r(\lambda, T)\,w_r(h)\,dh}{\int_0^H w_r(h)\,dh}. \qquad (4)$$

With known values of the temperature of the surface the computations of the weighting factors $k_\rho^*(\lambda, T_0)$ and $k_w^*(\lambda, T_0)$ are carried out from the data on the atmospheric models.

The coefficient $k_r^*(\lambda, T_0)$ is also a function of the dimensions of the raindrops.

Equation (3), taking (4) into account, leads to equations which connect the spectrum of absorption in the atmosphere with the values of the integral moisture content $\rho_\Sigma = \int_0^H \rho(h)\,dh$ and the water content $W_\Sigma = \int_0^H w(h)\,dh$,

$$\begin{aligned}
\tau(\lambda_1) &= \tau_k(\lambda_1) + k_\rho^*(\lambda_1, T_0)\,\rho_\Sigma + k_w^*(\lambda_1, T_0)\,w_\Sigma + k_r^*(\lambda_1, T_0)\,w_{\Sigma r}\\
&\cdots\cdots\cdots\cdots\cdots\cdots\cdots\cdots\cdots\cdots\\
\tau(\lambda_n) &= \tau_k(\lambda_n) + k_\rho^*(\lambda_n, T_0)\,\rho_\Sigma + k_w^*(\lambda_n, T_0)\,w_\Sigma + k_r^*(\lambda_n, T_0)\,w_{\Sigma r}.
\end{aligned} \qquad (5)$$

If we assume the integral absorption in the atmospheric oxygen $\tau_k(\lambda)$ and the weighting factors $k_\rho^*(\lambda, T_0)$, $k_w^*(\lambda, T_0)$, $k_r(\lambda, T_0)$ to be known values, we have a system of equations that will allow solution due to the difference in the spectral characteristics of attenuation in water vapor, dropping-liquid clouds and in rain. /156

3

The sensitivity of the radiometric method to measuring the

[1] $\gamma_{k\lambda}(h)$ is the coefficient of linear absorption in oxygen.

integral values of the moisture content and the water content may be evaluated using the relationships for small increments.

Let us represent (2) in the form

$$T_b(\lambda) = T_0(1 - R(\lambda))\, e^{-2\tau(\lambda)} + \Delta T_b(\lambda), \tag{6}$$

where the correction $\Delta T_b(\lambda)$ takes into account the nonisothermicity of the atmosphere.

By differentiating (6), in first approximation we have

$$\frac{dT_b(\lambda)}{d\tau} \approx 2R(\lambda)\, T_0 e^{-2\tau(\lambda)}. \tag{7}$$

According to (7) the minimal recordable change in the integral absorption is determined by the condition

$$\Delta\tau_{min} \approx \frac{\Delta T_{min}}{2T_0 R(\lambda)\, e^{-2\tau(\lambda)}}, \tag{8}$$

where $\Delta T_{min} = 3\sigma_b$ is the minimal recordable change in temperature, σ_b is the mean square value of the noise variations in the radio brightness.

The relationships for the minimal recordable values of the changes in moisture content and water content have the form

$$\Delta\rho_{\Sigma min} = \frac{\Delta T_{min}}{2T_0 R(\lambda)\, e^{-2\tau(\lambda)} k^*_\rho(\lambda, T_0)}, \tag{9}$$

$$\Delta w_{\Sigma min} \approx \frac{\Delta T_{min}}{2T_0 R(\lambda)\, e^{-2\tau(\lambda)} k^*_w(\lambda, T_0)}, \tag{10}$$

$$\Delta w_{\Sigma r\, min} \approx \frac{\Delta T_{min}}{2T_0 R(\lambda)\, e^{-2\tau(\lambda)} k^*_r(\lambda, T_0)}. \tag{11}$$

The maximum sensitivity to change of the moisture content is reached at a frequency of resonance absorption of water vapors f = 22, 23 GHz.

The value of the minimal recordable value $\Delta\rho\Sigma_{min}$ of the variation in moisture content for different values of the integral absorption τ with a value of the fluctuation threshold $\Delta T_{min} = 1^\circ$ is given on Table 1.

Table 1

τ	0.1	0.5	1
$\Delta_{\rho\,\Sigma min}$ g/cm^2	0.25	0.54	1.4

The sensitivity to change of the dropping water content, as the computations made using (10) show, in the shortwave part of the centimeter band depends little on frequency.

The dependence of the sensitivity to change in the moisture content $\Delta w_{\Sigma min}$ mm at a wave length of about 2 cm is shown on Table 2. /157

τ	0.1	0.5	1
$\Delta W_{\Sigma min}$ mm	10^{-1}	$2\cdot10^{-1}$	$6\cdot10^{-1}$

The sensitivity to change in water content with a cloud cover of moderate intensity is about 30% of the water reserve in the clouds.

Evaluations of the minimally detectable intensity of precipitations I_{min} mm/hr, with observations at a wave length of about 1 cm (where a pronounced spectral difference exists in the absorption in clouds and in rain) for an altitude of the lower edge of the cloud cover $H_0 \approx 1$ km, are shown on Table 3.

Table 3

τ	0.1	0.5	1
I_{min} mm/hr	2.5	5	10

At a wave length of about 1 cm, as a result of the significant amount of integral absorption, the sensitivity of the radiometric method allows detection of clouds of moderate intensity.

4

The precision of the radiometric method of determining the moisture content is limited by the effect of the instrumental and methodological errors.

The methodological errors arise due to unallowed-for variations in the weighting factors T^*, $k^*_\rho(\lambda, T_0)$, $k^*_w(\lambda, T_0)$ and $k^*_r(\lambda, T_0)$, which are included in equations (2) and (5). The variations in the weighting factors may, for example, occur due to deviation in finding the vertical distribution of temperature, moisture and water content from the distribution assumed in the computational model; the influence of the temperature changes in the absorption coefficients as a function of the sizes of the raindrops

and the influence of the scattering effects on large drops.

Additional errors may occur due to the absorption in dimers of the water vapors and the influence of the background radiations outside the main lobe of the antenna.

Instrumental errors are expressed by errors in calibrating the scale of radio brightness, by the influence of the natural fluctuational noises of the receiver, by the instability of the circuit, etc.

Correct allowance for the effect of methodological errors, characteristic of the radiometric method, requires inclusion of the generalized data on the distributions of meteorological parameters in the atmosphere.

Preliminary evaluations show that the sizes of the methodological errors, under the conditions when the integral absorption does not exceed 0.5, is 20 - 50% of the measurable values of the moisture content and water content.

The problem is significantly more complicated under the conditions of a cloud cover with gaps, partially overlapping the field of vision of the radiometric instrument.

REFERENCES

1. Dicke, R., R. Beringer, R.L. Kyhl and A.V. Vane: Atmospheric Absorption Measurements with a Microwave Radiometer. Phys. Rev., Vol. 70, p. 340, 1946. /158
2. Kislyakov, A.G. and K.S. Stankevich: Issledovaniye troposfernogo pogloshcheniya radiovoln radioastronomicheskimi metodami. (Investigation of Tropospheric Absorption of Radio Waves by Radiometric Methods)., Izv. VUZ, Radiofizika, Vol. X, No. 9-10, p. 1244, 1967.
3. Crawford, A.B. and D.C. Hogg: Measurement of Atmospheric Attenuation at Millimeter Wavelengths. Bell System Techn. J., Vol. 35, No. 4, p. 907, 1956.
4. Hogg, D.C. and R.A. Semplack: Estimated Sky Temperature Due to Rain in the Microwave Band., Bell Syst. Techn. J. Vol. 40, No. 3, p. 1331, 1961.
5. Straiton, A.W., C.W.Tolbert and C.O. Britt: Apparent Temperatures of Some Terrestial Materials and the Sun at 4.3 Millimeter Wavelengths., J. Appl. Phys., Vol. 29, No. 5, p. 776, 1958.
6. Ananov, N.I., Ye.A. Basharinov, K.P. Kidryashev and B.G. Kutuza: Fluktuatsii radioizlucheniya oblachnoy atmosfery v millimetrovom diapazone voln. (Fluctuations in Radio Emission from a Cloudy Atmosphere in the Millimeter Wave Length Band)., Radiotekhnika i elektronika, Vol. X, No. 11, p. 1941, 1965.

7. Basharinov, A.Ye., S.T. Yegorov, M.A. Kolosov and B.G. Kutuza: Patent No. 27927 of May 23, 1964, Claim to Patent No. 951474/38 of May 7, 1963.
8. Stepanenko, V.D.: Radiolokatsiya v meteorologii. (Radar in Meteorology), Gidrometeoizdat, 1966.

THERMAL RADIO EMISSION FROM AN ICE COVER IN THE UHF-BAND

L.T. Tuchkov, A.Ye. Basharinov, M.A. Kolosov and A.A. Kurskaya

ABSTRACT: The prospects of using the radiometric method for determining the parameters of the ice and snow covers are reviewed; this method has certain advantages at times, in comparison with the method of active probes. The observations of the thermal radio emission of the ice cover in the centimeter and decimeter bands were made in reservoirs both with fresh and with sea water. Variations were found in the radiobrightness temperatures from 110 to 200° K in observations of the ice cover in comparison with radiation from a water surface. The appearance of snow on the ice surface leads to an increase in the intensity of the radio emission from the cover. With an increase in the moisture content of the snow cover and ice, a decrease is observed in the radio brightness by 40 - 50° K. The possibility of finding the boundaries of the ice fields by a polarization selection of signals which are virtually independent of the thickness of the ice is noted.

1

In addition to the methods of studying the ice and snow covers /159 by active probes a radiometric method is now being developed to record the radiothermal emission from these covers [1,2].

The dependence of the emittance of the covers on their condition and their pronounced penetrability of radio waves in the UHF band, define the numerous possibilities of the radiometric method.

The emittance of the ice cover is determined by its absorption and reflecting properties and depends on the temperature, the salinity, the thickness of the cover, the presence of humidity in the liquid phase, the character of the underlying surface, the properties of the upper snow layer, etc.

The current of radiothermal emission is represented in the form of a superposition of a direct current of radiation from the ice layer and currents which arise due to reflections on the lower and upper boundaries.

Determination of the emittance and the character of the polar-

ization of the UHF radiation is made with the help of plane-stratified structure-type models, which differ in temperature, dielectric constant and size of the angle of losses.

The frequency characteristics of the linear absorption of the ice cover in the region where the angle of losses may be assumed constant has a dependence which is inverse to the wave length, that determines the increase in the penetrability of the radiation in the decimeter band in comparison with the penetrability in the centimeter and millimeter radio wave bands [3,4].

2

Observations of thermal radio emission from ice covers in the centimeter and millimeter bands were made on reservoirs with fresh and with sea water.

During the winter of 1962 - 1965 measurements were made on the Baltic Sea and on lakes in the Moscow and Leningrad Regions. In 1964 - 1965 observations were made of the radiation from ice on the Kara Sea.

In the observations of the intensity of radiation of the ice cover, forming on the surface of water, we found an increase in the radio emission in comparison with the radiation from an open water surface. The radiobrightness temperatures here were measured from T_b = 110° K for water to T_b = 200° K for new ice both for fresh and for sea reservoirs. /160

With an increase in the integral absorption along the line of sighting an increase is observed in the intensity of radiation and the radio brightness reaches 240 - 250° K.

The appearance of snow on the surface of the ice leads to an increase in the intensity of the radio emission from the cover. We found a dependence of the intensity of radiation on the density and structure of the snow. The observable changes in radio brightness are 20 - 30°

With an increase in the moisture content of the snow cover and ice a decrease is observed in the radio brightness by 40 - 50°.

Based on the measurements of the angular brightness characteristics of the vertically polarized component of the radiation from ice, we found an increase in the "effective" dielectric constant of the cover from 3 to 5.5 as a function of the moisture content of the ice.

In the presence of snow the effective dielectric constant of the cover with an increase in moisture content varied from 1.75 (with dry loose snow) to 5.5. In observing the intensity of the

radiation from sea ice we noted an increase in the absorption (in comparison with fresh ice). Change in salinity by 6 - 8% led to a change in the radio brightness by 20 - 30° [5].

3

In observing the radio emission under conditions of the formation of an ice cover on the surface of the water we noted an attenuation of polarization of the thermal radio emission. This phenonomen permits recording the boundaries of the ice fields by the polarization selection of signals received by the radiometric stations.

The conditions of detection of boundaries of ice fields by polarization selection of signals are virtually independent of the thickness of the ice.

The formation on the surface of ice of a layer of snow, just as the presence of irregularities on the surface of the interface water - ice and ice - air, produces an attenuation of the polarization of radiation.

4

The thermal radio emission represents an uncorrelated random process.

With the passage of the noisy signal along the circuit with a finite pass band a correlation bond is established between the instantaneous values of the noise voltage at the output of the circuit. If we represent the UHF circuit of the radiometric receiver in the form of an equivalent filter with a pass band Δf, we note that the period of time τ, during which the instantaneous values of the output voltage are found to be correlated, represents a value that is inverse to the pass band.

The thermal radio emission from water through a layer of ice represents a superposition of radiations emitted from the ice cover after multiple reflections in the layer of ice. In the case when the lag time due to sequential reflections $t_{lag} < \tau$, and the irregularities on the interface ice - water and ice air satisfy the criterion of Rayleigh irregularities, in the high-frequency circuit of the radiometric receiver we observe interference phenomena.

These interference phenomena produce oscillations in the output voltage. The character of the interference oscillations depends on the electrical properties of the ice cover and the parameters of the receiving instrument. /161

The examples probably are far from exhausting all the possibilities of the radiometric method of determining the parameters of ice and snow covers which have, in a number of cases, advantages in comparison with the method of active probing.

REFERENCES

1. Seling, T. and D. Nance: Electronics, No. 19, May, 1961.
2. Kennedy, I., R. Sakamoto and I. Ross: Meeting in Miami, 1965.
3. Gumming, W.J.: Appl. Phys., Vol. 23, Nos. 7 - 8, 1952.
4. Watt, A. and E. Maxwell: J. Res. Nat. Bur. Stand., Vol. 240, No. 1948.
5. Kurskaya, A.A., L.V. Fedorova and G.D. Yakovleva: Teplovoye izlucheniye l'da v santimetrovom i detsimetrovom diapazonakh. (Thermal Radiation from Ice in the Centimeter and Decimeter Bands)., See this Collection.

Translated for the National Aeronautics and Space Administration by:
Aztec School of Languages, Inc.,
Research Translation Division (332)
Maynard, Massachusetts
NASw-1692.

"The aeronautical and space activities of the United States shall be conducted so as to contribute . . . to the expansion of human knowledge of phenomena in the atmosphere and space. The Administration shall provide for the widest practicable and appropriate dissemination of information concerning its activities and the results thereof."

—NATIONAL AERONAUTICS AND SPACE ACT OF 1958

NASA SCIENTIFIC AND TECHNICAL PUBLICATIONS

TECHNICAL REPORTS: Scientific and technical information considered important, complete, and a lasting contribution to existing knowledge.

TECHNICAL NOTES: Information less broad in scope but nevertheless of importance as a contribution to existing knowledge.

TECHNICAL MEMORANDUMS: Information receiving limited distribution because of preliminary data, security classification, or other reasons.

CONTRACTOR REPORTS: Scientific and technical information generated under a NASA contract or grant and considered an important contribution to existing knowledge.

TECHNICAL TRANSLATIONS: Information published in a foreign language considered to merit NASA distribution in English.

SPECIAL PUBLICATIONS: Information derived from or of value to NASA activities. Publications include conference proceedings, monographs, data compilations, handbooks, sourcebooks, and special bibliographies.

TECHNOLOGY UTILIZATION PUBLICATIONS: Information on technology used by NASA that may be of particular interest in commercial and other non-aerospace applications. Publications include Tech Briefs, Technology Utilization Reports and Notes, and Technology Surveys.

Details on the availability of these publications may be obtained from:

SCIENTIFIC AND TECHNICAL INFORMATION DIVISION

NATIONAL AERONAUTICS AND SPACE ADMINISTRATION

Washington, D.C. 20546